

Johannes Silde

Assessing the impact of synthetic inertia controls in DFIG wind turbines on small-signal stability

Master's thesis in Energy and Environmental Engineering

Supervisor: Professor Olimpo Anaya-Lara

June 2021



Norwegian University of
Science and Technology

Johannes Silde

Assessing the impact of synthetic inertia controls in DFIG wind turbines on small-signal stability

Master's thesis in Energy and Environmental Engineering
Supervisor: Professor Olimpo Anaya-Lara
June 2021

Norwegian University of Science and Technology
Faculty of Information Technology and Electrical Engineering
Department of Electric Power Engineering

Abstract

The presence of renewable energy sources, in particular wind power, is rapidly increasing in the power system. The rotational speed of large wind turbines is regulated to obtain maximum power extraction from the wind. This speed regulation causes a decoupling between the mechanical rotation of the wind turbine and the electrical frequency of the power system. Because of this decoupling, implementing wind power to the power system reduce the system inertia and impairs the frequency stability. A popular solution to the inertia decrease is the synthetic inertia controller. This is a power reference manipulation technique in the wind turbine controls, causing fast and potentially significant power changes. The reference manipulation is, through a derivator, proportional to the change in frequency and the kinetic energy stored in the wind turbine rotation. This control makes the wind turbine provide an inertial power similar to a synchronous generator, counteracting frequency changes. It is expected that these synthetic inertia controllers will gain presence in the power system in the near future. Fast, reference-based power electronic converters will impact the power system stability. Therefore, this thesis examines how DFIG wind turbines with frequency service controls, including synthetic inertia controllers, affect the power system's small-signal stability.

The wind turbine technology considered is the type 3 doubly-fed induction generator. Kundur's two-area system is used for the analysis, where one of the synchronous generators is replaced with an aggregated wind turbine model. A test system is developed in DIgSILENT PowerFactory, where the wind turbine model is developed from the DFIG wind turbine template in the DIgSILENT library. Complete frequency service controls are designed, including a generic synthetic inertia controller. Comprehensive model verification is performed by reconstructing the test network in a second software, Matlab Simulink. Despite some modeling differences in the two software, a strong correspondence is obtained between the eigenvalue profiles, verifying the power system and wind turbine modeling.

Various sensitivity analyses are performed for wind power without frequency controls and synchronous generation. This is used to investigate the root of the eigenvalue movement obtained for the synthetic inertia controller's sensitivity analyses and better understand the DFIG wind turbines' impact on system stability. Without frequency controls, the wind turbines impair the small-signal stability, particularly the inter-area mode damping, motivated by the DFIG control system. However, including frequency controls in the wind turbines, the small-signal stability is enhanced, including reversing the impairing impact on the inter-area mode. The wind turbines will also create and excite small oscillatory eigenvalues, especially when using synthetic inertia controls. From the analysis of the dominant power system eigenvalues, the synthetic inertia derivator is a powerful system state. A decreasing derivator time constant better replicates the shape of the inertial contribution from a synchronous generator but also replicates increasing synchronous generator inertia towards the system eigenvalues. Therefore, by appropriate synthetic inertia derivator parameters, the wind turbine can impact the system eigenvalues with the desired generator inertia, and at the same time, provide frequency support through an inertial contribution in accordance with the stored kinetic energy in the wind turbine rotation.

Sammendrag

Tilstedeværelsen av fornybare energikilder, spesielt vindkraft, øker raskt i kraftsystemet. Bruk av vindturbiner medfører også utfordringer, da rotasjonshastigheten til store vindturbiner reguleres for å oppnå maksimal effektutvinning fra vinden. Hastighetsreguleringen forårsaker frakobling mellom den mekaniske rotasjonen til vindturbinen og den elektriske frekvensen til kraftsystemet. Frakoblingen fører til at økende implementering av vindkraft i kraftsystemet reduserer systemets treghetsmoment og svekker frekvensstabiliteten. En populær løsning på treghetsreduksjonen er syntetiske treghetsregulatorer. Dette er en manipulasjonsteknikk i effektreferansen til vindturbinen. Regulatoren forårsaker raske og potensielt betydelige effektendringer. Referansemanipulasjonen er gjennom en derivator proporsjonal med endringen i frekvens og gjennom rotasjonshastigheten proporsjonal med kinetisk energi lagret i vindturbinens rotasjon. Regulatoren får vindturbinen til å gi en effekt ved frekvensendringer som ligner på responsen til en synkron-generator, som motvirker frekvensendringer. Det forventes å finne flere og flere av disse syntetiske treghetsregulatorer i kraftsystemet i tiden som kommer. Raske, referansebaserte kraftelektronikkomformere vil påvirke kraftsystemets stabilitet. Denne masteroppgaven undersøker hvordan DFIG-vindturbiner med frekvenskontrollere, inkludert syntetiske treghetsregulatorer, påvirker kraftsystemets småsignal-stabilitet.

Vindturbinteknologien i fokus er type 3, dobbelmatet induksjonsgenerator. "Kundur's two-area system" brukes til analysen, der en av synkron-generatorene byttes til vindkraft. Et testsystem er utviklet i DIgSILENT PowerFactory, hvor vindturbinmodellen er utviklet fra DFIG vindturbinmalen, hentet fra DIgSILENT-biblioteket. En komplett frekvenskontroller er designet, bestående av syntetisk treghet- og primærkontroll. Omfattende modellverifisering er utført ved å rekonstruere modellen i programvaren Matlab Simulink. Til tross for enkelte modelleringsforskjeller i programvarene, oppnås en høy grad av korrespondanse mellom egenverdiprofilene. Dette bidrar til å verifisere kraftsystem- og vindturbinmodelleringen.

Flere følsomhetsanalyser utføres for vindkraft uten frekvenskontroll og synkron-generering. Dette brukes til å undersøke roten av egenverdibevegelsen til de ulike syntetiske treghetsregulator-analysene, samt gi bedre forståelse rundt DFIG-vindturbiners påvirkning på systemets stabilitet. Uten frekvenskontroll svekker vindturbinene småsignal-stabiliteten, spesielt dempingen av mellomområde-modusen, forårsaket av DFIG-kontrollsystemet. Ved å inkludere frekvenskontrolleren i vindturbinene forbedres småsignal-stabiliteten, og den svekkede påvirkningen på mellomområde-modusen reverseres. Vindturbinene både skaper og påvirker små oscillerende egenverdier, spesielt ved bruk av syntetiske treghetsregulatorer. Derivatoren i treghetsregulatoren har en høy påvirkning på egenverdiene i systemet. En reduserende tidskonstant i derivatoren vil bedre etterligne formen til treghetsbidraget fra en synkron-generator, men også etterligne økende synkron-generator-treghet mot systemets egenverdier. Derfor kan en syntetisk treghetsregulator med de riktige parameterne påvirke systemets egenverdier med ønsket treghet, og samtidig gi frekvensstøtte gjennom et treghetsbidrag i samsvar med den lagrede kinetiske energien i vindturbinens rotasjon.

Preface

This report is the Master's Thesis of a fifth-year student in Energy and Environmental Engineering at the Norwegian University of Science and Technology. The thesis is the graduating report in the course TET4905. The work builds on the author's pre-work in a specialization project [1] which provided valuable prior knowledge for DFIG wind turbine modeling and control.

A large thanks to the project supervisor, Professor Olimpo Anaya-Lara, at the Department of Electric Power Engineering at NTNU. His strong knowledge and engagement in the topic have been an important source of inspiration and guidance throughout the project.

Trondheim, June 9, 2021

Johannes Silde

Johannes Silde

Content

Abstract	iii
Sammendrag	v
Preface	vii
Content	ix
List of Figures	xii
List of Tables	xiv
Abbreviations	xv
1 Introduction	1
1.1 Background	2
1.2 Research challenges	3
1.3 Objectives	3
1.4 Contribution	4
1.5 Methodology	4
1.6 Structure of the report	5
2 Theoretical foundation	7
2.1 Introduction	8
2.2 Frequency control	9
2.3 DFIG wind turbine operation and control	10
2.3.1 Basic operation principles	10
2.3.2 Frequency service controls	12
2.4 Small-signal stability	13
2.4.1 The swing equation	14
2.4.2 System linearization	14
2.4.3 The eigenvalues and eigenvectors	15
3 Test power system implementation and validation	18
3.1 Introduction	19
3.2 Model design and implementation in DIgSILENT	19
3.2.1 Kundur's two-area system	19
3.2.2 Synchronous generation	20

3.2.3	Wind power integration	20
3.2.4	The design and functionality of the frequency service controls	22
3.3	Model verification	26
3.3.1	Model design and implementation in Simulink	26
3.3.2	Model synchronization	27
3.3.3	Modeling differences	27
3.3.4	Eigenvalue correspondence	27
4	Small-signal stability analysis of synchronous generation	31
4.1	Introduction	32
4.2	The turbine-governor control system	33
4.3	The AVR and PSS	34
4.4	The synchronous generator inertia	35
4.4.1	The local modes' connection to the generators for changing inertia	36
4.4.2	The inertia's effect on system dynamics	39
4.4.3	The inertia and PSS of synchronous generator 2	42
4.5	Loading	44
4.6	Inter-tie line length	44
5	Small-signal stability analysis of DFIG wind turbines	45
5.1	Wind power without frequency service controls	46
5.1.1	System introduction	46
5.1.2	Wind power penetration	47
5.1.3	The DFIG control system	49
5.1.4	The mechanical mode	53
5.1.5	Loading	54
5.1.6	Inter-tie line length	55
5.1.7	Key findings	56
5.2	Wind power with frequency service controls	57
5.2.1	System introduction	57
5.2.2	The synthetic inertia controller	57
5.2.3	The primary control	61
5.2.4	Wind power penetration	62
5.2.5	The parameters of the synthetic inertia derivator	67
5.2.6	The critical mode	69
5.2.7	Loading	71
5.2.8	Inter-tie line length	72
5.2.9	Key findings	73

6	Discussion	74
6.1	Model validation and evaluation	75
6.2	Comparison of the small-signal stability impact from the generation characteristics	76
6.2.1	General mode trajectories	76
6.2.2	The local modes	76
6.2.3	The inter-area mode	78
6.2.4	The small modes	79
6.2.5	Loading	80
6.2.6	Inter-tie line length	80
6.3	The synthetic inertia controller	81
7	Conclusion and further work	83
7.1	Conclusion	84
7.2	Further work	86
	References	87
	Appendix	91
A	The DIgSILENT model	92
A.1	Power system overview with the nominal power flow	92
A.2	The power system with implemented wind power, including the nominal power flow	93
A.3	The synchronous generators and their control system	94
A.4	The DFIG wind turbine and its control system	100
A.5	Extended results from the result comparison between DIgSILENT and Simulink .	109
B	The complete linearization	112
B.1	The eigenvalues for synchronous generation	112
B.2	The observability of the dominant eigenvalues in the synchronous generator speeds	113
B.3	The eigenvectors relating the states to the dominant eigenvalues for synchronous generation	114
B.4	The eigenvalues when generator 2 is wind power without frequency controls . . .	115
B.5	The eigenvectors relating the states to the dominant eigenvalues when generator 2 is wind power without frequency controls	116
B.6	The eigenvectors relating the synchronous generator speeds to the oscillatory modes	117
B.7	The eigenvalues when generator 2 is wind power with frequency controls	118
B.8	The eigenvectors relating the states to the dominant eigenvalues when generator 2 is wind power with frequency controls	119
C	Extended results from the stability analysis of synchronous generation	120
C.1	Simple analytical eigenvalue calculation	123
D	Extended results from the stability analysis of wind power without frequency service controls	125
E	Extended results from the stability analysis of wind power with frequency service controls	132

List of Figures

1.1	Global energy transformation goals.	2
2.1	Frequency dynamics at the sudden event of power generation shortage.	9
2.2	Schematic of a doubly-fed induction generator.	11
2.3	Power reference scheme with frequency service controls.	12
3.1	Kundur's Two-Area System.	20
3.2	The power response for a load step increase for wind turbines without frequency controls.	23
3.3	The DIgSILENT synthetic inertia controller.	23
3.4	The DIgSILENT primary controller.	25
3.5	The power response for a load step increase for wind turbines with frequency controls.	26
3.6	The eigenvalues from both Simulink and DIgSILENT for a purely synchronous generation.	28
3.7	The inter-area mode from DIgSILENT and Simulink for increasing wind power penetration.	30
3.8	The local mode one from DIgSILENT and Simulink for increasing wind power penetration.	30
3.9	The local mode two from DIgSILENT and Simulink for increasing wind power penetration.	30
4.1	The local modes for varying inertia in area one.	37
4.2	Zoomed edition of the local modes for varying inertia in area one.	37
4.3	The participation factors connecting the generator speeds to the local mode in area one.	38
4.4	The participation factors connecting the generator speeds to the local mode in area two.	38
4.5	The speed of generators 1 and 2 for a step increase of voltage reference at half inertia.	40
4.6	The speed of generators 1 and 2 for a step increase of voltage reference at nominal inertia.	40
4.7	The speed of generators 1 and 2 for a step increase of voltage reference at double inertia.	40
4.8	The simulated and calculated speed of generator 1 for a step increase of voltage reference.	41
4.9	The components of the calculated speed of generator 1 for a step increase of voltage reference.	41
4.10	The local modes for decreasing inertia and PSS gain in generator 2.	43
4.11	The inter-area mode for decreasing inertia and PSS gain in generator 2.	43
5.1	The local modes for increasing wind power penetration without frequency controls.	48
5.2	The inter-area mode for increasing wind power penetration without frequency controls.	48
5.3	The inter-area mode for increasing wind power penetration with very slow power regulators.	52
5.4	The mechanical mode as a function of the shaft stiffness K , damping D , and inertia H	54

5.5	The inter-area mode for a varying inertial contribution.	59
5.6	The inter-area mode for varying synthetic inertia derivator time constant.	59
5.7	The inter-area mode for varying droop, both for wind- and synchronous power.	62
5.8	The local modes for increasing wind power penetration with frequency controls.	64
5.9	The local modes for increasing wind power penetration using slow synthetic inertia derivators.	64
5.10	The inter-area mode for increasing wind power penetration with frequency controls.	66
5.11	The inter-area mode for increasing wind power penetration using a slow synthetic inertia derivator.	66
5.12	The inter-area mode for increasing wind power penetration using adoptive synthetic inertia derivator parameters.	68
5.13	The parameter function of the adoptive synthetic inertia derivator.	68
5.14	Modes 18 and 19 for increasing wind power penetration with frequency controls.	70
5.15	Sensitivity analysis of mode 18 towards the dominant states.	70
5.16	Modes 18 and 19 for increasing loading.	71
5.17	Modes 18 and 19, and 20 for increasing inter-tie line length.	73

List of Tables

4.1	The inter-area- and local modes for varying turbine governor gain.	33
4.2	The inter-area- and local modes for varying AVR gain.	34
4.3	The inter-area- and local modes for varying PSS gain.	34
4.4	The inter-area- and local modes for varying inertia of all four generators.	35
4.5	The inter-area- and local modes for varying inertia in the generators in area one.	35
4.6	The inter-area- and local modes for varying system loading.	44
4.7	The inter-area mode for varying inter-tie line length.	44
5.1	The inter-area mode for varying PI regulator speed of the rotor currents.	50
5.2	The inter-area mode for varying PI regulator speed of the active and reactive power . . .	51
5.3	The inter-area- and local mode for varying system loading. Generator 2 is wind power without frequency controls.	54
5.4	The inter-area mode and mode 20 for varying inter-tie line length. Generator 2 is wind power without frequency controls.	55
5.5	The synchronous generator inertia replicated by the synthetic inertia derivator.	66
5.6	The inter-area- and local mode for varying system loading. Generator 2 is wind power with frequency controls.	71
5.7	The inter-area mode for varying inter-tie line length. Generator 2 is wind power with frequency controls.	72

Abbreviations

AVR Automatic Voltage Regulator

DFIG Doubly-Fed Induction Generator

MPE Maximum Power Extraction

MPPT Maximum Power Point Tracking

PE Power Electronic

PI Proportional Integral

PSS Power System Stabilizer

RoCoF Rate of Change of Frequency

RSC Rotor Side Converter

SG Synchronous Generator

TSO Transmission System Operator

VSC Voltage Source Converter

Chapter 1

Introduction

This chapter gives an introduction to the work performed and to the report. A description of topic relevance, motivation of work, and thesis output is provided through the work's background, current research challenges, and contribution from this Master's thesis. The chapter also includes a description of how the work is performed and the structure of the report.

1.1 Background

The presence of wind power in the power system has increased rapidly in recent years. Environmental goals such as the Paris agreement [2] and goal number 7 in UNs sustainable development [3] are factors pushing the development forward. It is expected that wind power technology will continue to accelerate and gain a considerable portion of the power production in the grid. The global energy goals and the progress for integrating wind power technology in the power system are shown in figure 1.1. The goal is to cover 35% of the global power demand with wind power by 2050 [4]. This is an enormous increase from the 6% coverage in 2018.

The increasing penetration of wind power technology causes a decrease in power system ancillary services, especially frequency control [5, 6]. The displacement of synchronous generation causes an overall decrease in the physical power system inertia. The result is higher frequency deviations and more severe nadir points at power mismatch [7]. Traditionally, large conventional synchronous-based power plants supplied the required voltage- and frequency support, but as wind power penetration continues to increase, the dynamics in the power system change, triggering Grid Code requirements. Grid Codes have already started to address the possibilities for frequency service from wind farms and are expected to require primary control and synthetic inertia provision from wind farms as the penetration increases.

A popular means of realizing frequency service in wind turbines are the combination of primary control and synthetic inertia controllers [5, 6]. These are power reference manipulation techniques in the wind turbine controls, causing fast and potentially large power changes. By making the reference manipulation proportional to both the change of frequency and the kinetic energy stored in the wind turbine rotation, the wind turbines can replicate the inertial response from a synchronous generator. It is expected that these synthetic inertia controllers will gain presence in the power system in the near future, impacting the system dynamics.

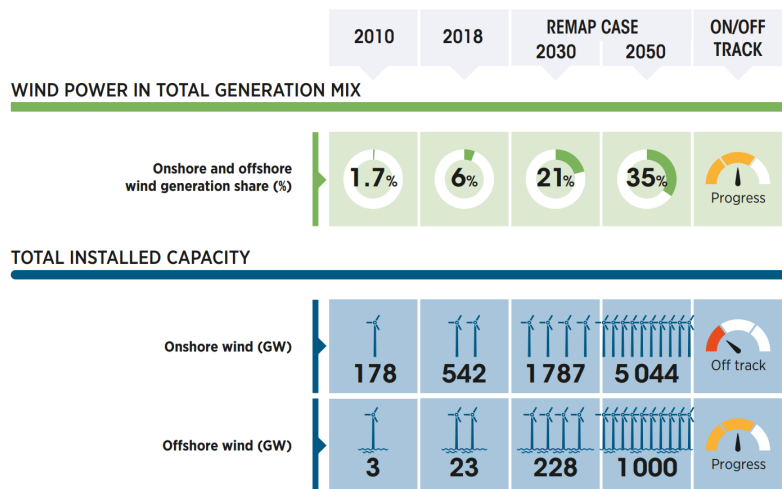


Figure 1.1: Global energy transformation goals [4].

1.2 Research challenges

In the coming years, the power system will experience growth in frequency service from renewable energy sources, especially wind turbines [6]. Power electronic converters partly or fully deliver the power from large wind turbines to the power system. The converters are based on switching logic and deliverers a power based on mathematically calculated reference values. This is another means of supplying power than through the widely used conventional synchronous generator.

Power electronic converter response is almost instantaneous and may cause challenges for the power system's small-signal stability. In particular, the inertial response is both a fast and extensive amount of power imposed on the power system. The impact of the system stability introduced by these fast power regulating controllers is not yet widely analyzed and understood. The literature is to some degree divided and inconclusive [8]. This thesis aims to shed light on how doubly-fed induction generator wind turbines equipped with frequency service controls, including synthetic inertia controllers, affect the power system's small-signal stability.

1.3 Objectives

The objective of this thesis is to provide insight into how synthetic inertia controllers in doubly-fed induction generator wind turbines affect the small-signal stability of the synchronous-based power systems. To achieving this, the objective is divided into two parts.

- Develop an inter-connected test system to analyze both inter-area- and local mode behavior. Analyze the impact from both synchronous- and wind power without frequency controls as a foundation and base of comparison for wind power equipped with synthetic inertia controls.
 - Create a fundamental understanding of the stability impact from characteristics of synchronous generation. Perform sensitivity analyses of the synchronous generation, focusing on the generator inertia, for later eigenvalue movement justification.
 - Replace synchronous generation with wind power, and identify and analyze relevant wind power characteristics' impact on the small-signal stability.
- Develop a generic frequency service controller and analyze the impact on the small-signal stability, focusing on the synthetic inertia controller.
 - Examine the stability impact when wind power with frequency controls replace synchronous- and wind power without frequency controls.
 - Identify and analyze connections between the synthetic inertia controller and the system stability.
 - Develop recommendations and considerations to be made when fitting synthetic inertia controllers in synchronous-based power systems.

1.4 Contribution

This thesis builds on a specialization project undertaken during the Autumn 2020 [1]. The project's focus was to gain a broad insight into DFIG wind power operation and control and develop a simulation model. However, the model is not used in this thesis as a change of software was chosen for simpler eigenvalue analysis. Nevertheless, some content in this report's introduction- and theoretical foundation chapters are inspired or gathered from the specialization project. The outline of the objective in this thesis corresponds to the described further work in the specialization project.

Wind turbines contributing to frequency service is an important yet large field within modern electrical power engineering. This thesis is not expected to solve nor create unambiguous solutions to the use of synthetic inertia controllers for improved system stability. However, the thesis contributes with well-documented development trends and argumentation of the small-signal stability impact from synthetic inertia controllers in DFIG wind turbines. The stability impact of wind power with frequency controls replacing both synchronous- and wind power without frequency controls are considered, giving a clear indication of potential stability improvement. The thesis presents compelling results of the power system's dominant eigenvalues' sensitivities towards the parameters in the synthetic inertia controller. Finally, remarks and recommendations for fitting synthetic inertia controllers in wind farms are given.

An output from the work performed in this thesis is two complete simulation models of Kundur's two-area system [9], in different software. As a part of the verification of the DIgSILENT model, the model is replicated in Matlab Simulink and verified by corresponding eigenvalue profiles. However, due to the time-consuming process of control replication and synchronization, only the thesis's primary software DIgSILENT contains frequency service control. The models are designed for stability analysis of wind power in inter-connected synchronous-based power systems. An eventual successor could use the models in conjunction with performing the recommended further work.

1.5 Methodology

Extensive simulation studies are performed together with a literature review to fulfill the thesis's objective. Kundur's two-area system is the inter-connected synchronous-based power system used for the small-signal stability analysis. This system allows for the analysis of both inter-area- and local modes.

The software DIgSILENT PowerFactory is used to carry out the analysis. The base of the wind turbine model is from the DFIG wind turbine template in the DIgSILENT library. Details of model construction and tuning are given in Section 3.2.3, including the modifications and the design of the frequency service controls. In order to verify the simulation model, the model is replicated in Matlab Simulink. Extensive control system- and parameter synchronization are performed in both synchronous generators and wind turbines. As a result, a high correspondence is obtained in the eigenvalue profiles between the two software, verifying the modeling. The result also corresponds with trends in previous research.

Sensitivity analyses between the system eigenvalues and various parameters are a central means of analysis in the thesis. For this purpose, the "Modal/Eigenvalue Analysis" tool in DIgSILENT is used. This tool linearizes the power system at the current state, which for all presented results are at steady-state, at the inertial conditions. The sensitivity analyses are performed by manually changing the parameters of interest, linearizing, and exporting the eigenvalues. The data is imported, analyzed, and manipulated into a tidy graphical representation in Matlab. For the analysis in Simulink, the "Model Linearizer" application is used. The linearized state space is calculated by choosing an arbitrary set of in- and output in the model. This is further used to calculate the system eigenvalues in Matlab.

The main mean of analysis in the thesis is eigenvalue sensitivity analyses and comparisons between the grid configurations. This report contains a "stand-alone" stability analysis, where extensive results representing a base of comparison are developed. The base includes analysis of the synchronous-based power system, focusing on the generator inertia, and analysis of wind power without frequency control, focusing on the wind power penetration level and the DFIG control system. The base provides a complete comparison platform to discuss similarities between the grid configurations to justify the obtained eigenvalue development.

The choice of relevant parameters for the sensitivity analyses is based on control relevance, eigenvectors relating the states to the modes, and experimental methods. As the analysis in the thesis is largely based on the comparison of eigenvalue development for a variety of sensitivity analyses for the different system configurations, extensive amounts of results are required. The essential results are included in the result and analysis chapters of the report while supporting results are included in the report appendix.

1.6 Structure of the report

The report is divided into an introduction, a theory, and a simulation model chapter, two result chapters, a discussion, and finally, a conclusion and further work chapter. The two result chapters contain the separate small-signal stability analysis of synchronous generation and wind power. The result chapters also include the analyses of the results, identifying important connections actively used to justify the chosen stability analyses. The report includes an extensive appendix. The appendix includes details about the model development and parameters, and all relevant numerical values for the complete linearization of the power system for the three configurations synchronous-, wind-, and wind power with frequency controls. Three extended result appendices are included, one for each system configuration. As the primary means of analyzing the small-signal stability in this thesis are results comparison, extensive amounts of results are required. The results are partly included in the appendix and referred to consecutively to achieve tidy and succinct result chapters. The figure numbering in the appendix contains the appendix letter for simple lookup.

Chapter 1 - Introduction: Description of the motivation and relevance, performed work and output, and how the work is performed and structured.

Chapter 2 - Theoretical foundation: Theoretical foundation of the report covering power system frequency dynamics and control, DFIG wind power, and small-signal stability.

Chapter 3 - Test power system implementation and validation: Development of the simulation model, including Kundur's two-area system, the synchronous generators, and wind turbines. The control system and aggregation model are presented together with the developed frequency controls. Finally, the model is validated by comparing the eigenvalue development in the DIgSILENT model against another software.

Chapter 4 - Small-signal stability analysis of synchronous generation: Presentation to the eigenvalue profile of Kundur's two-area system operated with conventional synchronous generation. Various system properties are examined, in particular generator inertia, to create a base of expectation and comparison for the later wind power analysis.

Chapter 5 - Small-signal stability analysis of DFIG wind turbines: Detailed analysis of DFIG wind turbine's impact on small-signal stability, both with- and without frequency controls. A particular focus on wind power penetration and the synthetic inertia derivator.

Chapter 6 - Discussion: Model evaluation, discussion of connections between the various sensitivity analyses, and description of important findings.

Chapter 7 - Conclusion and further work: Summary of substantial impact from synthetic inertia controllers on the small-signal stability, and important considerations when fitting synthetic inertia controllers in synchronous-based power systems. Finally, suggestions for further work.

Chapter 2

Theoretical foundation

This chapter presents the theoretical foundation of the thesis. First, the conventional power system's frequency dynamics and control are presented, focusing on the frequency drop and primary control. Next, basic operation and control of the DFIG wind turbine are considered, focusing on the frequency service controls, particularly the synthetic inertia controller. Finally, small-signal stability is considered. A mathematical description and deduction of system linearization are presented, including eigenvalue and eigenvector analysis.

2.1 Introduction

This chapter gives a theoretical introduction to the subjects in this thesis. Some of the content in the chapter is adapted from the author's preparatory project [1]. Frequency dynamics and control in conventional synchronous generators are presented to introduce the frequency service wind turbines should provide. Only a basic description of the Doubly-Fed Induction Generator (DFIG) operation and control is given. The focus is the frequency service controls, including the synthetic inertia controller, primary control, and the concept of deloading. This chapter also gives a theoretical introduction to small-signal stability. The result in the thesis is mainly based on linear analysis from DIGSILENT. Therefore, the chapter includes a description and a mathematical deduction of essential terms within the system state linearization and the resulting analysis of eigenproperties.

Traditionally, the power system was dominated by a few large, highly controllable synchronous generators. The modern trend in the power system is a more distributed generation [10]. This is a means of integrating renewable energy sources, including multiple generation units with lower power ratings. In comparison to conventional power generation, renewable power generation is in general of more varying nature. The power system must be designed to be reliable, controllable, and within the quality boundaries of harmonic pollution [11]. Wind power technology is a popular means of integrating renewable energy into the power system. The penetration of wind power technology into the power system has increased rapidly in the last years and is expected to continue to accelerate in the years to come. The global energy transformation goal [4] states that 35% of the global energy demand should be covered by wind power by 2050. Technology development for offshore power production has also in the last decade been gaining focus. Offshore wind power allows for larger area wind farms, stronger and less time-variant wind, and have less visual and environmental impact [12].

The power from large wind turbines is partly or fully supplied by Power Electronic (PE) converters, impacting the power system dynamics. Large wind turbines are operated with variable speed, preventing a natural inertial response at frequency events. Hence, the power system is dependent on conventional synchronous generators to supply the frequency support [6]. With the accelerating wind power penetration in the electrical power generation mix, wind turbine generators must also contribute with frequency service. Technology making wind turbines replicate synchronous generators' frequency behavior through PE converter control is available on the market and can be found in the power system today.

The European Grid Codes [13] require large wind farms to have the possibility to contribute with primary control within the requirements of the Transmission System Operator (TSO). The European Grid Codes also states that the TSO has the right to specify synthetic inertia provision from the wind farms. The requirements for frequency service are therefore dependent on the TSO. The Grid Codes by the Norwegian TSO Statnett [14] require large wind farms to be able to supply a frequency-controlled power reserve. Hence, the Norwegian Grid Codes require implemented primary control, but only active if re-

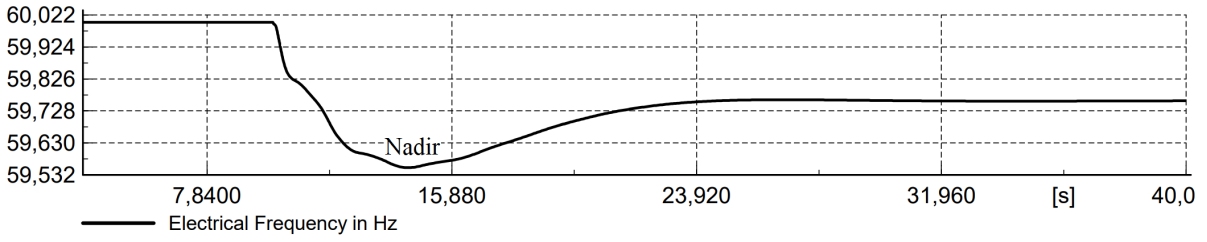


Figure 2.1: Frequency dynamics at the sudden event of power generation shortage.

quired by the system responsible. Synthetic inertia is similarly described in the Norwegian Grid Codes as a requirement if specified by the system responsible. Hence, frequency service from wind farms is dependent on the system responsible. Frequency service is, therefore, a highly relevant topic in the coming years.

This thesis considers the stability analysis impact from DFIG wind turbines with frequency service controls. A review of previous work on this subject is performed in [8]. The literature does not give a clear and general conclusion to variable speed wind turbine's effects on the power system stability. The effect is highly dependent on the implemented controls. Even though the literature is divided on the subject, making the following general remarks based on the trends is possible. The DFIG can enhance damping in power system oscillations but also impair the damping in inter-area oscillations. Frequency control in variable speed wind turbines is generally said to enhance the damping of power system oscillations.

2.2 Frequency control

This section describes the frequency dynamics and control of the power system, based on [15]. The focus is stage two and three, or the frequency drop and primary control. In the event of loss of generation, the frequency will drop at a rate determined by the system inertia. The frequency drop and the resulting inertial contributions typically last for a few to several seconds. Following the frequency drop, the primary control will converge the frequency onto a new value given by the new power equilibrium. The primary control is of longer nature, typically lasting for several seconds. Secondary control, or stage four, is not considered and is the control action of frequency restoration. The frequency dynamics and control for either step increase of loading or loss of generation are illustrated in figure 2.1.

A power mismatch results in increasing or decreasing system frequency. A typical frequency event is initiated by loss of generation, therefore a reducing frequency as in figure 2.1. The acceleration or deceleration ε obtained in the synchronous generators' rotational speed is dependent on the total inertia of the power system generators' H_{sum} , and their apparent power $S_{n,sum}$, shown in equation 2.1.

$$\varepsilon = \Delta P_{system} \frac{1}{2H_{sum}} \frac{S_{n,sum}}{\omega_s} \quad (2.1)$$

The generator inertia H is defined as the stored kinetic energy, with the unit seconds [15]. This is the time the generator can provide its rated power only through kinetic energy extraction. The stored kinetic energy in each generator determines its power contribution during a changing frequency. This can through

equation 2.1 be expressed as in equation 2.2. This individual power change in each generator during a frequency change is referred to as the inertial response. The equation shows how this contribution is proportional to the stored kinetic energy and the acceleration or the Rate of Change of Frequency (RoCoF) caused by the power mismatch.

$$\Delta P_i = 2H_i \varepsilon \frac{\omega_s}{S_{n,i}} \quad (2.2)$$

The RoCoF is a measure of the frequency event's severity and is a determining factor of the absolute deviation, the Nadir [6]. The RoCoF is inversely proportional to the system inertia, shown in equation 2.1. Hence, inertia is critical for obtaining a slow change in the system frequency at power mismatch.

Synchronous generators are constant speed generators, rotating their mass at speed proportional to the grid frequency. The inertia these rotating masses represent provides substantial energy storage. Power imbalances in the grid are effectively absorbed or supplied by small changes in the rotating masses' kinetic energy. For synchronous generators, this is physical energy available without control and is effectually instantaneously [16]. The rotation speed of the masses in the synchronous machines must be physically changed to change the grid frequency. The power system can not be operated without this inertia, providing a smoothing effect slowing any frequency change [16].

Primary control is the frequency dynamics stage, where the turbine governors regulate the power based on the grid frequency to achieve a new power equilibrium. Through the turbine governor, the generator speed is related to its power production. The power system's complete speed droop characteristics relate the change of power to the change of frequency. Large power systems consisting of several synchronous generators have a relatively flat characteristic, meaning that large power imbalances are required to cause considerable frequency change. A necessary power reserve is required to contribute to primary control to establish a new power equilibrium after a change in the power flow. If generators are operated at their maximum power output, they can not increase their power output to contribute to the primary control. The inertial response of synchronous generators is not dependent on a power reserve, as the inertial response is a physical resistance to a changing rotational speed.

2.3 DFIG wind turbine operation and control

2.3.1 Basic operation principles

Variable speed wind turbines are the modern choice of technology. Amongst the advantages for variable speed operation are reduced mechanical strain on the drive train and structure, increased power efficiency, and the ability of wind gust absorption [7]. The mechanical power from the wind depends on the wind turbine's physical size, wind speed, and the power coefficient [16]. The power coefficient is defined by the relation between the wind speed and the rotational speed of the wind turbine, referred to as the tip-speed ratio. Optimizing the rotational speed based on the wind speed enables Maximum Power Extraction (MPE) from the wind [7].

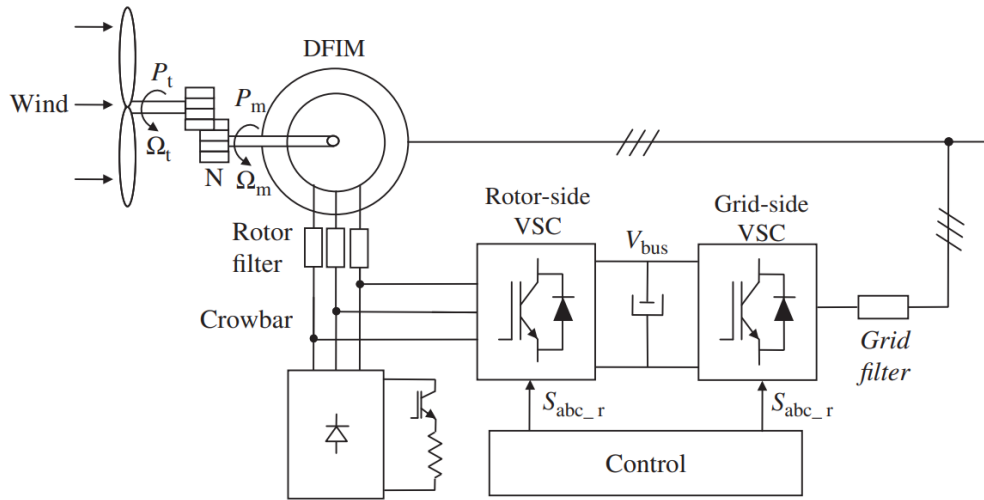


Figure 2.2: Schematic of a doubly-fed induction generator [17].

As the speed of variable speed wind turbines is regulated to maximize the power from the wind, the mechanical and electrical frequency of the wind turbine is decoupled [7]. Therefore, the kinetic energy stored in the wind turbine's rotation will neither release nor absorb energy from the grid during frequency events, unlike synchronous generators. Effectively, this means that variable speed wind turbines do not contribute to the system inertia. The increasing penetration of variable speed wind turbines will consequently result in higher frequency variations and -deviations at power imbalances [6]. For large wind speeds, the pitch controller limits the mechanical power the wind turbine absorbs from the wind to prevent overloading. This is a rotation of the wind turbine airfoil itself [7].

The wind turbine technology considered in this thesis is the type 3 doubly-fed induction generator. The DFIG is a wound rotor machine where the rotor windings are made available through slip rings. A schematic of a DFIG configuration is shown in figure 2.2. The stator winding is directly connected to the grid, and the rotor winding is connected through a back-to-back Voltage Source Converter (VSC) topology [7]. The Rotor Side Converter (RSC) regulates the active- and reactive power from the stator [7, 18]. The required rotor voltage to obtain the desired operation is calculated in the RSC controls and applied to the RSC through pulse-width modulation to realize the rotor voltage. The RSC energizes the rotor windings by charging or extracting energy from the DC-link capacitor. The grid side converter regulates the DC-link capacitor's voltage by delivering or consuming power from the grid. As the speed of the wind turbine is regulated based on the wind speed, the slip of the induction machine will vary [18]. The frequency of the rotor voltage reference calculated by the RSC controls corresponds with the induction machine slip. The stator will deliver power for all operating speeds, while the rotor will deliver or consume power dependent on the rotational speed. PE equipment is sensitive to overvoltage and overcurrent. Therefore, the DFIG is equipped with a rotor short-circuiting, thyristor controlled, resistor or a crowbar [19].

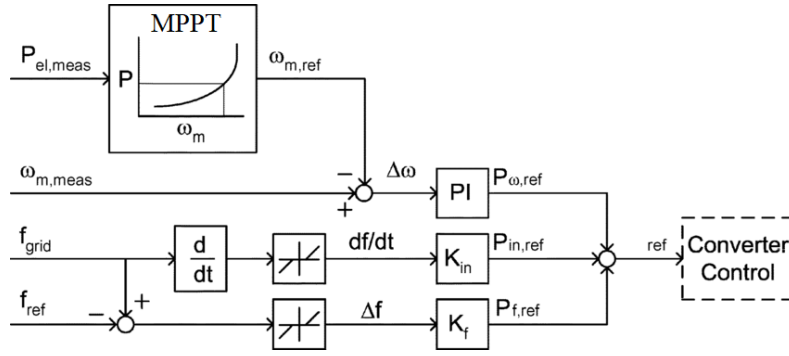


Figure 2.3: Power reference scheme with frequency service controls. The reference is composed of MPPT, synthetic inertia, and primary control [24].

2.3.2 Frequency service controls

The increasing penetration of wind power cause reducing system inertia. Variable speed wind turbines do not have a natural inertial response but can replicate one through PE control. A popular means of providing frequency support from wind turbines is the combination of synthetic inertia- and primary control strategies. As the decreasing power system inertia is a growing concern, much research is performed in the field of frequency support from wind turbines [20, 21, 22, 23]. The literature generally suggests a power reference manipulation proportional to the derivative of the grid frequency. The objective of the controllers is to provide frequency support by replicating the behavior of conventional synchronous generators. A schematic of such a power reference modification scheme is shown in figure 2.3. This scheme corresponds to the control system in the constructed DIGSILENT simulation model. The Maximum Power Point Tracker (MPPT) power reference is manipulated to provide an inertial- and a primary control contribution.

The inertial response is a short-term supply of additional power during a changing frequency to limit the RoCoF and the nadir [6]. The power reference manipulation realizing the inertia response is shown in equation 2.3. The inertial coefficient $K_{inertia} = 2H$ is proportional to the generator inertia. A consequence of kinetic energy extraction is wind turbine deceleration. By making the contribution proportional to the stored kinetic energy, the inertial contribution is based on the same foundation as for synchronous generators, causing a similar deceleration. A change in the wind turbine's rotational speed causes deviation from the MPPT speed and, consequently, a power decrease in the following speed restoration phase. The stored kinetic energy in the wind turbine rotation is proportional to its rotational speed and, though the MPPT, dependent on the wind speed. A typical synchronous-based power plant inertia is 2 – 10 seconds, given by the combined generator- and turbine inertia, dependent on the turbine type and operation speed (poles) [25]. For wind turbines, typical inertia is between 2 – 6 seconds [24]. The stored kinetic energy is therefore not necessarily reduced by introducing wind turbine power. However, it must be accessed through PE control.

The primary control contribution is a long-term power delivery, proportional to the deviation to the nominal grid frequency, shown in equation 2.4 [6]. The objective is to converge the frequency by creating a new power equilibrium. Unlike the inertial response, a deloading strategy is, for the primary control contribution, required to increase the power output for the duration of the frequency event, as the power can not be at the expense of stored kinetic energy.

$$\Delta P_{inertia} = K_{inertia} f_{pu} \frac{df}{dt} \quad (2.3)$$

$$\Delta P_{pri} = K_{droop}(f_{pu} - 1) \quad (2.4)$$

Variable speed wind turbines are operated at speeds given by the MPPT, operating at MPE. The wind turbine must be operated with a power reserve, realized by a deloading strategy [6], to replicate synchronous generators' behavior at frequency events. This can either be achieved by pitch- or speed control. The deloading strategy developed in the simulation model is pitch-based. This is the rotation of the airfoil blades themselves to reduce the power absorbed by the wind. A power increase is obtained by optimizing the pitch at a frequency event [26]. Deloading causes a portion of the potentially absorbed energy in the wind to be "spilled". A consequence of deloading is a possible CO_2 emission increase [27] if the power replacing the power reduction is not based on renewable energy sources.

2.4 Small-signal stability

This thesis focus on the small-signal stability impact from DFIG wind turbines with frequency service controls. Therefore, a theoretical introduction to small-signal stability is presented. The focus is on the means of analysis. The process of linearizing the state space is mathematically deduced, including the fundamental swing equation defining the dynamics of the generator speed and -angle state. From the linearized state space, the eigenproperties of the state matrix are presented. If not stated otherwise, the complete section is based on [9].

Small-signal stability analysis describes the power system's ability to maintain synchronism when subjected to a small disturbance. A disturbance is defined as small if the synchronous machines' operation point is changed to such a small degree that the linear analysis of the system can describe the following dynamics. The system is small-signal unstable if the rotor angle steadily increases or if the rotor angle oscillations increase after a small disturbance. For the small-signal stability analysis, the state space is developed. For this purpose, the concept of states is central. The state of the system is the least amount of system information required to determine future behavior. The state space is a Euclidean space that, by the state trajectory, describes the movement of the system state. The state of the system is divided into state variables. This is the minimal set of linearly independent system variables that gives a complete description of the system's behavior, together with the system inputs. The state variables can be the physical quantities generator speed, angle or voltage, or abstract mathematical variables within the control system or differential equations describing the system dynamics.

2.4.1 The swing equation

For the stability analysis requiring the state-space formulation, the differential equation describing the rotor angle and speed dynamics are considered [25]. The swing equation describes the rotor dynamics in electrical machines based on Newton's second law. The equation describes the power balance of a rotating machine, shown in equation 2.5. The input power, working to accelerate the machine, is the applied mechanical power on the shaft. The power working to decelerate the machine is the sum of electrical- and damping power. Only at an equilibrium between the powers is the rotation speed constant. For a motor, the signs are opposite.

$$2H \frac{S_n}{\omega_s} \frac{d^2\delta}{dt^2} = P_m - P_e - P_d \quad (2.5)$$

Where H is the inertia, and S_n and ω_s are rated power and synchronous speed, P_m, P_e, P_d are mechanical-, electrical- and damping power, respectively. Whenever the speed of the synchronous generator differs from synchronous speed, the damper winding will, through its penetrating flux, induce a current, causing a damping power working to restore the generator speed [15]. Therefore, the synchronizing power from the damper can be both positive and negative. The swing equation is, in appendix C.1, used to deduce a simplified analytical calculation of the Kundur's two-area system's eigenvalues for an uncontrolled synchronous generation.

2.4.2 System linearization

Eigenanalysis is the main mean of small-signal stability analysis and is extensively used in this thesis. A mathematical deduction from the state space resulting in the eigenproperties of the state matrix is presented to give a broader understanding of the mathematical background of the linearization used in the thesis' analysis. The complete deduction is based on [9]. Small bold letters symbolize vectors, while large bold letters are matrices.

By considering an autonomous system, meaning that the state variable derivatives are independent of time, the change in the state variables $\dot{\mathbf{x}}$ can be expressed as a function of the system inputs \mathbf{u} and the state variable themselves \mathbf{x} . The state variable development in equation 2.6 describe the state of the system. It is also common to define a system output vector \mathbf{y} . However, due to relevance, this is not included.

$$\dot{\mathbf{x}} = f(\mathbf{x}, \mathbf{u}) \quad (2.6)$$

For the stability analysis, the development of the system state is linearized. The linearization is considered at steady-state, at the system equilibrium. At the system equilibrium, the change in the state variables is zero, mathematically expressed in equation 2.7.

$$\dot{\mathbf{x}}_0 = f(\mathbf{x}_0, \mathbf{u}_0) = 0 \quad (2.7)$$

A small change from the equilibrium is considered, shown in equation 2.8, to analyze how a small disturbance affects the state variables.

$$\dot{\mathbf{x}} = \dot{\mathbf{x}}_0 + \Delta\dot{\mathbf{x}} = f(\mathbf{x}_0 + \Delta\mathbf{x}, \mathbf{u}_0 + \Delta\mathbf{u}) \quad (2.8)$$

By expressing the small perturbation of the non-linear functions as a Taylor's series, the expression can be simplified, shown in equation 2.9. This by using the initial state change of zero.

$$\dot{x}_i = f_i(\mathbf{x}_0 + \Delta\mathbf{x}, \mathbf{u}_0 + \Delta\mathbf{u}) = \frac{\partial f_i}{\partial x_1} \Delta x_1 + \dots + \frac{\partial f_i}{\partial x_n} \Delta x_n + \frac{\partial f_i}{\partial u_1} \Delta u_1 + \dots + \frac{\partial f_i}{\partial u_r} \Delta u_r \quad (2.9)$$

From the Taylor's series, the partial derivatives can be gathered into matrices. This gives the standard form of the linearized state space, shown in equation 2.10.

$$\Delta\dot{\mathbf{x}} = \mathbf{A}\Delta\mathbf{x} + \mathbf{B}\Delta\mathbf{u} \quad (2.10)$$

The \mathbf{A} matrix, shown in equation 2.11, is commonly referred to as the state matrix. This is the Jacobian matrix consisting of the sensitivities or the partial derivatives evaluated at the system's steady-state.

$$\mathbf{A} = \begin{bmatrix} \frac{\partial f_1}{\partial x_1} & \dots & \frac{\partial f_1}{\partial x_n} \\ \dots & \dots & \dots \\ \frac{\partial f_n}{\partial x_1} & \dots & \frac{\partial f_n}{\partial x_n} \end{bmatrix} \quad (2.11)$$

The state matrix is a powerful tool for the stability analysis of the power system. From the eigenproperties of the state matrix, the small-signal stability is evaluated. By considering the Laplace transform of the linearized state space, the expression can further be developed, shown in equation 2.12.

$$\mathcal{L}(\Delta\dot{\mathbf{x}}) = s\Delta\mathbf{x}(s) - \Delta\mathbf{x}(0) = \mathbf{A}\Delta\mathbf{x}(s) + \mathbf{B}\Delta\mathbf{u}(s) \quad (2.12)$$

$$\Delta\mathbf{x}(s) = (s\mathbf{I} - \mathbf{A})^{-1}(\Delta\mathbf{x}(0) + \mathbf{B}\Delta\mathbf{u}(s)) = \frac{adj(s\mathbf{I} - \mathbf{A})}{det(s\mathbf{I} - \mathbf{A})}(\Delta\mathbf{x}(0) + \mathbf{B}\Delta\mathbf{u}(s))$$

From the manipulated expression, the poles of the linearized state space are given by the roots of the nominator, shown in equation 2.13.

$$det(s\mathbf{I} - \mathbf{A}) = 0 \quad (2.13)$$

This is referred to as the characteristic equation of the state matrix. The values of s satisfying the equation are the eigenvalues of the state matrix. For power systems, all values of the state matrix are real, causing all complex eigenvalues to occur in conjugate pairs.

2.4.3 The eigenvalues and eigenvectors

The eigenvalues from the state matrix predict the power system behavior against small disturbances through state development. As the state space is evaluated at steady-state, the eigenvalues only accurately describe this operation point. The dimension of the state matrix determines the number of eigenvalues λ . An eigenvalue can have two parts, one real and one imaginary. The real component gives the damping, and the imaginary gives the oscillation frequency. The relations are shown in equation 2.14.

$$\lambda = \sigma \pm j\omega \quad f = \frac{\omega}{2\pi} \quad \zeta = \frac{-\sigma}{\sqrt{\sigma^2 + \omega^2}} \quad (2.14)$$

The damping ratio ζ determines the contribution's rate of decay. Hence, a large positive value is desired for stability. The system is stable if the real part of the eigenvalues is negative, meaning positive damping and a decaying contribution. The system is unstable if containing an eigenvalue with a positive real part.

For large power systems, the eigenvalues can either be of local- or global nature. Local modes typically have oscillation frequencies in the range of 0.7-2.0Hz. These modes may be associated with rotor angle oscillations of single- or a group of generators oscillating against the rest of the system or by generators in proximity oscillating against each other. Global modes are caused by interactions between groups of generators located in different areas. The frequency of the global or inter-area modes ranges between 0.1-0.7Hz, dependent on the number of generators involved in the oscillation. The modes can be characterized based on their oscillation frequency and their connection strength to the state variables of generator speed or rotor angle.

The eigenvectors define the connection between the system's state variables and the eigenvalues. The right eigenvector ϕ_{ki} measures the activity in the k th state x_k from the i th mode λ_i . The left eigenvector ψ_{ik} weighs the contribution of this state's activity to the mode. The right eigenvector ϕ , shown in equation 2.15, is a column vector, the i th column relates the i th eigenvalue to the system states.

$$\mathbf{A}\phi_i = \lambda_i\phi_i \quad (2.15)$$

For each eigenvalue, there is an n -long column vector. These can be gathered in a matrix Φ , shown in equation 2.16, relating all eigenvalues and states.

$$\Phi = [\phi_1, \phi_2, \dots, \phi_n] = \begin{bmatrix} \phi_{11} & \dots & \phi_{1n} \\ \dots & \dots & \dots \\ \phi_{n1} & \dots & \phi_{nn} \end{bmatrix} \quad (2.16)$$

In the same way, the left eigenvector ψ , shown in equation 2.17, has n -rows, where the i th row relates the i th eigenvalue to the system states. The left eigenvectors can also be gathered in a matrix Ψ by transposing the row vectors.

$$\psi_i\mathbf{A} = \lambda_i\psi_i \quad (2.17)$$

From equation 2.15 and 2.17, multiplying the vectors with a scalar is also a solution. The participation factor is defined to create an expression of connection strength between states and modes without units and scaling. The participation factor matrix \mathbf{P} is shown in equation 2.18. This combines the measure of state activity from the modes, and the weight of state contribution to the mode, making the participation factor dimensionless. Therefore, the participation factor measures the relative participation between a state variable and a mode.

$$\mathbf{P} = [\mathbf{p}_1, \mathbf{p}_2, \dots, \mathbf{p}_n] = \begin{bmatrix} \phi_{11}\psi_{11} & \dots & \phi_{1n}\psi_{n1} \\ \dots & \dots & \dots \\ \phi_{n1}\psi_{1n} & \dots & \phi_{nn}\psi_{nn} \end{bmatrix} \quad (2.18)$$

In the literature, the transformed state variable vector \mathbf{z} is typically used [9]. This variable transform causes decoupling between the state variables. From this transformation, the controllability and observability matrix is defined, using the system matrices \mathbf{B} and \mathbf{C} . For simple eigenvector discussion in the thesis, the right- and left eigenvectors are directly referred to as observability and controllability. In theory, these are only identical for an excitation vector of unity [28].

The eigenproperties of the state matrix can be used to predict the state variable response for small disturbances. The complete equation for the time response in the state variables is shown in equation 2.19. The coefficient c_i represents the magnitude of excitation of the i th mode, dependent on the nature of the disturbance. This coefficient is given by the multiplication of the left eigenvector ψ_i , and the initial conditions at the linearization $\Delta \mathbf{x}(0)$.

$$\Delta \mathbf{x}(t) = \sum_{i=1}^n \phi_i c_i e^{\lambda_i t} \quad (2.19)$$

For complex eigenvalues, the excitation coefficients are also complex, with appropriate values to make the state variable response real, shown in equation 2.20.

$$\Delta x_i(t) = e^{\sigma_i t} \sin(\omega_i t + \theta_i) \quad (2.20)$$

Identifying the excitation coefficient can be challenging and are for the simple theoretical example in chapter 4 experimentally replicated.

Chapter 3

Test power system implementation and validation

This chapter presents the DIGSILENT model. The power system model is presented, together with the synchronous generator- and wind turbine models. The modeling and functionality of the wind turbine's frequency service controls are considered. Finally, the model is replicated in Simulink to validate the model using the eigenvalue development.

3.1 Introduction

This chapter presents the simulation model and its verification. To limit the chapter's length and allow for detailed visualization, the control system, parameters, and dynamical simulations are in the Appendix A. The modeling of Kundur's two-area system is presented, first with synchronous generation. Including the generator modeling, both in terms of the electrical parameters and the control system. Further, the DFIG wind turbines are presented, including the various modifications. As the used wind turbine template does not offer frequency controls, a generic frequency service controller is designed, including synthetic inertia and primary controls. The modeling technique of these controls, including parameter adjustment and functionality, is presented through dynamical simulations of power mismatches.

The control system of the synchronous generators in DIgSILENT is constructed to be replicable in Matlab Simulink. The complete model is reconstructed in Simulink to verify the DFIG wind power modeling and the base system with the synchronous generation. The model synchronization and differences are presented. Some modeling differences exist between the software as the DFIG wind turbine templates are used as a base in both DIgSILENT and Simulink. In particular, three differences stand out, the DC-link voltage, speed controller, and the turbine shaft. The eigenvalue profile is compared between the software to validate the DIgSILENT model. A particular focus is given to the development for increasing penetration of wind power. The three main modeling differences cause some differences. However, high correspondence is obtained for the three dominant eigenvalues of the system.

3.2 Model design and implementation in DIgSILENT

3.2.1 Kundur's two-area system

For the stability analysis, Kundur's two-area system is used [9]. This is a power system constructed to analyze the eigenvalue profile of interconnected power systems. The systems, shown in figure 3.1, consist of two areas connected by two parallel inter-tie lines of 220km. Each area consists of two generation units. The Kundur's two-area system model in DIgSILENT, including the nominal power flow, is shown in Appendix A.1.

The system is fully symmetrical over bus 8, with some differences in the loading. The power system configuration and parameters correspond to the original system, including the system frequency of 60Hz. However, the power flow is slightly different and is adjusted to correspond with the enhanced system in the standard model of Kundur's two-area system in Simulink [29]. The adjustment is an increase in capacitors of 187MVar in each area for improved voltage profile, causing a slight increase in the inter-area power flow to 413MW.

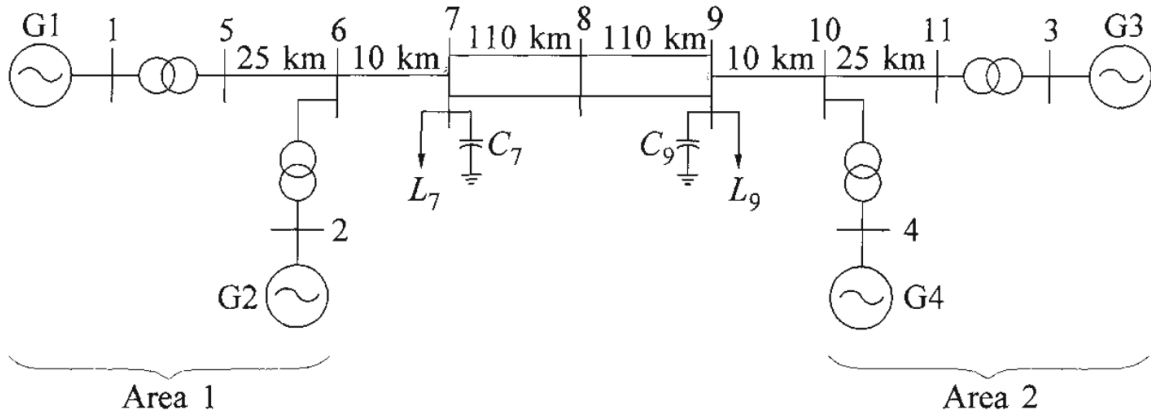


Figure 3.1: Kundur's Two-Area System [9].

3.2.2 Synchronous generation

For the base case, all four generators are synchronous. The parameters of the generators, including the control system, are shown in Appendix A.3. The generators are 900MVA and are nominally loaded at about 80% with an active power of 700MW. The exception is generator 3, loaded with 719MW, shown in Appendix A.1. Generator 1 operates as the slack bus in the system. Except for the generator inertia, the generators in areas one and -two are identical. The generator inertia is $H = 6.5s$ in area one and $H = 6.175s$ in area two. The parameters of the synchronous generators are shown in figure A.1.

The four generators are fully controlled with identical control systems, including turbine governors, automatic voltage regulators (AVR), and power system stabilizers (PSS), all active for the presented simulation unless otherwise stated. The control system is designed to represent a generic model and with the possibility to be recreated in Simulink. The generators have steam turbines, shown with the governor in figure A.2. As the governor gain only multiplies with the speed deviation, the primary control droop is equal to the inverse of the gain. The nominal gain $K=20$ in figure A.3 equals a droop of 5%. The AVR is shown in figure A.4, with the parameters shown in figure A.5. An AVR compatible with PSS manipulation is chosen. The PSS circuit with parameters is shown in figure A.6 and A.7.

3.2.3 Wind power integration

For the wind power integration, the 1.5MW DFIG wind turbine template from the DIgSILENT library is used [30]. This is a complete wind turbine model containing the DFIG, rotor voltage control based on power and current regulation, and a shaft connecting the generator to the aerodynamic model of the turbine. The power reference is calculated to achieve MPE from the wind. The induction machine has an apparent power of $1.5/0.9 = 1.67MVA$. The model includes a step-up transformer from the wind turbine generator voltage of 690V to the voltage of 20kV at the generator 2 bus. The DFIG and the control system are presented in Appendix A.4, including a detailed description of the generic DFIG frame. Only the parts considered in the later sensitivity analysis and the parts modified are included. The parameters of the DFIG are shown in figure A.9, including its inertia at nominal speed $H = 5.04s$.

The wind turbine is connected at the generator 2 bus, shown in Appendix A.2. As the wind turbine generator operates at a lower voltage than synchronous generator 2, two transformers are required. Hence, the wind turbines have to produce 707.4MW to achieve the same power delivery to generator 2 bus. The model includes reactive power regulation, operated to achieve the voltage 1 p.u. at the generator 2 bus, similar to synchronous generation. The wind turbine template does not include the DC-link voltage in the DFIG VSC. Hence, the model neglects the DC-link voltage dynamics. As shown in the generic DFIG frame in figure A.10, the calculated rotor voltage in the controls is applied directly to the DFIG's rotor windings.

The "number of parallel machines" function in DIgSILENT is used to make the wind turbine into an adequately large wind farm [30]. In accordance with [31], the internal dynamics of the single wind turbine is preserved by using single wind turbine currents in the control system. This is achieved by increasing the base values of the wind turbine's current- and power controls to follow the number of parallel machines, keeping the p.u. currents constant. This aggregation technique is commonly referred to as "full aggregation" [32], and neglects the differences in wind speed and mechanical power absorption in the different wind turbines. In transient studies, the wind speed is typically considered constant over the short period considered [31]. Therefore, the wind speed variations are not expected to have a considerable impact on the small-signal stability.

The model neglects the cables connecting the wind turbines to the step-up transformer and the cables connecting the step-up transformer to the main transformer. These simplifications are based on the assumption that the transformers represent a more significant impedance than the connecting cables [31]. The number of parallel transformers is increased equally as the number of parallel wind turbines for increased wind power penetration. The number of parallel machines is referred to as the aggregation number m , where the aggregation number $m = \frac{900}{1.5/0.9} = 540$ is required to fully replace synchronous generator 2 with wind power.

Exploring the varying nature of the wind is not in the scope of this thesis. The focus is the stability impact from wind power replacement of a 900MVA synchronous generator producing 700MW. At aggregation number 540, the 900MVA wind farm produces 810MW at nominal wind speed. For the wind turbines to contribute with frequency service, the wind turbines need to be operated with the necessary power reserve. Therefore, the wind farm is operated at the wind speed allowing for the nominal power production of 810MW, with the deloading resulting in the desired power production of 707.4MW, both of which resulting in the wind turbine rotational speed 1.2p.u. For all simulations in the report, the wind turbines are operated with a deloading pitch of 5 degrees giving the desired power reserve of approximately 12.5%.

3.2.4 The design and functionality of the frequency service controls

The DFIG wind turbine template in DIgSILENT is equipped with a power reduction ability at over-frequency but not complete frequency service controls. Therefore, new frequency controls are designed with synthetic inertia and primary control. The complete frequency service controls are shown in figure A.11 with the parameters in figure A.12.

Challenges arise when introducing the synthetic inertia derivator into the control system. The parameters of the Proportional Integral (PI) regulators in the power- and current controllers have to be adjusted to be compatible with the derivator. Simulations show that a sensitive derivator is required to achieve an inertial contribution with a similar form as for a synchronous generator. Increasing the derivator sensitivity does, however, trigger controller instability towards the PI regulators. Having slow PI regulators, they are not able to realize the fast and extensive power from the synthetic inertia controller. Therefore, a compromise is made between the speed of the PI regulators and the synthetic inertia derivator giving the best overall performance.

Dynamical simulations are performed to illustrate the functionality of the frequency controls. In addition to the simulations in this section, complementary simulations are included in Appendix A.4. Firstly, the wind turbines' behavior to power mismatch without frequency controls is examined. A step increase in loading of 300MW is performed at bus 7. Figure 3.2 shows all generators' power response when generator 2 is wind power without frequency controls. A power response is obtained in the wind turbines despite the lack of designated controls. Some power oscillations are expected as the wind turbines are the closest generation unit to the load step, experiencing the most significant voltage drop from the event. A large induced current occurs in the stator as this is directly connected to the power system. The current and voltage magnitude response is shown in figure A.13. This response also corresponds to the power response from an inertialess synchronous generation in figure C.6. Therefore, the power response from the wind turbines without frequency controls is not inertial but an electrical response caused by a large induced current due to the steep load change. As the power change only occurs in the electrical machine and not in the reference values, the contribution is quickly counteracted. For faster controls, as in figure D.7, the duration of the power oscillation reduces. The size and form are dependent on the steepness of the load change and the load change's location, meaning the impedance between the load change and the wind turbines.

Specialized controls are designed to make the DFIG replicate the behavior of a synchronous generator. The frequency service is a combination of synthetic inertia and primary control. The controls are tested against multiple load changes to ensure robustness and accurate replication of a synchronous generator's response.

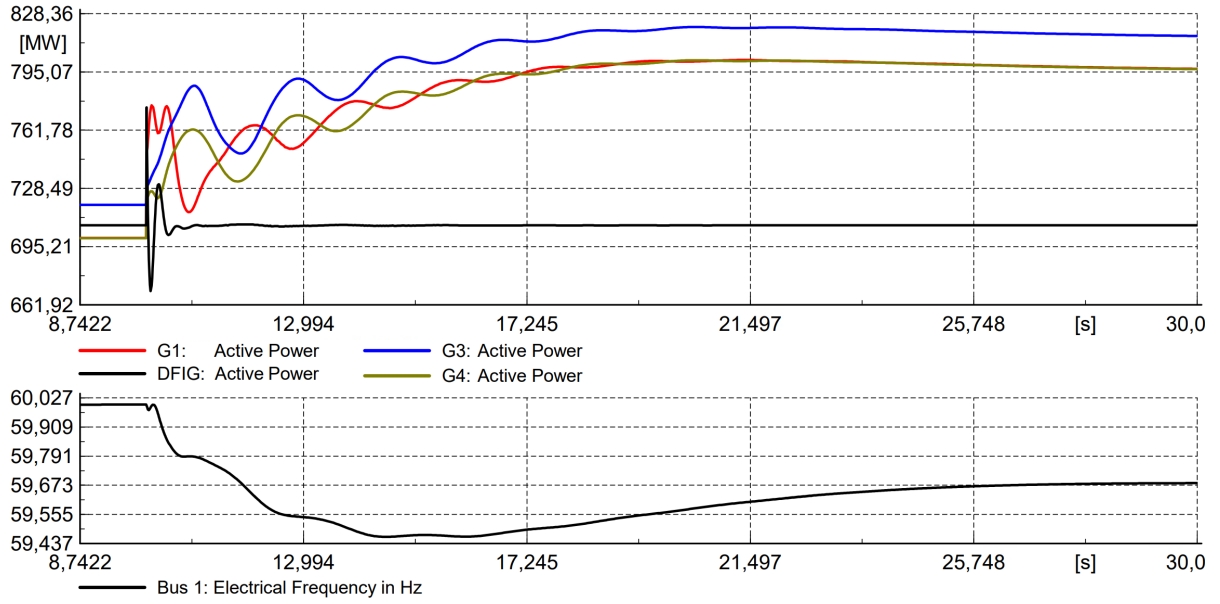


Figure 3.2: The active power- and frequency response for a load step increase of 300MW at $t=10$ s on bus 7. Generator 2 is wind power without frequency controls.

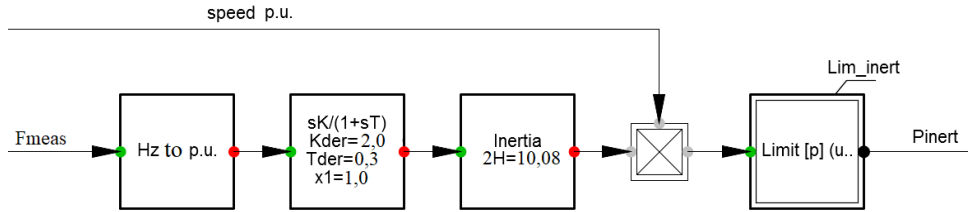


Figure 3.3: The DigSILENT synthetic inertia controller.

The synthetic inertia controller

The wind turbines should supply a short-term power as a changing frequency to participate in a slow rate of frequency change in the event of a power mismatch. As described in Section 2.3, this is realized by manipulating the power reference of the wind turbines with a contribution both proportional to the change in frequency and the inertia stored in the wind turbine rotation. The controls realizing this is shown in figure 3.3. This power is added to the power reference of the machine. A saturation block limits both the inertial- and primary control contribution. This is nominally at 0.3p.u. shown in figure A.12.

The control loop's functionality is illustrated in figure A.14, where a load step of 300MW occurs at bus 7. The synthetic inertia control is able to make the wind turbines rapidly release a significant additional amount of power, replicating the natural inertial response of a synchronous generator. The magnitude of the inertial contribution from the wind turbines is approximately the same as for the synchronous generators. The wind turbines are operated at a wind speed resulting in a turbine speed of 1.2p.u. Hence, the inertia of the wind turbines is $H = 5.04 * 1.2 = 6.05s$, close to the inertia of the synchronous generators. The inertial contribution is extracted from the kinetic energy of the wind turbine. Hence, at the expense of the rotor speed. The speed of the wind turbines and synchronous generator 1 is shown in

figure A.15, where the wind turbines suffer a similar deceleration as synchronous generator 1. A similar deceleration verifies the size of the inertial contribution produced by the synthetic inertia controls. A too-large deceleration would indicate a too large inertial contribution, not in accordance with the wind turbine's inertia.

The oscillations in the wind turbine speed are caused by the mechanical mode in the two-mass shaft model, analyzed in section 5.1.4. As the rotor is decelerated, the speed of the turbine differs from the optimal speed given by the MPPT. Therefore, to accelerate the machine, the power controller reduce the power output after the inertial response, causing an adverse effect on the primary control. A simple relation is constructed between the inertial contribution and the pitch angle to minimize this effect, further elaborated in Appendix A.4. However, the inertial response is much faster than the mechanical power increase, and reduced power output occurs regardless. This pitch-based power increase is active for the simulation in figure A.14.

Compared to the base case in figure 3.2, the inertial controls do not significantly improve the nadir. Still, the contribution is able to reduce the steepness of the frequency change, and in doing so, delaying the occurrence of the nadir. The inertial response does not help to establish a new power equilibrium to aid the frequency convergence. For this purpose, primary contribution controls are designed. The wind turbines' electrical power response from the voltage drop and induced stator current occurs for all the presented dynamical simulations. This is not a characteristic for the wind turbines and also occurs when generator 2 is synchronous, shown in figure A.8. This is a characteristic for this specific load event, where the load is step is located at the bus closest to the generator 2 bus. However, the fast power decrease after the initial peak only occurs in the wind turbines and is a consequence of its control system working to counteract the induced current.

The primary controller

Primary control is a power change, typically lasting for several seconds, proportional to the frequency deviation to converge a changing frequency by establishing a power generation and -consumption equilibrium. As the power reference of the wind turbines is created based on its speed to achieve MPE, simple power reference modification is counteracted after some time. The long-term power change can not be extracted or absorbed by the turbine's kinetic energy but requires a mechanical power increase. For this purpose, the wind turbines are operated deloaded with adaptive pitch control.

The control is shown in figure 3.4. This can be considered as a pitch controller regulated with a proportional regulator based on the frequency deviation. By using a PI regulator, the pitch would be regulated until the frequency is restored to nominal, effectively replicating secondary control action. As the pitch angle has a nonlinear relation to the mechanical power extracted from the wind, a direct droop-based gain will not have the desired effect. A frequency deviation to pitch ratio is therefore designed to achieve the desired response, shown in figure A.12. The coefficient relating frequency deviation to pitch angle

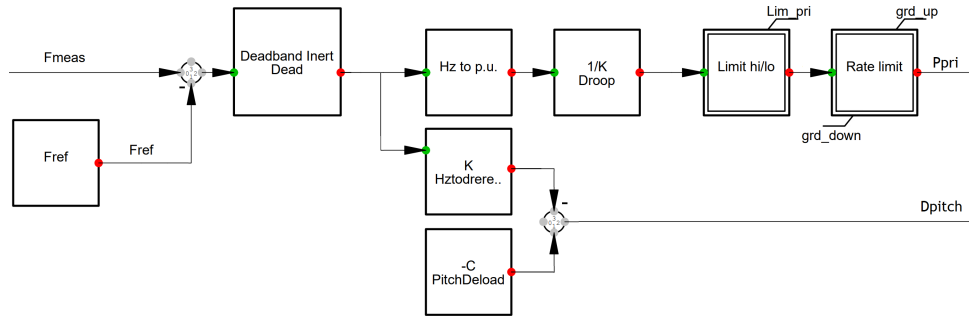


Figure 3.4: The DigSILENT primary controller.

is tuned to correspond with the synchronous generators' droop of 5% for a power mismatch of 300MW. Due to the nonlinearity, the coefficient is different for positive and negative frequency deviations, further described in Appendix A.4.

The obtained active power response from the wind turbines and the synchronous generators in the power system using this pitch control is shown in figure A.16. Only the pitch-based primary control is active. The droop of the synchronous generators defines the new frequency given by the equilibrium of the power balance. When the wind turbines contribute to primary control, the generators are not decelerated as much before realizing the power equilibrium. Hence, the frequency converges onto a frequency differing less from the nominal. As the pitch-based primary control ensures an increased power output before the nadir occurs, the nadir is elevated. However, as the synthetic inertia controls are not active, it occurs at approximately the same time as for the base case.

The purely pitch-based primary control accelerates the wind turbine, causing a new, increased power reference. However, the process is slow compared to the synchronous generators. Therefore, a control acting on the power reference simultaneously as the pitch regulation is implemented. The complete control is shown in figure 3.4. The contribution P_{pri} is added to the power reference. The active power response for this configuration is shown in figure A.17. The combination of power reference manipulation and pitch control causes a faster response, improved nadir, and a lower frequency deviation.

The power response with the complete frequency service controls is shown in figure 3.5, and with a longer timescale in figure A.18. The synthetic inertia controls ensure a delayed nadir. A greater improvement might be expected when activating the inertia controller. This is a consequence of the inertial response in synchronous generator 1, which is greatly reduced as the wind turbines contribute with inertial power. By comparing the frequency response from the wind turbines with the frequency response from synchronous generator 2 in figure A.8, the nadir actually improves. This should not be taken as a general indicator but rather a consequence of the sizeable deloading angle and the consequent rapid and significant primary control contribution from the wind turbine, eventually converging at the desired 5% droop. As the inertial response from the wind turbine, contrary to the synchronous generator response, is reduced after the electrical response from the induced current, a steeper RoCoF is obtained for the wind power.

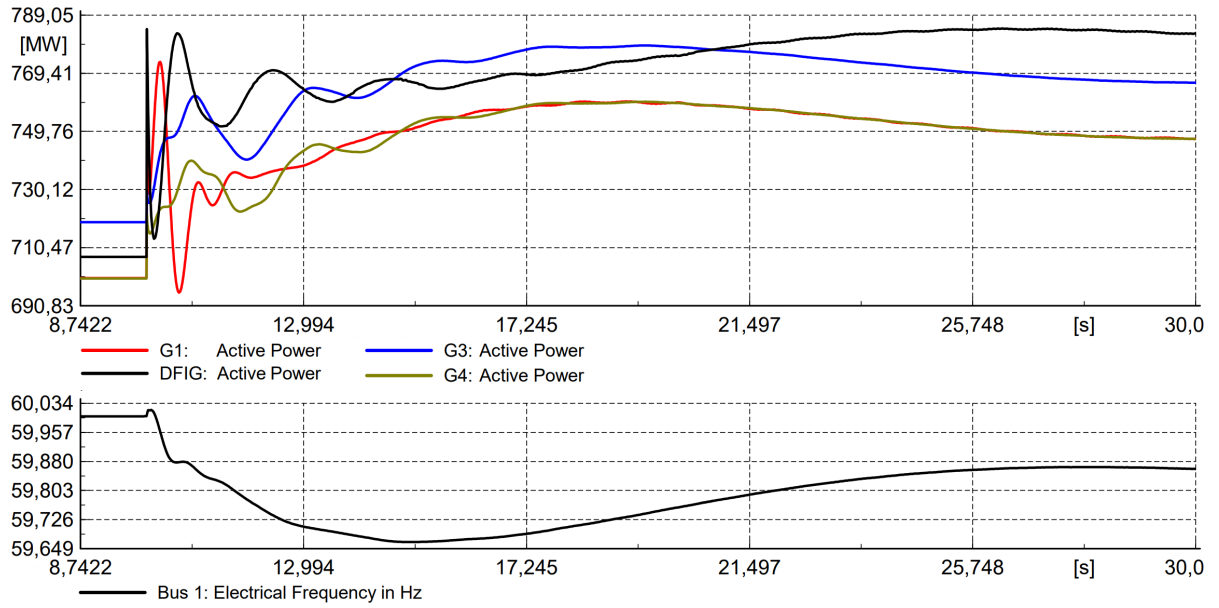


Figure 3.5: The active- power and frequency response for a load step increase of 300MW at $t=10$ s on bus 7. Generator 2 is wind power using the complete frequency service controls.

3.3 Model verification

3.3.1 Model design and implementation in Simulink

The DIgSILENT model is reconstructed in Matlab Simulink for verification. For this purpose, the Simulink template "Performance of Three PSS for Interarea Oscillations" is used [29]. This is a complete model of Kundur's two-area system, including the synchronous generators. Like the DIgSILENT model, all four synchronous generators are fully controlled, with identical control systems, including steam turbine governors, AVR, and PSSs. Three PSS configurations are provided in the model, where the PSS called " $\Delta\omega$ PSS Kundur" is used. This PSS ensures stable operation and corresponds with the PSS used in DIgSILENT. Area one of the Simulink model, including wind power, is shown in figure A.25. For the wind turbine, the template "Doubly-Fed Induction Generator Phasor Type" is used. In this model, the calculated contribution from the wind turbine is applied to the power system by controlled current sources. Aggregation is achieved by multiplying this current reference with the aggregation number.

As most of the DIgSILENT model results are eigenvalue development, the model is verified by eigenvalue comparison for a wind power penetration increase. The "Model Linearizer" application is used to linearize the Simulink model by choosing a system input and output. The state matrix is extracted from the linear system output and used in Matlab to calculate the eigenvalues. For the penetration increase, the eigenvalues from Simulink are calculated by choosing the aggregation number for the "Parameter Variation" function in the linearizer tool. It is also used to decrease the apparent power of synchronous generator 2, similar to the increase of the wind turbine and step-up transformer. Construction and synchronizing of the frequency controls across the two software are not considered. This is a time-consuming process and is suggested as part of the further work to validate the results further.

3.3.2 Model synchronization

Accurate synchronization of the models is required to achieve similar eigenvalue profiles between the software. The original parameters from Kundur's system are used for lines, synchronous generators, and loading. For an improved voltage profile, the capacitive shunt batteries in the Simulink template are increased with 187MVar. This is replicated in the DIgSILENT model. Further, a great effort is put into synchronizing the control system of the synchronous generators. In the construction phase of the DIgSILENT model, a thorough library search was performed to find a steam turbine governor, AVR, and PSS to match the narrow selection in Simulink.

The electrical values of the wind turbine in Simulink are replicated in DIgSILENT and presented in the section above. However, the step-up transformer in DIgSILENT is replicated in Simulink. The control structure of the DFIG in DIgSILENT and Simulink has multiple fundamental differences, challenging the synchronization. Therefore, direct replication of the PI regulator parameters is not possible. Instead, numerous simulations are performed, considering the eigenvalues and the dynamic performance of the wind turbines to fine-tune the synchronization of the wind turbines.

3.3.3 Modeling differences

For the control system of the synchronous generators, quite similar models are identified across the software. However, the control system modeling in the DFIG wind turbine templates is different, making the synchronization difficult. For instance, the speed regulation. In Simulink, the power reference is calculated based on the generator speed and the optimal power coefficient. For a generator speed lower than the optimal value, the electrical power is lower than the mechanical power, and the generator is accelerated onto the optimum [1]. In DIgSILENT, there is a designated PI regulated speed controller, constructing the power reference based on the speed deviation to the speed given by the MPPT.

The Simulink model includes a complete model of the VSC, including the DC-link voltage. This is not considered in DIgSILENT, assuming a constant DC-link voltage and optimal PE converter operation. The shaft connecting the wind turbine blades to the generator is in DIgSILENT modeled as two masses, connected by a spring. In Simulink, the mechanical power from the turbine is applied directly to the machine and does not consider the possibility of shaft oscillations.

3.3.4 Eigenvalue correspondence

This section presents the eigenvalue correspondence between the two software. The results considered for the validation do, naturally, represent essential results for the thesis. The focus in this section is the correspondence between the software to validate the DIgSILENT modeling. The interpretation of the eigenvalue development itself is analyzed in chapter 4 and 5.

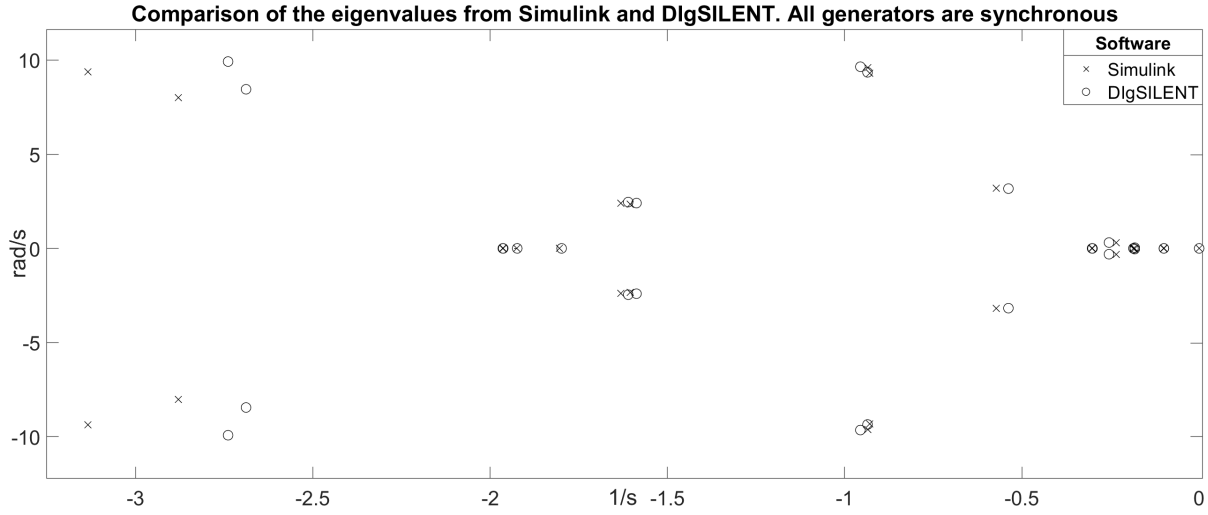


Figure 3.6: The eigenvalues from both Simulink and DIgSILENT for a purely synchronous generation.

The eigenvalue profile of the power system operated purely with synchronous power for both software is shown in figure 3.6. The results show a good correspondence between the software. The four pairs of oscillatory modes with the highest damping are related to the AVRs and are not focused in the thesis. The result shows that, in particular, the local modes correspond well, but also the inter-area modes. These are the modes of focus in the thesis and, therefore, the modes of focus in the synchronization. Their observability towards the generator speed states is examined to further investigate the dominant mode's correspondence between the software. The observability in Simulink is shown in figure A.29 and in figure B.1 for DIgSILENT. The result shows that the observability of the dominant modes in the generator speeds is near identical between the software, strengthening the base network's modeling validity.

The power system's impact from replacing synchronous generator 2 with wind power is considered to analyze the validity of the wind power modeling. A high correspondence is obtained shown in figure A.26, where the differences are similar as for the case of pure synchronous generation. In the thesis, several sensitivity analyses are analyzed for a variety of wind power scenarios. The eigenvalue development for an increasing wind power penetration is therefore considered. The development of the eigenvalues is shown in figure A.27. As the dominant eigenvalues are of interest, figure 3.7, 3.8, and 3.9 shows the development of the inter-area- and local modes one and two respectively. The development trends between the software are very similar. The initial and the final deviation are similar, strengthening the wind power modeling. The largest deviation is obtained in the path of local mode one, where DIgSILENT indicates more of a circular movement. The deviation between the initial and final values also differs most for this mode. In section 4.4.1, it is shown that the mode referred to as the local mode in area one in this section initially is the local mode in area two and opposite.

From figure A.27, Simulink has an oscillatory mode of about $-1.6 \pm 15i$, which does not exist in DIgSILENT. A linear analysis shows that this mode is linked to the dynamics of the DC-link voltage. The figure also shows that DIgSILENT has a mode of about $-0.2 \pm 7i$, not existing in Simulink. This mode is analyzed in section 5.1.4 and is a mechanical mode linked to the shaft. The later analysis in the thesis shows that one of the small modes becomes critical for several sensitivity analyses performed with the frequency controls. Therefore, the small mode development is considered between the software, shown in figure A.28. The development of the two best damped small oscillatory modes corresponds between the software, but the mode that is later referred to as the critical mode only exists in the DIgSILENT. This mode is analyzed in section 5.2.6, shown to be linked to the speed controller and speed variation of the shaft, both of which are not included in the Simulink model.

The results show that the development trends of the dominant eigenvalues correspond well between the software. The slight numerical deviation is mainly caused by the deviation from the synchronous generation and could probably be improved by further fine-tuning the synchronization. The great similarities between the development trends in the dominant modes for the penetration increase of wind power validate the wind power modeling. However, three modes not corresponding between the software are identified, all linked to modeling differences. In particular, the DC-link voltage, speed controller, and the turbine shaft.

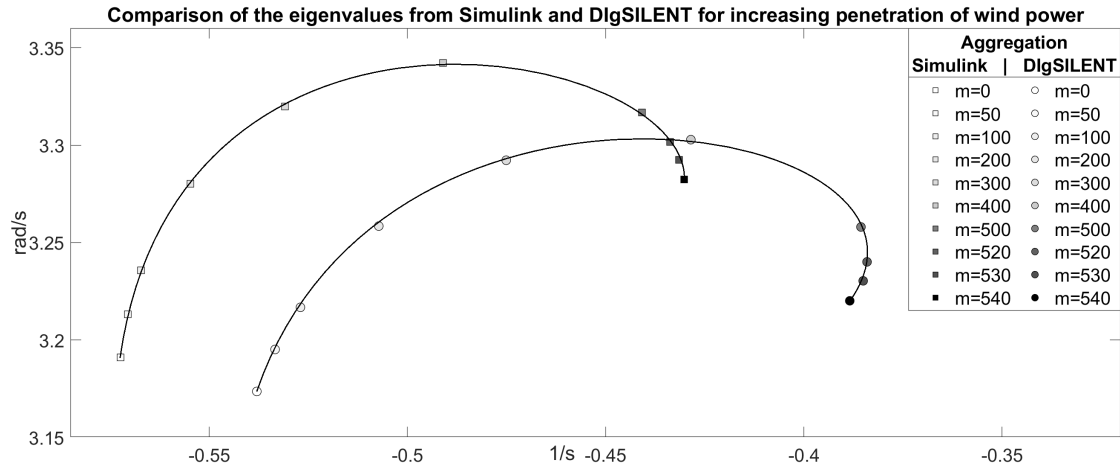


Figure 3.7: The inter-area mode from DIgSILENT and Simulink for increasing wind power penetration. No frequency controls are active.

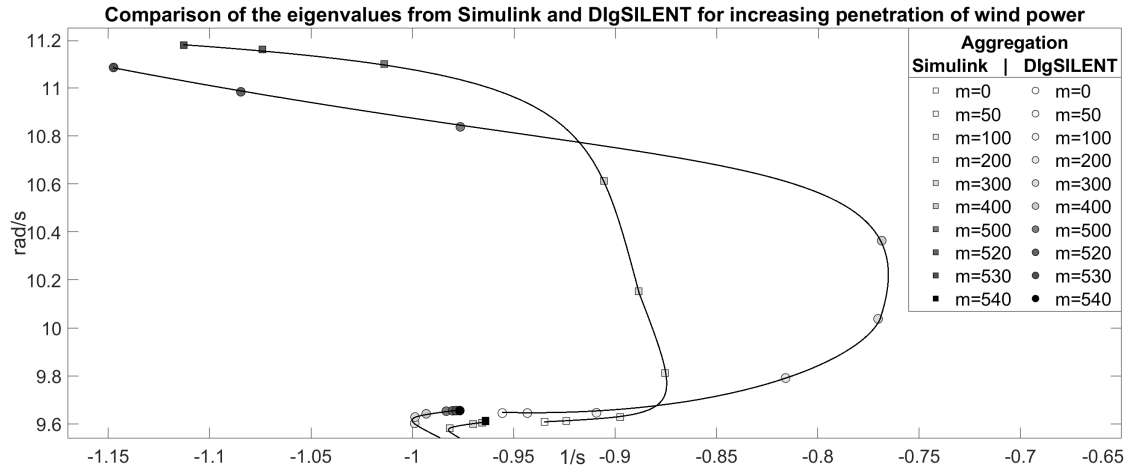


Figure 3.8: The local mode in area one from DIgSILENT and Simulink for increasing wind power penetration. No frequency controls are active.

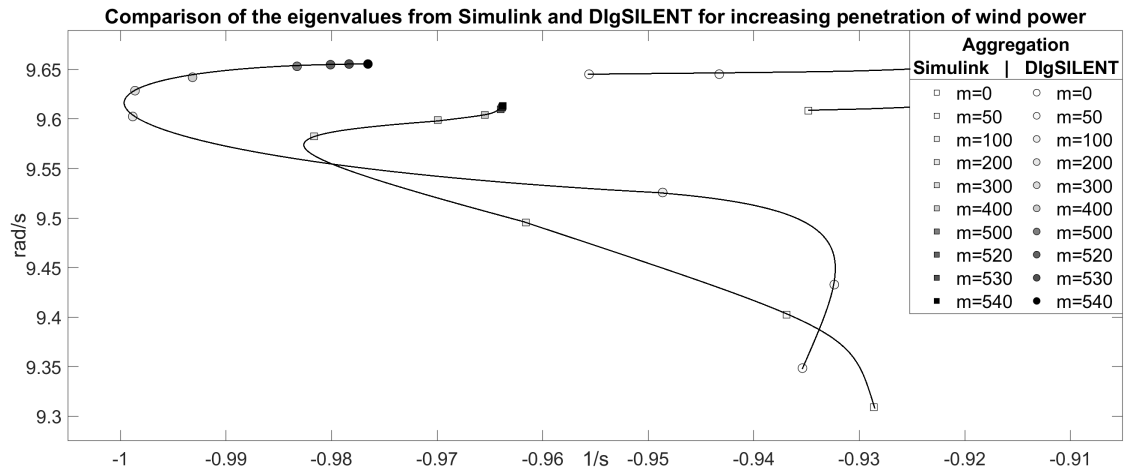


Figure 3.9: The local mode in area two from DIgSILENT and Simulink for increasing wind power penetration. No frequency controls are active.

Chapter 4

Small-signal stability analysis of synchronous generation

This chapter presents the analysis of the small-signal stability of Kundur's two-area system operated with synchronous generation. The purpose is to get familiar with the eigenvalue profile and the sensitivity of the eigenvalues towards the generation controls, system parameters, and configuration. The results in the chapter serve as a base of comparison and expectation for the later wind power implementation.

4.1 Introduction

This chapter presents a small-signal stability analysis of Kundur's two-area system operated with purely synchronous generation. The purpose is to get familiar with how the control system, generation, and grid configurations affect the system stability. The results also serve as a base of comparison and expectation for the later wind power implementation. Multiple sensitivity analyses are performed through parameter sweeps on control- and machine parameters to analyze their impact on the system stability. The control system parameters are examined before a thorough analysis of the power system inertia. A great concern with wind power implementation is the decreasing power system inertia. Therefore, several cases are analyzed within the topic of generator inertia. Lastly, the system loading and inter-tie line length is examined. This is also analyzed for wind power to explore possible differences in the stability impact. In this chapter, the main mean of result presentation is tables. This gives a tidy presentation of eigenvalue movement and includes the numerical values, also for the damping ratios. A visual representation is chosen for the later analysis of wind power implementation, where more of a trend development is of focus. As this chapter focus on synchronous generation, the synchronous generators are commonly referred to as generators.

When referring to the eigenvalues, three quantities are used. The imaginary part, describing the oscillation frequency of the contribution, the real part, referred to as the damping, describing the duration of the contribution, and the damping ratio, giving the rate of decay. The damping ratio is referred to as improved or enhanced if either the imaginary part decreases or the real part increases. The real part, or the damping of the eigenvalues, is for a stable system negative. Therefore, increased damping refers to an increased absolute value of the real part, meaning a larger negative value.

The focus of the linearization is the three dominant modes. The complete linearization of the system is shown in Appendix B. All eigenvalues are shown in Appendix B.1, and the eigenvectors connecting the system states to the dominant modes are shown in Appendix B.3. As described in Section 3.2.2, all generators are fully controlled, equipped with steam turbine governors, and AVRs with PSSs. The control structures and the belonging parameters are shown in Appendix A.3. The most important results from the stability analysis are included in this chapter. In Appendix C, extended results are included. These are referred to consecutively when relevant. The appendix also includes a simple mathematical description of the system eigenvalues for an uncontrolled system, only based on generator speed and -angle. The formulas give a simple description of important parameters for the dominant modes. A final expression is developed to justify the development of the inter-area mode for varying inertia. For the complex power system with several controlled generation units, the order of the system makes simple analytical calculations difficult.

Table 4.1: The inter-area- and local modes for varying turbine governor gain.

Gain factor	inter-area mode		Local mode, area 1		Local mode, area 2	
	Eigenvalue	zeta [%]	Eigenvalue	zeta [%]	Eigenvalue	zeta [%]
0.1	$-0.515 \pm 3.098i$	16.4	$-0.955 \pm 9.339i$	10.17	$-0.975 \pm 9.636i$	10.07
1	$-0.538 \pm 3.174i$	16.71	$-0.936 \pm 9.349i$	9.96	$-0.956 \pm 9.645i$	9.86
4	$-0.594 \pm 3.423i$	17.10	$-0.873 \pm 9.381i$	9.27	$-0.891 \pm 9.678i$	9.168
10	$-0.640 \pm 3.890i$	16.23	$-0.750 \pm 9.447i$	7.91	$-0.765 \pm 9.744i$	7.83
20	$-0.631 \pm 4.556i$	13.72	$-0.552 \pm 9.561i$	5.76	$-0.564 \pm 9.858i$	5.71

4.2 The turbine-governor control system

The turbine governor is the controller responsible for regulating the mechanical power of the generators [15]. A sensitivity analysis of the governor gain is performed to analyze the governor's impact on the small-signal stability. For the governor used in DigSILENT, increasing the gain is effectively the same as decreasing the droop, as the gain is only applied to the speed difference, shown in figure A.2.

The result from the sensitivity analysis are shown in table 4.1, where the gain factor is multiplied with the base gain of 20, from figure A.3. This gain equals the droop 5%. The result shows how the two local modes become more oscillatory as the gain increase, as the damping ratios decrease. The inter-area mode performs a circular motion, where increasing gain firstly increasing the damping before reducing it. The result shows that a fast or a sensitive controller is achieved at the expense of system stability. All three dominant modes become unstable at a gain factor of about 75. A dynamic simulation is performed to illustrate how the gain or the droop affects the power system dynamics for a power mismatch.

Figure C.1 and C.2 shows the active power response from the generators, and the system frequency for a load increase of 31% = 300MW. In figure C.1, the governor is operated at the nominal gain of 20, meaning a droop of 5%, while in figure C.2, the gain is 80, meaning a droop of 1.25%. A more violent response is obtained for the increased gain. The enlarged power contribution causes an elevated nadir, a greater overshoot, and an improved steady-state frequency. The decreased droop causes the generators to deliver a greater power increase per frequency decrease, resulting in a lower frequency deviation at frequency convergence. The result also shows that the inertial response is unaffected by the gain change. The inertial contribution from synchronous generators is a physical resistance to a changing rotational speed and not a matter of control. From table 4.1, a small impact is obtained in the system stability for the gain factor of 4, while the dynamics performance is greatly impacted.

Table 4.2: The inter-area- and local modes for varying AVR gain.

	inter-area mode		Local mode, area 1		Local mode, area 2	
Gain factor	Eigenvalue	zeta [%]	Eigenvalue	zeta [%]	Eigenvalue	zeta [%]
0.25	$-0.823 \pm 3.394i$	23.57	$-0.940 \pm 7.713i$	12.10	$-0.952 \pm 7.994i$	11.83
0.5	$-0.629 \pm 3.204i$	19.26	$-1.029 \pm 8.481i$	12.04	$-1.040 \pm 8.777i$	11.77
1	$-0.538 \pm 3.174i$	16.71	$-0.936 \pm 9.349i$	9.96	$-0.956 \pm 9.645i$	9.86
5	$-0.470 \pm 3.169i$	14.67	$-0.503 \pm 10.628i$	4.73	$-0.558 \pm 10.893i$	5.12

Table 4.3: The inter-area- and local modes for varying PSS gain.

	inter-area mode		Local mode, area 1		Local mode, area 2	
Gain factor	Eigenvalue	zeta [%]	Eigenvalue	zeta [%]	Eigenvalue	zeta [%]
0	$0.178 \pm 4.075i$	-4.36	$-0.349 \pm 6.986i$	4.99	$-0.376 \pm 7.182i$	5.23
0.5	$-0.325 \pm 3.655i$	8.86	$-0.809 \pm 8.294i$	9.71	$-0.824 \pm 8.547i$	9.60
1	$-0.538 \pm 3.174i$	16.71	$-0.936 \pm 9.349i$	9.96	$-0.956 \pm 9.645i$	9.86
2	$-0.577 \pm 2.518i$	22.34	$-1.032 \pm 10.997i$	9.34	$-1.059 \pm 11.376i$	9.27
4	$-0.459 \pm 1.898i$	23.51	$-1.155 \pm 13.531i$	8.51	$-1.193 \pm 14.036i$	8.47

4.3 The AVR and PSS

The AVR is the controller responsible for voltage control through reactive power regulation. The PSS is a control loop in the AVR, providing a damping component [33]. Sensitivity analyses are performed on the controllers to analyze how they affect the power system stability. The relation between the dominant eigenvalues and the AVR gain is shown in table 4.2. The gain factor is multiplied with the base gain of 200, from figure A.5. The result shows how the local modes' damping is decreased as the gain increase. From the local modes' damping, the modes perform a circular movement around the gain factor of 0.5. As the gain increases, the damping ratio reduces. The inter-area mode damping is also highly affected by the AVR gain. The movement is dominated by the real part, reducing the inter-area mode damping ratio for a faster AVR. The result shows that the dominant eigenvalues are sensitive towards the AVR gain.

From Appendix B.3, the PSSs hold great control over the dominant modes. Particularly the state variable x_1 , related to the high pass filter shown in figure A.6. The gain sweep of the PSS is shown in table 4.3. The gain factor is multiplied with the base gain of 12, from figure A.7. The result shows how the local modes' damping increase as the gain factor increase. The inter-area mode damping is highly affected by the PSS gain, where the damping is dependent on the PSS to ensure a negative real part, and hence, a stable system. As the gain factor exceeds 2, the damping ratio of the local modes starts to decrease due to the increasing imaginary part, and the inter-area mode damping starts to decrease, despite the continuously increasing damping ratio.

Table 4.4: The inter-area- and local modes for varying inertia of all four generators.

	inter-area mode		Local mode, area 1		Local mode, area 2	
Inertia factor	Eigenvalue	zeta [%]	Eigenvalue	zeta [%]	Eigenvalue	zeta [%]
0.25	$-1.571 \pm 3.859i$	37.71	$-1.256 \pm 17.918i$	6.99	$-1.289 \pm 18.571i$	6.92
0.5	$-1.083 \pm 3.681i$	28.23	$-0.962 \pm 12.774i$	7.51	$-0.986 \pm 13.224i$	7.44
1	$-0.538 \pm 3.174i$	16.71	$-0.936 \pm 9.349i$	9.96	$-0.956 \pm 9.645i$	9.86
2	$-0.216 \pm 2.481i$	8.67	$-1.266 \pm 7.083i$	17.59	$-1.240 \pm 7.235i$	16.89
4	$-0.083 \pm 1.849i$	4.48	$-1.904 \pm 5.730i$	31.53	$-1.815 \pm 5.756i$	30.07

Table 4.5: The inter-area- and local modes for varying inertia in the generators in area one.

	inter-area mode		Local mode, area 1		Local mode, area 2	
Inertia factor	Eigenvalue	zeta [%]	Eigenvalue	zeta [%]	Eigenvalue	zeta [%]
0.25	$-1.012 \pm 3.664i$	26.62	$-1.007 \pm 9.764i$	10.26	$-1.253 \pm 17.912i$	6.98
0.5	$-0.7445 \pm 3.482i$	20.91	$-0.938 \pm 9.682i$	9.64	$-0.955 \pm 12.770i$	7.46
1	$-0.538 \pm 3.174i$	16.71	$-0.936 \pm 9.349i$	9.96	$-0.956 \pm 9.645i$	9.86
2	$-0.453 \pm 2.864i$	15.62	$-1.265 \pm 7.09i$	17.56	$-0.980 \pm 9.638i$	10.12
4	$-0.454 \pm 2.626i$	17.04	$-1.899 \pm 5.728i$	31.47	$-0.987 \pm 9.637i$	10.19

4.4 The synchronous generator inertia

The system inertia can be considered as the breaks of changes in the system and is a critical system characteristic of remaining stable during disturbances. The eigenvalues are calculated for multiple inertias to analyze how the system inertia impacts the power system stability. The inertia factor is multiplied with the base inertias of 6.5s and 6.175s, from figure A.1. The inertia sweep of all four generators is shown in table 4.4. The two local modes move in vary similar paths, increasing the damping ratio as the inertia increases. However, inter-area mode damping highly reduces as the system inertia increase. This can be mathematical justified by the simple expression deduced in Appendix C.1, showing that an inertia increase in either area reduces the inter-area mode damping. The result shows a strong connection between all three dominant eigenvalues and the generator inertias. When the system inertia decrease, the inter-area mode damping ratio increase, and the local mode damping ratio decrease, becoming dominant.

Only the inertia on area one is considered to analyze how the difference in the area inertias affects the eigenvalues. The result in table 4.5 shows how the local mode in area one, for increasing inertia, follows the same path as for increasing inertia of all generator. On the other hand, when the inertia in area one decreases, the local mode in area one is little affected. However, the local mode in area two is affected, following the path of the local mode in area one for the decreasing inertia of all generators. This indicates that the connection between the generator groups and the belonging local mode is affected as the inertia in area one decreases below the inertia in area two, requiring further analysis.

4.4.1 The local modes' connection to the generators for changing inertia

For the later analysis of wind power, synchronous generator 2 is replaced by DFIG wind power. Therefore, a thorough analysis of inertia decrease in area one is considered. When increasing the inertia in area one, the local mode's damping ratio improves, and the local mode in area two is little affected. However, when decreasing the inertia in area one, the local mode in area two is the mode affected. By analyzing the local modes in detail, the local modes do not cross each other for decreasing inertia in area one but instead perform a sort of exchange between the areas. A possible explanation is the disturbance of the inertia balance, where area one no longer represents the largest source of stored kinetic energy.

The complete path of the local modes for the inertia sweep of the generators in area one between the factors 0.25-2 is shown in figure 4.1. The factors are multiplied with the nominal inertia of 6.5s from figure A.1. When zooming into the part where the inertia of the two areas cross, shown in figure 4.2, the local mode in area one is the mode affected by increasing inertia, and the local mode in area two is the mode affected by decreasing inertia. The local modes can be characterized based on their participation factors. The concept of participation factors is described in Section 2.4.3. The participation factors, linking the local modes to the generator speed states, as a function of the generator inertia in area one is shown in figure 4.3 and 4.4. The size of the participation factors is relative, meaning that the state with the highest participation factor towards the mode has the size 1.

The participation factors show that as the inertia of the generators in area one reaches the inertia $H=6.11s$, the connection strength highly change. As the inertia in area one decreases, and the local mode in area two starts to move, the connection to the generators in area two weakens. At the same time, the generators in area one gain a stronger connection. Therefore, as the inertia in area one decreases towards the inertia in area two, area two's local mode gradually becomes the local mode in area one and opposite. When the inertia of the generators in area one is at 6.11s, the participation factors show that the local modes are as dominant in both areas.

The path of the local modes can for the inertia sweep be further analyzed, bearing in mind the changing connection strength between the generators and the local modes. The inertia of 6.11s is marked in figure 4.2. The blue line shows the mode initially representing the local mode in area two. After point 6.11s, following the direction of the arrow, the generators in area one becomes dominant. This is visible in the movement path, where the path highly changes and starts to replicate the expected development of the mode from the inertia sweep of all generators in table 4.4. From the complete movement of the eigenvalues in figure 4.1, the local mode in area one performs a circular movement, starting with inertia above nominal as the green line and finish with inertia below nominal, as the blue line. This path also corresponds with the path of the local mode in area one for the inertia sweep of all generators table 4.4. This further supports the hypothesis of motivation from the changed inertia balance, as area one has the highest inertia for all points in table 4.4. It is expected to obtain a similar behavior of the local modes when generator 2 is replaced by wind power, as DFIGs do not contribute to physical inertia.

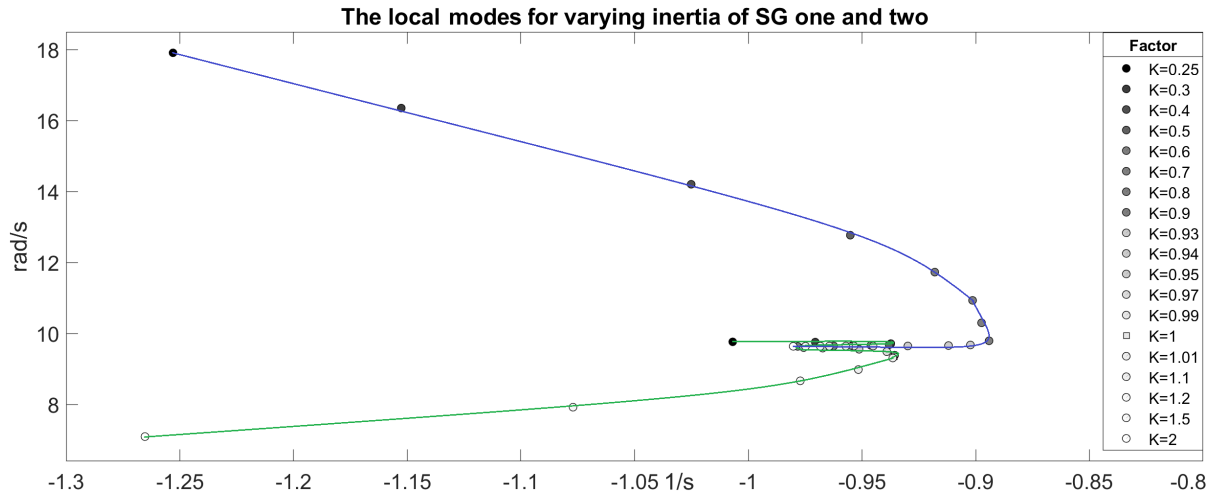


Figure 4.1: The local modes for varying inertia in area one. The green line is the path of the mode initially representing the local mode in area one. Likewise, the blue line is the local mode in area two. The square is for nominal inertia.

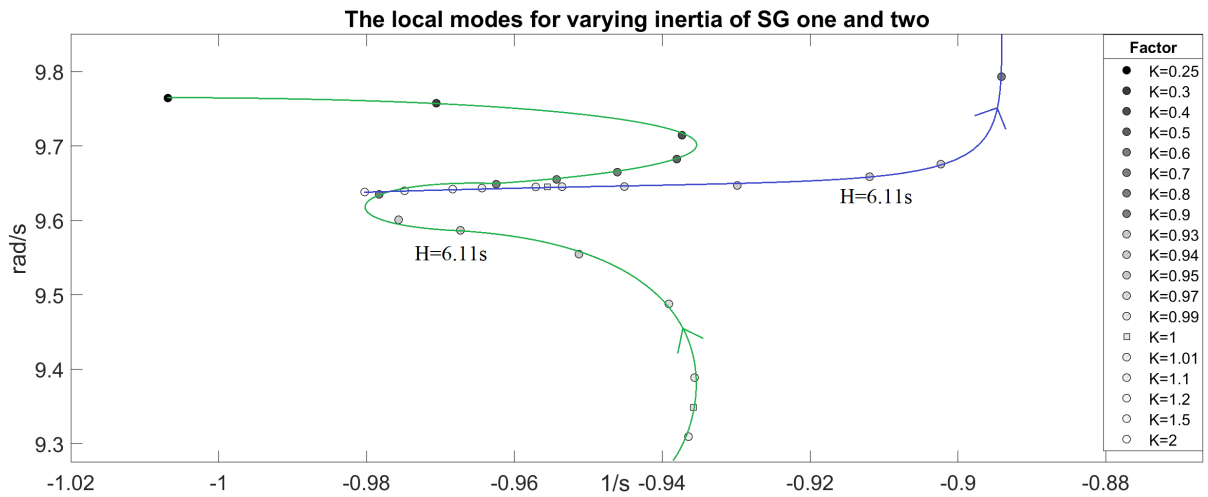


Figure 4.2: Zoomed edition of the local modes for varying inertia in area one. The green line is the path of the mode initially representing the local mode in area one. Likewise, the blue line is the local mode in area two. The square is for nominal inertia. The arrows point in the direction of decreasing inertia.

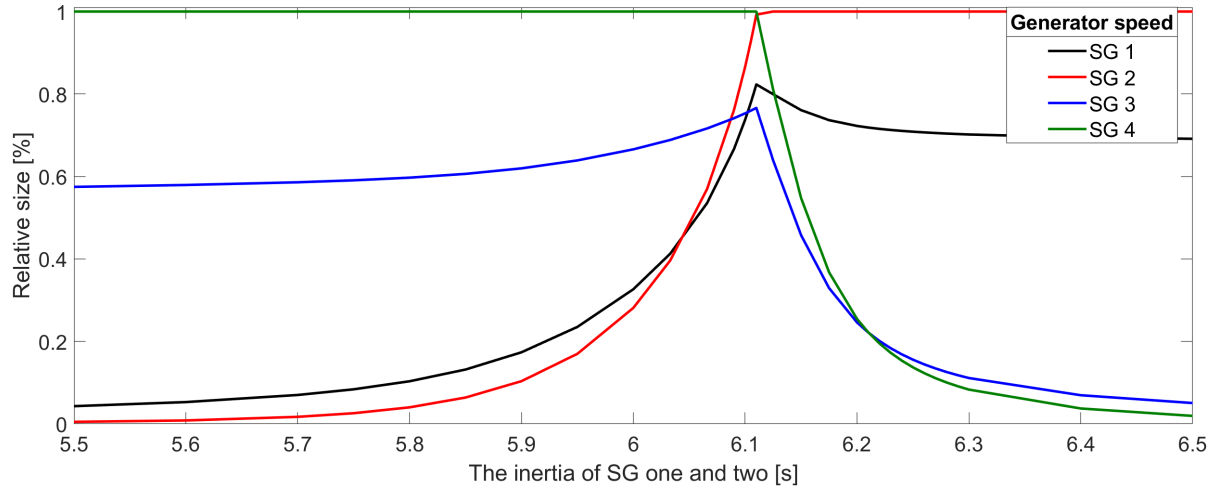


Figure 4.3: The participation factors connecting the generator speed states to the mode initially representing the local mode in area one.

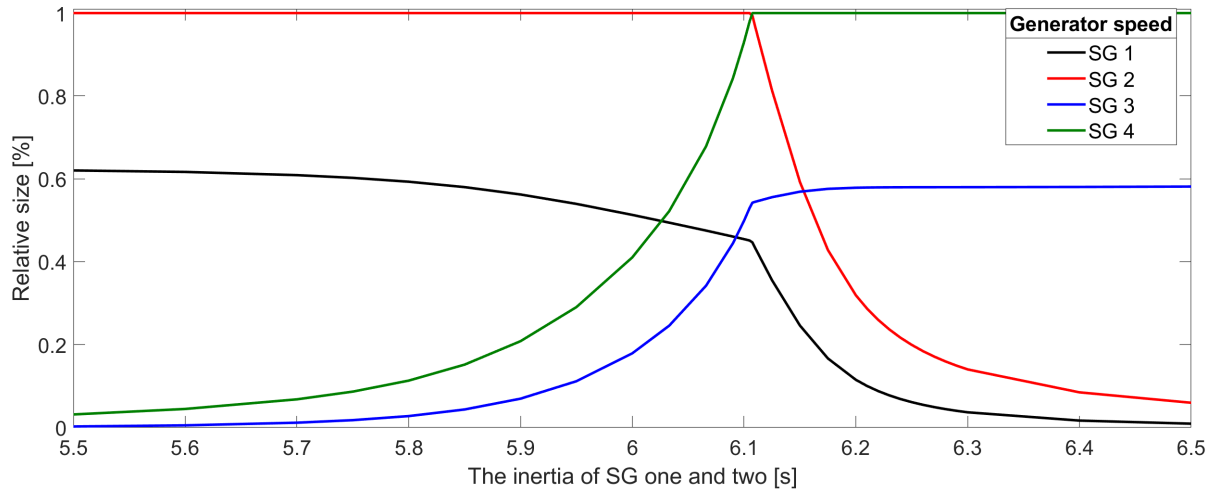


Figure 4.4: The participation factors connecting the generator speed states to the mode initially representing the local mode in area two.

4.4.2 The inertia's effect on system dynamics

System inertia is essential to counteract frequency changes in the power system and to slow down system oscillations. The generator inertia is stored kinetic energy in the generator and turbine rotation. Energy will either be released or absorbed from the kinetic energy in the rotation, working to counteracting any speed oscillation. A small disturbance is considered for a selection of generator inertias, visualizing the dominant eigenvalues in the generator speeds to investigate the importance of the system inertia. The voltage reference of generator 1 is increased to 1.05 at $t=0$ s and back to 1.00 at $t=0.1$ s. The three generator inertias analyzed are half, nominal, and double. The inertia is changed proportionally on all generators. The result is, therefore, a dynamic simulation of the linearization in table 4.4.

The result is shown in figure 4.5, 4.6, and 4.7. Only the generator speeds in area one are included. Hence, the local mode in area one and the inter-area mode is dominant, described by the observability shown in figure B.1. For half inertia, the mode nominally local in area two dominates the high-frequency oscillations as this becomes the local mode in area one, described in the section above. As the inertia decrease, the generator speed oscillation's frequency and amplitude increase. The oscillation frequency corresponds with the imaginary part of the eigenvalues in table 4.4. The table shows how the damping of the inter-area mode decrease as the inertia increase. This is also visible in the dynamic simulations, where the largest inertia causes the longest duration of low-frequency oscillations.

A clear distinction is visible between the contribution from the local- and inter-area mode. In particular, for generator 1 with the smallest inertia, the fast oscillations from the local mode oscillate around the slow oscillations from the inter-area mode. The local mode makes the two generators in area one oscillate agings each other, visible by comparing the fast oscillations from the two generator speeds. This can be mathematically explained by the observability of the local mode, shown in figure B.1, where the angle difference is about 180 degrees. As shown in the figure and described in Section 2.4.3, this is general; local modes make generators within an area oscillating against each other. The figure also shows that the inter-area mode makes the generators in one area oscillate together against the generators in the other.

The speed oscillations are composed of several components. The theoretical oscillation in the speed of generator 1 is calculated to examine the components. The calculation is performed for the nominal inertia, corresponding to the linearization in Appendix B. The right eigenvector and the excitation coefficient describe the relation between the eigenvalues and the oscillations in the time domain, described in Section 2.4.3. For the theoretical calculation, the excitation coefficient is, for the three dominant modes, experimental replicated and put to zero for the remaining. Therefore, only the right eigenvector is used to describes the amplitude and phase shift of the contribution from the eigenvalues, shown in equation 4.1. As a consequence of the neglected excitation, two synchronizing coefficients are defined to synchronize the oscillations, effectively replicating the coefficient. The speed response of generator 1 from figure 4.6 is theoretically replicated by the equation using $K = 0.01$ and $\rho = 5.49$ s, shown in figure 4.8.

$$\Delta x(t) = |\phi| e^{\sigma(t-\rho)} \sin(\omega(t-\rho) - \angle\phi) * K \quad (4.1)$$

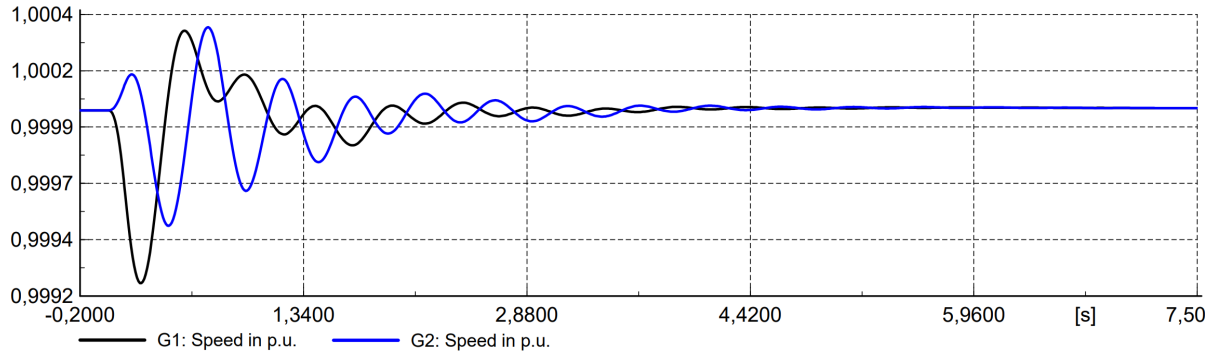


Figure 4.5: The speed of generators 1 and 2 for a step increase of voltage reference in generator 1, of 5% between $t=0-0.1$ s. The inertia of all generators is half their nominal values.

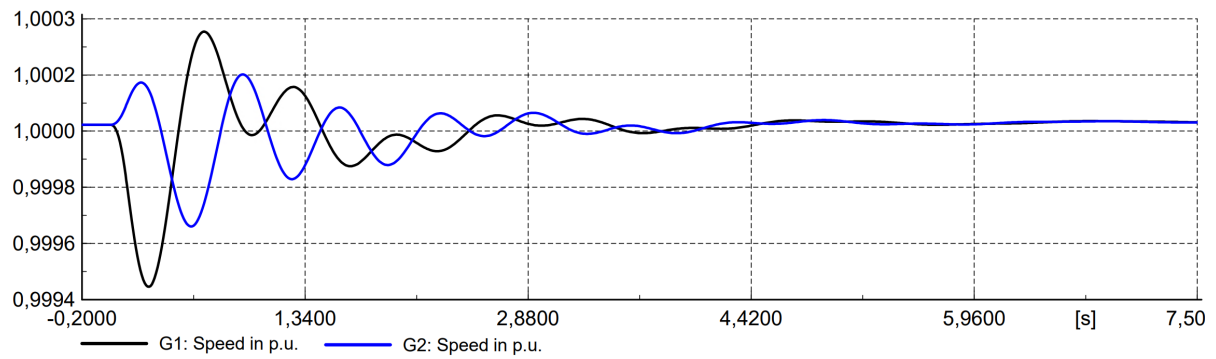


Figure 4.6: The speed of generators 1 and 2 for a step increase of voltage reference in generator 1, of 5% between $t=0-0.1$ s. The inertia of all generators is at their nominal values.

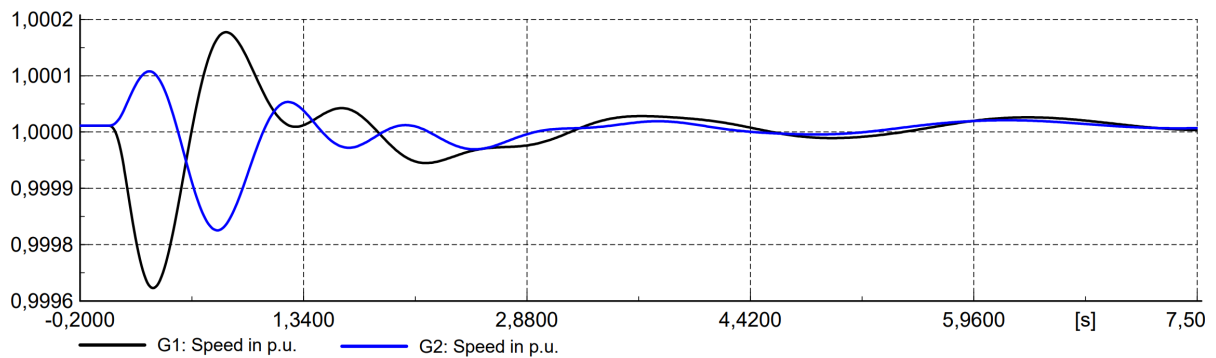


Figure 4.7: The speed of generators 1 and 2 for a step increase of voltage reference in generator 1, of 5% between $t=0-0.1$ s. The inertia of all generators is double their nominal values.

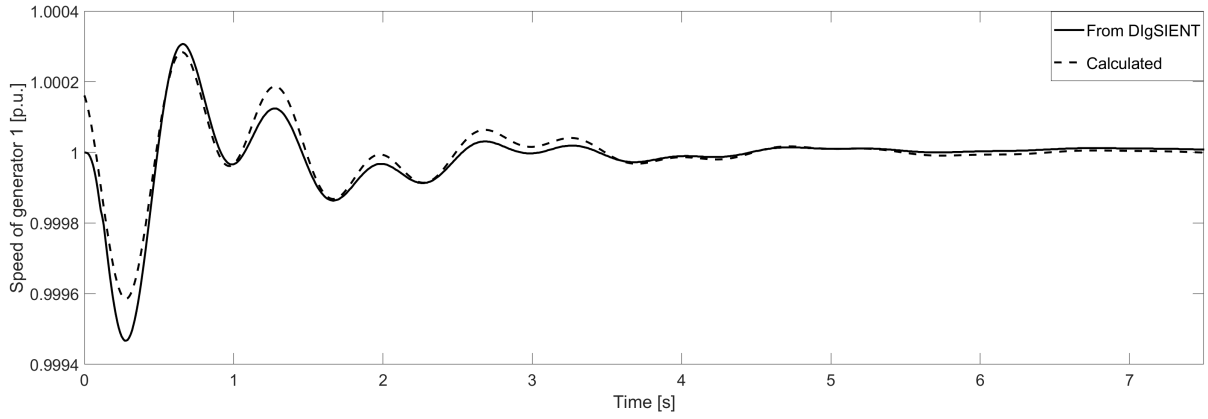


Figure 4.8: The simulated and theoretically calculated speed of generator 1 for a step increase of voltage reference in generator 1, of 5% between $t=0-0.1s$.

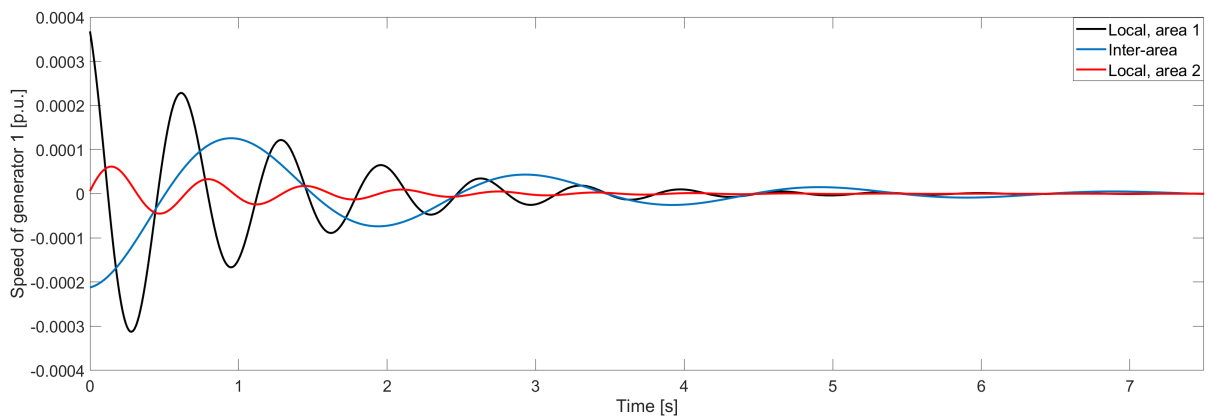


Figure 4.9: The three components of the theoretically calculated speed of generator 1 for a step increase of voltage reference in generator 1, of 5% between $t=0-0.1s$.

The correspondence between the simulated and calculated response is not of particular interest due to the simplified calculation. Only the inter-area- and local modes are included and are simplified to have equal event excitation. Nevertheless, similar oscillations confirm that these are the dominant modes in the generator oscillations after the small disturbance. This means that these are the eigenvalues with the greatest observability in the generator speeds, and are the eigenvalues excited by the disturbance. To analyze the contribution from the three dominant modes, figure 4.9 shows the individual contributions from the three modes. Their sum equals the calculated response in figure 4.8. The local mode in area one firstly dominant the oscillation but decays faster than the inter-area mode as the local mode's real part is larger. The inter-area mode has slower oscillations, causing the local mode to oscillate around its contribution, most visible at $t \approx 0.75$ s in figure 4.8. The contribution from the local mode in area two is small but visible.

4.4.3 The inertia and PSS of synchronous generator 2

The results confirm that system inertia is essential to limit the power system oscillations. Therefore, as generator 2 is to be replaced by wind power, having zero apparent inertia towards the system, larger power system oscillations are expected. Further analysis is performed to analyze the differences between a grid with decreasing system inertia and a grid with increasing wind power penetration. In addition to the impact on the eigenvalue profile, an inertia-less machine will naturally not contribute with inertial power. Figure C.6 shows the power response from the generators when generator 2 has approximately zero inertia and its consequent lack of inertial response. Some active power response is obtained by the high rate of change of voltage and induced current, further described in Section 3.2.4. However, the generator still contributes with primary control power, as the turbine governor action is unchanged.

When wind power replaces synchronous generation, both the system inertia and the power contribution from generation units equipped with the stability properties of the PSS are reduced. Therefore, a parameter sweep is performed to analyze the difference between increasing wind power penetration and decreasing generator inertia and PSS contribution. Both the inertia and PSS gain are decreased proportionally to replicate the increasing wind penetration shown in figure 4.10 and 4.11. A visual representation is chosen for a simple comparison of movement trends for the later wind power analysis.

Decreasing inertia in area one changes the connection between the local modes and the belonging generators, explained in detail in Section 4.4.1. Therefore, the mode of interest is the mode initially local in area two. The local mode movement is similar to the inertia sweep in area one, but when also decreasing the PSS gain, and only considering generator 2, a smother circular movement is obtained. The inter-area mode damping is shown to improve for decreasing inertia and PSS gain. From table 4.5, decreasing inertia improves the inter-area mode damping, and from table 4.3, a decreasing PSS gain reduce the inter-area mode damping. The parameter sweep in figure 4.11 show that the decreasing inertia effect dominates, and the inter-area mode damping increase for a decreasing factor. The mode that becomes the local mode in area two is little affected by the inertia and PSS gain decrease in generator 2.

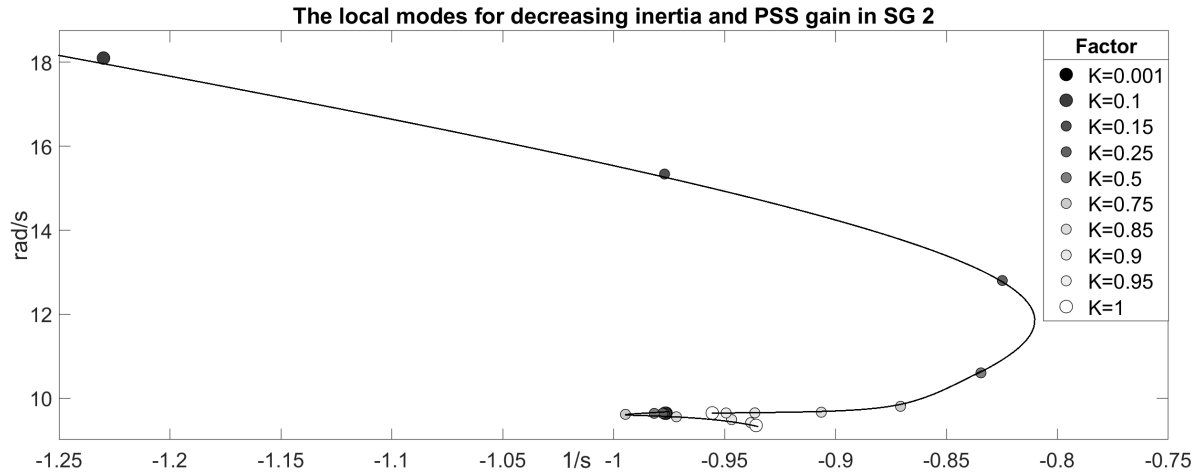


Figure 4.10: The local modes for decreasing inertia and PSS gain in generator 2.

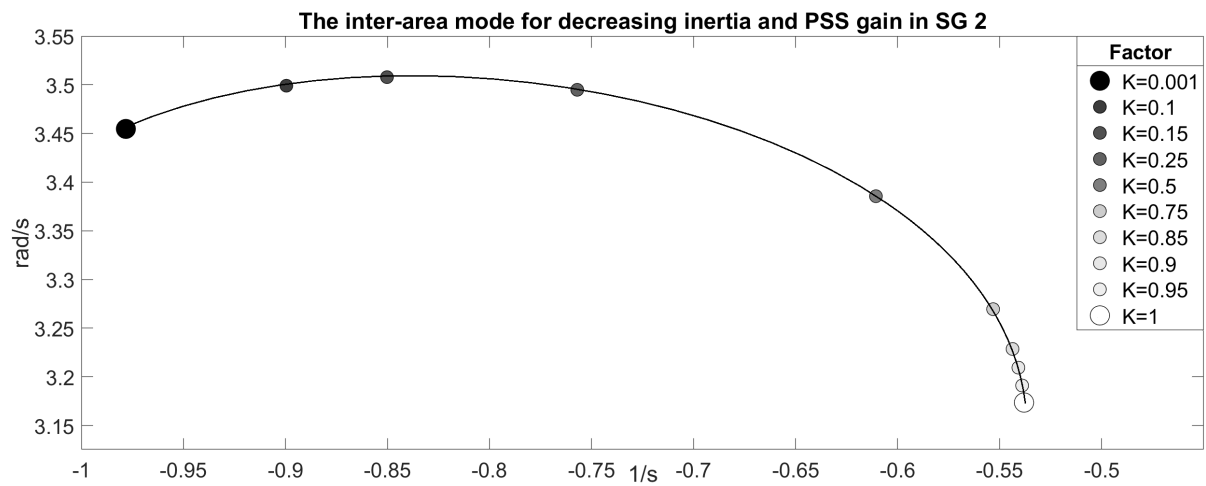


Figure 4.11: The inter-area mode for decreasing inertia and PSS gain in generator 2.

Table 4.6: The inter-area- and local modes for varying system loading.

	inter-area mode		Local mode, area 1		Local mode, area 2	
Loading factor	Eigenvalue	zeta [%]	Eigenvalue	zeta [%]	Eigenvalue	zeta [%]
0.5	$-0.9213 \pm 3.186i$	27.78	$-1.242 \pm 9.427i$	13.06	$-1.149 \pm 9.776i$	11.67
0.75	$-0.695 \pm 3.258i$	20.86	$-1.051 \pm 9.440i$	11.07	$-1.039 \pm 9.761i$	10.58
1	$-0.538 \pm 3.174i$	16.71	$-0.936 \pm 9.349i$	9.96	$-0.956 \pm 9.645i$	9.86
1.25	$-0.430 \pm 2.955i$	14.40	$-0.856 \pm 9.238i$	9.23	$-0.891 \pm 9.530i$	9.31
1.5	$-0.352 \pm 2.622i$	13.31	$-0.792 \pm 9.120i$	8.65	$-0.857 \pm 9.418i$	9.06

Table 4.7: The inter-area mode for varying inter-tie line length.

Length factor	Eigenvalue	f [Hz]	zeta [%]
0.5	$-0.9918 \pm 3.764i$	0.599	25.48
1	$-0.5380 \pm 3.1736i$	0.505	16.71
1.5	$-0.3683 \pm 2.5922i$	0.4126	14.07

4.5 Loading

Table 4.6 shows how the inter-area- and local modes change as the system loading is varied. The capacitive shunt batteries are unchanged, while both the active and reactive loading is varied. The generation percentage is varied similarly to the loading, with some difference to ensure that the slack bus (generator 1) is loaded equally to the other generators. The result shows how the real value dominates the movement of the modes. A high loading impairs the system's stability, causing a more oscillatory system. The power system does, however, remain stable for all loading factors. As the reactive power increase, the generators are no longer able to maintain the voltage on the loading buses, decreasing the effective loading. The resulting voltages at loading factor 1.5 are 0.901 and 0.905 on buses 7 and 9, respectively, where the resulting generator loading is between 104 and 111%.

4.6 Inter-tie line length

A sensitivity analysis of the inter-tie line length is considered to analyze how the connection strength of the two areas affects the system stability. The power flow in the inter-tie line is kept constant by varying the active load in area two. The reactive power increase as the line length increase. The inter-area mode is the mode primarily affected and, therefore, the mode of interest. Table 4.7 shows the development of the inter-area mode as the length of the inter-tie line increase. The damping of the mode is highly dependent on the line length and is reduced as the length increase. The system remains stable for the line lengths presented. For length factors above 2, it is no longer sufficient to increase the loading in area two to keep the power transfer constant, as the reactive power supply no longer is able to sustain the voltage on the load bus in area two.

Chapter 5

Small-signal stability analysis of DFIG wind turbines

This chapter presents the analysis of the small-signal stability of Kundur's two-area system with implemented DFIG wind power. The impact of wind power with- and without frequency service controls is analyzed separately. The stability impact from the DFIG controls and wind power penetration level is considered, but of particular focus is the synthetic inertia controller. Detailed analysis of eigenvalue development and movement justification is provided.

5.1 Wind power without frequency service controls

5.1.1 System introduction

This section presents the stability analysis of Kundur's two-area system when synchronous generator 2 is replaced with wind power without frequency control. The wind turbine model is described in Section 3.2.3. The DFIG template's power ramping function at over frequency is not active. The objective of this section is to understand how the characteristics of the DFIG wind turbine affect the power system stability. Multiple sensitivity analyses are performed, examining the power system's eigenvalue dependency towards the DFIG parameters. The eigenvalue development for wind power penetration increase is evaluated and compared to the relevant results from the synchronous generation for justification. As the synchronous generation results are referred to frequently, synchronous generators are in this chapter referred to as SGs.

A particular focus is given to the two DFIG controllers regulating the power and current output. The controllers are shown to have significant control over the inter-area mode and are used to analyze the mode's movement for increasing wind power penetration. The dynamic performance of the controllers is evaluated for the different scenarios to better understand the eigenvalue development. Only the eigenvalue development is included in the text to achieve a tidy and succinct result presentation. The extended result, including the dynamic simulations, are in Appendix D. Further, the DFIG shaft introduces a mechanical mode to the system. As this mode is the power system's poorest damped mode, it is examined to ensure that it is an internal mode in the DFIG shaft with a small impact on the synchronous generators. Lastly, the system loading and inter-tie line length is examined. This is analyzed for all three power generation characteristics considered to explore possible differences in the stability impact.

The base values for the parameters used for the sensitivity analyses and the additional controls introduced to the wind turbine are shown in Appendix A.4. The complete linearization of the power system is shown in Appendix B, with the eigenvalues for wind power without frequency controls in Appendix B.4. The eigenvectors relating the dominant eigenvalues to the system states are shown in Appendix B.5. The eigenvectors relating the speed of the SGs to all oscillatory modes are shown in Appendix B.6.

The literature does not draw a clear conclusion on the DFIG wind turbine's impact on system stability. The control systems of the DFIG are essential, where voltage control, regulating the reactive power, has an important impact on the system stability [8]. The general trend in the literature is that the DFIG can enhance the system stability but decrease the damping of the inter-area modes. From [34], the inter-area mode is the mode most sensitive towards the wind power implementation, where wind power location, penetration level, and system stress are important factors. From [35, 36], DFIG wind power shows trends of decreasing the inter-area mode damping.

5.1.2 Wind power penetration

The power system stability impact from an increasing wind power penetration is examined by performing an aggregation sweep. The number of parallel wind turbines and transformers is increased similarly to the apparent power decrease of SG 2. For the aggregating number $m = 0$, the wind turbine and transformer are disconnected, and for the aggregation 540, SG 2 is disconnected. The development of the dominant modes is shown in figure 5.1, and 5.2.

By replacing synchronous generation with wind power, the inertia in the area decreases. The decreasing inertia causes the inertia in area two to exceed the inertia in area one, disturbing the connection between the local modes and the belonging SGs, explained in Section 4.4.1. Therefore, the local mode initially local in area two is the mode of interest. The results show how the damping of the mode first decreases before increasing for the largest penetration levels. As SG 2 is disconnected at aggregation 540, the local mode in area one no longer exists, as there is only one SG in the area. The development trend of both local modes bears a remarkable resemblance to the development of the PSS and inertia sweep of SG 2 in figure 4.10. However, the development of the imaginary part of the mode local in area one is not as severe for the wind power penetration increase.

Figure 4.10 shows the local mode development for reduced inertia and PSS gain of SG 2, and figure C.3 shows the local mode development for only reduced inertia of SG 2. When comparing the wind power penetration increase with these figures, the result bears the best resemblance to reducing both generator inertia and PSS gain. This means that the driving factor for the movement of the local mode for increasing penetration of DFIG wind power is the reduction of both physical inertia and PSS-equipped power. The high correspondence indicates that the DFIG controls have a negligible impact on the local modes. This corresponds with the linear analysis in Appendix B.5, showing that the wind turbines have very small control over the local mode.

The inter-area mode development in figure 5.2 has a notable damping decrease as the penetration of wind power increases. From the inertia sweep of SGs in table 4.4 and 4.5, decreasing inertia is expected to increase the damping of the inter-area mode. Also, the inertia and PSS sweep of SG 2 in figure 4.11 suggest increasing damping. This means that the movement of the inter-area mode for increasing penetration of wind power, contrary to the local mode, is not dominated by the replaced inertia and PSS-equipped power but rather another DFIG characteristic.

For the wind power penetration increase, movement is obtained in three pairs of small oscillatory modes, shown in figure D.3. These are not focused in this section as they remain stable for the sensitivity analyses considered. However, these modes are excited by the frequency controls, where in particular, modes 18 and 19 in Appendix B.4 becomes critical for several sensitivity analyses. From figure D.3, modes 18 and 19 remain unchanged during the increasing penetration of wind power without frequency controls.

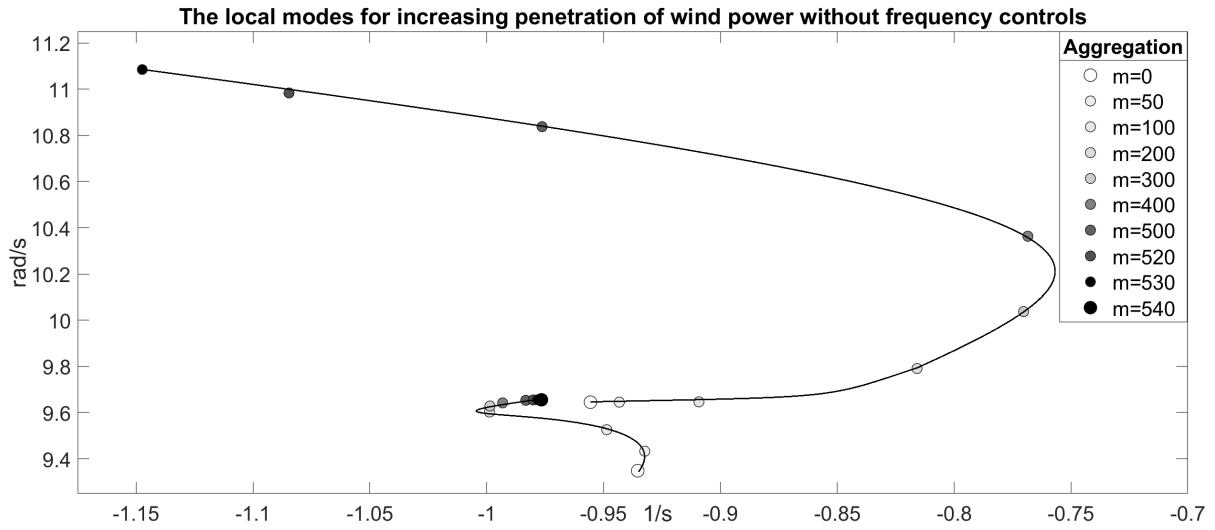


Figure 5.1: The local modes for increasing wind power penetration without frequency controls. An aggregation of $m = 540$ equals complete wind power replacement of SG 2.

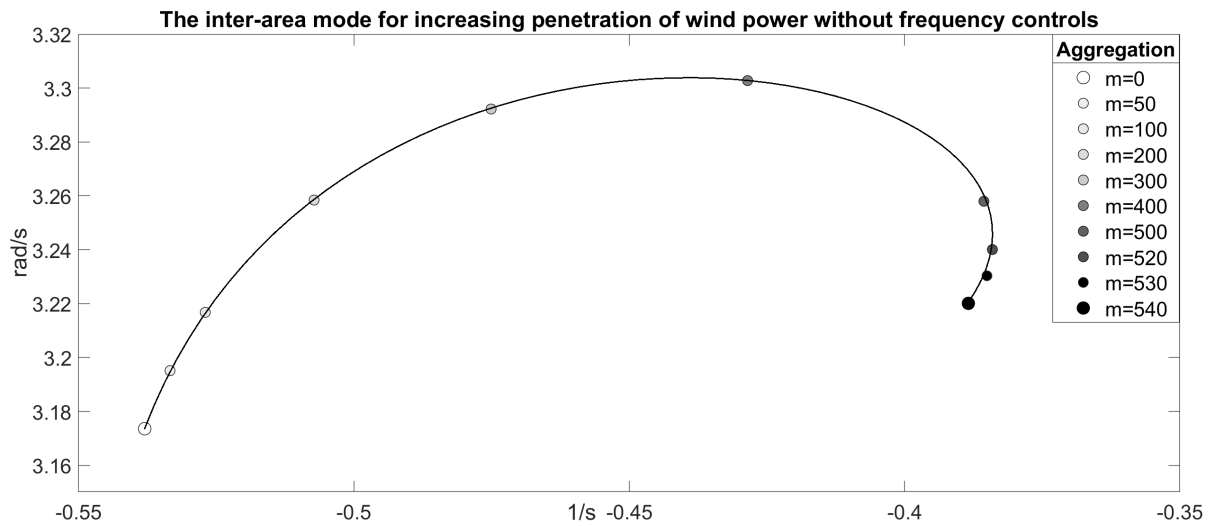


Figure 5.2: The inter-area mode for increasing wind power penetration without frequency controls. An aggregation of $m = 540$ equals complete wind power replacement of SG 2.

The results show that a more oscillatory system is obtained when wind power replaces synchronous generation. As the power system's remaining three SG are equipped with PSSs, the inter-area mode is still well damped. The local mode in area two is little affected by the wind power penetration increase. The decreased inter-area mode damping for the implementation of DFIG wind power corresponds to the literature presented in the section's introduction. From Appendix B.5, the wind turbine's control system holds a non-negligible control over the inter-area mode. Hence, the control system is examined to understand the decreasing inter-area mode damping.

5.1.3 The DFIG control system

The regulators in the control system are examined to gain a better insight into the DFIG's impact on the power system stability. From Appendix B.5, the regulators do hold some control over the inter-area mode. The deviation between the wind power penetration increase in figure 5.2 and the inertia and PSS decrease of SG 2 in figure 4.11 might, therefore, be improved by control adjustment. The speed of the rotor current regulators is important for the behavior of the generator's active and reactive power output. The current regulators are shown in figure A.19, with the parameters in figure A.20. The rotor current is regulated in the synchronous reference frame [17], where the d-component current regulates the active power, and the q-component current regulates the reactive power.

A sensitivity analysis of the system eigenvalues and the PI regulators of the current controller is performed. A slight movement is obtained in multiple eigenvalues during the parameter sweep, but only the inter-area mode is affected for the dominant modes. This corresponds with the x_d and x_q states controllability towards the inter-area mode from Appendix B.5. The low impact on the local mode corresponds with low controllability from these states and the consequent high correspondence between the local mode development for the wind power penetration increase and the inertia and PSS decrease of SG 2.

For the parameter sweep, both current component regulators are varied proportionally. The relation between the proportional and integral parameters is kept constant, given by the integrator time constant, and only the gain factor is varied. The result is shown in table 5.1, where the factors are chosen to illustrate the movement path of the inter-area mode. A great movement is obtained, dominated by the real part. Slowing down the regulators, the inter-area mode damping decreases until the gain factor is reduced to 10%, where the damping increases. For gain factors above 5, the system becomes highly unstable, and the linearization tool fails. The controller's significant control over the inter-area mode demonstrates the controller's ability to affect the inter-area mode for an increasing wind power penetration.

A dynamic simulation is performed to gain a broader understanding of the improved damping for the slow regulators. For a load step close to the wind turbines, the induction machine experience a steep change of rotor current and grid voltage. For slow controls, the wind turbines will not be regulated onto their supposed operation, and an unfavorable response is obtained. A step increase in loading is

Table 5.1: The inter-area mode for varying PI regulator speed of the dq components of the rotor current. The relation between the P and I components is constant and multiplied by the gain factor.

Gain factor	Eigenvalue	zeta [%]
5	$-0.409 \pm 3.229i$	12.57
1	$-0.388 \pm 3.220i$	11.96
0.2	$-0.284 \pm 3.140i$	9.01
0.1	$-0.200 \pm 2.960i$	6.74
0.035	$-0.299 \pm 2.181i$	13.58

performed when the current controls are deactivated, effectively replicating the response of very slow controls. The result in figure D.4 shows a significant power response from the wind turbine. Because the current controls are disabled, the new current reference from the power controller is not realized, decelerating the machines, eventually causing generator trip. However, the result shows that some natural inertial response is obtained, possibly explaining the improved damping for the slow controls.

To further analyze the control system's impact on the inter-area mode movement, the power regulators are examined. The power regulators are shown in figure A.21, with the parameters in figure A.22. The power controllers are also composed of two PI regulators, separately regulating the active- and reactive power. Similar to the rotor current sweep, the two regulators are varied proportionally while the relation between the proportional and integral components is kept constant. The result, in table 5.2, is very similar to that of the current controller. The real part dominates the mode movement. The inter-area mode damping reduces for a slow controller until the controller speed 5%, where the damping starts to increase. Increasing the gain factor above five has little effect on the damping and causes an increased power ripple. Further, the dynamic impact from the slow controllers is considered to examine the motivation of the inter-area mode movement.

To replicating very slow controls, the power controller is deactivated. This results in constant rotor current references, given by the initial conditions. The rotor current regulators will therefore regulate the rotor voltages to achieve these currents. The result is shown in figure D.5. The dynamic power response is remarkable, where a natural inertial response very similar to that of a SG is obtained. Natural inertial responses are not obtained from variable speed wind turbines as DFIGs, since they are operated at rotational speeds based on the wind and not the grid frequency, explained in Section 2.3. However, when the controls are slowed down, there is no longer a complete speed decoupling. It should be noted that the high correspondence towards the inertial contribution from the SG is a consequence of the nominal rotor current controls. For faster rotor current controls, the minor response in figure D.6 is obtained. For slower controls, the response moves towards the massive response of deactivated current controls in figure D.4. The obtained response in figure D.5 shows that the current controls are able to regulate the power back to steady-state.

Table 5.2: The inter-area mode for varying PI regulator speed of both active- and reactive power. The relation between the P and I components is constant and multiplied by the gain factor.

Gain factor	Eigenvalue	zeta [%]
5	$-0.405 \pm 3.254i$	12.35
1	$-0.388 \pm 3.220i$	11.96
0.1	$-0.328 \pm 3.146i$	10.04
0.05	$-0.239 \pm 2.986i$	7.98
0.02	$-0.408 \pm 2.470i$	16.30

The dynamic simulations of the load step show how the active power response from the wind turbines is highly dependent on the regulators. For the nominal power and current controls, the speed of the DFIG is independent of the grid frequency, only obtaining minor oscillations, shown in figure D.8. When deactivating or slowing down the power controls, a natural inertial response is obtained, at the expense of stored kinetic energy, hence, deceleration of the machine shown in figure D.9. This natural inertia response is highly dependent on the speed of the current controllers. For deactivated power controls and nominal current controls, the natural inertial contribution is not in accordance with the stored kinetic energy, decelerating the wind turbine to a greater extent than SG 1. For fast controllers, the natural inertia response completely disappears, shown in figure D.7. Therefore, speeding up the controls can be considered the process of decoupling the speed of the induction machine from the electrical frequency of the grid.

The rotor voltage realizes the calculated DFIG operation from the controls. Hence all regulators involved impact the response. The nominal controls of the DFIG model are, as described in Section 3.2.4, designed to be compatible with the derivator in the synthetic inertia controls and to give the best power regulation. The load event for the deactivated power controls in figure D.5 might suggest that inertial contribution could be realized only using slow power controls. The presented dynamic simulations are considered to understand the controllers' functionality, as they highly affect the inter-area mode damping. Deactivating the controls is not possible as the current reference constructed by the power regulators ensures equilibrium between mechanical and electrical power for varying wind speed to achieve speed regulation and MPE, and voltage support.

The significant development of the inter-area mode for the parameter sweeps in both controllers shows significant dependency and emphasizes the importance of controller adjustment. Therefore, the controls play an essential role in the deviation between the wind power penetration increase in figure 5.2, and the inertia and PSS decrease of SG 2 in figure 4.11. To further confirm this, the movement of the inter-area mode is investigated for a wind power penetration increase where the power controls are deactivated, shown in figure 5.3. Deactivating the power controls is not a realistic operation condition but is performed for eigenvalue movement justification. The result in figure 5.3 shows that the inter-area mode

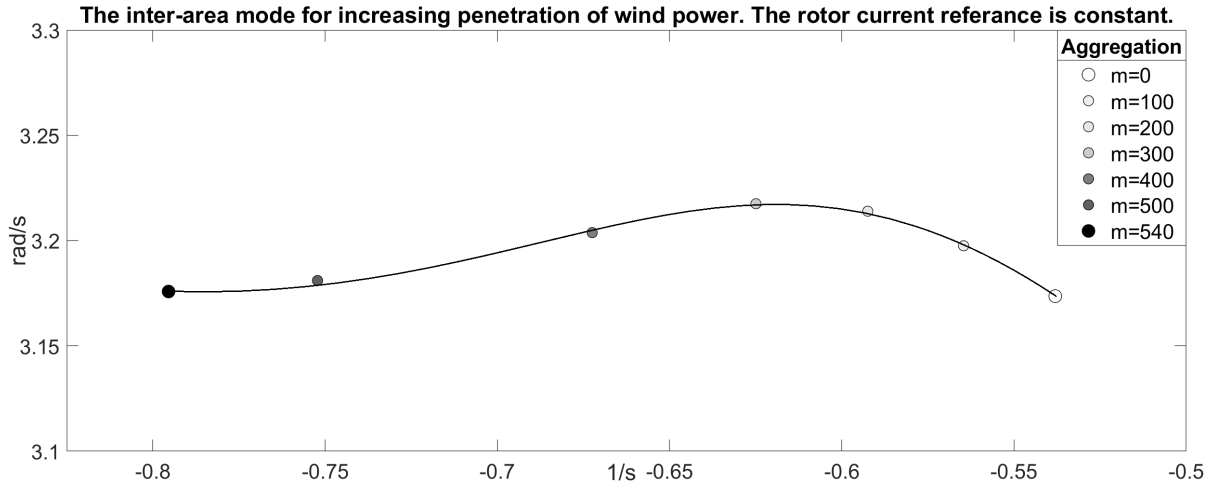


Figure 5.3: The inter-area mode for increasing wind power penetration. The power regulator in the DFIG is deactivated, meaning that the wind turbines are operated with constant rotor current references. An aggregation of $m = 540$ equals complete wind power replacement of SG 2.

now moves similarly as the parameter sweep of the inertia and PSS gain of SG 2, where the inter-area mode damping increase as the wind power penetration increase. Thus, the development trends of the inter-area mode correspond, and the numerical values could probably be further synchronized through fine-tuning.

The stability analysis performed in this section shows that the controls of the DFIG play a major role in the small-signal stability, particularly the inter-area mode. The speed of the power and rotor current regulators is shown to hold a high control of the inter-area mode. There is a complicated relationship between the regulator speed and the inter-area mode, including circular movements. Increasing the speed of the regulators increase the damping to a small degree but quickly causes instability in the form of simulations divergence. When highly reducing the speed of the regulators, the power response resembles an SG through a natural inertial contribution.

With slow controls, the movement of the inter-area mode bears a greater resemblance to the expected movement. Wind power penetration increase with controls so slow that an inertia response is obtained is required to replicate the inter-area movement of inertia decrease from SG 2. This is contradictory but points a finger towards the PI regulators. Very slow regulators are required to achieve the desired stability improvement to the point where the wind turbine is uncontrollable. Therefore, the results offer insight into the decreasing inter-area mode damping for increasing wind power penetration, yet not a solution.

5.1.4 The mechanical mode

The generic shaft of the DFIG is modeled as a two-mass shaft, described in Section 3.2. This means that the speed of the wind turbine and the generator is connected through a spring causing torsional vibration and hence, a mechanical mode, describing the natural frequency of vibration [37]. The mathematical formulas and importance of accurate modeling and parameters of the shaft are described in [38], where the DIgSILENT model is based on the lumped inertia formula. In [39], the participation factors are used, in a three-mass model, to determine which modes are connected to the DFIG shaft angle and speed, and hence, are mechanical modes. The possibility of damping mechanical modes caused by torsional vibration utilizing power reference manipulation is explored in [40].

Based on this literature, this section aims to verify that mode 29 in Appendix B.4 is a mechanical mode and to analyze how this mode affects the power system stability. The eigenvectors relating all the oscillatory modes to the SG speeds are shown in Appendix B.6. Amongst the SG speed states, the eigenvectors show that the mechanical mode has the strongest connection to SG 1. For this state, the mechanical mode has controllability of 0.032, observability of 0.205, and a participation factor of 0.00165 relative to the inter-area mode. Hence, the SG speed has a weak connection to the mechanical mode. The eigenvectors relating the mechanical mode to the system states are shown in figure D.10. The state with the strongest connection to the mode is "dphi12". This is the change of the angle difference between the turbine and generator speed. Further, the DFIG generator speed and change of turbine speed states are dominant. Hence, the mode has the strongest connection to the mechanical movement of the DFIG shaft.

A sensitivity analysis is performed towards the shaft stiffness K , damping D , and inertia H shown in figure 5.4 to examine the mechanical mode's connection to the shaft parameters. The shaft, and the parameters are shown in figure A.23 and A.24. The parameter sweep shows how decreased stiffness, increased damping, and decreased inertia improve the damping of the mechanical mode. The extended sensitivity analysis in figure D.11 together with figure 5.4 shows that the inter-area and local mode is little affected and has a weak connection to the shaft parameters.

The torsional vibrations, described by the mechanical mode, causes oscillations in the turbine power whenever the mechanical or the electrical torque is changed. In the case of a sudden load change, the electric power from the DFIG will experience fast change. Hence, oscillations are obtained in the shaft during the synchronization of the turbine and generator speed. The turbine power oscillations for a step increase in loading are shown in figure D.12. The period of the oscillations is measured to 0.928s, corresponding with the frequency given by the mechanical mode $p = 1/f = 1/\frac{\omega_{29}}{2\pi} = 0.928s$. In addition to the weak connection identified between mechanical mode and the SG speeds in the linear analyses, the SG speeds are evaluated for a small disturbance, shown in figure D.13. The result show oscillations dominated by the inter-area mode, where the SGs in area two oscillate against the SG in area one, with a frequency given by the inter-area mode $p = 1/f = 1/\frac{\omega_{35}}{2\pi} = 1.95s$.

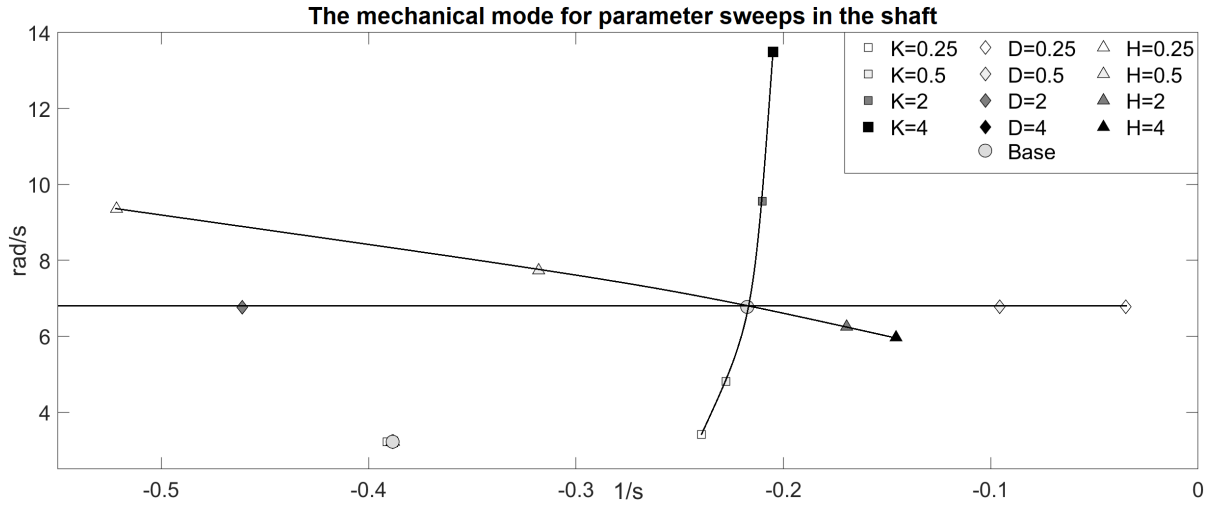


Figure 5.4: The mechanical mode in the DFIG shaft as a function of the shaft stiffness K , damping D , and inertia H .

Table 5.3: The inter-area- and local mode for varying system loading. Generator 2 is wind power without frequency controls.

	Inter-area mode		Local mode	
Loading factor	Eigenvalue	zeta [%]	Eigenvalue	zeta [%]
0.5	$-1.055 \pm 3.273i$	30.68	$-1.111 \pm 9.826i$	11.24
0.75	$-0.709 \pm 3.426i$	20.27	$-1.055 \pm 9.806i$	10.70
1	$-0.388 \pm 3.220i$	11.96	$-0.977 \pm 9.66i$	10.06
1.25	$-0.143 \pm 2.610i$	5.47	$-0.9209 \pm 9.531i$	9.62
1.5	$0.0035 \pm 1.681i$	-0.21	$-0.895 \pm 9.417i$	9.46

In this section, mode 29 is examined as this is the system eigenvalues with the poorest damping. The result shows that this is a mechanical mode connected to the shaft of the DFIG, causing torsional oscillations in the shaft for electrical and mechanical speed mismatch. The mode has a weak connection to the SG speeds and is only affected by the parameters of the shaft. Mode 29 is therefore not a mode of further interest.

5.1.5 Loading

Table 5.3 shows how the inter-area- and local modes change as the system loading is varied. The capacitive shunt batteries are unchanged, while both the active and reactive loading is varied. The generation percentage is varied similarly to the loading, with some difference to ensure that the slack bus (SG 1) is loaded equally to the other generators. The result shows how the real value dominates the movement of the modes. A high loading impairs the system's stability, causing a more oscillatory system. The system becomes small-signal unstable by the inter-area mode at the loading factor of 1.5.

Table 5.4: The inter-area mode and mode 20 for varying inter-tie line length. Generator 2 is wind power without frequency controls.

Length factor	Inter-area mode		Mode 20	
	Eigenvalue	zeta [%]	Eigenvalue	zeta [%]
0.5	$-1.092 \pm 3.914i$	26.87	-0.0996	100
1	$-0.388 \pm 3.220i$	11.96	-0.09939	100
1.5	$-0.121 \pm 2.256i$	5.36	-0.0986	100
1.85	$-0.041 \pm 1.345i$	3.05	-0.0525	100
1.875	$-0.046 \pm 1.257i$	3.66	0.0179	-100

5.1.6 Inter-tie line length

A parameter sweep is performed of the inter-tie line length to analyze how the connection strength of the two areas affects the system stability. The power flow in the inter-tie line is kept constant by varying the active load in area two. The reactive power increase as the line length increase. The inter-area mode is the dominant mode primarily affected and, therefore, the mode of interest. Table 5.4 shows the development of the inter-area mode as the length of the inter-tie line increase. The damping of the mode is highly dependent on the line length and is reduced as the length increase. As the length increase above 1.5, the mode does a circular movement, never reaching a real part below $-0.0411/s$. The damping ratio of the inter-area mode is very small for the length factor 1.5 and above.

The system becomes unstable for length factors above 1.85, caused by mode 20 from Appendix B.4. The movement of the mode is therefore included in table 5.4, and visualized in figure D.14. Similar modes are obtained in the power system for synchronous generation, modes 10-12 in Appendix B.1. These modes do, however, not move during the inter-tie line sweep in table 4.7. To gain a deeper understanding of the movement of mode 20, the states controlling the development is evaluated for the nominal line length, shown in figure D.15, the length factor 1.85, shown in figure D.16, and the length factor 1.875, shown in figure D.17. For nominal line length, the mode is controlled by the intermediate and medium pressure states $x3$ and $x4$ in the SG steam turbines, shown in figure A.2. For increasing line length, the DFIG speed-controller becomes the controlling state, together with the SG speeds. As the mode becomes unstable, the speed of the SGs becomes dominant, together with the speed change state xH in the DFIG shaft.

No significant impact is obtained in the mode when changing the wind turbine inertia or the parameters of the speed controller. However, changing the power and current controllers affects the mode, in particular the current controller. By highly reducing the speed of the current controllers, the mode damping increase, but does not become stable before the controller are slowed down to the point where it is disabled.

5.1.7 Key findings

- For increasing penetration of DFIG wind power, the local mode damping decrease for low penetration levels, and increase as the penetration increase. The inter-area mode damping decrease as the penetration level increase.
 - The driving factors for the local mode movement are the reduction of inertia and PSS-equipped power.
 - The driving factor for the inter-area mode movement is the DFIG control regulators. Slow controls improve the damping. A strong connection between the controllers and inter-area mode is identified, emphasizing the importance of appropriate adjustment.
- When highly reducing the speed of the DFIG control regulators, an inertial response similar to a synchronous generator is obtained at frequency events.
- Speeding up the DFIG controllers can be considered the process of decoupling the speed of the induction machine from the electrical frequency of the grid.
- A mechanical mode is obtained in the DFIG shaft. The mode has a weak connection to the synchronous generator speeds and is only affected by the parameters of the DFIG shaft.

5.2 Wind power with frequency service controls

5.2.1 System introduction

This section presents the stability analysis of Kundur's two-area system when generator 2 is DFIG wind power with frequency controls. A thorough analysis of the frequency controls is performed, focusing on the synthetic inertia controller. The small-signal stability impact from the synthetic inertia controller's parameters, determining the size and form of the inertial contribution, is analyzed separately. The eigenvalue development is also examined for increasing wind power penetration, showing promising results. The synthetic inertia derivator can be adjusted to separately determine the inertial contribution providing frequency support and the inertial behavior towards the system eigenvalues. A relation between the synthetic inertia derivator parameters and its apparent inertia towards the inter-area mode is developed.

Three pairs of minor complex conjugate modes are analyzed. In particular, the poorest damped pair is focused, referred to as the critical modes, causing instability for several sensitivity analyses. The three pairs of oscillatory modes have an amplitude below 10% of the inter-area mode, therefore referred to as the small modes. Lastly, the system loading and inter-tie line length is examined. This is analyzed for all three power generation characteristics considered to explore possible stability impact differences.

The base values for the parameters sweeps and the additional controls introduced to the wind turbine are shown in appendix A.4. The complete linearization of the power system is shown in appendix B. All eigenvalues are shown in appendix B.7. The eigenvalues in focus are the dominant modes, where the eigenvectors relating these eigenvalues to the states in the power system are shown in appendix B.8. Many simulations are performed, including several sensitivity analyses and dynamic simulations to understand the results and identify relevant connections for eigenvalue movement justification. Therefore, in addition to the presented results in this section, extended results from the stability analysis are included in appendix E. The figures are referred to when relevant.

The literature available on the small-signal stability impact from DFIG wind turbines with synthetic inertia controllers is limited. From the general review in [8], frequency controllers in DFIGs are said to have a positive impact on the eigenvalue damping. In [41], DFIG wind turbine equipped with frequency controllers is shown to damp the power system eigenvalues, in particular the inter-area mode.

5.2.2 The synthetic inertia controller

This section analyzes how the synthetic inertia controller impacts the power system stability. From the linear analysis in appendix B.8, the system state representing the synthetic inertia derivator holds the highest control over the inter-area mode. Therefore, adjustment of the synthetic inertia controller is expected to cause a notable impact on the mode. The size and form of the contribution are separately analyzed. For the parameter sweeps, the saturation block of the inertial contribution is deactivated.

The size of the inertial contribution

The size of the inertial contribution is dependent on the change of frequency and the stored kinetic energy in the wind turbine, described in Section 2.3. This is translated to the synthetic inertia controller by the frequency derivative and speed of the wind turbine in p.u. described in Section 3.2.4. By changing the size of the calculated inertial contribution, the wind turbine will no longer contribute with inertial power on the same basis as SGs. The nominal inertial contribution is validated to be in correspondence with the kinetic energy in figure A.15, where the wind turbine is decelerated, similar to an SG. A sensitivity analysis is performed to examine the stability impact on the size of the inertial contribution.

The development of the inter-area mode for a varying inertial contribution is shown in figure 5.5. The inertia factor is multiplied with the calculated inertial contribution in the frequency controls shown in figure A.11. For the factor of zero, the mode equals the inter-area mode without frequency controls, with a small deviation given by the primary control, considered in the section below. The development of the inter-area mode shows how the damping improves as the wind turbines contribute with inertial power. The mode's damping continues to increase as the inertia factor exceeds the nominal at $Kf = 1$.

Substantial and unrealistic inertial contributions are required to make the system unstable. The movement of the local- and small modes are shown in figure E.1 and E.2, respectively. Three pairs of small modes are affected by the inertia sweep, 18 and 19, 23 and 24, and 31 and 32, from appendix B.7. As the inertia factor increase, the first modes to cause small-signal instability are modes 18 and 19. These modes will be shown to cause instability for multiple of the sensitivity analyses and are further examined in section 5.2.6. The local mode in area two is little affected by the inertia sweep.

The form of the inertial contribution

To further understand how the synthetic inertia controller affects the power system stability, the properties of the derivator are considered. Reducing the time constant of the derivator makes the frequency controller more sensitive to frequency changes, affecting the size and form of the inertial contribution. Therefore, to achieve constant frequency support during the sensitivity analysis of the synthetic inertia derivator time constant, the gain is adjusted to keep the inertial contribution in accordance with the wind turbine's kinetic energy. A small time constant is desired to achieve a sensitive frequency controller. When reducing the time constant below 0.3 times the nominal, controller instability occurs between the PI regulators of the power and current regulators and the derivator. The sensitivity analysis of the synthetic inertia derivator is shown in figure 5.6. The inter-area mode is shown to have a strong connection to the derivator. A fast derivator or a small time constant causes a decreasing inter-area mode damping.

Reducing the derivator time constant can be considered the process of connecting the wind turbine inertia to the grid frequency. A logical comparison is, therefore, the inertia sweep of SG 2 in figure C.5. Making the frequency controller more sensitive to frequency changes by reducing the derivator time constant,

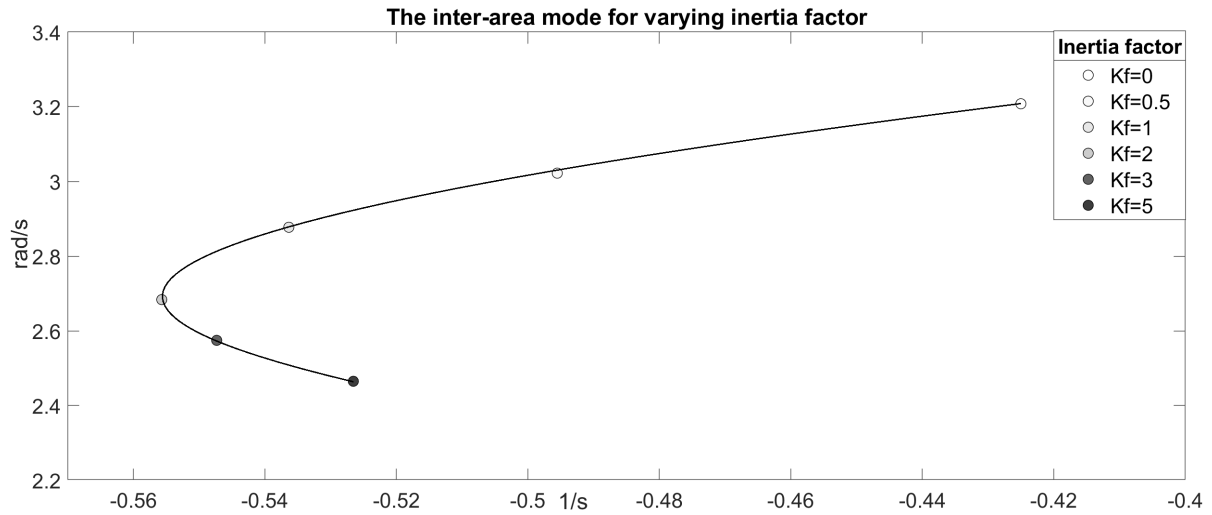


Figure 5.5: The inter-area mode for a varying inertial contribution.

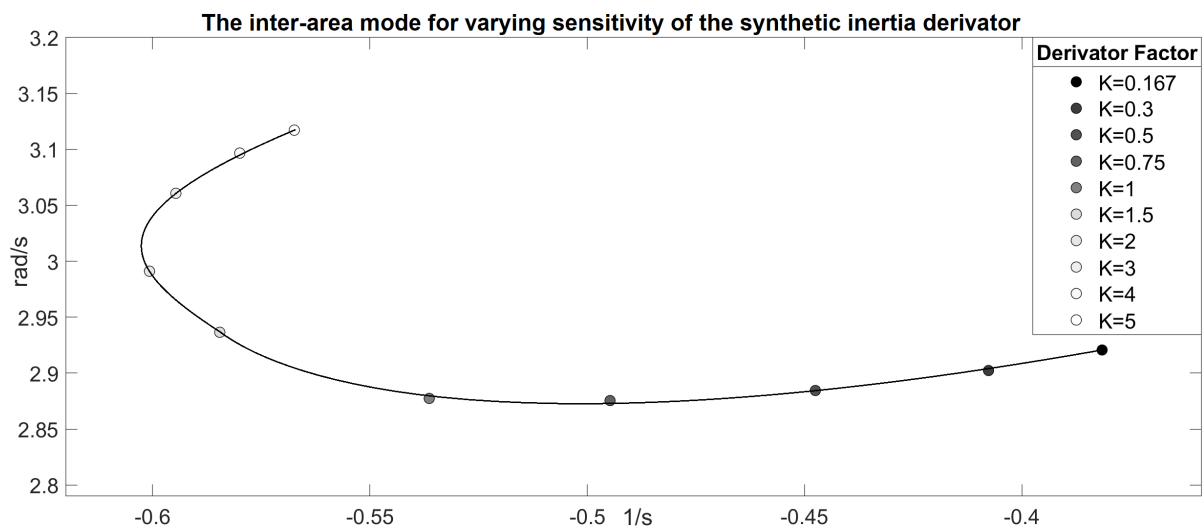


Figure 5.6: The inter-area mode for varying synthetic inertia derivator time constant. The gain of the derivator is regulated to keep the size of the inertial contribution constant.

similar to increasing the inertia of SG 2, reduces the inter-area mode damping. There are some differences between the two figures. The inertia decrease of SG 2 does not cause a circular movement, decreasing the damping for the lowest inertias, as for the derivator. The smallest derivator time constant values also cause lower inter-area mode damping than the inertia increase in SG 2, but this is due to the SG's limited inertia factor interval. A greater correspondence might be obtained by further examining the PSS of SG 2 and the controls of the DFIG. However, the comparison shows similar movement trends, indicating that a sensitive synthetic inertia derivator replicates the behavior of physical inertia on the inter-area mode. The inter-area mode damping is reduced further by a sensitive derivator than for the nominal for SG 2. This indicates that the synthetic inertia derivator of the wind turbines, potentially, could be used to define the physical inertia the power system eigenvalues experience from the wind turbines.

Dynamic simulations are performed for the different derivators to evaluate the shape of the inertial responses to understand why a sensitive inertia controller replicates inertial behavior towards the inter-area mode. Figure E.3 and E.4 shows the active power response for a step load increase for a fast- and slow synthetic inertia derivator, respectively. The result shows that a fast derivator achieves an inertial contribution much more similar to an SG. This corresponds well with the sensitivity analysis of the derivator. An inertial behavior is obtained towards the inter-area mode for the synthetic inertia controller, best replicating the inertial contribution from an SG. During the time constant sweep, the gain of the derivator is adjusted to achieve a constant impact on the kinetic energy of the wind turbine. The different derivators result in different inertial contribution shapes and also different frequency support. A small difference exists between the obtained nadir for the two derivator speeds. A lower RoCoF is obtained for the sensitive derivator as this reacts faster to the changing frequency. The gain adjustment might not be perfect and could cause some of the similarities between the inter-area mode's sensitivity towards the inertia factor and the derivator time constant. A potential gain adjustment deviation could also be part of the root to the deviation between the inter-area mode's sensitivity towards the derivator time constant and the inertia of SG 2.

Similar to the eigenvalue analysis of the inertia size, movement is obtained in the small modes during the derivator time constant sweep. The development of the small modes 18 and 19, 23 and 24, and 31 and 32 are shown in figure E.5 and E.6. The eigenvalue development is included both with- and without the gain adjustment required to keep the inertial contribution constant. This illustrates that only changing the time constant has little impact on the mode development. The critical modes 18 and 19 are little affected by the derivator, regardless of the gain adjustment. Modes 23 and 24, and 31 and 32 are little affected by only changing the derivator time constant. However, when the gain is adjusted to keep the inertial contribution constant, the mode development is similar to the inertia increase in figure E.2, meaning that the gain increase dominates the mode development. The modes do not experience significant change for the great variety of derivator factors considered. Hence, the inter-area mode is the mode primarily affected by the adjustment of the synthetic inertia derivator time constant.

This section analyzed the synthetic inertia controller's impact on the system stability. The results show that the inter-area mode is highly affected by the controller. Also, some of the small oscillatory modes in the system are affected by the synthetic inertia controller. However, substantial and unrealistic parameters are required to affect the small modes to a critical extent. The local mode in area two has a weak connection to the synthetic inertia controller in the wind turbines in area one. The results show that an inertial contribution from the wind turbines improves the damping of the inter-area mode. However, having a too-fast synthetic inertia controller impairs the damping. Inertial contributions are obtained for the variety of derivator parameters in the synthetic inertia controller. The choice of parameters does, however, highly impact the damping of the inter-area mode. The trends in the results indicate that speeding up the derivator in the inertia controller replicates the behavior of increasing the inertia of an SG. Hence, the synthetic inertia controller can not only dynamically give short-term frequency support but also replicate SG inertia on the eigenvalues. It should be noted that even though the derivator impacts the inter-area mode similarly to SG inertia, a local mode in area one is not obtained.

5.2.3 The primary control

For the wind turbines to contribute with primary control, the frequency controls include a power contribution proportional to the deviation between the measured and nominal frequency. A sensitivity analysis is performed of the droop to analyze how the wind turbines' primary control affects power system stability. The wind turbines' primary control is achieved through a combination of pitch control and power reference manipulation. The power reference manipulation speeds up the primary control contribution, as the pitch control is dependent on the speed controller to increase the power reference, described in Section 3.2.4. The power reference manipulation is used for the parameter sweep to indicate the eigenvalue movement for a more sensitive primary controller.

The result is shown in figure 5.7. The inter-area mode is the dominant mode primarily affected and, therefore, the mode of interest. The figure also includes the inter-area mode movement for a varying droop of generator 2 when it is synchronous. The droop factors are chosen to highlight the mode movement. It should be noted that the power reference modification in the wind turbine controls is adjusted to achieve a primary control contribution equal to the contribution from the SGs. As the reference manipulation is added to the speed controller reference, which is being increased by the pitch controller, the droop of the power reference manipulation in the wind turbines is not equal to that of the SG.

The result shows that the movement trends of the inter-area mode for a varying droop are similar for wind- and synchronous power. The damping increase as the droop decrease. There are only minor differences in the inter-area mode for the nominal droop $K = 1$ between the two generation characteristics. However, deactivating the droop controller in the wind turbine causes a more considerable decrease in the inter-area mode damping than deactivating the droop controller of the SG. For the SG droop variation, also the local mode in area one is affected, further described in Section 4.2.

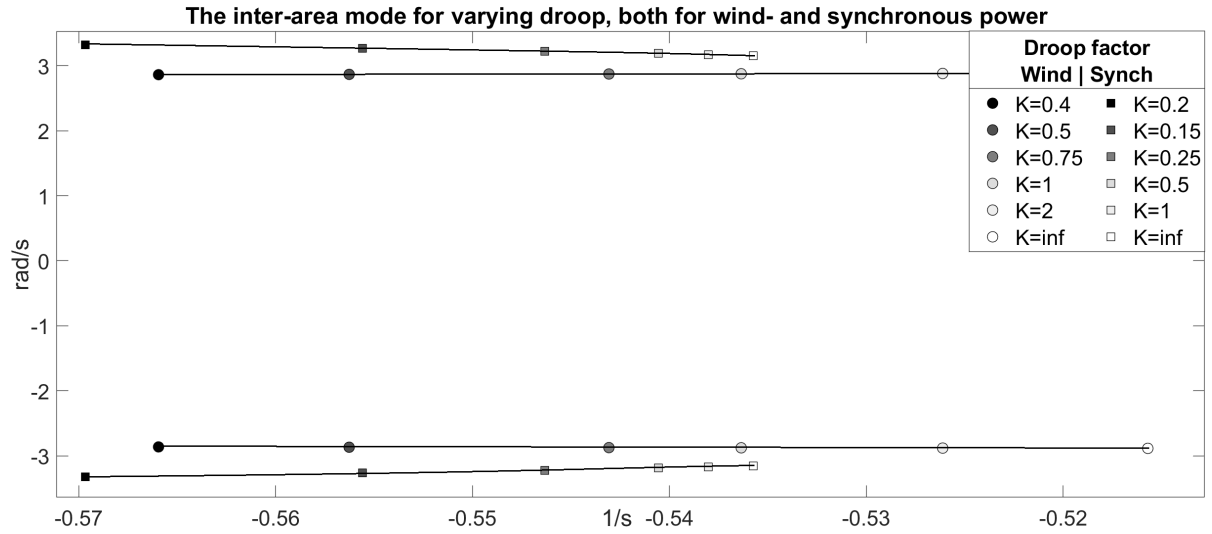


Figure 5.7: The inter-area mode for varying droop of generator 2, both for wind- and synchronous power.

The result shows a relatively weak connection between the inter-area mode and the wind turbines' primary controller. An inter-area mode damping ratio increase from 17.59% to 18.32% is obtained. Similar to the inertia sweeps, also the small oscillatory modes are affected by the changing droop. The development of modes 18 and 19, 23 and 24, and 31 and 32 are shown in figure E.7. The development trends are equal to the inertia sweep. The primary controller has an improving impact on modes 31 and 32, and an impairing impact on modes 18 and 19. However, significant variations are required in the droop controller to obtain great moments. The three pairs of small modes are affected by the power reference manipulation from both the inertia and primary control. With a focus on modes 18 and 19, Section 5.2.6 shows that these modes are linked to the speed of the wind turbines, explaining the modes' impact from the power reference manipulations.

5.2.4 Wind power penetration

The power system stability impact from the increasing penetration of DFIG wind power equipped with frequency controllers is examined. From the analysis of the synthetic inertia derivator, the results indicate that the controller is not only able to contribute with inertial power during a changing frequency but also replicate SG inertia on the inter-area mode. This is the base for the penetration increase, where an aggregation sweep is performed both for the nominal synthetic inertia derivator $T_{der} = 0.3, K_{inert} = 2$, and for a slow derivator $T_{der} = 1.2, K_{inert} = 2.75$. The movement of the local modes during the wind power penetration increase is shown in figure 5.8 and 5.9. For complete wind power replacement of SG 2, the local mode in area one disappears, independent of the frequency controls and its tuning.

The wind power penetration increase shows exciting and convincing results. For the nominal synthetic inertia derivator, the local mode in area one is affected, while for a slow derivator, the local mode in area two is affected. As analyzed in Section 4.4.1, when the inertia in area one is reduced below the inertia of area two, the local modes do not cross each other but rather perform an exchange between the SG groups, defined by the connection strength to the SG speeds. The penetration increase for the nominal synthetic inertia controls shows that the local modes do not experience this exchange, indicating that the inertia balance between the areas remains unchanged. Therefore, the movement of the local mode in area one during the wind power penetration increase is motivated by another system characteristic. For the slow synthetic inertia derivator in figure 5.9 it is, however, the local mode in area two experiencing the movement, indicating that the inertia in area one is reduced below the inertia in area two. This shows that a sensitive inertia controller replicates inertia behavior also towards the local modes. When the speed of the synthetic inertia derivator is reduced, the wind turbines still contribute with inertial power, shown in figure E.4. Hence, slow synthetic inertia controls contribute to frequency service but do not have an as severe inertial effect on the eigenvalues.

The penetration increase of wind power without frequency control, in Section 5.1.2, described a local mode movement both motivated by the reduction of inertia and PSS equipped power. However, the penetration increase of wind power with frequency controls does not seem to be affected by the reducing PSS power. In particular, from the result with the slow inertia derivator, the local mode movement bears a greater resemblance to the inertia sweep of SG 2 where the PSS is unchanged in figure C.4, than to the sweep of both inertia and PSS gain in figure 4.10. Hence, a positive impact is obtained on the power system stability from the frequency service controls. The same goes for wind power penetration with nominal synthetic inertia controls. The local mode movement bears greater resemblance to the load reduction in table 4.6, than to the PSS gain reduction in table 4.3, indicating that the local mode movement is motivated by the reducing percentage of synchronous based generation in area one, rather than the reducing portion of PSS-equipped power.

The movement of the inter-area mode is highly affected by the regulators in the control system, analyzed in Section 5.1.3. Reducing the speed of the converters is shown to make the induction machine behave more like an SG as the connection between the mechanical and electrical speed is strengthened. However, fast converters are required to realize the inertial contribution, therefore making further analysis of the parameters of the PI regulators difficult. The inter-area movement for a nominal- and slow synthetic inertia derivator is shown in figure 5.10 and 5.11 respectively. The two synthetic inertia controllers achieve approximately the same damping for the complete replacement of SG 2, improving the inter-area mode damping. The slow derivator obtains greater imaginary- and real parts. The relation between the inter-area modes for the two controls, for complete penetration, corresponds with the sensitivity analysis of the synthetic inertia derivator in figure 5.6. The slow controller is the derivator factor $K = 4$, hence increased both imaginary- and real parts. This also corresponds with the decreased inertia of SG 2 in figure C.5.

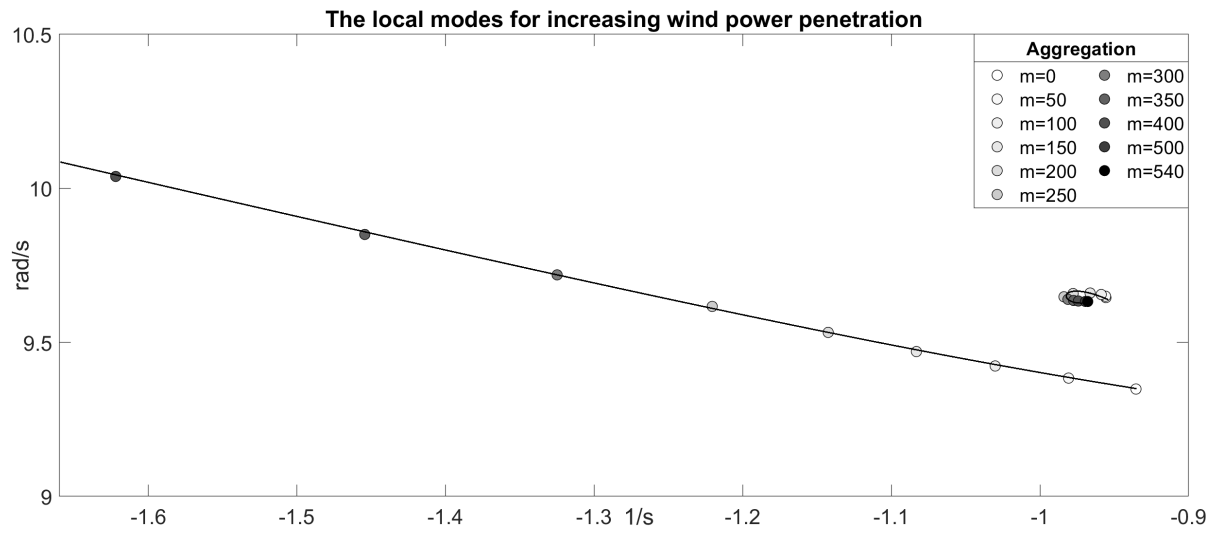


Figure 5.8: The local modes for increasing wind power penetration with frequency controls.

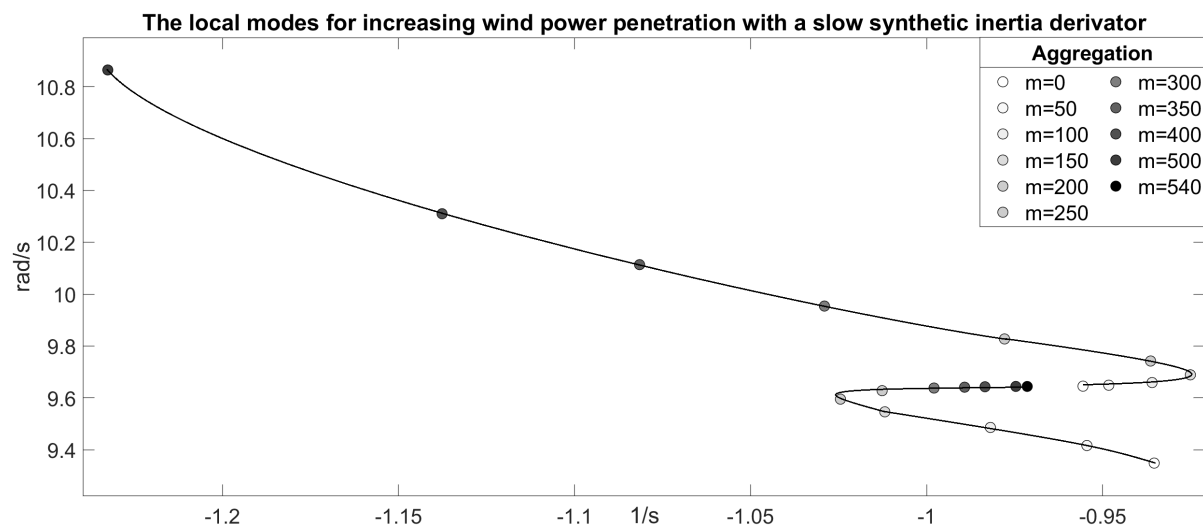


Figure 5.9: The local modes for increasing wind power penetration with frequency controls, using a slow synthetic inertia derivator.

Circular movement paths are obtained in the inter-area mode during the penetration increase. In particular, for the nominal controls, the damping is reduced when the replacement of SG 2 is increased between 100/540 to 400/540. However, the changes are minor, where the development of the inter-area damping spans between $-0.5451/s$ and $-0.51/s$. At the same time, the imaginary part is decreased, keeping the damping ratio fairly unchanged. The inter-area mode damping is increased for both the synthetic inertia controls when the penetration exceeds 400/540. For the nominal controls, the real value is relatively similar for zero and full wind power penetration. As the imaginary part decrease, the damping ratio is enhanced by the wind power. Further examination of the circular movements in the inter-area mode during the penetration increase is not considered. The inter-area mode is previously shown to be highly dependent on the DFIG controllers. The movement of the local modes is also shown to be motivated by the replacement of synchronous power. Most of the presented sensitivity analyses in the frequency controller also involve circular movements. The circular movements of the inter-area mode are therefore expected to be a combination of these factors.

During the wind power penetration increase, movement is obtained in the small modes, shown in figure E.8. The penetration increase shows that modes 31 and 32 in appendix B.7 has their origin from the synchronous generation modes 18 and 19 in appendix B.1, and the modes 23 and 24 have their origin from the synchronous generation modes 13 and 14. The dominant states for these two pairs of small oscillatory modes are shown in figure E.9. Both these small modes are, for synchronous generation, linked to the SG speeds and the PSS. As SG 2 is replaced with wind power with frequency controls, the states related to the wind turbine speed also become dominant, particularly the synthetic inertia derivator state. The same eigenvector profile is obtained for wind power without frequency controls, except for the derivator state. The result also corresponds to the analysis of the critical modes 18 and 19 in Section 5.2.6. However, the critical modes do not exist for pure synchronous generation and are introduced to the system by the wind turbines. Therefore, DFIG wind turbines will create and excite small oscillatory power system eigenvalues, mainly when using frequency service controls.

This section examines how the power system stability is affected by increasing wind power penetration equipped with frequency service controls. Based on the analysis of the synthetic inertia controller in section 5.2.2, the penetration increase is performed with both fast- (the nominal) and slow synthetic inertia derivator. The objective is to determine if a sensitive derivator replicates inertial behavior towards the dominant eigenvalues. The analysis focuses on the local- and the inter-area mode, but the small oscillatory modes are also included as they are affected by the synthetic inertia controller. The results clearly indicate, by the movement of both inter-area- and local mode, that a sensitive synthetic inertia derivator replicates SG inertia behavior towards the small-signal stability.

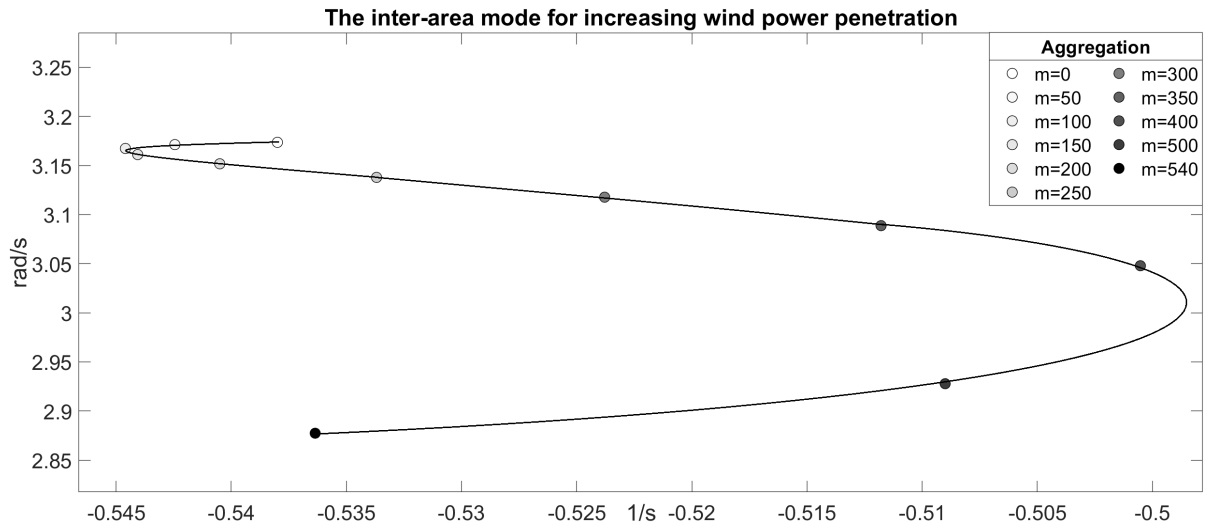


Figure 5.10: The inter-area mode for increasing wind power penetration with frequency controls.

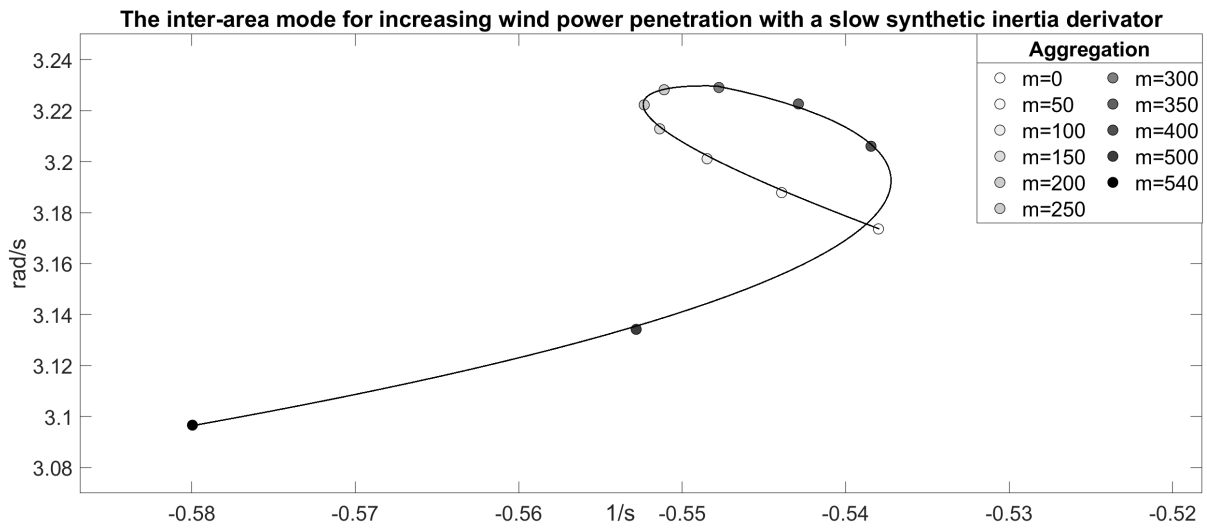


Figure 5.11: The inter-area mode for increasing wind power penetration with frequency controls, using a slow synthetic inertia derivator.

Table 5.5: The synchronous generator inertia, the synthetic inertia derivator time constant replicate towards the inter-area mode.

Synthetic inertia derivator			Synchronous generator inertia	
Time constant [s]	Gain	Inter-area mode	Inertia H [s]	Inter-area mode
0.55	2.21	$-0.598 \pm 2.974i$	3.5	$-0.598 \pm 3.262i$
0.375	2.06	$-0.565 \pm 2.906i$	5	$-0.565 \pm 3.218i$
0.3	2	$-0.536 \pm 2.877i$	6.5	$-0.538 \pm 3.174i$
0.23	1.79	$-0.498 \pm 2.875i$	10	$-0.498 \pm 3.0765i$
0.191	1.673	$-0.474 \pm 2.878i$	15	$-0.474 \pm 2.958i$

5.2.5 The parameters of the synthetic inertia derivator

The parameters' inertial effect on the inter-area mode

The presented results show that appropriate adjustment of the synthetic inertia derivator can replicate inertial behavior towards both dominant modes. Therefore, a concrete relation between the derivator and the physical inertia it represents towards the power system eigenvalues is developed. Table 5.5 shows the relation between the derivator time constant and the SG inertia it represents towards the inter-area mode. The gain of the derivator is adjusted to make the inertial contribution follow the kinetic energy stored in the wind turbine's rotation for the various time constants.

The inter-area mode movement in table 5.5 does, for the synthetic inertia derivator parameters follow the path in figure 5.6, and for the SG inertias follow the path in figure C.5. The derivator parameters are adjusted to obtain identical inter-area mode damping. The nominal controls are not designed based on the replaced SG inertia and do not have identical real parts. From figure 5.6, the synthetic inertia controller is, for a constant inertial contribution, unable to produce a real part below approximately $-0.61/s$. Hence, the controller has the lower limit $H = 3.5s$ of replicated physical inertia. For the presented parameters, the local mode in area two is little affected.

The table shows that SG inertia between 3.5-15s can be replicated using a derivator time constant between 0.55-0.191s. From figure 5.6, this is the interval 1.83-0.64 of the derivator factors. Hence, only a small portion of the potential derivator time constants are used to achieve great differences in the apparent inertia towards the power system eigenvalues. From the result, the derivator parameters can be expressed as a function of the SG inertia replaced by the wind turbines to achieve constant inertial impact on the inter-area mode. The synthetic inertia time constant T as a function of the desired inertia towards the eigenvalues are shown in equation 5.1. The required derivator gain K to keep the inertial contribution constant, in accordance with the kinetic energy of the wind turbine, is shown in equation 5.2. A derivator with these parameters effectively draws the inter-area mode movement in figure 5.6.

$$T(H) = 0.1550845 + \frac{689031.5449}{1 + (2303.89H)^{1.598037}} \quad (5.1)$$

$$K(H) = 1.446835 + \frac{1.00399}{1 + (0.14371H)^{1.63622}} \quad (5.2)$$

These are the derivator parameters required to keep the inter-area mode damping constant for complete wind power replacement of an SG with the inertia H . However, the damping of the inter-area mode during the wind power penetration increase is shown to vary.

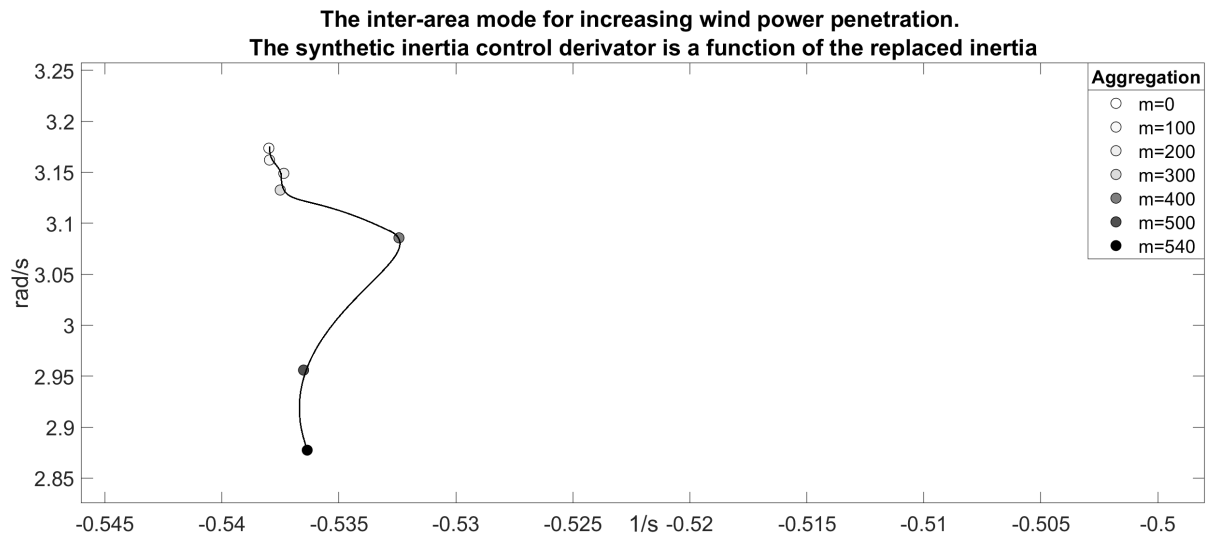


Figure 5.12: The inter-area mode for increasing wind power penetration with frequency controls, using adoptive synthetic inertia derivator parameters.

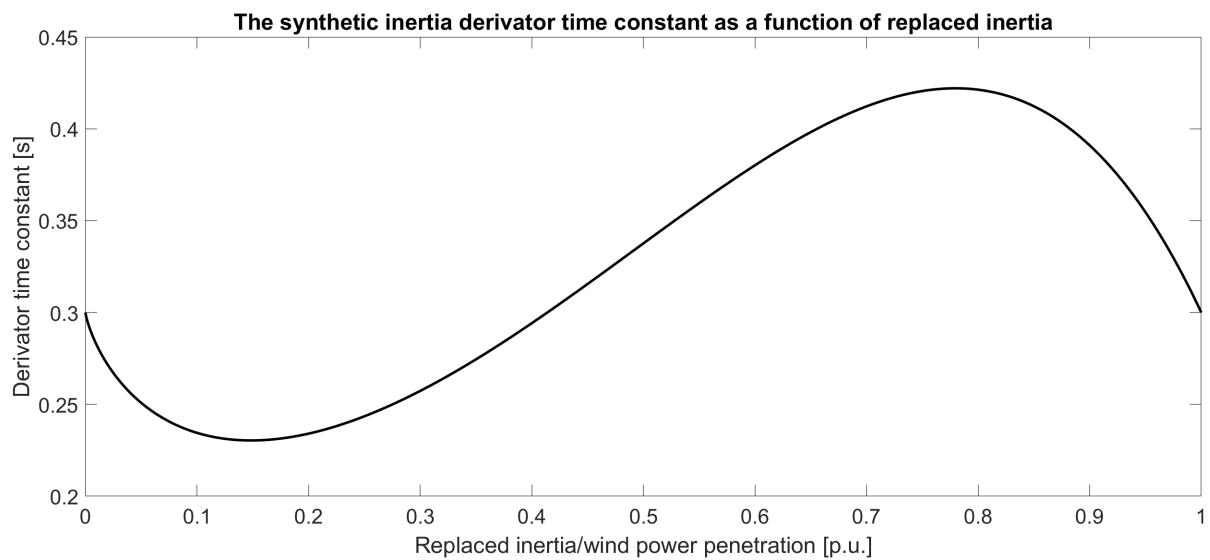


Figure 5.13: The parameters of the adoptive synthetic inertia derivator as a function of wind power penetration.

Parameter variation during the wind power penetration increase

For the wind power penetration increase in figure 5.10, the inter-area mode does not move in a straight line between the inter-area modes in table 5.5, but rather through circular motions. By adjusting the synthetic inertia derivator time constant appropriately during the penetration increase, the impact on the inter-area mode can be minimized. The inter-area mode movement in figure 5.12 is obtained when varying the derivator parameters as a function of the penetration level. The derivator time constant used in the figure as a function of the wind power penetration or the replaced inertia in p.u. is shown in equation 5.3.

$$T(H) = T(H = 1)(1 + 155 * (H - 0.991H^{0.99} - 0.009H^{5.2})) \quad H \text{ in p.u.} \quad (5.3)$$

In the equation, the time constant is in seconds, and the inertia replaced H in p.u. From table 5.5, $T(H = 1) = 0.3$ for an SG inertia of 6.5s. The equation is visualized in figure 5.13. The gain is adjusted to keep the inertial contribution constant. The time constant begins and ends the penetration increase with the value given by the SG inertia to be replaced. The variations in the time constant are developed to counteract the variations in the inter-area mode for increasing penetration. For perfect adjustment of the time constant, the inter-area mode could move in a straight line between the mode's position in the transition between synchronous- and wind power. The equation is not expected to be generic but illustrates the variety of possibilities in the synthetic inertia controller to improve the behavior of the inter-area mode.

5.2.6 The critical mode

Modes 18 and 19 in appendix B.7 cause instability for several sensitivity analyses of DFIG wind power with frequency controls. Figure 5.14 show modes 18 and 19 for increasing penetration of wind power with frequency controls. These modes do not exist for a pure synchronous generation but are introduced to the power system by the wind turbines. The modes' damping decreases during the wind power penetration increase.

To examine which states are linked to the modes, linear analysis is performed, shown in figure E.10. The modes are linked to the speed of the DFIG, in particular, the speed controller. The state of the synthetic inertia derivator x_1 , from figure A.11, has the greatest control over the modes. Based on the eigenvectors, parameter sweeps are performed on parameters related to the relevant states. The sensitivity analysis is shown in figure 5.15. The numerical values are chosen to highlight mode movement. The mode is highly sensitive to the gain of the speed controller, where the damping improves for a faster speed controller. The mode is also sensitive to the shaft inertia. From the previous section, the mode is not sensitive towards the time constant of the derivator. Therefore, only the mode movement for a varying inertia factor K_f is considered.

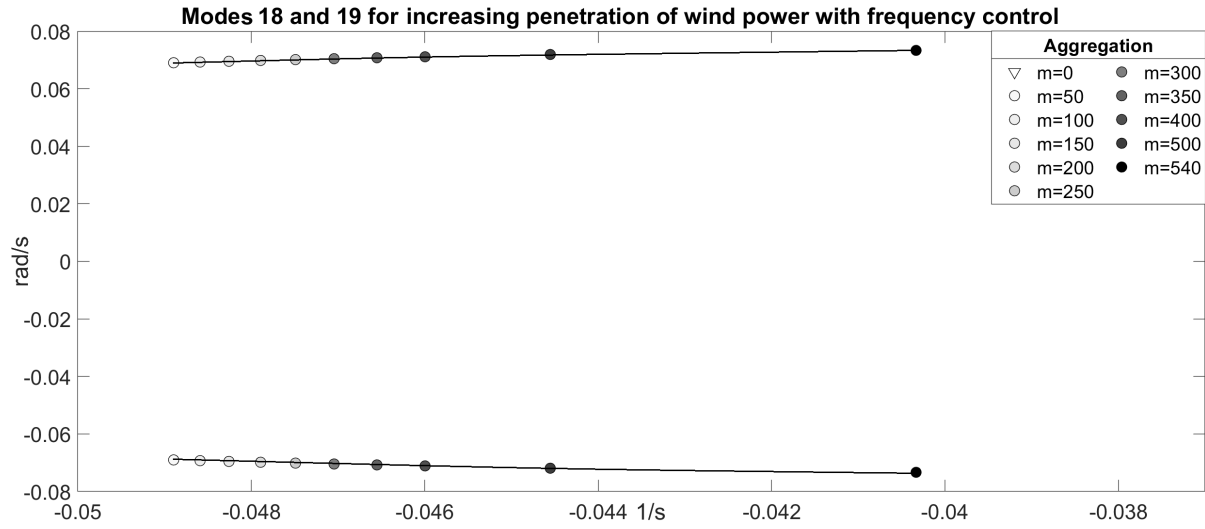
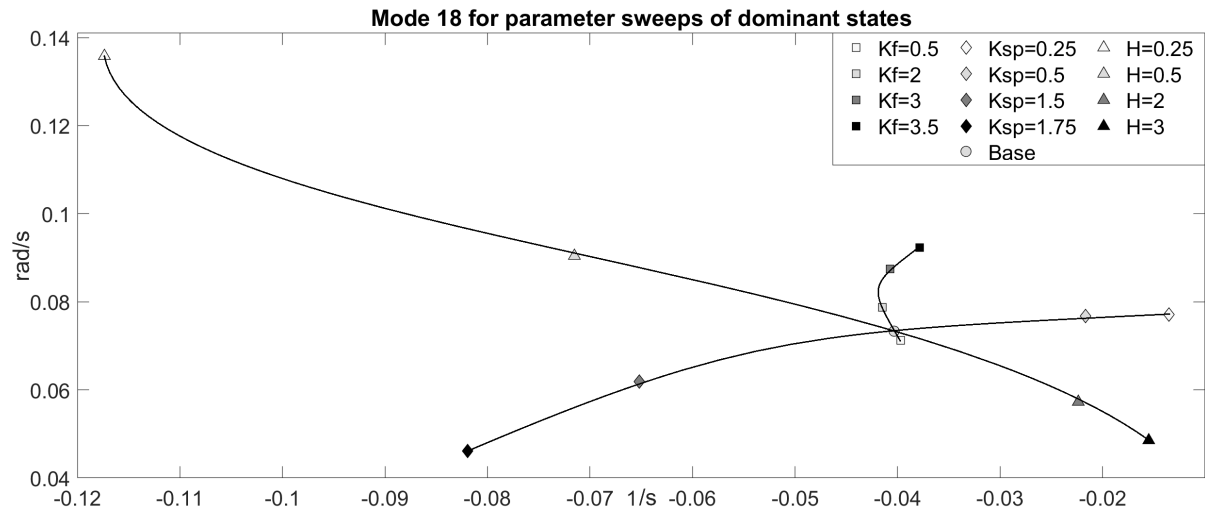


Figure 5.14: Modes 18 and 19 for increasing wind power penetration with frequency controls.

Figure 5.15: Sensitivity analysis of mode 18 for synthetic inertia gain K_f , speed controller gain K_{sp} , and inertia H .

The linear analysis shows that the mode is related to the speed of the machine, and hence, the power balance, explaining the mode sensitivities. A faster speed controller will keep the speed of the wind turbine more constant, increasing inertia will slow down any speed change, and decreasing inertial contribution will reduce the power imbalance the power manipulations represent. The mode's connection to the wind turbine speed also explains why increasing power reference manipulation of both synthetic inertia and primary control highly impacts and impairs the damping. It should be noted that adjustment of the speed controller does not realize stable operation for the exaggerated parameter sweeps, causing instability from modes 18 and 19. Nevertheless, as these modes become critical for several sensitivity analyses, the speed controller should be explored further to examine a possible stability enhancement. This is suggested as part of the further work on this thesis.

Table 5.6: The inter-area- and local mode for varying system loading. Generator 2 is wind power with frequency controls.

Loading factor	Inter-area mode		Local mode	
	Eigenvalue	zeta [%]	Eigenvalue	zeta [%]
0.5	$-0.972 \pm 3.101i$	29.91	$-1.138 \pm 9.803i$	11.53
0.75	$-0.722 \pm 3.108i$	22.63	$-1.055 \pm 9.761i$	10.75
1	$-0.536 \pm 2.877i$	18.32	$-0.968 \pm 9.633i$	10.00
1.25	$-0.356 \pm 2.465i$	14.29	$-0.910 \pm 9.516i$	9.52
1.5	$-0.191 \pm 1.962i$	9.69	$-0.888 \pm 9.403i$	9.4

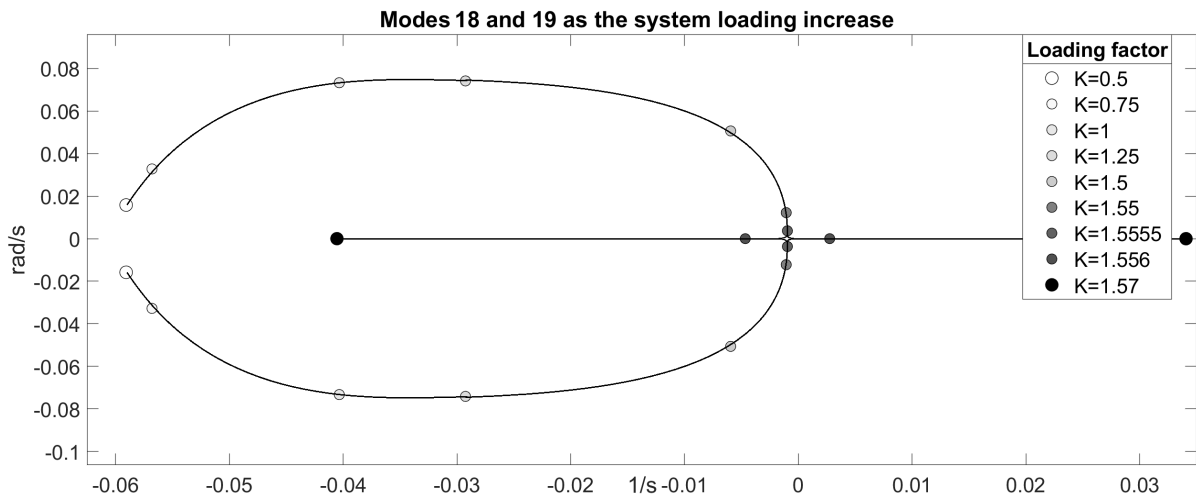


Figure 5.16: Modes 18 and 19 for increasing loading. Mode 17 and the zero modes are not included as no movement is obtained during the load increase.

5.2.7 Loading

Table 5.6 shows how the inter-area- and local modes change as the system loading is varied. The capacitive shunt batteries are unchanged, while both the active and reactive loading is varied. The generation percentage is varied similarly to the loading, with some difference to ensure that the slack bus (SG 1) is loaded equally to the other generators. The result shows how the real value dominates the movement of the modes. A high loading impairs the system's stability, causing a more oscillatory system. The inter-area- and local mode is stable during the load increase, but the critical modes 18 and 19 cause instability for loading above 155%. The movement of modes 18 and 19 is shown in figure 5.16. The modes perform a circular movement and become purely real, making the system unstable as the loading factor increases from 1.5555 to 1.556. The modes become more sensitive to the loading increase at the largest loadings. Modes 23 and 24 in appendix B.7 have the same movement pattern, but as these are better damped, modes 18 and 19 first obtain a positive real part. For 150% loading, the system voltage is reduced, and the generators are loaded between 103% and 112%, dependent on their reactive power delivery. Hence, this is not a feasible operation, despite the small-signal stable system.

Table 5.7: The inter-area mode for varying inter-tie line length. Generator 2 is wind power with frequency controls.

Length factor	Eigenvalue	zeta [%]
0.5	$-0.998 \pm 3.648i$	26.39
1	$-0.536 \pm 2.877i$	18.32
1.5	$-0.302 \pm 2.138i$	13.99

5.2.8 Inter-tie line length

A parameter sweep is performed of the inter-tie line length to analyze how the connection strength of the two areas affects the system stability. The power flow in the inter-tie line is kept constant by varying the active load in area two. The reactive power increase as the line length increase. The inter-area mode is the dominant mode primarily affected and, therefore, the mode of interest. Table 5.7 shows the development of the inter-area mode as the length of the inter-tie line increase. The damping of the mode is highly dependent on the line length and is reduced as the length increase. The inter-area mode remains stable as the length of the inter-tie line increase. The reactive power delivery is highly increased as the line length increase. As the length factor reaches 1.87, modes 18 and 19 cause instability, moving similarly as for the loading increase. The complete path of modes 18 and 19, and 20 is shown in figure 5.17, including an extensive amount of length-points to highlight the movement path.

An interesting relation is obtained between mode 20 and modes 18 and 19. Mode 20 was the mode causing instability for the inter-tie line length increase without frequency controls, at the same line length. As the line length increases, the imaginary part of modes 18 and 19 decreases. Like the load increase, the modes become purely real, moving on both the positive and negative real axes. When the mode, moving on the negative axis, encounters mode 20, they emerge and start to move towards the initial placement of modes 18 and 19. By comparing the movement of modes 18 and 19 with- and without frequency controls in figure 5.17 and D.14, it is clear that the frequency controls excite the critical modes 18 and 19.

Mode 17 and the zero modes are not affected by the inter-tie line length. This is shown in figure 5.17 where the symbols for $L = 0.5$ and $L = 2.2$ overlap. The analysis of modes 18 and 19 in Section 5.2.6 shows how the modes has the strongest link to the speed controller, change in turbine speed, and synthetic inertia controller. When mode 20 started to move for the increasing inter-tie line length increase without frequency controls, the same states became dominant. The system also becomes unstable at the same inter-tie line length. It should be noted that adjusting the parameters connected to these states does not allow for a stable system for the line lengths making the system unstable. Having a faster speed controller would improve the damping of modes 18 and 19 for nominal conditions, possibly affect the mode movement, but is not be able to counteract the positive real part for the longest lengths. Modes 18 and 19 do not cause instability before the extensive length factor $L = 1.87$. Hence, exaggerated lengths are required, and the system is considered robust towards the length variation.

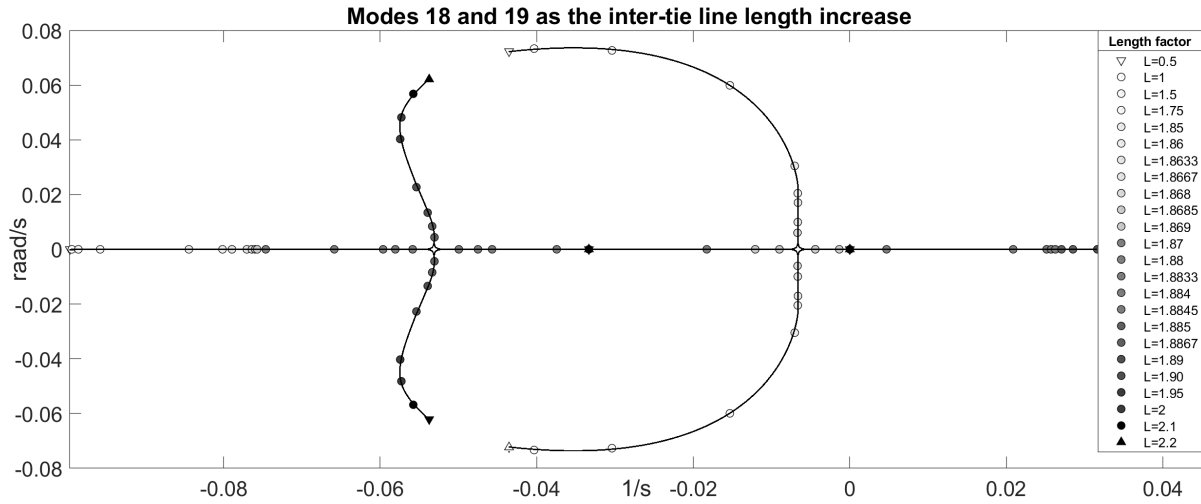


Figure 5.17: Modes 18 and 19, and 20 for increasing inter-tie line length.

5.2.9 Key findings

- For increasing penetration of DFIG wind power with frequency controls, both inter-area- and local mode damping increase. For implemented wind power, a great stability advantage is achieved by activating the frequency controls.
- The time constant and gain of the synthetic inertia controller can be adjusted separately to control the shape and size of the inertial contribution, respectively.
- The inter-area mode has a strong connection to the synthetic inertia derivator. The damping of the mode increase for an increased inertial contribution.
- The system eigenvalues react to a sensitive derivator similar to synchronous generator inertia.
- The synthetic inertia derivator parameters can be adjusted to achieve the desired apparent inertia towards the system eigenvalues, and at the same time, contribute with frequency support through an inertial contribution in accordance with the wind turbine's kinetic energy.
- DFIG wind turbines, particularly with synthetic inertia controls, create and excite small oscillatory modes.

Chapter 6

Discussion

This chapter provides a discussion of the results by comparing the results between the different system configurations. The validity and performance of the DIgSILENT model are evaluated. The impact on the local-, inter-area-, and small modes are separately discussed. The stability robustness is evaluated for the different generation techniques by system loading and inter-tie connection strength. Finally, general remarks and recommendations are considered for the synthetic inertia controller.

6.1 Model validation and evaluation

Thorough model validation is performed, where the eigenvalue profile obtained in DIgSILENT is compared with an equal system in Matlab Simulink. The comparison shows a good correspondence between the three dominant modes, both for synchronous- and wind power. This strengthens the validity of the stability development trends presented in this thesis. However, there are some fundamental differences in the wind turbine modeling between Simulink and DIgSILENT. Three significant modeling differences are DC-link voltage, designated PI regulated speed controller, and two-mass shaft. The lack of DC-link voltage dynamics in the DIgSILENT model excludes an oscillatory mode and its potential stability impact. In particular, the inertial contribution is a significant and fast power change and might cause considerable voltage variations in the DC-link voltage, affecting the presented results. On the other hand, the DC-link voltage mode obtained in Simulink is well damped, and therefore not expected to have a too considerable stability impact.

The speed controller and the state of the speed variation in the turbine shaft are shown to be essential states for the small modes. The development of the two small modes with the highest damping corresponds with the Simulink model, hence, validated. However, the critical mode is not obtained in Simulink due to the lack of speed controller and shaft modeling. The DIgSILENT modeling, particularly the shaft, is considered to be the more realistic modeling. Therefore, the critical mode is expected to be a real challenge when fitting synthetic inertia controllers in DFIG wind turbines. However, the development of the mode is not validated. For the model validation, the wind turbine models in both software are fully aggregated without distribution cables. Therefore, the impact from the aggregation technique and the neglected cables are not a part of the validation, and the impact on the results is not examined.

Every wind power analysis is performed at a constant deloading of about 12.5% and a constant wind speed. The deloading is large enough to realize the optimal power response for the presented frequency events, meaning no response saturation is required. The impact from a varying deloading or a varying wind speed is not considered. It might be argued that the case considered represents the highest impact on the power system. Decreasing the wind speed would cause a lower generator speed than the considered speed of 1.2p.u. and hence a smaller inertial contribution. Also, decreasing the deloading could trigger the need to saturate the inertial- or primary control contribution not to exceed the generator's power rating or the potential mechanical power in the wind. The voltage control from the wind turbines is, in the presented literature, said to have a significant impact on the eigenvalue profile. A strong sensitivity is also identified between the eigenvalues and the synchronous generators' AVR. The voltage support is not a focus in this thesis. Nevertheless, the wind turbines are equipped with voltage controllers for reactive power contribution, requiring a thorough synchronization between DIgSILENT and Simulink to achieve equal eigenvalue profiles. Remarkable correspondence is obtained in the stability impact when introducing the DFIG wind turbines in the two separate software. Therefore, the modeling is considered to have strong validity.

6.2 Comparison of the small-signal stability impact from the generation characteristics

6.2.1 General mode trajectories

Introducing DFIG wind power without frequency controls to the power system impairs the small-signal stability. For low wind power penetration, the local mode damping experience a slight reduction, and for increasing wind power penetration, the inter-area mode damping reduce. The dominant modes are for the base network well-damped, avoiding a critical impact. Therefore, increasing penetration of DFIG wind power without frequency controls reduces the frequency stiffness and worsens the nadir, and impairs the small-signal stability. The general trend in the presented literature is a possible stability enhancement but a decreased inter-area mode damping. This corresponds with the results in this thesis, where the inter-area mode damping decreases for all penetration levels. However, the stability enhancement from the local mode damping is only obtained for high penetration levels.

A very favorable impact is obtained by fitting frequency service controls in the wind turbines. Both frequency support and small-signal stability are improved using the synthetic inertia controller. The initial negative impact on the local mode is eliminated, and the inter-area mode damping is improved by the correct adjustment of the synthetic inertia derivator. The topic of synthetic inertia controller's impact on small-signal stability is not yet highly researched. The improving development trends presented in this thesis corresponds with the results from two articles presented within the topic.

6.2.2 The local modes

Introducing DFIG wind power without frequency controls to the power system, the local mode damping is reduced for low wind power penetration levels and increases for large penetration levels. When fitting frequency service controls in the wind turbines, the local mode damping improves for all penetration levels. The local mode in area one disappears as synchronous generator 2 is completely replaced with wind power, independent of the frequency controls.

A variety of eigenvalue sensitivity analyses is performed for synchronous generator inertia to understand the motivation of the eigenvalue movement when increasing the penetration of DFIG wind power. Since the wind power is connected in the area with the largest inertia, the well-documented local mode exchange occurs. Reducing the inertia in area one causes the synchronous generator speeds in area two to lose connection to their local mode while the synchronous generators in area one gain connection to the mode. In the same way, the synchronous generators in area two strengthen their connection to the local mode in area one. The connection change between the local modes and the synchronous generator groups does not occur at precisely the same inertias. This could be caused by various system characteristics and might be linked to the differences in area loading and the inter-area power flow.

Wind power penetration variations are used to understand the local modes' impact from the wind turbines. In particular, three configurations are considered for wind power penetration analysis to understand the local modes' development. These are wind power without frequency controls, with slow synthetic inertia derivator, and with nominal synthetic inertia controls. The increase of the imaginary part in the local mode is smaller than the comparing synchronous generator sensitivity analysis for all wind power penetration increases. From the analysis of synchronous generation, the high oscillation frequency increase in the local mode is motivated by the decreasing inertia. The lower imaginary part for the wind power penetration is favorable, as it increases the damping ratio of the mode. The nature of this limitation is not identified. It could either be considered an indication of a small inertial impact from the wind turbines or a consequence of the nature of the penetration increase, where the inertia of the synchronous generator is constant while its apparent power is reduced. Nevertheless, wind power penetration increase is part of the model validation, showing the same development of the imaginary part in Simulink. Despite the final size of the imaginary part, a remarkable resemblance is obtained between the penetration increases and the constructed synchronous generator justification scenarios, giving a strong indication of the motivation of the mode movement.

The local mode development for the wind power penetration increase without frequency controls is similar to reducing inertia and PSS gain in synchronous generator 2. This means that the local mode development is motivated by the reducing inertia the DFIG wind turbines present and the reducing portion of the power production equipped with the stabilizing feature of the PSS. The high correspondence between the two sensitivity analyses is further supported by the linear analysis, suggesting a DFIG control system with little control over the local modes. The local mode development is similar for the wind power penetration without- and with slow synthetic inertia controls. However, using a slow synthetic inertia controller, the movement bears the best resemblance to the sole reduction of synchronous generator inertia. Hence, the replacement of PSS-equipped power no longer seems to be a driving factor for the local modes' when equipping the wind power with synthetic inertia controls.

Which area's local mode is affected by the wind power penetration increase indicates the inertia balance between the areas. For inertia reduction of synchronous generator 2 and the wind power penetration increases without- and with slow synthetic inertia controls, the local mode in area two is affected. This is caused by the change in inertia balance, further causing the change in connection strength between the local modes and synchronous generator groups. However, for the nominal synthetic inertia controller, the local mode in area one is affected. This indicates an unchanged inertia balance between the two areas. Hence, the local modes react to a sensitive synthetic inertia derivator in the same way as for the physical inertia of a synchronous generator. The movement of the local mode is, for wind power penetration increase with the nominal frequency controls, dominated by the real part, highly improving the damping. As the apparent inertia towards the local mode seems fairly unaffected, the movement of the mode does not resemble any of the inertia changing sensitivity analyses of synchronous generation. However, the local mode movement resembles the synchronous generation's load reduction, indicating a movement motivated by the reducing portion of synchronous power.

6.2.3 The inter-area mode

Introducing DFIG wind power without frequency controls to the power system impair the inter-area mode damping. When fitting frequency service controls in the wind turbines, the inter-area mode damping is highly improved. Wind power with the appropriate synthetic inertia tuning can also improve the inter-area mode damping compared to synchronous generation. From the analysis of synchronous generation, the damping of the inter-area mode is expected to increase for decreasing inertia. However, the damping decrease for increasing penetration of wind power without frequency controls. The system linearization shows that the DFIG control system holds a control over the inter-area mode, and a strong connection is identified from the sensitivity analysis. This might be part of the root of the divided literature on eigenvalue impact from DFIG wind power. The choice of control parameters and -topology highly impact the system stability. The controls in the DIgSILENT model are chosen to give the best dynamical performance, and at the same time, be compatible with the synthetic inertia derivator. Despite the presented modeling differences between the DFIG wind turbines in DIgSILENT and Simulink, a very strong correspondence is obtained in the inter-area mode movement for increasing wind power penetration.

Excessively slowing down the DFIG controls improves the inter-area mode damping. The speed of the regulators is essential for the dynamic performance of the wind turbines. Having slow controls strengthens the connection between the mechanical speed of the wind turbine and the electrical frequency of the power system. The development of the inter-area mode shows a greater resemblance to the decreasing inertia and PSS gain of synchronous generator 2 when performing the penetration increase with wind power having deactivated power regulators, symbolizing very slow regulators. The slow power controls cause a natural inertial response from the wind turbines. This is contradictory and does not explain the inter-area mode's better replication of reducing inertia and PSS gain in synchronous generator 2. However, the great change in the inter-area mode's movement path confirms that the DFIG controls significantly impact the mode. Fast controllers are required to achieve the fast power reference change from the synthetic inertia controls. The stability impact from the speed of the DFIG controls using synthetic inertia controls is not examined, as a varying speed would cause varying frequency support, hence a compound system impact.

By introducing the synthetic inertia controls to the wind turbine, the inter-area mode damping ratio is enhanced from 13.13% to 18.33%. Hence, a clear stability advantage operating the wind turbines with synthetic inertia controls. The state representing the synthetic inertia derivator is, above the synchronous generator speeds, the state with the highest control over the inter-area mode. The damping ratio of the inter-area mode is also improved when replacing the fully controlled synchronous generator with wind power equipped with complete frequency service controls. During the wind power penetration increase, circular movements are obtained in the inter-area mode path, causing a slight reduction in the damping.

The inter-area mode is highly sensitive towards the synthetic inertia derivator, where a connection is developed between the speed of the derivator and the physical inertia it represents towards the mode. A sensitive derivator, similarly to synchronous generator inertia, reduces the inter-area mode damping. The

derivator can therefore be adjusted to represent the inertia giving the best small-signal stability, and at the same time provide frequency support by an inertial contribution defined by its kinetic energy. Equipping the wind turbines with controls to contribute with primary control, similar to the synchronous generator turbine governor, improves the inter-area mode damping. The damping improvement of introducing the nominal primary control is minor, where the primary control has a greater impact on the dynamic frequency convergence process than on the eigenvalue profile.

6.2.4 The small modes

From various synthetic inertia sensitivity analyses, movement is obtained in three pairs of small oscillatory modes. The modes have an amplitude below 10% of the inter-area mode. Particularly modes 18 and 19 can challenge the system stability. These modes are introduced to the system by the wind turbines, independent of the frequency controls. The modes are closely linked to the speed variation of the DFIG, where the speed controller, change of turbine speed, and the synthetic inertia derivator are the states with the strongest connection. The two best-damped pairs of small oscillatory modes, 23 and 24, and 31 and 32, originate from synchronous generation, both related to generator speed and PSS. However, when synchronous generator 2 is replaced with wind power, the DFIG speed-related states become dominant.

The synthetic inertia derivator holds the greatest control over all the small oscillatory modes. Because of the connection to the DFIG speed, the two components of the power reference manipulation from the frequency controller highly impact the modes. Exaggerated parameters are required, also for the critical mode, to obtain critical movement. Increasing penetration of wind power reduces the damping of the small modes, particularly the critical mode. However, the critical mode remains fairly constant for increasing wind power penetration without frequency control, emphasizing the synthetic inertia controls' impact on the mode. The speed controller of the wind turbine has a strong connection to the critical mode and can be adjusted to achieve better damping at nominal conditions. However, for the exaggerated parameter sweeps causing instability, control adjustment does not achieve stable operation.

For the inter-tie line increase for wind power without frequency control, the small mode eventually causing the instability is also motivated by the DFIG speed-related states. The movement of the small oscillatory modes is not analyzed in detail for the case of wind power without frequency controls, as minor movement is obtained. Nevertheless, all three modes exist, showing that the synthetic inertia derivator does not impose any of the modes on the system but rather excites them. From the model validation, the critical modes are not obtained in Simulink. Hence, these modes are not validated. This is expected to result from the lack of a designated PI regulated speed controller and a two-mass shaft model in the verification software Simulink. The states these two represent are dominant in all three small modes. However, despite the difference in modeling, the movement of the two best damped small oscillatory modes is validated by Simulink for increasing wind power penetration without frequency control. Hence, introducing wind turbines, particularly with frequency controls, will create and excite small modes in the power system, where the driving states are related to the speed variation of the DFIG.

6.2.5 Loading

The system loading is varied in all three power system configurations to analyze differences in the stability impact for wind- and synchronous power. For the highest loading of 150%, the generation units of all grid configurations are overloaded. This is not a feasible operation state but considered to examine differences in development trends for the three configurations. Different numerical values would be obtained by fine-tuning the controls, particularly in the voltage controller of the wind turbines. The constructed scenarios where the wind turbines contribute equally as the synchronous generators for a varying loading are not realistic and require a wind speed following the system loading. Also, for wind turbines with frequency controls, an overloaded wind turbine can not supply frequency service. Hence, the loading scenarios and numerical values are not expected to be accurate but to indicate the development trends.

The system consisting of purely synchronous generation shows the most favorable stability impact for the increasing load. The damping of all three dominant modes reduce as the loading increase but remains well damped. When generator 2 is wind power without frequency controls, the nominal inter-area mode damping is lower. The inter-area mode also becomes more sensitive to the load increase, causing the mode damping to be highly reduced for the loading of 125% and to cause instability at the highest loading 150%. When generator 2 is wind power, the local mode in area two seems to be less affected by the load increase, probably caused by the reactive power distribution defined by the voltage regulators. When including the frequency controls in the wind turbines, the nominal inter-area mode damping is higher. Even though the damping ratio nominally is higher than for a pure synchronous generation, the mode obtains lower damping ratios as the loading increase. This is similar to the result from the wind turbines without frequency controls, where the inter-area mode damping becomes more sensitive to loading change. Similarly, the local mode in area two also seems to be less affected.

By including the frequency controls, the modes representing the dominant modes for nominal conditions remain stable for the selection of loading. However, the system obtains a pair of poorly damped modes, 18 and 19, for the largest loading, making the system unstable as the loading reaches 155.6%. Extensive and unrealistic loading is required to make these modes critical. A more robust and less loading sensitive stability is achieved by including the frequency controls in the wind turbines.

6.2.6 Inter-tie line length

Similar to the system loading, the connection strength of the two areas is varied for all three power system configurations to analyze differences in the stability impact. During the inter-tie line variation, the power flow between the two areas is kept constant. As the line length increase, the reactive power demand increase, reducing the voltage at the load buses. The foundation for the line length increase is important for the obtained eigenvalues. Different eigenvalues are obtained if not keeping the active power flow constant or if changing the capacitive shunt batteries according to the reactive power demand. The focus is the stability impact from the different power generation characteristics. Hence, the numerical values are not of particular interest but rather the development trend differences.

The inter-area mode remains stable between the length factors 0.5 to 1.5 for all three configurations. Like the load variation, the mode is more sensitive for the inter-tie line length when generator 2 is wind power. When increasing the length factor towards 2, the system with synchronous generation remains stable but struggles to keep the inter-tie line power flow constant because of the high reactive power demand. The system becomes unstable for both wind power configurations at the length factor 1.87, but not by the inter-area mode. For wind power without frequency controls, a small mode is excited by the states related to the DFIG speed, particularly the speed controller. For wind power with frequency controls, the critical modes 18 and 19 cause the instability, also excited by the speed controller, but together with the synthetic inertia derivator. Modes 18 and 19 remain fairly constant for the length increase without frequency controls, emphasizing the synthetic inertia derivator's excitation of the mode.

Even though synchronous generation causes the least impact on the inter-area mode from the inter-tie connection strength, the power system stability is robust for the wind power configurations. The great inter-tie length of $1.87 \cdot 220\text{km}$ is required to provoke instability for the wind power configurations. When introducing frequency controls in the wind turbines, both the initial inter-area mode damping and the negative impact from the length variation is reduced.

6.3 The synthetic inertia controller

Both improved small-signal stability and frequency stability are achieved by including the synthetic inertia controller in the wind turbines. By manipulating the power reference of the wind turbines with a contribution proportional to the change in frequency, an inertial contribution similar to the natural inertial response from a synchronous generator is obtained. Through the wind turbine's rotational speed, the contribution is made proportional to the wind turbine's stored kinetic energy, ensuring a power contribution not extensively decelerating the wind turbine.

The synthetic inertia derivator defines the link between the stored kinetic energy of the wind turbine rotation and frequency oscillations in the power system, effectively working as the brakes of an oscillating system. Potentially, the gain of the derivator can make the wind turbine contribute with inertial power larger than what the stored kinetic energy allows, larger than that of a synchronous generator. In the same way, the time constant of the derivator can make the wind turbine replicate generator inertias towards the eigenvalue profile, independent of the wind turbine inertia. The power of the synthetic inertia derivator is emphasized in the linear analysis, where the derivator holds the greatest control over the inter-area mode. Therefore, the adjustment of the derivator parameters is essential for both frequency support and small-signal stability.

The wind turbines' inertial contribution should correspond with the stored kinetic energy of wind turbine rotation, causing a generator deceleration similar to that of the synchronous generators in the system. However, the desired apparent inertial impact on the system eigenvalues, given by the synthetic inertia derivator time constant, is not as unambiguous. The inter-area mode damping decrease when either the synchronous generator inertia- or the derivator sensitivity increase. From the perspective of inter-area mode, low apparent inertia is favorable, below the inertia of the synchronous generator being replaced. For the local modes, from the analysis of synchronous generator inertia, decreasing inertia cause decreasing damping ratio. The same trend is obtained for increasing wind power penetration with a slow synthetic inertia derivator, particularly for low penetration levels. Therefore, the general recommendation is to make the wind turbines impact the system inertia as little as possible by making the apparent inertia from the wind turbine equal to the synchronous generator being replacing, or to a typical synchronous generator. This will both increase the local mode damping and reduce the oscillation frequency of the inter-area mode, improving the damping ratio of both dominant power system eigenvalues.

For this purpose, an equation is developed, relating the synthetic inertia derivator time constant to the physical inertia it represents towards the inter-area mode. The real part dominates the movement of the inter-area mode when varying the sensitivity or the time constant of the derivator. Therefore, the equation is based on equal inter-area mode damping. When changing the time constant of the derivator, the gain has to be adjusted accordingly to keep the inertial contraction constant and in accordance with the wind turbine's stored kinetic energy. The relation between the time constant and the physical inertia it represents towards the inter-area mode is developed between a synchronous generator and a wind farm with equal power ratings. It is based only on a single power system configuration and a single location of wind power implementation. Therefore, the numerical values are not expected to be general but give a numerical example to a generic relation.

Chapter 7

Conclusion and further work

This chapter concludes the fulfillment of the thesis objective. First, a short description of key results is given, focusing on the impact of the synthetic inertia controller, including remarks and recommendations. Finally, suggestions for further work are proposed.

7.1 Conclusion

This thesis presents a thorough analysis of how synthetic inertia controllers in doubly-fed induction generator wind turbines affect the small-signal stability of the synchronous-based power systems. An extensive analysis is performed for wind power without frequency controls and synchronous generation. This provides insight into the DFIG wind turbines' impact on the power system stability and serves as a base to analyze the root of the eigenvalue movement for the various sensitivity analyses. Of particular focus is the inter-area- and local modes, as these are the dominant eigenvalues. The local mode in area one disappears for complete wind power replacement of synchronous generator two, regardless of frequency controls. Wind power without frequency controls impairs the small-signal stability. The local mode damping reduces for low penetration levels, where the movement is mainly motivated by the reducing system inertia and the portion of power generation equipped with PSSs. The inter-area mode damping reduces for all penetration levels. However, the movement is not motivated by the reducing inertia but by the DFIG controls, where fast power and rotor current regulators reduce the damping. When including frequency service controls in the wind turbines, the damping of both dominant eigenvalues improves.

When introducing DFIG wind turbines to the power system, particularly with frequency controls, the wind turbines will create and excite the power system's small oscillatory eigenvalues. These eigenvalues gain a strong connection to the states related to the DFIG wind turbine's speed, particularly the speed controller and synthetic inertia derivator. Even though exaggerated parameter changes are required to provoke instability from these modes, special considerations should be given when tuning the controls, especially the DFIG speed controller. Implementing DFIG wind power in the power system, a slight reduction in the small-signal stability robustness is obtained. In particular, the inter-area mode becomes more sensitive to system changes. However, using frequency controls in the wind turbines, the power system has a nominal well-damped eigenvalue profile. Therefore, sizeable system changes are required to impose stability challenges.

The frequency service controls are composed of a synthetic inertia controller and primary control. The primary control has the similar, minor improving impact on the inter-area mode damping as the droop controller of the synchronous generator turbine governor. The controller in focus, the synthetic inertia controller, modifies the power reference of the wind turbines during a changing frequency to release or absorb an inertial power counteracting the frequency change, effectively replicating the frequency behavior of a synchronous generator. However, the synthetic inertia controller does not only improve the frequency quality but also strengthen the power system's small-signal stability. In particular, the inter-area mode, but also the local mode damping, highly improves when including the synthetic inertia controller in the wind turbines. The synthetic inertia derivator represents a powerful state in the power system. It effectively defines the link between the stored kinetic energy of the wind turbine rotation and the frequency oscillations in the power system. Furthermore, the derivator represents the power system state with the greatest control over the inter-area mode, above the speed of the synchronous generators.

The synthetic inertia derivator is composed of a gain and a time constant. The gain affects the size of the power reference modification and the resulting inertial contribution. The derivator gain can potentially make the wind turbines contribute with inertial power larger than a synchronous generator, larger than what the stored kinetic energy allows, causing excessive speed change in the wind turbine. Increasing the size of the inertial contribution improves the inter-area mode damping. The time constant of the synthetic inertia derivator defines the shape of the inertial contribution. Decreasing the time constant makes the derivator more sensitive to frequency changes, resulting in an inertial contribution shape more similar to that of a synchronous generator. In addition, decreasing the derivator time constant replicates increasing synchronous generator inertia towards the system eigenvalues. Hence, the apparent inertia the wind turbines represent towards the small-signal stability is defined by the sensitivity of the synthetic inertia derivator. Therefore, by correctly adjusting the derivator parameters, the wind turbines can impact the small-signal stability with inertia similar to a synchronous generator, and at the same time, contribute to frequency support by an inertial contribution in accordance with the wind turbines' stored kinetic energy.

A relation between the time constant of the synthetic inertia derivator and the physical inertia it represents towards the inter-area mode is developed. Only a small time constant change is required to affect the apparent inertia towards the inter-area mode significantly. The synthetic inertia derivator should be adjusted to replicate the apparent inertia causing the most favorable impact on both the inter-area- and local modes. This can be achieved by replicating the inertia of the synchronous generator being replaced or, generally, the inertia of a typical synchronous generator. The numerical values in the developed relation are not expected to be generic but to be used as a starting point for further fine-tuning when fitting synthetic inertia controllers in synchronous-based power systems. Changing the time constant of the synthetic inertia derivator, both the shape and size of the inertial contribution are affected. Therefore, as the time constant is adjusted, the gain of the derivator must be adjusted accordingly to ensure an inertial contribution in accordance with the stored kinetic energy. By this recommendation, wind turbines equipped with frequency service controls, including a synthetic inertia controller, can both provide frequency support through an inertial contribution and have a favorable impact on the power system's small-signal stability.

7.2 Further work

This thesis provides insight into how DFIG wind turbines with frequency service control impact the power system's small-signal stability. However, much research remains to understand the full impact. Therefore, suggestions for further work on the thesis are included. A part of the contribution from the thesis is the developed, verified DIgSILENT model. The DIgSILENT model and the verification model in Simulink are submitted to the project supervisor for a possible successor. Therefore, further development of the models is relevant.

- For the complete analysis in this thesis, all synchronous generators have steam turbines and are equipped with PSSs. Therefore, an interesting study case is to analyze if the small-signal stability is impacted differently with different synchronous generator turbines and PSSs.
- For the complete analysis in this thesis, only a single power system and only a single location of wind power implementation are considered. Several power system configurations and implementation locations should be analyzed to investigate the presented results' generic validity.
- The wind turbine deloading is constant for all presented results. The impact of the deloading could be examined, where the potential impact from contribution saturation should be considered.
- The speed controller is not explicitly analyzed. The controller holds a strong control over the small modes, where an increased gain is shown to improve the critical mode's damping. The possibilities to improve the damping of the small modes should be examined further together with the speed controller's impact on the dominant modes.
- As the DIgSILENT- and Simulink model used for verification is made available to a possible successor, the model verification could be expanded to include the frequency controls. For further model verification, the key result in this thesis, the sensitivity between the derivator time constant and the inter-area mode, should be considered. This requires the development of the frequency service controls in the Simulink model. Also, the critical mode could be considered in further model validation. It is also relevant to implement the DC-link voltage dynamics in the DIgSILENT model to analyze possible impacts. If implementing frequency controls in the Simulink model, this model could be used to analyze the DC-link voltage's impact.

References

- [1] Silde Johannes. “Simulation model development of a DFIG wind turbine with frequency service for small-signal stability analysis”. In: (2020).
- [2] United Nations Climate Change. “The Paris Agreement”. In: (2015). URL: <https://unfccc.int/process-and-meetings/the-paris-agreement/the-paris-agreement>.
- [3] United Nations. “Sustainable Development Goal 7: Ensure access to affordable, reliable, sustainable and modern energy”. In: (). URL: <https://www.un.org/sustainabledevelopment/energy/>.
- [4] International Renewable Energy Agency. “Future of Wind:investment, technology, grid integration and socio-economic aspects (A Global Energy Transformation paper)”. In: 88 (Oct. 2019).
- [5] Ayman Attya and Jose Luis Dominguez-Garcia. “Provision of Ancillary Services by Wind Power Generators”. In: *Advances in Modelling and Control of Wind and Hydrogenerators*. Ed. by Amir Ebrahimi. Rijeka: IntechOpen, 2020. Chap. 6. DOI: 10.5772/intechopen.90235. URL: <https://doi.org/10.5772/intechopen.90235>.
- [6] O. Anaya-Lara et al. “Intelligent control mechanisms for provision of virtual inertia”. In: *Integrated Research Programme on Wind Energy* (2016).
- [7] B. Fox et al. *Wind Power Integration: Connection and System Operational Aspects*. Energy Engineering. Institution of Engineering and Technology, 2007. Chap. 3. ISBN: 9780863414497. URL: <https://books.google.no/books?id=LTuo24RfTGoC>.
- [8] José Luis Domínguez-García et al. “Power oscillation damping supported by wind power: A review”. In: *Renewable and Sustainable Energy Reviews* 16.7 (2012), pp. 4994–5006. ISSN: 1364-0321. DOI: <https://doi.org/10.1016/j.rser.2012.03.063>. URL: <http://www.sciencedirect.com/science/article/pii/S136403211200247X>.
- [9] P. Kundur, N.J. Balu, and M.G. Lauby. *Power System Stability and Control*. EPRI power system engineering series. McGraw-Hill Education, 1994. Chap. 12. ISBN: 9780070359581. URL: <https://books.google.no/books?id=2cbvyf8Ly4AC>.
- [10] Patricio Salmerón Revuelta, Salvador Pérez Litrán, and Jaime Prieto Thomas. “8 - Distributed Generation”. In: *Active Power Line Conditioners*. Ed. by Patricio Salmerón Revuelta, Salvador Pérez Litrán, and Jaime Prieto Thomas. San Diego: Academic Press, 2016, pp. 285–322. ISBN: 978-0-12-803216-9. DOI: <https://doi.org/10.1016/B978-0-12-803216-9.00008-0>. URL: <http://www.sciencedirect.com/science/article/pii/B9780128032169000080>.

- [11] G. Pepermans et al. “Distributed generation: definition, benefits and issues”. In: *Energy Policy* 33.6 (2005), pp. 787–798. ISSN: 0301-4215. DOI: <https://doi.org/10.1016/j.enpol.2003.10.004>. URL: <http://www.sciencedirect.com/science/article/pii/S0301421503003069>.
- [12] X. Yang and K. Bai. “Development and prospects of offshore wind power”. In: *2010 World Non-Grid-Connected Wind Power and Energy Conference*. 2010, pp. 1–4. DOI: 10.1109/WWEC.2010.5673138.
- [13] The European Union. “COMMISSION REGULATION (EU) 2016/631”. In: Apr. 2016.
- [14] Statnett. “Nasjonal veileder for funksjonskrav i kraftsystemet (NVF)”. In: July 2020. Chap. 14.
- [15] J. Machowski, J.W. Bialek, and J. Bumby. *Power System Dynamics: Stability and Control*. Wiley, 2011. Chap. 5. ISBN: 9781119965053. URL: <https://books.google.no/books?id=wZv92UdKxi4C>.
- [16] “Introduction to A Wind Energy Generation System”. In: *Doubly Fed Induction Machine*. John Wiley & Sons, Ltd, 2011. Chap. 1, pp. 1–85. ISBN: 9781118104965. URL: <https://onlinelibrary.wiley.com/doi/abs/10.1002/9781118104965.ch1>.
- [17] Gonzalo Abad and Grzegorz Iwanski. “Properties and Control of a Doubly Fed Induction Machine”. In: *Power Electronics for Renewable Energy Systems, Transportation and Industrial Applications*. John Wiley & Sons, Ltd, 2014. Chap. 10, pp. 270–318. ISBN: 9781118755525. URL: <https://onlinelibrary.wiley.com/doi/abs/10.1002/9781118755525.ch10>.
- [18] John Fletcher and Jin Yang. “Introduction to the Doubly-Fed Induction Generator for Wind Power Applications”. In: *Paths to Sustainable Energy*. Ed. by Jatin Nathwani and Artie Ng. Rijeka: IntechOpen, 2010. Chap. 14. DOI: 10.5772/12889. URL: <https://doi.org/10.5772/12889>.
- [19] Maurício BC Salles et al. “Crowbar system in doubly fed induction wind generators”. In: *Energies* 3.4 (2010), pp. 738–753.
- [20] Q. Gao and R. Preece. “Improving frequency stability in low inertia power systems using synthetic inertia from wind turbines”. In: *2017 IEEE Manchester PowerTech*. 2017, pp. 1–6. DOI: 10.1109/PTC.2017.7980836.
- [21] H. Dharmawardena, K. Uhlen, and S. S. Gjerde. “Modelling wind farm with synthetic inertia for power system dynamic studies”. In: *2016 IEEE International Energy Conference (ENERGYCON)*. 2016, pp. 1–6. DOI: 10.1109/ENERGYCON.2016.7514098.
- [22] X. Tian et al. “Coordinative control strategy of virtual inertia and primary frequency of DFIGs based wind farms”. In: *2016 IEEE PES Asia-Pacific Power and Energy Engineering Conference (APPEEC)*. 2016, pp. 2169–2174. DOI: 10.1109/APPEEC.2016.7779871.
- [23] D. Sun et al. “Influence of virtual inertia in wind turbines on large scale power grid frequency characteristics”. In: *8th Renewable Power Generation Conference (RPG 2019)*. 2019, pp. 1–6. DOI: 10.1049/cp.2019.0274.
- [24] J. Morren et al. “Wind turbines emulating inertia and supporting primary frequency control”. In: *IEEE Transactions on Power Systems* 21.1 (2006), pp. 433–434.

- [25] P. Kundur, N.J. Balu, and M.G. Lauby. *Power System Stability and Control*. EPRI power system engineering series. McGraw-Hill Education, 1994. Chap. 3. ISBN: 9780070359581. URL: <https://books.google.no/books?id=2cbvyf8Ly4AC>.
- [26] L. Holdsworth, J. B. Ekanayake, and N. Jenkins. “Power system frequency response from fixed speed and doubly fed induction generator-based wind turbines”. In: *Wind Energy* 7.1 (2004), pp. 21–35. DOI: 10.1002/we.105. eprint: <https://onlinelibrary.wiley.com/doi/pdf/10.1002/we.105>. URL: <https://onlinelibrary.wiley.com/doi/abs/10.1002/we.105>.
- [27] O. Anaya-Lara et al. “Contribution of DFIG-based wind farms to power system short-term frequency regulation”. In: *IEE Proceedings - Generation, Transmission and Distribution* 153.2 (2006), pp. 164–170. DOI: 10.1049/ip-gtd:20050264.
- [28] DIgSILENT PowerFactory. “User Manual”. In: (2020).
- [29] *Performance of Three PSS for Interarea Oscillations*. 2020. URL: <https://www.mathworks.com/help/phymod/sps/ug/performance-of-three-pss-for-interarea-oscillations.html>.
- [30] DIgSILENT PowerFactory. “Technical Reference, DIgSILENT Doubly Fed Induction Generator Templates”. In: (2020).
- [31] A. Shafiu et al. “Aggregated Wind Turbine Models for Power System Dynamic Studies”. In: *Wind Engineering* 30.3 (2006), pp. 171–185. URL: <https://doi.org/10.1260/030952406778606205>.
- [32] H. Liu and Z. Chen. “Aggregated Modelling for Wind Farms for Power System Transient Stability Studies”. In: *2012 Asia-Pacific Power and Energy Engineering Conference*. 2012, pp. 1–6. DOI: 10.1109/APPEEC.2012.6307118.
- [33] J. Machowski, J.W. Bialek, and J. Bumby. *Power System Dynamics: Stability and Control*. Wiley, 2011. Chap. 10. ISBN: 9781119965053. URL: <https://books.google.no/books?id=wZv92UdKxi4C>.
- [34] José Rueda and F. Shewarega. “Small Signal Stability of Power Systems with Large Scale Wind Power Integration”. In: Jan. 2009.
- [35] Espen Hagstrøm, Ian Norheim, and Kjetil Uhlen. “Large-scale wind power integration in Norway and impact on damping in the Nordic grid”. In: *Wind Energy* 8 (July 2005), pp. 375–384. DOI: 10.1002/we.168.
- [36] H.M. Fayek et al. “The impact of DFIG and FSIG wind farms on the small signal stability of a power system”. In: *2014 5th International Conference on Intelligent and Advanced Systems (ICIAS)*. 2014, pp. 1–6. DOI: 10.1109/ICIAS.2014.6869505.
- [37] Olimpo Anaya-Lara et al. “Wind Energy Generation: Modelling and Control”. In: Jan. 2009. Chap. 7, Influence of Rotor Dynamics on Wind Turbine Operation, pp. 121–133. ISBN: 0470714336.
- [38] E. Prasanthi and K. N. Shubhanga. “Stability analysis of a grid connected DFIG based WECS with two-mass shaft modeling”. In: *2016 IEEE Annual India Conference (INDICON)*. 2016, pp. 1–6. DOI: 10.1109/INDICON.2016.7838953.

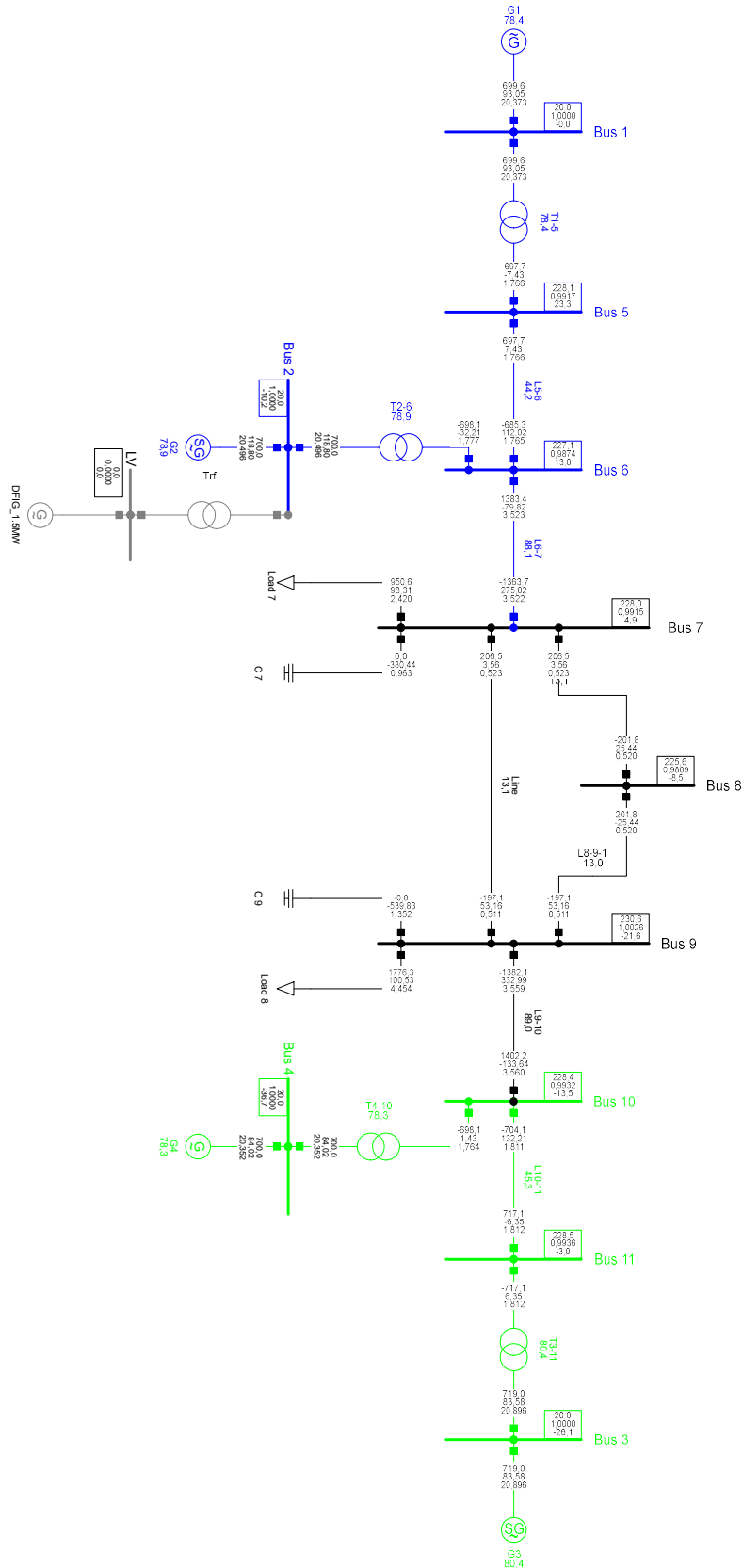
- [39] Yu Songtao et al. “Torsional vibration characteristic study of the grid-connected DFIG wind turbine”. In: *IOP Conference Series: Earth and Environmental Science* 52 (Jan. 2017), p. 012022. DOI: 10.1088/1742-6596/52/1/012022.
- [40] Libo Liu et al. “A Damping Method for Torsional Vibrations in a DFIG Wind Turbine System Based on Small-Signal Analysis”. In: *Electric Power Components and Systems* 45.5 (2017), pp. 560–573. DOI: 10.1080/15325008.2016.1274344. URL: <https://doi.org/10.1080/15325008.2016.1274344>.
- [41] R.D. Fernández, R.J. Mantz, and P.E. Battaiotto. “Potential contribution of wind farms to damp oscillations in weak grids with high wind penetration”. In: *Renewable and Sustainable Energy Reviews* 12.6 (2008), pp. 1692–1711. ISSN: 1364-0321. DOI: <https://doi.org/10.1016/j.rser.2007.01.013>. URL: <https://www.sciencedirect.com/science/article/pii/S1364032107000330>.

Appendix

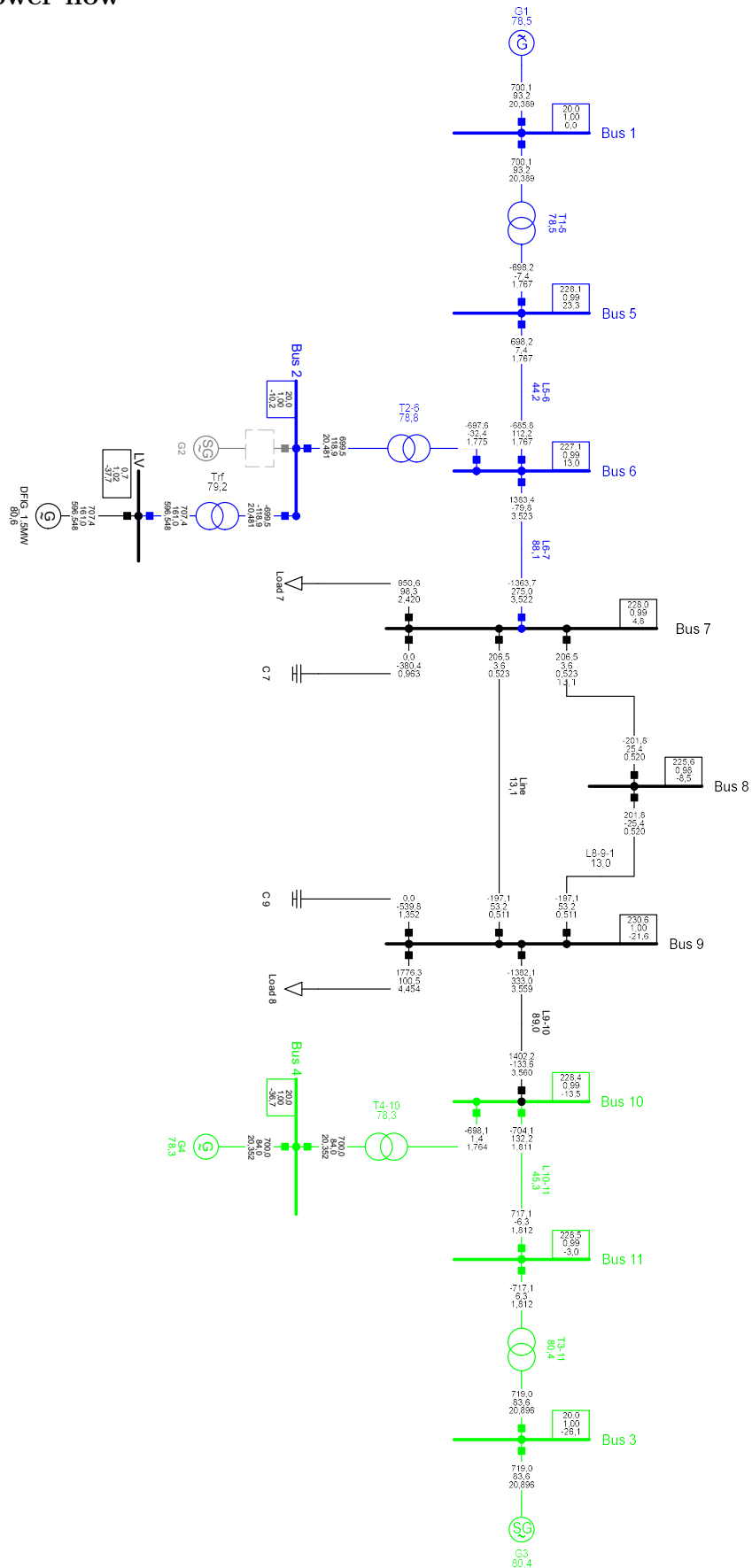
A	The DIgSILENT model	92
A.1	Power system overview with the nominal power flow	92
A.2	The power system with implemented wind power, including the nominal power flow	93
A.3	The synchronous generators and their control system	94
A.4	The DFIG wind turbine and its control system	100
A.5	Extended results from the result comparison between DIgSILENT and Simulink .	109
B	The complete linearization	112
B.1	The eigenvalues for synchronous generation	112
B.2	The observability of the dominant eigenvalues in the synchronous generator speeds	113
B.3	The eigenvectors relating the states to the dominant eigenvalues for synchronous generation	114
B.4	The eigenvalues when generator 2 is wind power without frequency controls . . .	115
B.5	The eigenvectors relating the states to the dominant eigenvalues when generator 2 is wind power without frequency controls	116
B.6	The eigenvectors relating the synchronous generator speeds to the oscillatory modes	117
B.7	The eigenvalues when generator 2 is wind power with frequency controls	118
B.8	The eigenvectors relating the states to the dominant eigenvalues when generator 2 is wind power with frequency controls	119
C	Extended results from the stability analysis of synchronous generation	120
C.1	Simple analytical eigenvalue calculation	123
D	Extended results from the stability analysis of wind power without frequency service controls	125
E	Extended results from the stability analysis of wind power with frequency service controls	132

A The DIgSILENT model

A.1 Power system overview with the nominal power flow



A.2 The power system with implemented wind power, including the nominal power flow



A.3 The synchronous generators and their control system

Name		Generators 1 and 2 Type Kundur	
Nominal Apparent Power	900,	MVA	
Nominal Voltage	20,	kV	
Power Factor	1,		
No. of Phases	3		
Connection	Y		
Model	Standard	Input parameters	Short-Circuit data
Inertia			
Input Mode	Inertia Constant H (rated to Pgn)		
Inertia Constant H (rated to Pgn)	6,5	s	
Stator parameters		Synchronous Reactances	
rstr	0,0025	p.u.	
xl	0,2	p.u.	
		xd	1,8
		xq	1,7
Rotor Type		Rotor mutual reactances	
<input type="radio"/> Salient pole <input checked="" type="radio"/> Round Rotor		xrld	0,
		xrlq	0,
Transient Time Constants		Transient Reactances	
Td0'	8,	s	
Tq0'	0,4	s	
		xd'	0,3
		xq'	0,55
Subtransient Time Constants		Subtransient Reactances	
Td0''	0,03	s	
Tq0''	0,05	s	
		xd''	0,25
		xq''	0,25

Figure A.1: The parameters of SG 1 and -2. SG 3 and -4 are identical but with inertia constants $H=6.175s$.

gov_1IEEG1: IEEE Type 1 Speed-Governing Model

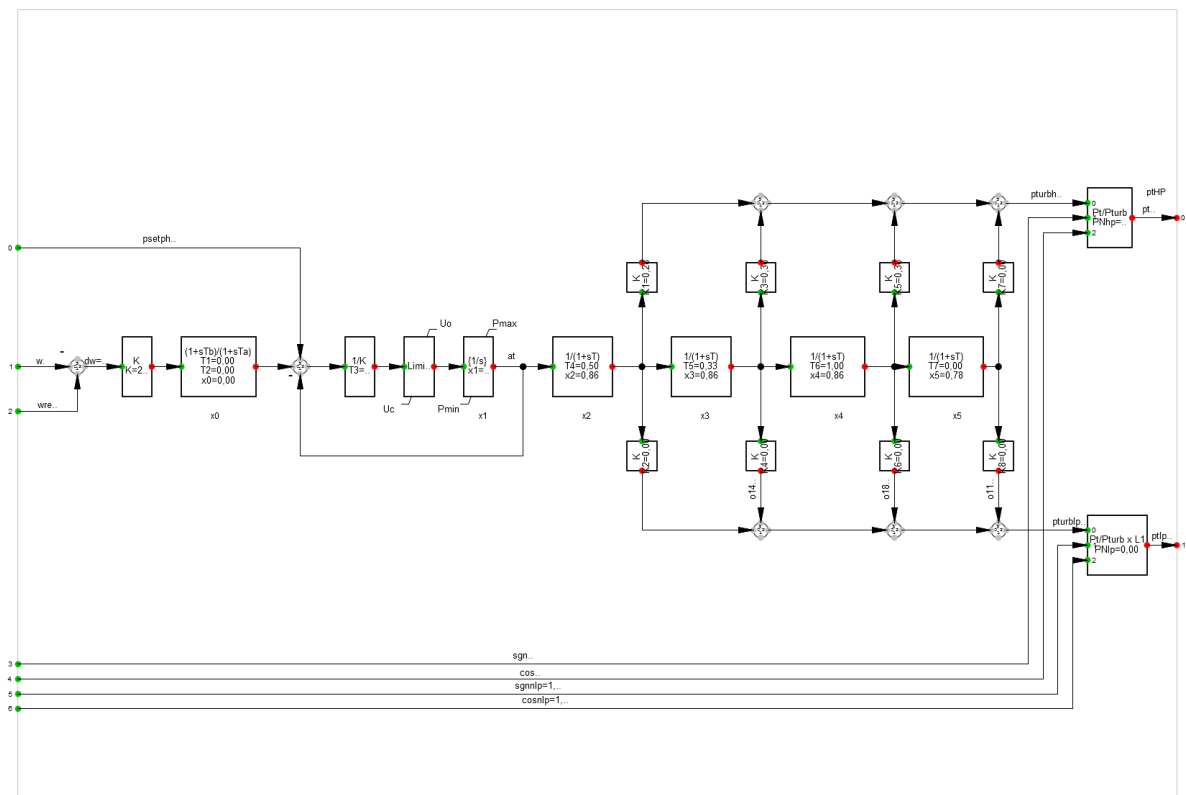


Figure A.2: The synchronous generators' steam turbine and governor.

gov Common Model - Two Area\Plant_G1\IEEEG1.ElmDsl X

Basic Data

Description

General Advanced 1 Advanced 2 Advanced 3

Name: IEEEG1

Model Definition: ▼ → User Defined Models\gov_IEEEG1

Configuration Script: →

☐ Out of Service ☐ A-stable integration algorithm

	Parameter
K	Controller Gain [p.u.]
T1	Governor Time Constant [s]
T2	Governor Derivative Time Constant [s]
T3	Servo Time Constant [s]
K1	High Pressure Turbine Factor [p.u.]
K2	High Pressure Turbine Factor [p.u.]
T5	Intermediate Pressure Turbine Time Constant [s]
K3	Intermediate Pressure Turbine Factor [p.u.]
K4	Intermediate Pressure Turbine Factor [p.u.]
T6	Medium Pressure Turbine Time Constant [s]
K5	Medium Pressure Turbine Factor [p.u.]
K6	Medium Pressure Turbine Factor [p.u.]
T4	High Pressure Turbine Time Constant [s]
T7	Low Pressure Turbine Time Constant [s]
K7	Low Pressure Turbine Factor [p.u.]
K8	Low Pressure Turbine Factor [p.u.]
PNhp	HP Turbine Rated Power(=0->PNhp=PgnnHp) [M...
PNlp	LP Turbine Rated Power(=0->PNlp=Pgnnlp) [MW]
Uc	Valve Closing Time [p.u./s]
Pmin	Minimum Gate Limit [p.u.]
Uo	Valve Opening Time [p.u./s]
Pmax	Maximum Gate Limit [p.u.]

Export to Clipboard Set to default

OK

Cancel

Events

Arrays/Matrices

Figure A.3: The parameters of the synchronous generators' steam turbine and governor.

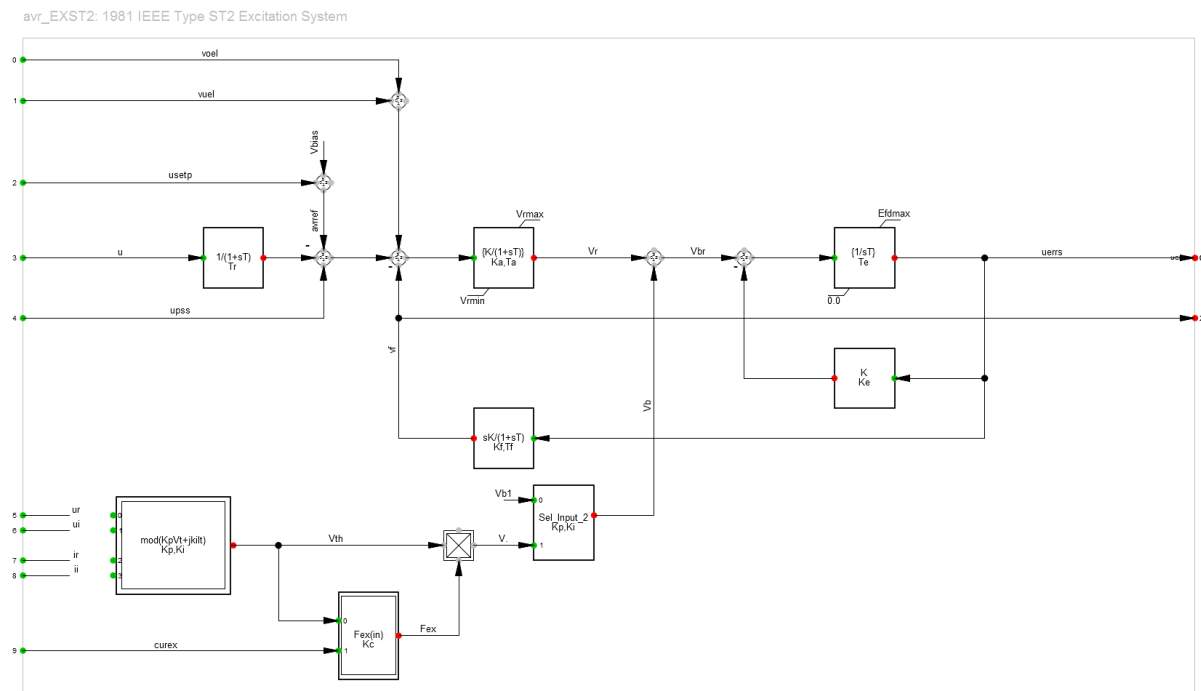


Figure A.4: The synchronous generators' AVR.

Basic Data

Description

General

Advanced 1

Advanced 2

Advanced 3

Name

EXST2

Model Definition

▼

→

User Defined Models\avr_EXST2

Configuration Script

→

☐ Out of Service
 ☐ A-stable integration algorithm

	Parameter	
Tr	Measurement Delay [s]	0,02
Ka	Controller Gain [pu]	200,
Ta	Controller Time Constant [s]	0,001
Ke	Exciter Constant [pu]	1,
Te	Exciter Time Constant [s]	0,000001
Kf	Stabilization Path Gain [pu]	0,001
Tf	Stabilization Path Time Constant [s]	0,1
Kp	Voltage Factor [pu]	0,
Ki	Current Factor [pu]	1,
Kc	Excitation Current Factor [pu]	0,5
Vrmin	Controller Output Minimum [pu]	-10,
Vrmax	Controller Output Maximum [pu]	10,
Efdmax	Exciter Maximum Output [pu]	12,3

Export to Clipboard

Set to default

OK

Cancel

Events

Arrays/Matrices

Figure A.5: The parameters of the synchronous generators' AVR.

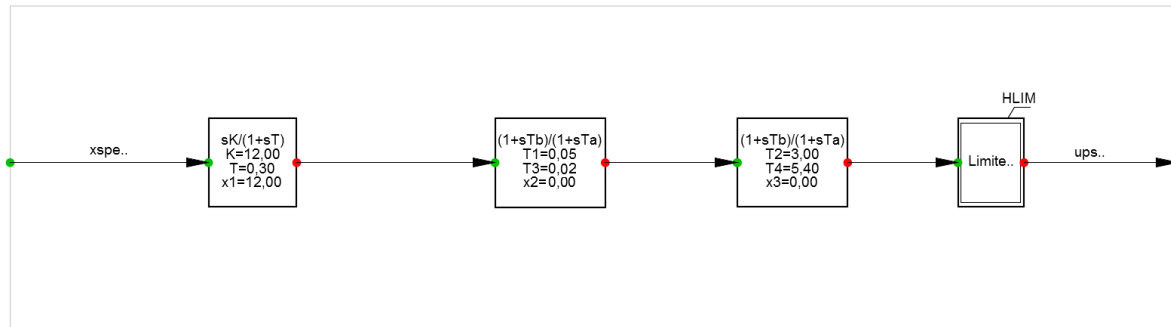
pss_STAB1: Speed Sensitive Stabilizing Model


Figure A.6: The synchronous generators' PSS.

pss Common Model - Two Area\Plant_G1\STAB1.ElmDsl

Basic Data

Description

General Advanced 1 Advanced 2 Advanced 3

Name: STAB1

Model Definition: [User Defined Models\pss_STAB1](#)

Configuration Script: [→](#)

☐ Out of Service ☐ A-stable integration algorithm

	Parameter
K Stabilizer Gain [pu]	12,
T Washout integrate time constant [s]	0,3
T2 Second Lead/Lag derivative time constant [s]	3,
T4 Second Lead/Lag delay time constant [s]	5,4
T1 First Lead/Lag derivative time constant [s]	0,05
T3 First Lead/Lag delay time constant [s]	0,02
HLIM Signal pss maximum [pu]	0,15

Export to Clipboard Set to default

OK

Cancel

Events

Arrays/Matrices

Figure A.7: The parameters of the synchronous generators' PSS.

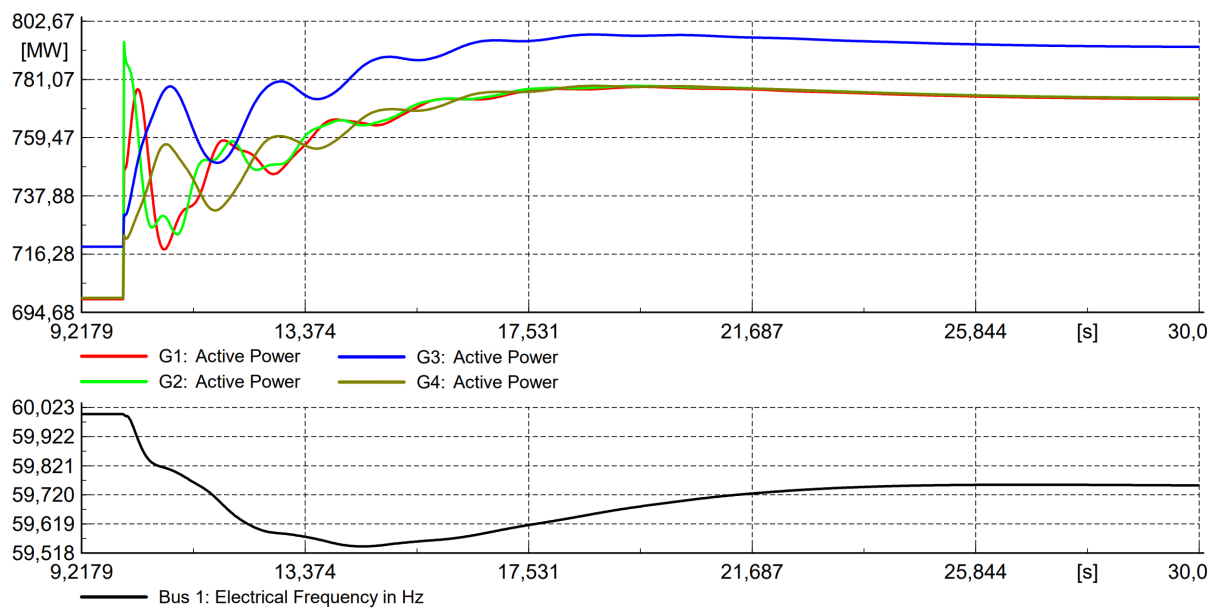


Figure A.8: The power- and frequency response for a load step of 300MW at $t=10$ s on bus 7. All generators are synchronous.

A.4 The DFIG wind turbine and its control system

Name

IG1.5MW

OK

Rated Voltage

0,69

kV

Cancel

Input Mode

☒ Slip-Torque/Current Characteristic
 ☐ Electrical Parameter

Calculate

Power Rating

☐ Rated Apparent Power

1666,664

kVA

☒ Rated Mechanical Power

1500,

kW

Rated Power Factor

0,91248

Efficiency at nominal Operation

98,63244

%

Nominal Frequency

60,

Hz

Nominal Speed

1193,942

rpm

No of Pole Pairs

3

Connection

Y

▼

Rotor

☒ Single Cage
 ☐ Double Cage

Moment of Inertia

481,1716

kgm²

Acceleration Time Constant

5,04

s

Locked Rotor Current (I_{lr}/I_n)

3,132307

p.u.

Locked Rotor Torque

0,04883664

p.u.

R/X Locked Rotor

0,03624122

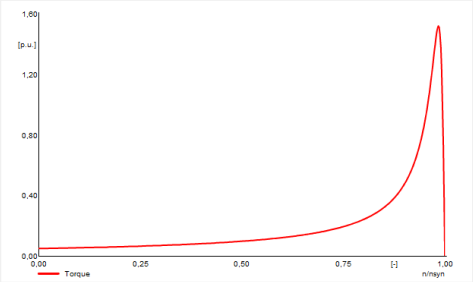
Torque at Stalling Point

1,703815

p.u.

Slip at Stalling Point

0,015



Stator Resistance R_s

0,00706

p.u.

Stator Reactance X_s

0,171

p.u.

Mag. Reactance X_m

2,9

p.u.

Figure A.9: The parameters of the induction machine.

The generic DFIG frame used in DIgSILENT is shown in figure A.10. This is the standard frame from the built-in DFIG model in DIgSILENT, with some adjustments.

- The "MPT" block calculates the optimal speed based on the generator speed and power production.
- This speed reference is further made into a power reference in the "Speed-controller" block based on PI regulation of the speed deviation.
- The speed reference is manipulated in the "Frequency mod" block, realizing inertial response and primary control. From the "Frequency mod" block, the pitch manipulation for primary control is fed to the pitch controller and the power reference to the PQ controller.
- The "PQ controller" calculates the dq-rotor reference currents based on PI regulation of the active- and reactive power deviation.
- Both the measured and reference dq-rotor currents are fed to the "Ir_ctrl", PI regulating the current deviation, creating the rotor voltage reference.
- Cross-couplings are canceled from the rotor voltages in the "Compensation ElmCom" block.
- The rotor voltage from the compensation block is together with the mechanical power from the shaft applied to the induction machine, the "DFIG ElmAsm" block. The induction machine supplies the rotor speed for the MPT, the rotor currents for the current regulator through the "current measurement" block, and the angles for the cancellation and measurement blocks.
- The mechanics consist of the pitch controller, turbine, and shaft. The power from the wind is provided by the turbine, based on wind speed, rotor speed, and pitch angle. The mechanical power of the DFIG is the power from the shaft, modeled as a spring synchronizing the turbine and generator speed.

The complete frequency service controls presented in section 3.2.4 is show in figure A.11. This is the content of the "Frequency mod" block in figure A.10. These controls are used to illustrate the functionality in chapter 3, and for the small-signal stability analysis in chapter 5.

The pitch-control is divided into two parts, one for above and one for below nominal frequency. This is due to the pitch angle's nonlinear relation to the mechanical power. Therefore, the factor between frequency deviation and pitch is different for the positive and negative loops. The factors are chosen to equal a droop of approximately 5% for a step increase and -decrease of 300MW at bus 7. The primary control pitch is either added or subtracted from the deloading pitch to realize the appropriate power increase or decrease. For the inertial response to affect the wind turbine speed as little as possible, a contribution proportional to the inertial response is added to the primary control's pitch angle. Also this pitch contribution is divided into a positive and negative part only to affect the pitch angle as the frequency is falling or raising towards the nadir. This ensures no negative, slowing impact on the pitch when the frequency converges onto the new value after the nadir.

Frame DFIG Generic:

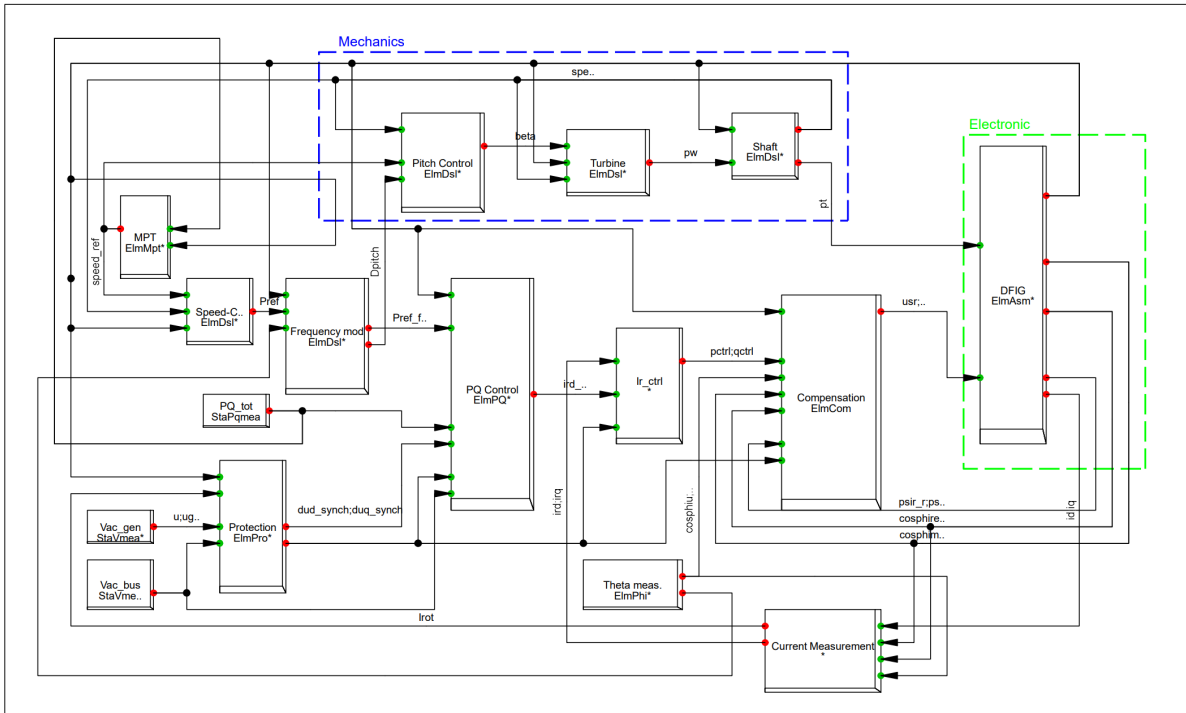


Figure A.10: The DFIG control frame.

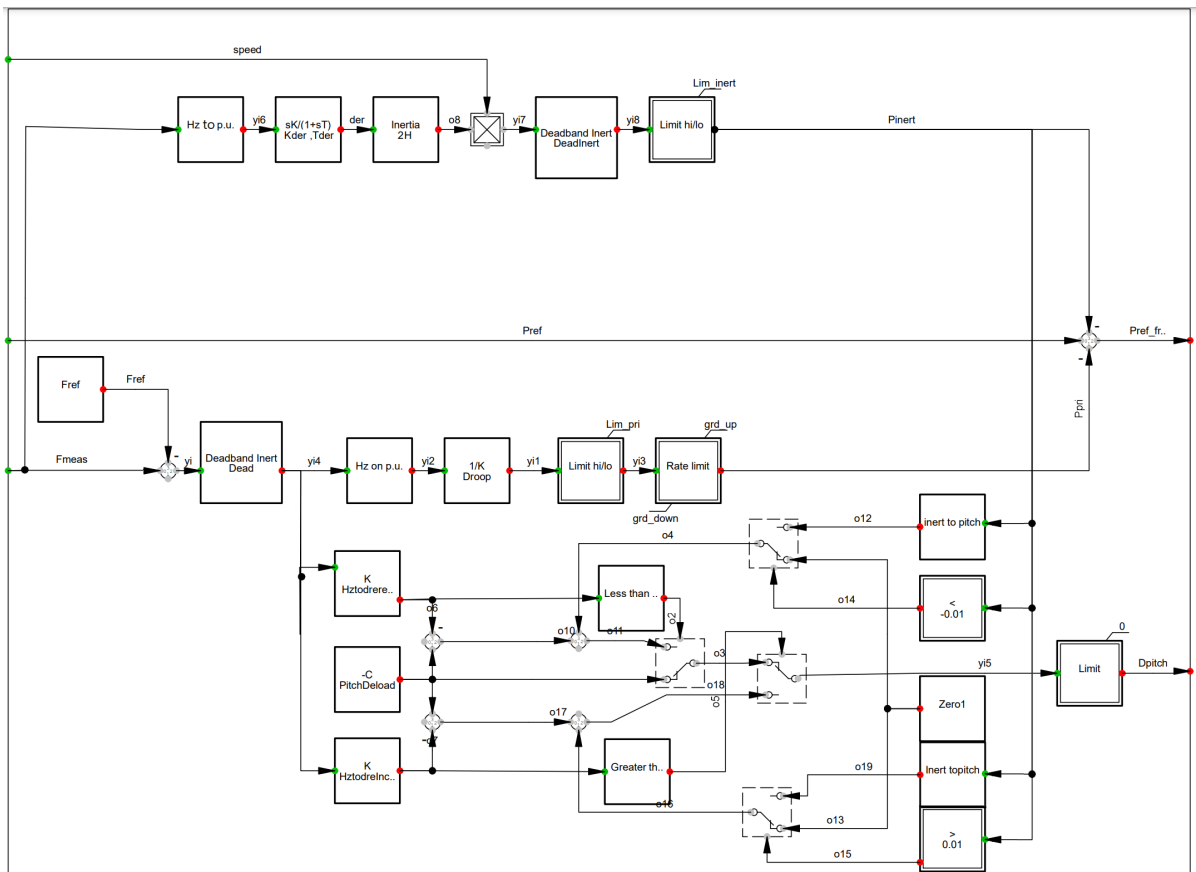


Figure A.11: The complete frequency service controls.

Common Model - Two Area\DFIG Control\Frequency.ElmDsl

Basic Data

Description

General Advanced 1 Advanced 2 Advanced 3

Name: Frequency

Model Definition: ...Hz\Library\DFIG Model\Freqservice

Configuration Script: →

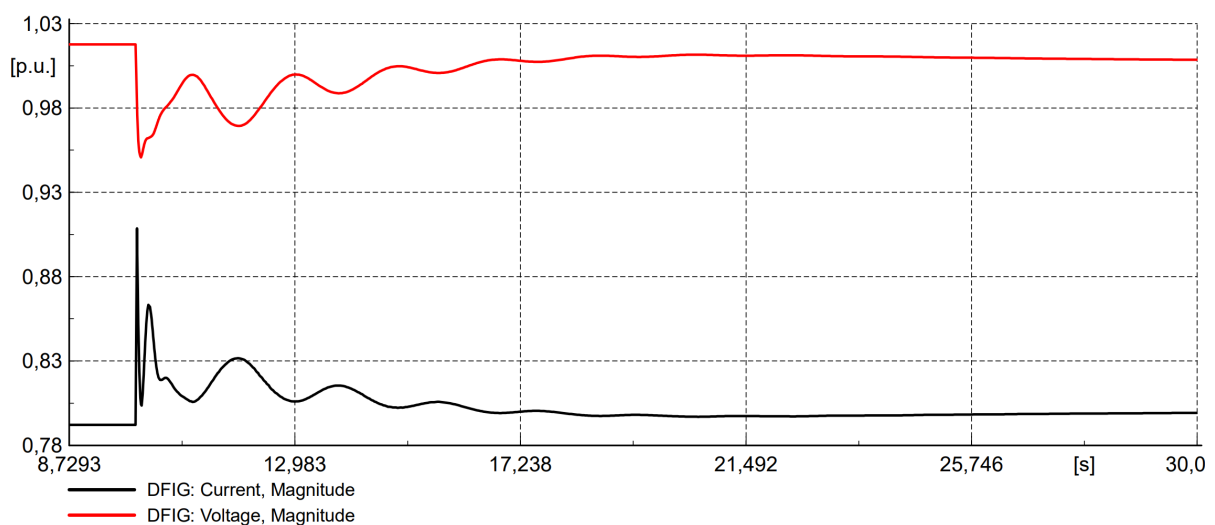
☐ Out of Service ☐ A-stable integration algorithm

	Parameter
Deadband for Primary control [Hz]	0,
Droop, Pu power to Pu frequency [%]	0,2
HztodgreIncrease Frequency deviation to pitch angle rati...	4,35
Hztodgrereduce Frequency deviation to pitch angle ratio...	4,85
PitchDeload [degrees]	5,
Kder Gain for frequency darivative	2,
Tder Timeconstant for frequency darivative [s]	0,3
H Intertia [s]	5,04
grd_down	-0,1
Lim_pri Limit to primary control in p.u. [Scalar]	0,3
Lim_inert Limit for inertia contribution [Scalar]	0,3
grd_up	0,1

Export to Clipboard Set to default

OK Cancel Events Arrays/Matrices

Figure A.12: The parameters of the frequency controls.

Figure A.13: The DFIG's current- and voltage amplitude response for a load step of 300MW at $t=10s$ on bus 7. No frequency controls are active.

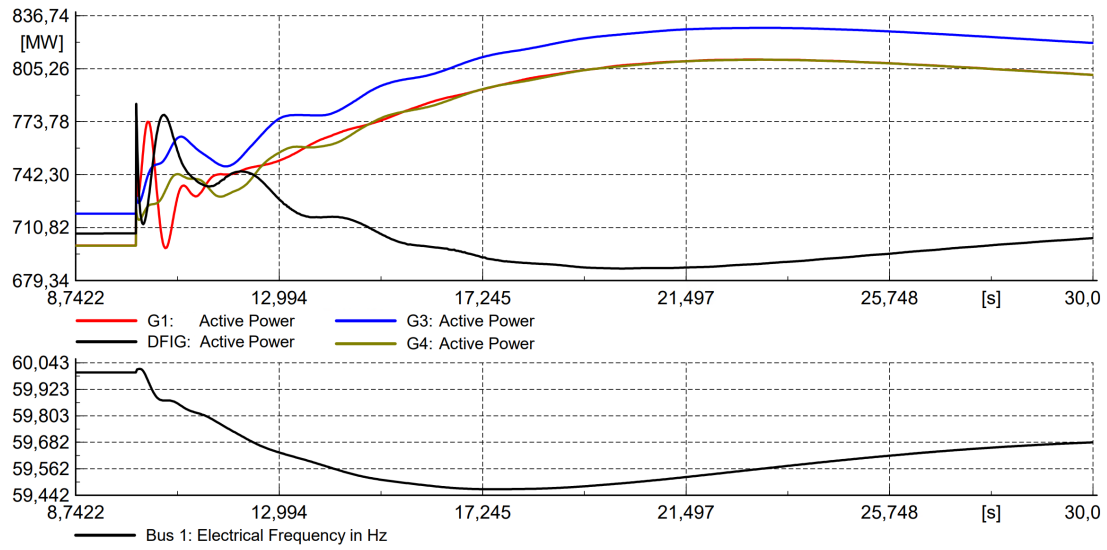


Figure A.14: The power- and frequency response for a load step increase of 300MW at $t=10$ s on bus 7, using only the synthetic inertia controls.

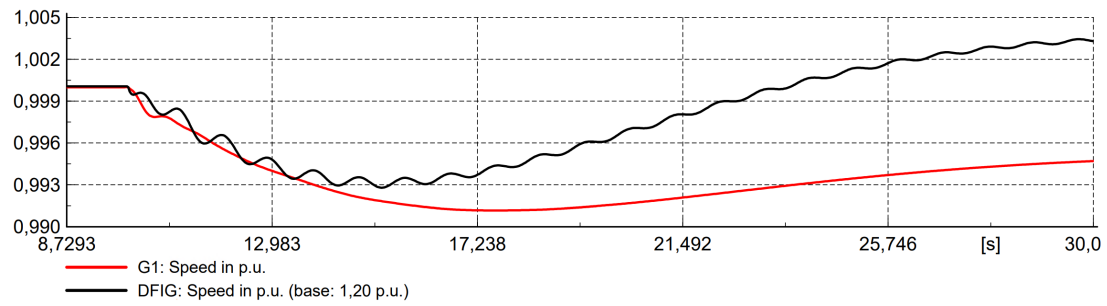


Figure A.15: The speed response of SG 1, and the wind turbine operated with only synthetic inertia controls. A load step of 300MW occurs at $t=10$ s on bus 7.

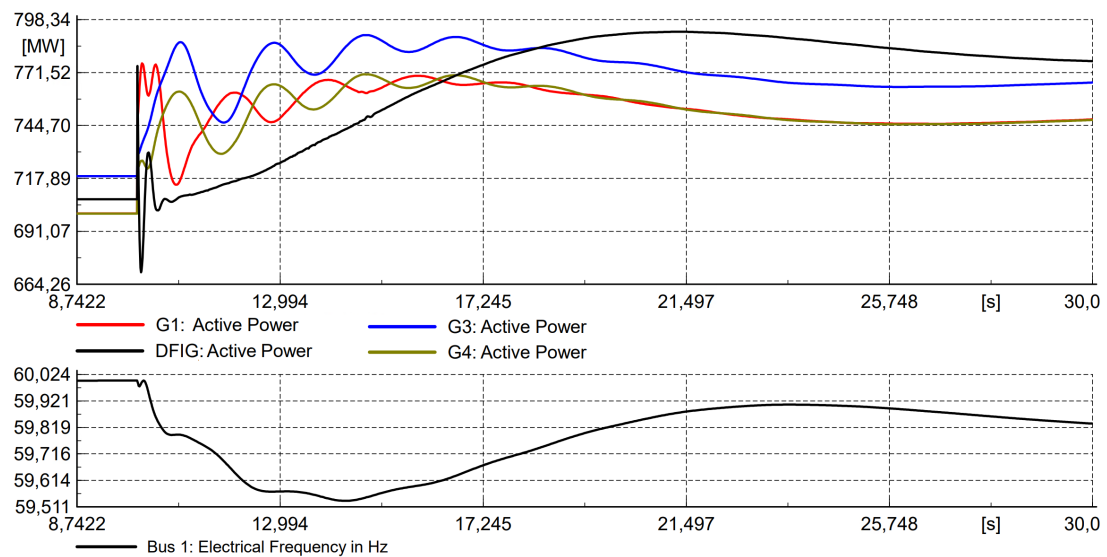


Figure A.16: The active power response for a load step of 300MW at $t=10$ s on bus 7, using only pitch-based primary control.

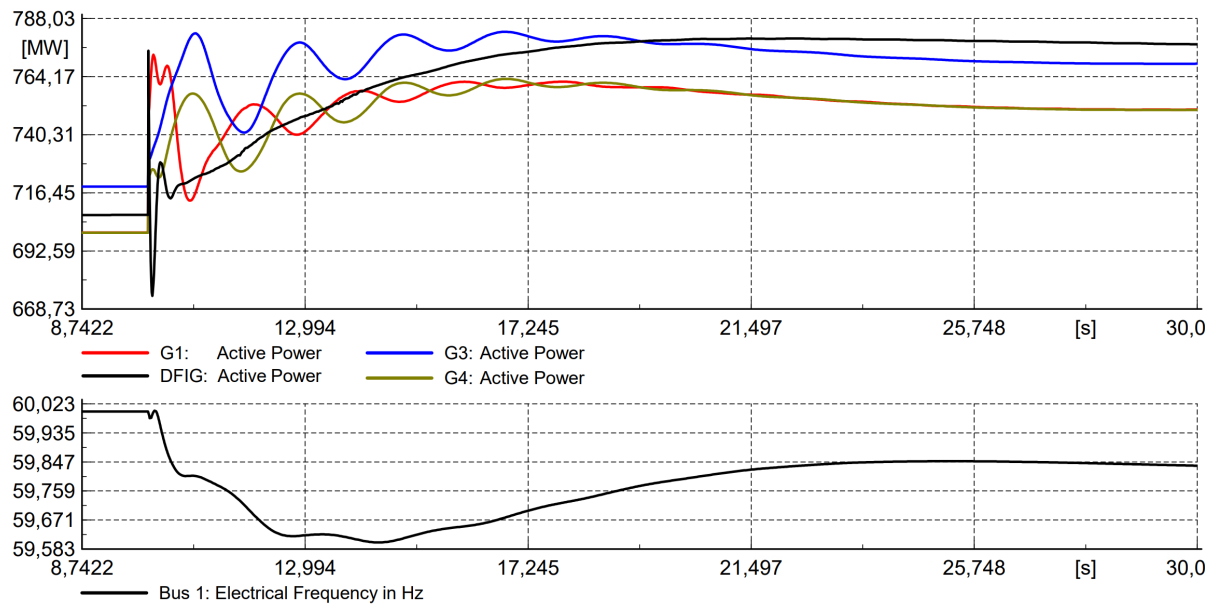


Figure A.17: The active power response for a load step of 300MW at $t=10$ s on bus 7, using both reference modification and pitch-based primary control.

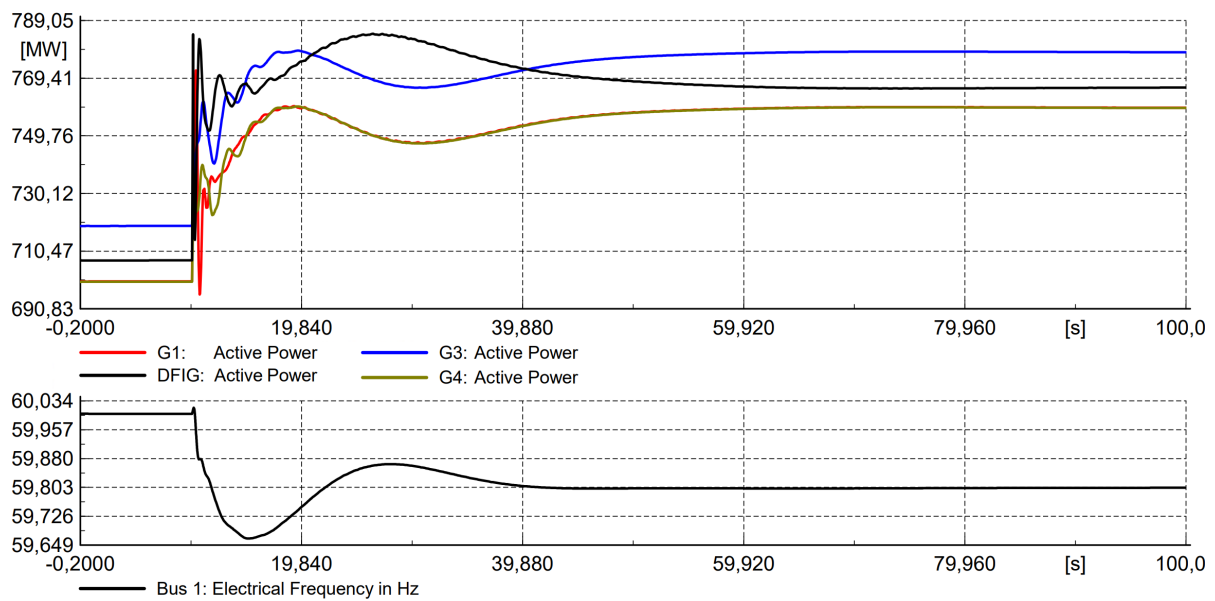


Figure A.18: The active power response for a load step increase of 300MW at $t=10$ s on bus 7, using the complete frequency service controls.

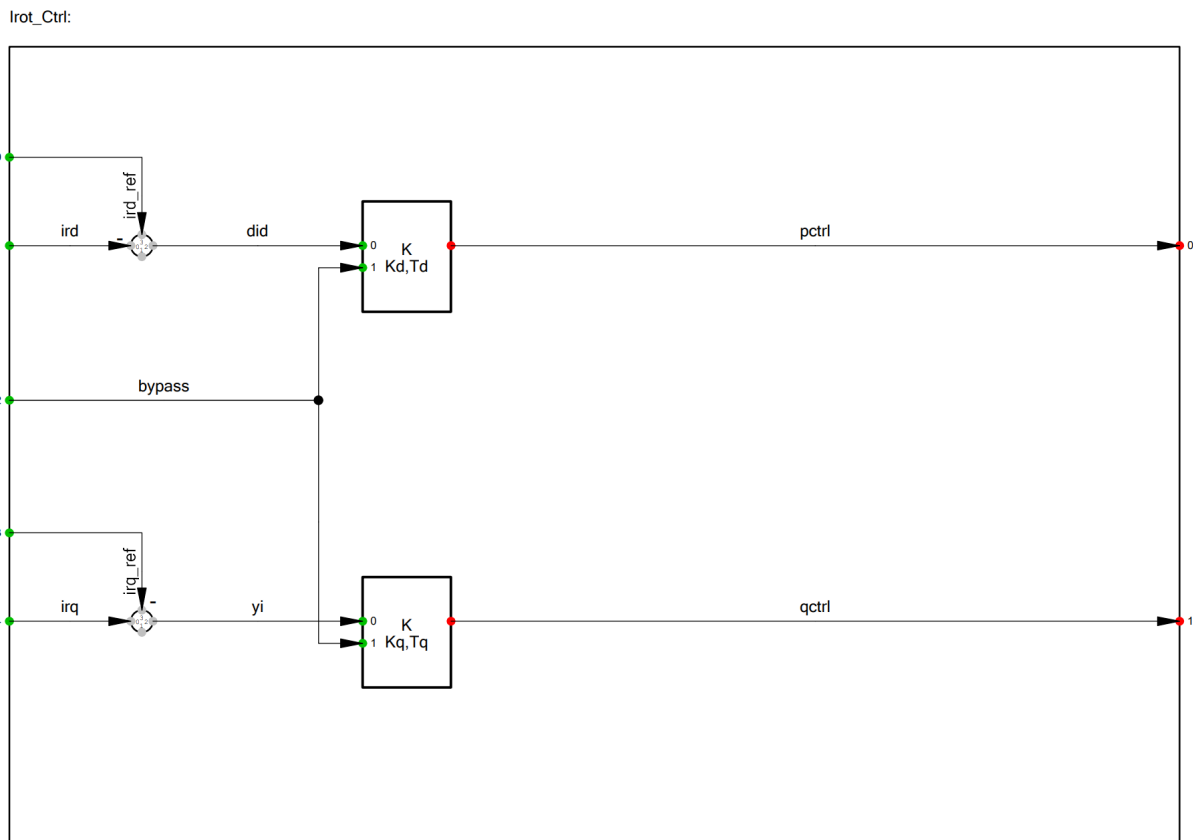


Figure A.19: The rotor current controller of the built-in DFIG in DiGSILENT.

dsl Common Model - Two Area\DFIG Control\Irot-Ctrl.ElmDsl

Basic Data	General	Advanced 1	Advanced 2	Advanced 3										
Description	<p>Name: Irot-Ctrl</p> <p>Model Definition: ... 50Hz\Library\DFIG Model\Irot_Ctrl</p> <p>Configuration Script: →</p> <p><input type="checkbox"/> Out of Service <input type="checkbox"/> A-stable integration algorithm</p> <table border="1"> <thead> <tr> <th>Parameter</th> <th>Value</th> </tr> </thead> <tbody> <tr> <td>Kd</td> <td>0,00496</td> </tr> <tr> <td>Td</td> <td>0,128</td> </tr> <tr> <td>Kq</td> <td>0,0496</td> </tr> <tr> <td>Tq</td> <td>0,0128</td> </tr> </tbody> </table> <p>Export to Clipboard Set to default</p>	Parameter	Value	Kd	0,00496	Td	0,128	Kq	0,0496	Tq	0,0128			
Parameter	Value													
Kd	0,00496													
Td	0,128													
Kq	0,0496													
Tq	0,0128													

OK Cancel Events Arrays/Matrices

Figure A.20: The parameters of the rotor current controller.

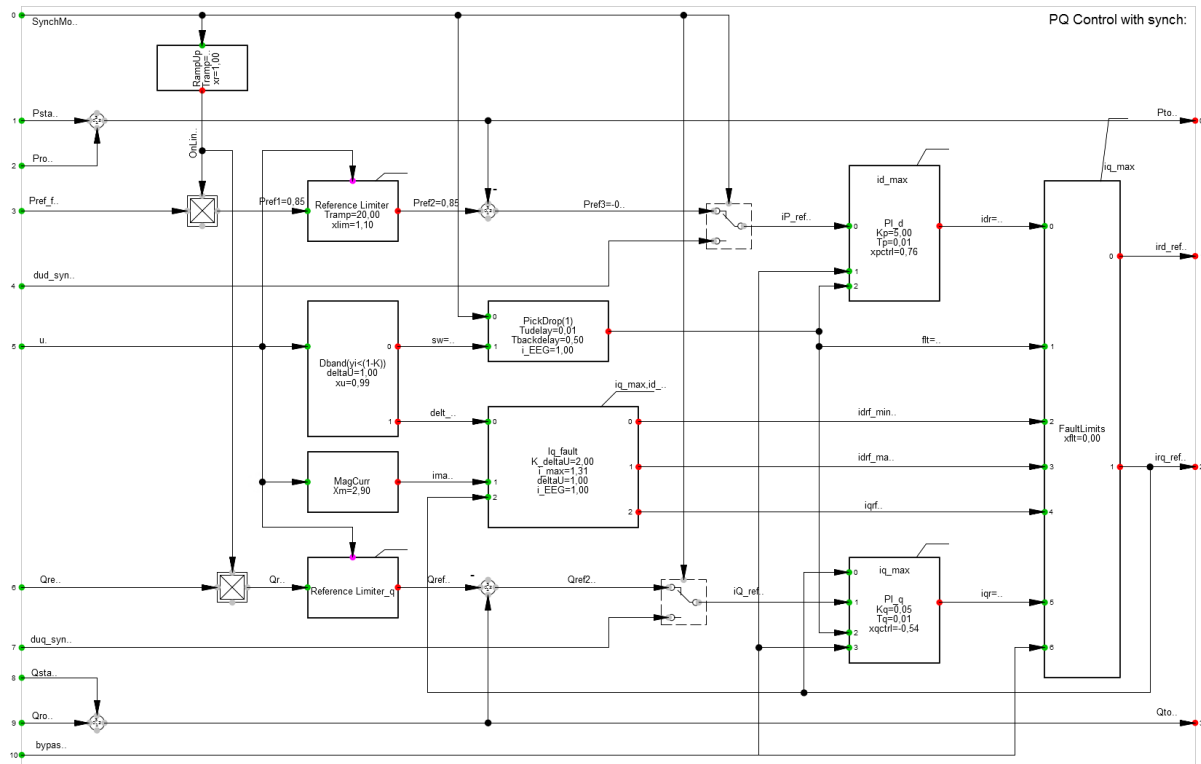


Figure A.21: The power controller of the built-in DFIG in DIGSILENT.

dsi Common Model - Two Area\DFIG Control\PQ control.ElmDsl*

Basic Data	
Description	

General		Advanced 1	Advanced 2	Advanced 3
Name	PQ control			
Model Definition	...ined Models\PQ Control with synch			
Configuration Script				
<input type="checkbox"/> Out of Service	<input type="checkbox"/> A-stable integration algorithm			
Parameter				
Kp : Active Power Control Gain [p.u.]	5,			
Tp : Active Power Control Time Constant [s]	0,01			
Kq : Reactive Power Control Gain [p.u.]	0,05			
Tq : Reactive Power Control Time Constant [s]	0,01			
Xm : Magnetizing reactance at Pbase [p.u.]	2,9			
deltaU : Voltage Dead Band [p.u.]	1,			
K_deltaU : Reactive support gain	2,			
i_max : Combined current limit [p.u.]	1,31			
i_EEG : FRT mode: 0=acc. TC2007, 1=acc. SDLWindV	1,			
Tudelay : Delay for activating dyn. voltage support [s]	0,01			
Tbackdelay : Delay for deactivating voltage support [s]	0,5			
Tramp : Power return ramp rate (PT1) [p.u./s]	20,			
id_max : id current limit [p.u.]	10,			
iq_max : iq current limit [p.u.]	10,			

Figure A.22: The parameters of the power controller.

Shaft_Generic:

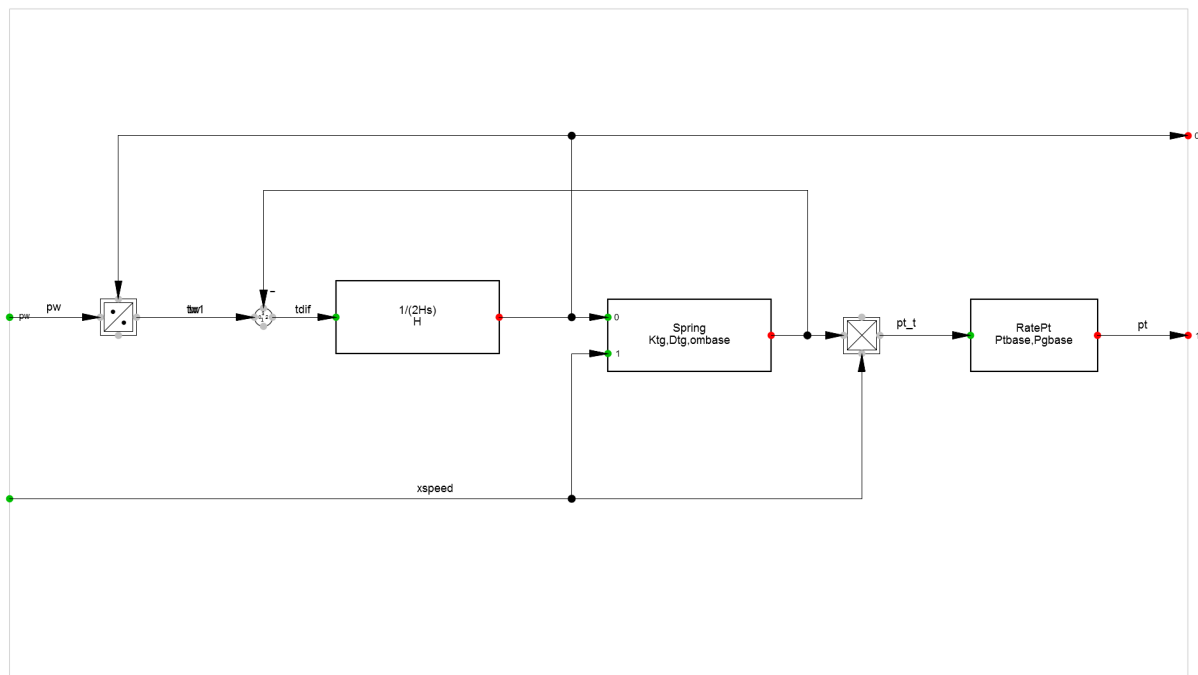


Figure A.23: The shaft model of the built-in DFIG in DIgSILENT.

dsi Common Model - Two Area\DFIG Control\Shaft.ElmDsl

Basic Data

Description

General Advanced 1 Advanced 2 Advanced 3

Name

Model Definition ...\Library\DFIG Model\Shaft_Generic

Configuration Script

☐ Out of Service ☐ A-stable integration algorithm

Parameter	
H	5,04
Ptbase	2,22
Pgbase	1,947
Ktg	80,27
Dtg	1,5
ombase	1,745

Figure A.24: The parameters of the shaft of the built-in DFIG in DIgSILENT.

A.5 Extended results from the result comparison between DIgSILENT and Simulink

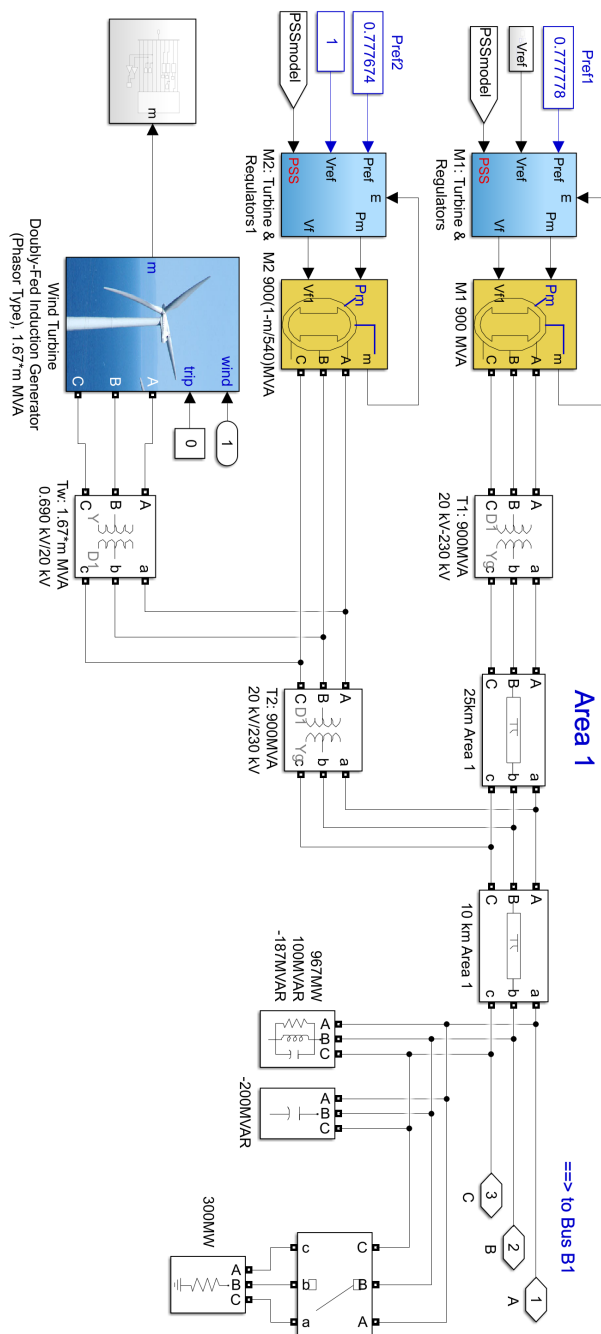


Figure A.25: Area one in Kundur’s two-area system in Simulink.

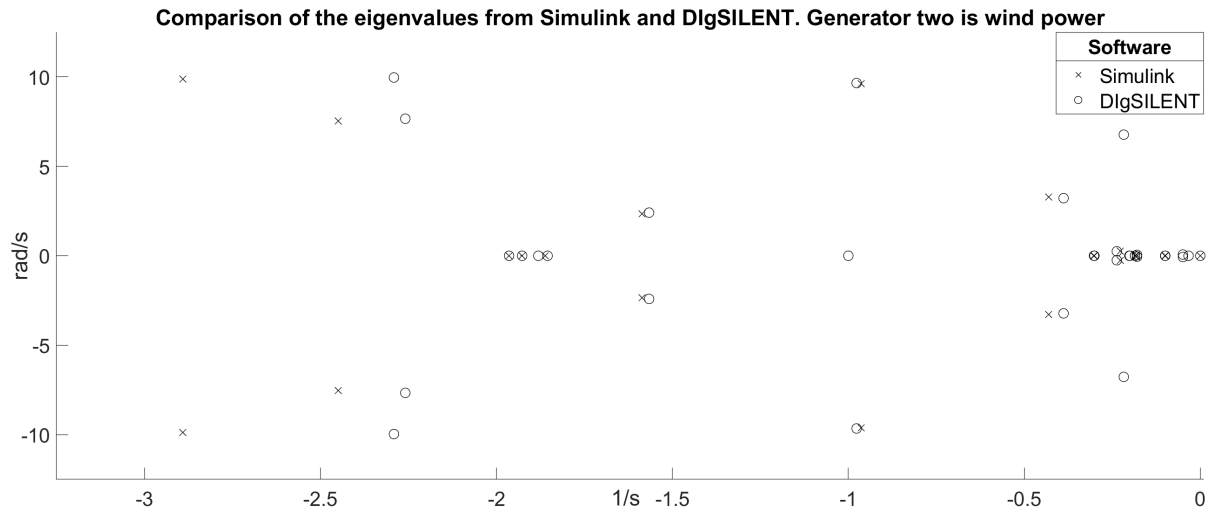


Figure A.26: The eigenvalues for both Simulink and DIgSILENT when generator two is wind power. No frequency controls are active.

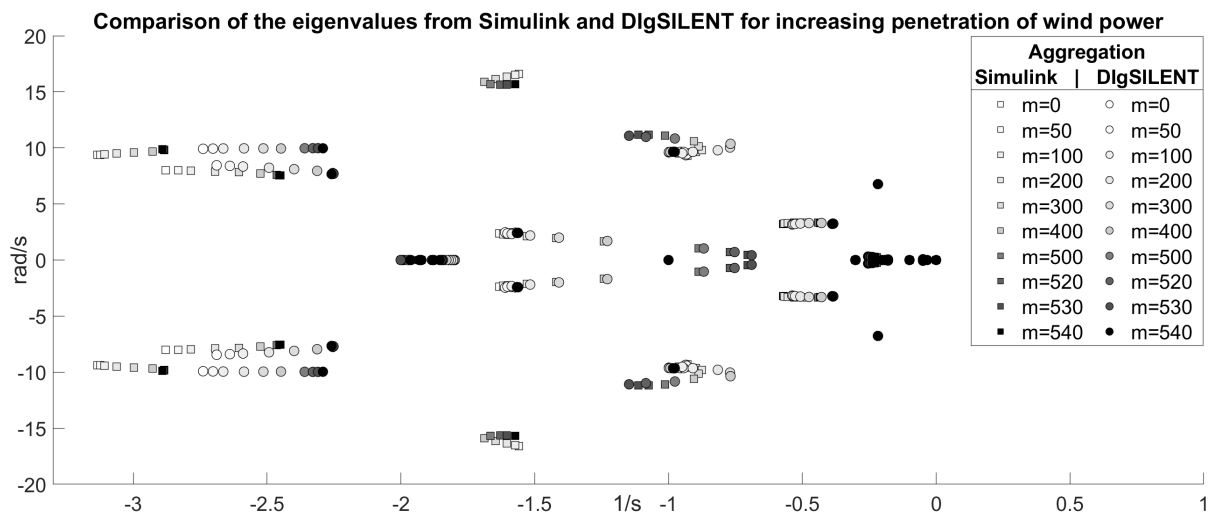


Figure A.27: All eigenvalues for both Simulink and DIgSILENT for increasing penetration of wind power. No frequency controls are active.

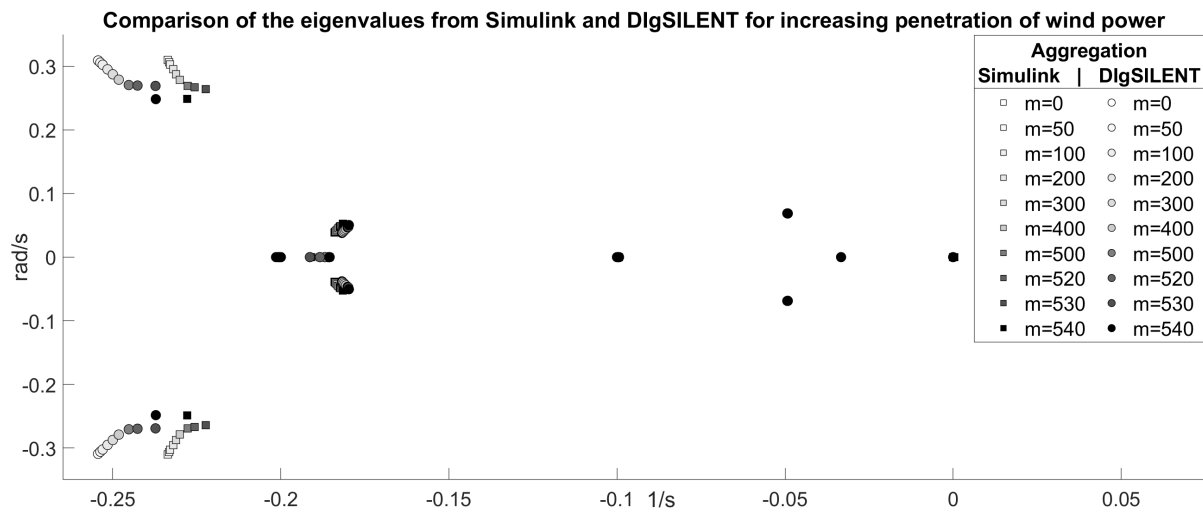


Figure A.28: The small eigenvalues for both Simulink and DIgSILENT for increasing penetration of wind power. No frequency controls are active.

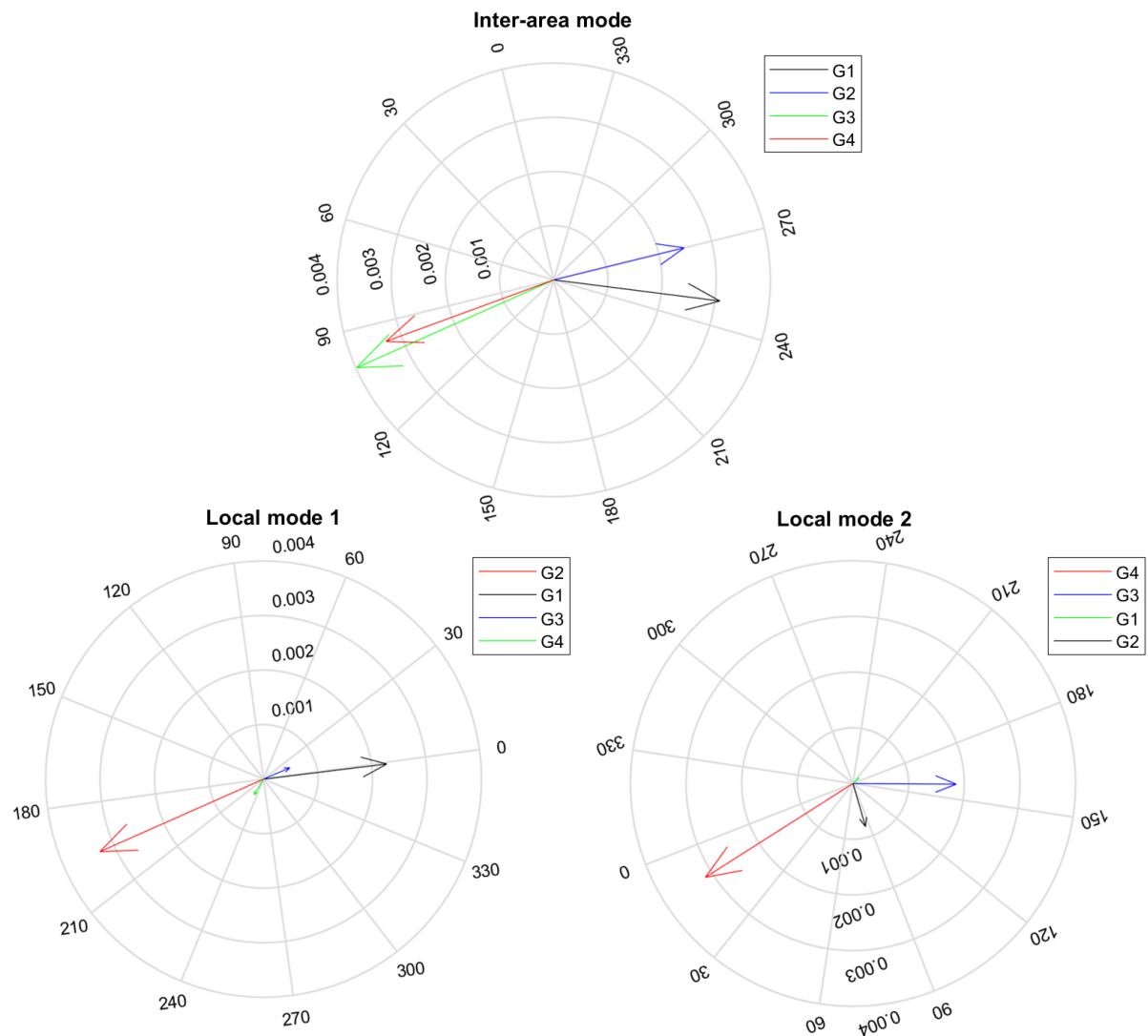


Figure A.29: The observability of the three dominant modes in the synchronous generator speeds from Simulink. The vectors are rotated based in the orientation in DIgSILENT, shown in figure B.1.

B The complete linearization

B.1 The eigenvalues for synchronous generation

Number	Eigenvalue	Frequency	Damping Ratio
1	0	0,000	0
9	0	0,000	0
10	-0,099400667133	0,000	1
11	-0,099741623455	0,000	1
12	-0,099746078877	0,000	1
13	-0,18181024069+0,038054093053i	0,006	0,978789776
14	-0,18181024069-0,038054093053i	0,006	0,978789776
15	-0,18548625812	0,000	1
16	-0,18553539798	0,000	1
17	-0,18556409896	0,000	1
18	-0,25436056896+0,30923830354i	0,049	0,635251362
19	-0,25436056896-0,30923830354i	0,049	0,635251362
20	-0,30089183111	0,000	1
21	-0,30208090481	0,000	1
22	-0,30209783276	0,000	1
23	-0,53803117326+3,1736292557i	0,505	0,167146857
24	-0,53803117326-3,1736292557i	0,505	0,167146857
25	-0,93580620096+9,3488002893i	1,488	0,099601318
26	-0,93580620096-9,3488002893i	1,488	0,099601318
27	-0,9555416635+9,6452112033i	1,535	0,098586409
28	-0,9555416635-9,6452112033i	1,535	0,098586409
29	-1,5871218224+2,4062808687i	0,383	0,550594842
30	-1,5871218224-2,4062808687i	0,383	0,550594842
31	-1,6102425445+2,4592496432i	0,391	0,5477906
32	-1,6102425445-2,4592496432i	0,391	0,5477906
33	-1,7982111419	0,000	1
34	-1,9234207066	0,000	1
35	-1,9629481445	0,000	1
36	-1,9641127951	0,000	1
37	-2,6879160373+8,4475049668i	1,344	0,303211191
38	-2,6879160373-8,4475049668i	1,344	0,303211191
39	-2,7386810816+9,9196362512i	1,579	0,26613034
40	-2,7386810816-9,9196362512i	1,579	0,26613034
41	-3,9812739042	0,000	1
42	-4,6651326814+0,44454309892i	0,071	0,995490542
43	-4,6651326814-0,44454309892i	0,071	0,995490542
44	-5,1963972244	0,000	1
45	-5,896070231+0,024706356376i	0,004	0,999991221
46	-5,896070231-0,024706356376i	0,004	0,999991221
47	-6,498755784+0,47737082023i	0,076	0,997312997
48	-6,498755784-0,47737082023i	0,076	0,997312997
49	-6,5485044674+0,51794205679i	0,082	0,996886734
50	-6,5485044674-0,51794205679i	0,082	0,996886734
51	-6,8308217491	0,000	1
52	-6,8759933134	0,000	1
53	-19,484285407	0,000	1
54	-20,838396187	0,000	1
55	-25,485459463	0,000	1
56	-25,624844257	0,000	1
57	-27,595772084	0,000	1
58	-28,738186453	0,000	1
59	-32,252522612	0,000	1
60	-32,358361326	0,000	1
61	-50	0,000	1
62	-50	0,000	1
63	-50	0,000	1
64	-50	0,000	1
65	-51,631604172	0,000	1
66	-51,641358957	0,000	1
67	-51,990441523	0,000	1
68	-52,167682562	0,000	1
69	-3012,7590053	0,000	1
70	-3012,759306	0,000	1
71	-3012,7736431	0,000	1
72	-3012,7834847	0,000	1
73	-997993,94967	0,000	1
74	-997993,94967	0,000	1
75	-997993,94967	0,000	1
76	-997993,94967	0,000	1

B.2 The observability of the dominant eigenvalues in the synchronous generator speeds

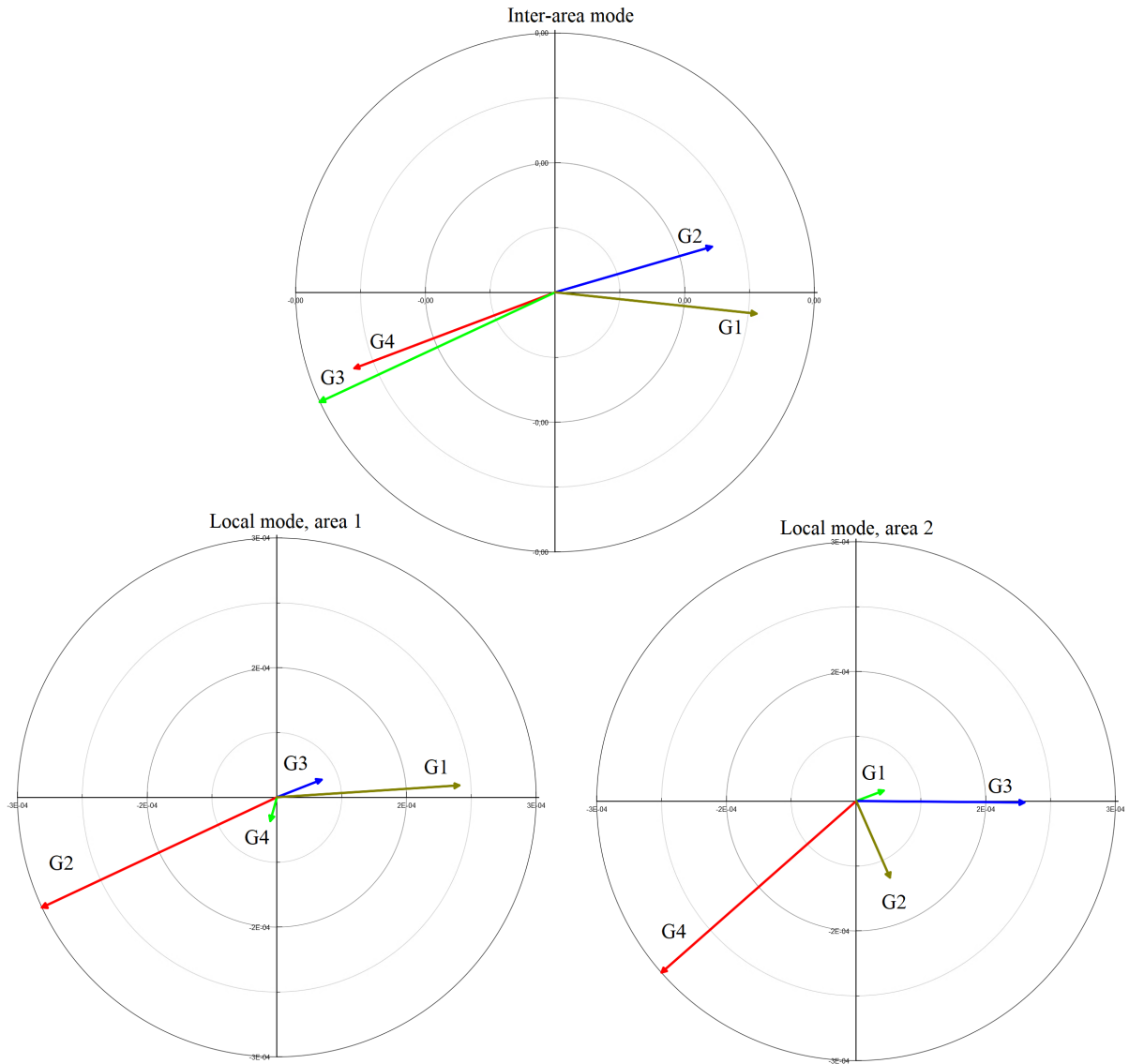


Figure B.1: The observability of the inter-area- and local modes in the synchronous generator speeds from DIgSILENT.

B.3 The eigenvectors relating the states to the dominant eigenvalues for synchronous generation

State name	State variable	Interarea mode (23)			Local mode, area 1 (25)			Local mode, area (27)		
		Controllability	Observability	Participation	Controllability	Observability	Participation	Controllability	Observability	Participation
Plant_G1; EXST2; xa	xa	0,000	0,625	0,000	0,000	0,879	0,003	0,000	0,450	0,000
Plant_G1; EXST2; xe	xe	0,000	0,625	0,000	0,000	0,879	0,000	0,000	0,450	0,000
Plant_G1; EXST2; xf	xf	0,000	0,626	0,024	0,000	0,675	0,296	0,000	0,341	0,012
Plant_G1; EXST2; xr	xr	0,003	0,016	0,013	0,004	0,004	0,051	0,000	0,004	0,004
Plant_G1; IEEE1; x0	x0	0,000	0,000	0,000	0,000	0,000	0,000	0,000	0,000	0,000
Plant_G1; IEEE1; x1	x1	0,002	0,021	0,011	0,000	0,003	0,004	0,000	0,000	0,000
Plant_G1; IEEE1; x2	x2	0,006	0,012	0,021	0,002	0,001	0,004	0,000	0,000	0,000
Plant_G1; IEEE1; x3	x3	0,009	0,001	0,003	0,003	0,000	0,000	0,000	0,000	0,000
Plant_G1; IEEE1; x4	x4	0,009	0,000	0,000	0,003	0,000	0,000	0,000	0,000	0,000
Plant_G1; IEEE1; x5	x5	0,000	0,000	0,000	0,000	0,000	0,000	0,000	0,000	0,000
Plant_G1; STAB1; x1	x1	0,061	0,010	0,176	0,039	0,001	0,115	0,003	0,000	0,001
Plant_G1; STAB1; x2	x2	0,002	0,034	0,022	0,003	0,009	0,089	0,000	0,001	0,001
Plant_G1; STAB1; x3	x3	0,019	0,002	0,010	0,009	0,000	0,005	0,001	0,000	0,000
Plant_G2; EXST2; xa	xa	0,000	0,537	0,000	0,000	1,000	0,003	0,000	0,574	0,000
Plant_G2; EXST2; xe	xe	0,000	0,537	0,000	0,000	1,000	0,000	0,000	0,574	0,000
Plant_G2; EXST2; xf	xf	0,000	0,538	0,021	0,000	0,768	0,335	0,000	0,434	0,036
Plant_G2; EXST2; xr	xr	0,003	0,014	0,011	0,004	0,006	0,072	0,001	0,005	0,011
Plant_G2; IEEE1; x0	x0	0,000	0,000	0,000	0,000	0,000	0,000	0,000	0,000	0,000
Plant_G2; IEEE1; x1	x1	0,002	0,017	0,007	0,000	0,004	0,005	0,000	0,001	0,000
Plant_G2; IEEE1; x2	x2	0,005	0,010	0,015	0,002	0,001	0,006	0,000	0,000	0,000
Plant_G2; IEEE1; x3	x3	0,008	0,001	0,002	0,003	0,000	0,000	0,001	0,000	0,000
Plant_G2; IEEE1; x4	x4	0,008	0,000	0,000	0,003	0,000	0,000	0,001	0,000	0,000
Plant_G2; IEEE1; x5	x5	0,000	0,000	0,000	0,000	0,000	0,000	0,000	0,000	0,000
Plant_G2; STAB1; x1	x1	0,060	0,008	0,140	0,039	0,001	0,162	0,007	0,000	0,009
Plant_G2; STAB1; x2	x2	0,002	0,027	0,018	0,003	0,013	0,125	0,001	0,004	0,007
Plant_G2; STAB1; x3	x3	0,019	0,002	0,008	0,009	0,000	0,007	0,002	0,000	0,000
Plant_G3; EXST2; xa	xa	0,000	0,975	0,000	0,000	0,296	0,000	0,000	1,000	0,003
Plant_G3; EXST2; xe	xe	0,000	0,975	0,000	0,000	0,296	0,000	0,000	1,000	0,000
Plant_G3; EXST2; xf	xf	0,000	0,977	0,040	0,000	0,227	0,031	0,000	0,756	0,315
Plant_G3; EXST2; xr	xr	0,003	0,028	0,023	0,001	0,002	0,007	0,004	0,006	0,071
Plant_G3; IEEE1; x0	x0	0,000	0,000	0,000	0,000	0,000	0,000	0,000	0,000	0,000
Plant_G3; IEEE1; x1	x1	0,002	0,027	0,014	0,000	0,001	0,000	0,000	0,003	0,003
Plant_G3; IEEE1; x2	x2	0,006	0,016	0,027	0,001	0,000	0,000	0,002	0,001	0,003
Plant_G3; IEEE1; x3	x3	0,009	0,001	0,004	0,001	0,000	0,000	0,003	0,000	0,000
Plant_G3; IEEE1; x4	x4	0,009	0,000	0,000	0,001	0,000	0,000	0,003	0,000	0,000
Plant_G3; IEEE1; x5	x5	0,000	0,000	0,000	0,000	0,000	0,000	0,000	0,000	0,000
Plant_G3; STAB1; x1	x1	0,064	0,013	0,239	0,012	0,000	0,009	0,036	0,001	0,093
Plant_G3; STAB1; x2	x2	0,002	0,044	0,030	0,001	0,002	0,007	0,003	0,008	0,075
Plant_G3; STAB1; x3	x3	0,021	0,002	0,014	0,003	0,000	0,000	0,008	0,000	0,004
Plant_G4; EXST2; xa	xa	0,000	0,998	0,000	0,000	0,187	0,000	0,000	0,924	0,003
Plant_G4; EXST2; xe	xe	0,000	0,998	0,000	0,000	0,187	0,000	0,000	0,924	0,000
Plant_G4; EXST2; xf	xf	0,000	1,000	0,040	0,000	0,143	0,011	0,000	0,699	0,321
Plant_G4; EXST2; xr	xr	0,003	0,024	0,019	0,001	0,002	0,004	0,004	0,007	0,086
Plant_G4; IEEE1; x0	x0	0,000	0,000	0,000	0,000	0,000	0,000	0,000	0,000	0,000
Plant_G4; IEEE1; x1	x1	0,002	0,023	0,010	0,000	0,000	0,000	0,000	0,004	0,005
Plant_G4; IEEE1; x2	x2	0,005	0,013	0,020	0,000	0,000	0,000	0,002	0,001	0,006
Plant_G4; IEEE1; x3	x3	0,008	0,001	0,003	0,001	0,000	0,000	0,003	0,000	0,000
Plant_G4; IEEE1; x4	x4	0,008	0,000	0,000	0,001	0,000	0,000	0,003	0,000	0,000
Plant_G4; IEEE1; x5	x5	0,000	0,000	0,000	0,000	0,000	0,000	0,000	0,000	0,000
Plant_G4; STAB1; x1	x1	0,062	0,011	0,190	0,007	0,000	0,003	0,039	0,001	0,158
Plant_G4; STAB1; x2	x2	0,002	0,036	0,024	0,001	0,001	0,002	0,003	0,013	0,128
Plant_G4; STAB1; x3	x3	0,020	0,002	0,011	0,002	0,000	0,000	0,009	0,000	0,007
Two Area; G1; phi	phi	0,013	0,051	0,189	0,013	0,023	0,884	0,001	0,004	0,015
Two Area; G1; psi1d	psi1d	0,000	0,026	0,003	0,003	0,008	0,062	0,000	0,005	0,003
Two Area; G1; psi1q	psi1q	0,006	0,009	0,016	0,004	0,002	0,021	0,000	0,001	0,001
Two Area; G1; psi2q	psi2q	0,004	0,009	0,009	0,002	0,002	0,008	0,000	0,001	0,000
Two Area; G1; psifd	psifd	0,006	0,030	0,054	0,016	0,012	0,575	0,001	0,006	0,023
Two Area; G1; speed	speed	1,000	0,001	0,307	0,979	0,000	0,691	0,081	0,000	0,009
Two Area; G2; phi	phi	0,011	0,000	0,000	0,013	0,000	0,000	0,003	0,000	0,000
Two Area; G2; psi1d	psi1d	0,000	0,014	0,001	0,003	0,011	0,081	0,000	0,007	0,010
Two Area; G2; psi1q	psi1q	0,005	0,016	0,024	0,003	0,006	0,046	0,001	0,003	0,006
Two Area; G2; psi2q	psi2q	0,003	0,016	0,014	0,001	0,005	0,019	0,000	0,002	0,002
Two Area; G2; psifd	psifd	0,006	0,020	0,035	0,016	0,015	0,683	0,003	0,008	0,072
Two Area; G2; speed	speed	0,872	0,001	0,216	1,000	0,000	1,000	0,185	0,000	0,059
Two Area; G3; phi	phi	0,013	0,270	1,000	0,003	0,016	0,154	0,012	0,008	0,285
Two Area; G3; psi1d	psi1d	0,000	0,047	0,005	0,001	0,003	0,007	0,002	0,010	0,077
Two Area; G3; psi1q	psi1q	0,006	0,015	0,027	0,001	0,001	0,002	0,003	0,002	0,020
Two Area; G3; psi2q	psi2q	0,004	0,015	0,016	0,000	0,001	0,001	0,001	0,002	0,008
Two Area; G3; psifd	psifd	0,007	0,042	0,080	0,005	0,004	0,060	0,015	0,014	0,619
Two Area; G3; speed	speed	0,971	0,001	0,381	0,271	0,000	0,050	0,896	0,000	0,581
Two Area; G4; phi	phi	0,011	0,242	0,755	0,003	0,013	0,119	0,014	0,012	0,514
Two Area; G4; psi1d	psi1d	0,000	0,046	0,005	0,000	0,003	0,003	0,003	0,011	0,088
Two Area; G4; psi1q	psi1q	0,006	0,016	0,025	0,001	0,001	0,003	0,003	0,006	0,057
Two Area; G4; psi2q	psi2q	0,003	0,016	0,014	0,000	0,001	0,001	0,002	0,005	0,023
Two Area; G4; psifd	psifd	0,007	0,043	0,079	0,003	0,003	0,021	0,016	0,013	0,669
Two Area; G4; speed	speed	0,851	0,001	0,277	0,206	0,000	0,019	1,000	0,000	1,000

B.4 The eigenvalues when generator 2 is wind power without frequency controls

Number	Eigenvalue	Frequency	Damping Ratio
1	0	0,000	0
15	0	0,000	0
16	-0,000000000002	0,000	0
17	-0,033333333333	0,000	1
18	-0,049337252223+0,068821798927i	0,011	0,582635677
19	-0,049337252223-0,068821798927i	0,011	0,582635677
20	-0,099388472534	0,000	1
21	-0,099746184636	0,000	1
22	-0,1	0,000	1
23	-0,17977037713+0,050467047687i	0,008	0,962781161
24	-0,17977037713-0,050467047687i	0,008	0,962781161
25	-0,18548455819	0,000	1
26	-0,18557575694	0,000	1
27	-0,2	0,000	1
28	-0,20143140772	0,000	1
29	-0,21744138422+6,7713410049i	1,078	0,032095468
30	-0,21744138422-6,7713410049i	1,078	0,032095468
31	-0,23719736948+0,24849035197i	0,040	0,690478844
32	-0,23719736948-0,24849035197i	0,040	0,690478844
33	-0,30086805955	0,000	1
34	-0,30209857751	0,000	1
35	-0,38842146251+3,2201001123i	0,512	0,119755945
36	-0,38842146251-3,2201001123i	0,512	0,119755945
37	-0,9765594381+9,6554990313i	1,537	0,100626871
38	-0,9765594381-9,6554990313i	1,537	0,100626871
39	-1	0,000	1
40	-1	0,000	1
41	-1,5662610723+2,4117201106i	0,384	0,544656577
42	-1,5662610723-2,4117201106i	0,384	0,544656577
43	-1,8546612153	0,000	1
44	-1,8809343518	0,000	1
45	-1,9269829674	0,000	1
46	-1,9641657312	0,000	1
47	-2,2589652922+7,6622913113i	1,219	0,282782693
48	-2,2589652922-7,6622913113i	1,219	0,282782693
49	-2,2912166961+9,966278392i	1,586	0,224052279
50	-2,2912166961-9,966278392i	1,586	0,224052279
51	-3,3333333333	0,000	1
52	-4,0795357159	0,000	1
53	-4,6279896031	0,000	1
54	-4,7852284343+1,0057155557i	0,160	0,978619854
55	-4,7852284343-1,0057155557i	0,160	0,978619854
56	-5,2541770103	0,000	1
57	-5,8741501632	0,000	1
58	-6,552531792+0,50620571834i	0,081	0,997029243
59	-6,552531792-0,50620571834i	0,081	0,997029243
60	-6,846044296	0,000	1
61	-6,9520501403	0,000	1
62	-6,9812182742+19,111336955i	3,042	0,343116195
63	-6,9812182742-19,111336955i	3,042	0,343116195
64	-7,6882561872	0,000	1
65	-18,086548015	0,000	1
66	-20	0,000	1
67	-20	0,000	1
68	-20,102128348	0,000	1
69	-20,55973057	0,000	1
70	-25,612398544	0,000	1
71	-28,292353077	0,000	1
72	-29,814987104	0,000	1
73	-32,31988354	0,000	1
74	-40,87709102+12,757962332i	2,030	0,954587146
75	-40,87709102-12,757962332i	2,030	0,954587146
76	-50	0,000	1
77	-50	0	1
78	-50	0	1
79	-51,634561771	0	1
80	-51,962224287	0	1
81	-52,190412925	0	1
82	-100	0	1
83	-103,06566059	0	1
84	-3012,759233	0	1
85	-3012,7676161	0	1
86	-3012,7802586	0	1
87	-997993,94967	0	1
88	-997993,94967	0	1
89	-997993,94967	0	1

B.5 The eigenvectors relating the states to the dominant eigenvalues when generator 2 is wind power without frequency controls

State name	State variable	Interarea mode (35)			Local mode, area 2 (37)		
		Controllability	Observability	Participation	Controllability	Observability	Participation
DFIG Control; Irot-Ctrl; xd	xd	0,007	0,003	0,011	0,001	0,000	0,001
DFIG Control; Irot-Ctrl; xq	xq	0,005	0,005	0,015	0,001	0,001	0,002
DFIG Control; MPT; xp	xp	0,000	0,000	0,000	0,000	0,000	0,000
DFIG Control; PLL WT; x1	x1	0,000	0,020	0,001	0,000	0,001	0,000
DFIG Control; PLL WT; x2	x2	0,000	0,099	0,020	0,000	0,006	0,001
DFIG Control; PQ control; xflt	xflt	0,000	0,000	0,000	0,000	0,000	0,000
DFIG Control; PQ control; xlim	xlim	0,000	0,000	0,000	0,000	0,000	0,000
DFIG Control; PQ control; xpctrl	xpctrl	0,000	0,200	0,011	0,000	0,107	0,002
DFIG Control; PQ control; xqctrl	xqctrl	0,006	0,008	0,032	0,000	0,001	0,001
DFIG Control; PQ control; xr	xr	0,000	0,000	0,000	0,000	0,000	0,000
DFIG Control; PQ control; xu	xu	0,000	0,000	0,000	0,000	0,000	0,000
DFIG Control; Pitch Control; xder	xder	0,000	0,000	0,000	0,000	0,000	0,000
DFIG Control; Pitch Control; xip	xip	0,000	0,000	0,000	0,000	0,000	0,000
DFIG Control; Pitch Control; xp	xp	0,000	0,000	0,000	0,000	0,000	0,000
DFIG Control; Shaft; dphi12	dphi12	0,024	0,000	0,000	0,000	0,000	0,000
DFIG Control; Shaft; xH	xH	0,013	0,000	0,000	0,000	0,000	0,000
DFIG Control; Speed-Controller; xi	xi	0,009	0,000	0,000	0,000	0,000	0,000
DFIG Control; Speed-Controller; xpc	xpc	0,013	0,000	0,000	0,000	0,000	0,000
Plant_G1; EXST2; xa	xa	0,000	1,000	0,001	0,000	0,713	0,000
Plant_G1; EXST2; xe	xe	0,000	1,000	0,000	0,000	0,713	0,000
Plant_G1; EXST2; xf	xf	0,000	0,987	0,119	0,000	0,540	0,030
Plant_G1; EXST2; xr	xr	0,004	0,005	0,012	0,000	0,006	0,009
Plant_G1; IEEEG1; x0	x0	0,000	0,000	0,000	0,000	0,000	0,000
Plant_G1; IEEEG1; x1	x1	0,002	0,012	0,012	0,000	0,002	0,000
Plant_G1; IEEEG1; x2	x2	0,006	0,007	0,024	0,000	0,000	0,000
Plant_G1; IEEEG1; x3	x3	0,009	0,001	0,003	0,000	0,000	0,000
Plant_G1; IEEEG1; x4	x4	0,009	0,000	0,000	0,000	0,000	0,000
Plant_G1; IEEEG1; x5	x5	0,000	0,000	0,000	0,000	0,000	0,000
Plant_G1; STAB1; x1	x1	0,086	0,006	0,303	0,004	0,001	0,008
Plant_G1; STAB1; x2	x2	0,003	0,019	0,039	0,000	0,006	0,007
Plant_G1; STAB1; x3	x3	0,028	0,001	0,018	0,001	0,000	0,000
Plant_G3; EXST2; xa	xa	0,000	0,816	0,000	0,000	1,000	0,003
Plant_G3; EXST2; xe	xe	0,000	0,816	0,000	0,000	1,000	0,000
Plant_G3; EXST2; xf	xf	0,000	0,805	0,043	0,000	0,757	0,356
Plant_G3; EXST2; xr	xr	0,002	0,022	0,024	0,004	0,007	0,086
Plant_G3; IEEEG1; x0	x0	0,000	0,000	0,000	0,000	0,000	0,000
Plant_G3; IEEEG1; x1	x1	0,001	0,021	0,015	0,000	0,002	0,003
Plant_G3; IEEEG1; x2	x2	0,004	0,012	0,029	0,002	0,000	0,003
Plant_G3; IEEEG1; x3	x3	0,006	0,001	0,004	0,003	0,000	0,000
Plant_G3; IEEEG1; x4	x4	0,006	0,000	0,000	0,003	0,000	0,000
Plant_G3; IEEEG1; x5	x5	0,000	0,000	0,000	0,000	0,000	0,000
Plant_G3; STAB1; x1	x1	0,038	0,010	0,234	0,035	0,001	0,094
Plant_G3; STAB1; x2	x2	0,001	0,034	0,030	0,003	0,007	0,077
Plant_G3; STAB1; x3	x3	0,012	0,002	0,014	0,008	0,000	0,004
Plant_G4; EXST2; xa	xa	0,000	0,907	0,000	0,000	0,899	0,003
Plant_G4; EXST2; xe	xe	0,000	0,907	0,000	0,000	0,899	0,000
Plant_G4; EXST2; xf	xf	0,000	0,895	0,047	0,000	0,680	0,356
Plant_G4; EXST2; xr	xr	0,002	0,019	0,020	0,004	0,008	0,104
Plant_G4; IEEEG1; x0	x0	0,000	0,000	0,000	0,000	0,000	0,000
Plant_G4; IEEEG1; x1	x1	0,001	0,018	0,011	0,000	0,003	0,005
Plant_G4; IEEEG1; x2	x2	0,004	0,010	0,021	0,002	0,001	0,006
Plant_G4; IEEEG1; x3	x3	0,005	0,001	0,003	0,003	0,000	0,000
Plant_G4; IEEEG1; x4	x4	0,005	0,000	0,000	0,003	0,000	0,000
Plant_G4; IEEEG1; x5	x5	0,000	0,000	0,000	0,000	0,000	0,000
Plant_G4; STAB1; x1	x1	0,038	0,009	0,194	0,039	0,001	0,159
Plant_G4; STAB1; x2	x2	0,001	0,028	0,025	0,003	0,011	0,129
Plant_G4; STAB1; x3	x3	0,012	0,002	0,012	0,009	0,000	0,007
Two Area; DFIG_1.5MW; cosphiu	cosphiu	0,000	0,015	0,000	0,000	0,004	0,000
Two Area; DFIG_1.5MW; phim	phim	0,000	0,073	0,000	0,000	0,007	0,000
Two Area; DFIG_1.5MW; psiA1_i	psiA1_i	0,000	0,009	0,000	0,000	0,003	0,000
Two Area; DFIG_1.5MW; psiA1_r	psiA1_r	0,000	0,049	0,002	0,000	0,012	0,001
Two Area; DFIG_1.5MW; psiA2_i	psiA2_i	0,000	0,000	0,000	0,000	0,000	0,000
Two Area; DFIG_1.5MW; psiA2_r	psiA2_r	0,000	0,000	0,000	0,000	0,000	0,000
Two Area; DFIG_1.5MW; psiB_i	psiB_i	0,000	0,000	0,000	0,000	0,000	0,000
Two Area; DFIG_1.5MW; psiB_r	psiB_r	0,000	0,000	0,000	0,000	0,000	0,000
Two Area; DFIG_1.5MW; sinphiu	sinphiu	0,000	0,019	0,000	0,000	0,006	0,000
Two Area; DFIG_1.5MW; speed	speed	0,002	0,000	0,000	0,000	0,000	0,000
Two Area; G1; phi	phi	0,015	0,000	0,000	0,002	0,000	0,000
Two Area; G1; psi1d	psi1d	0,001	0,033	0,012	0,000	0,009	0,009
Two Area; G1; psi1q	psi1q	0,008	0,022	0,099	0,001	0,004	0,008
Two Area; G1; psi2q	psi2q	0,004	0,022	0,057	0,000	0,003	0,003
Two Area; G1; psifd	psifd	0,010	0,041	0,236	0,002	0,010	0,061
Two Area; G1; speed	speed	1,000	0,001	0,384	0,107	0,000	0,053
Two Area; G3; phi	phi	0,008	0,197	1,000	0,012	0,009	0,397
Two Area; G3; psi1d	psi1d	0,000	0,038	0,006	0,002	0,011	0,090
Two Area; G3; psi1q	psi1q	0,004	0,013	0,032	0,003	0,002	0,022
Two Area; G3; psi2q	psi2q	0,002	0,013	0,018	0,001	0,002	0,009
Two Area; G3; psifd	psifd	0,004	0,035	0,088	0,015	0,014	0,698
Two Area; G3; speed	speed	0,658	0,001	0,443	0,896	0,000	0,592
Two Area; G4; phi	phi	0,007	0,178	0,760	0,014	0,008	0,371
Two Area; G4; psi1d	psi1d	0,000	0,040	0,006	0,003	0,011	0,102
Two Area; G4; psi1q	psi1q	0,003	0,015	0,032	0,003	0,006	0,065
Two Area; G4; psi2q	psi2q	0,002	0,015	0,018	0,002	0,005	0,026
Two Area; G4; psifd	psifd	0,004	0,039	0,097	0,016	0,013	0,738
Two Area; G4; speed	speed	0,572	0,001	0,321	1,000	0,000	1,000

B.6 The eigenvectors relating the synchronous generator speeds to the oscillatory modes

State	Eigenvalues				Eigenvector		
	Mode index	Real	Imag	Damping	Control	Obs	Part
Two Area; G1; speed	18	-0,049337	0,068822	0,582633	0,00269	0,000015	0,000143
Two Area; G1; speed	23	-0,17977	0,050467	0,962781	0,734503	0,000494	0,062646
Two Area; G1; speed	29	-0,217441	6,771341	0,032095	0,031903	0,000131	0,000634
Two Area; G1; speed	31	-0,237197	0,24849	0,690479	1	0,0009	0,382127
Two Area; G1; speed	35	-0,388421	3,2201	0,119756	1	0,000639	0,383677
Two Area; G1; speed	37	-0,976559	9,655499	0,100627	0,106683	0,000142	0,052591
Two Area; G1; speed	41	-1,566261	2,41172	0,544657	0,261631	0,000076	0,012439
Two Area; G1; speed	47	-2,258965	7,662291	0,282783	0,884313	0,000179	0,2432
Two Area; G1; speed	49	-2,291217	9,966278	0,224052	0,326068	0,00019	0,198404
Two Area; G1; speed	54	-4,785228	1,005716	0,97862	1	0,000056	0,1054
Two Area; G1; speed	58	-6,552532	0,506206	0,997029	0,127643	0,000014	0,00203
Two Area; G1; speed	62	-6,981218	19,111337	0,343116	1	0,000109	0,061167
Two Area; G1; speed	74	-40,877091	12,757962	0,954587	0,188377	0,000021	0,000675
Two Area; G3; speed	18	-0,049337	0,068822	0,582633	0,001002	0,000015	0,000053
Two Area; G3; speed	23	-0,17977	0,050467	0,962781	0,140203	0,000494	0,011955
Two Area; G3; speed	29	-0,217441	6,771341	0,032095	0,027209	0,000033	0,000134
Two Area; G3; speed	31	-0,237197	0,24849	0,690479	0,193857	0,000898	0,07392
Two Area; G3; speed	35	-0,388421	3,2201	0,119756	0,657677	0,001121	0,442956
Two Area; G3; speed	37	-0,976559	9,655499	0,100627	0,896224	0,00019	0,592251
Two Area; G3; speed	41	-1,566261	2,41172	0,544657	0,7193	0,000371	0,167279
Two Area; G3; speed	47	-2,258965	7,662291	0,282783	1	0,000067	0,103616
Two Area; G3; speed	49	-2,291217	9,966278	0,224052	0,700597	0,000125	0,280075
Two Area; G3; speed	54	-4,785228	1,005716	0,97862	0,44174	0,000074	0,06134
Two Area; G3; speed	58	-6,552532	0,506206	0,997029	0,876245	0,000113	0,112018
Two Area; G3; speed	62	-6,981218	19,111337	0,343116	0,119676	0,000016	0,001104
Two Area; G3; speed	74	-40,877091	12,757962	0,954587	0,07322	0,000003	0,000037
Two Area; G4; speed	18	-0,049337	0,068822	0,582633	0,00103	0,000015	0,000055
Two Area; G4; speed	23	-0,17977	0,050467	0,962781	0,122008	0,000494	0,010403
Two Area; G4; speed	29	-0,217441	6,771341	0,032095	0,010776	0,000024	0,000039
Two Area; G4; speed	31	-0,237197	0,24849	0,690479	0,170193	0,000898	0,064892
Two Area; G4; speed	35	-0,388421	3,2201	0,119756	0,57233	0,000934	0,321068
Two Area; G4; speed	37	-0,976559	9,655499	0,100627	1	0,000287	1
Two Area; G4; speed	41	-1,566261	2,41172	0,544657	1	0,000342	0,214684
Two Area; G4; speed	47	-2,258965	7,662291	0,282783	0,424845	0,000044	0,02844
Two Area; G4; speed	49	-2,291217	9,966278	0,224052	1	0,000132	0,422787
Two Area; G4; speed	54	-4,785228	1,005716	0,97862	0,430064	0,000064	0,051636
Two Area; G4; speed	58	-6,552532	0,506206	0,997029	1	0,000109	0,123265
Two Area; G4; speed	62	-6,981218	19,111337	0,343116	0,297209	0,00003	0,005018
Two Area; G4; speed	74	-40,877091	12,757962	0,954587	0,125634	0,000003	0,000072

B.7 The eigenvalues when generator 2 is wind power with frequency controls

Number	Eigenvalue	Frequency	Damping Ratio
1	0	0,000	0
15	0	0,000	0
16	-0,000000000014	0,000	0
17	-0,033333333333	0,000	1
18	-0,040333022894+0,073336798853i	0,012	0,481898418
19	-0,040333022894-0,073336798853i	0,012	0,481898418
20	-0,099388108786	0,000	1
21	-0,099746184635	0,000	1
22	-0,1	0,000	1
23	-0,17461389098+0,056147702258i	0,009	0,951993916
24	-0,17461389098-0,056147702258i	0,009	0,951993916
25	-0,18548457222	0,000	1
26	-0,18557576136	0,000	1
27	-0,2	0,000	1
28	-0,20144086309	0,000	1
29	-0,20922608395+6,752850331i	1,075	0,030968513
30	-0,20922608395-6,752850331i	1,075	0,030968513
31	-0,21926759624+0,15568509582i	0,025	0,815374028
32	-0,21926759624-0,15568509582i	0,025	0,815374028
33	-0,30087243301	0,000	1
34	-0,30209857757	0,000	1
35	-0,5363531084+2,8773646228i	0,458	0,183247858
36	-0,5363531084-2,8773646228i	0,458	0,183247858
37	-0,967834221+9,6325466388i	1,533	0,099972068
38	-0,967834221-9,6325466388i	1,533	0,099972068
39	-1	0,000	1
40	-1	0,000	1
41	-1,5575018672+2,4132997461i	0,384	0,54225821
42	-1,5575018672-2,4132997461i	0,384	0,54225821
43	-1,8944773732	0,000	1
44	-1,942641173+0,03081609609i	0,005	0,999874207
45	-1,942641173-0,03081609609i	0,005	0,999874207
46	-1,964163525	0,000	1
47	-2,2551235934+8,7426577509i	1,391	0,249769384
48	-2,2551235934-8,7426577509i	1,391	0,249769384
49	-2,3328375087+10,095424536i	1,607	0,225145769
50	-2,3328375087-10,095424536i	1,607	0,225145769
51	-2,952437806+3,9051094331i	0,622	0,603081513
52	-2,952437806-3,9051094331i	0,622	0,603081513
53	-4,045357571+0,09319716625i	0,015	0,99973473
54	-4,045357571-0,09319716625i	0,015	0,99973473
55	-4,8051662241	0,000	1
56	-5,2860021896	0,000	1
57	-5,8806476311	0,000	1
58	-6,4478280197+0,12200576761i	0,019	0,999821027
59	-6,4478280197-0,12200576761i	0,019	0,999821027
60	-6,5701462409+0,50489801416i	0,080	0,99706026
61	-6,5701462409-0,50489801416i	0,080	0,99706026
62	-6,8517986296	0,000	1
63	-7,8956018818	0,000	1
64	-19,240669983	0,000	1
65	-19,873116588	0,000	1
66	-20	0,000	1
67	-20	0,000	1
68	-20,616676317	0,000	1
69	-25,612827748	0,000	1
70	-28,221010469	0,000	1
71	-29,724489509	0,000	1
72	-32,320266181	0,000	1
73	-42,896193223+11,58441533i	1,844	0,965415244
74	-42,896193223-11,58441533i	1,844	0,965415244
75	-50	0,000	1
76	-50	0,000	1
77	-50	0	1
78	-51,634664339	0	1
79	-51,964354118	0	1
80	-52,22986932	0	1
81	-68,039340109	0	1
82	-100	0	1
83	-109,76100599	0	1
84	-3012,7592331	0	1
85	-3012,7676183	0	1
86	-3012,7802587	0	1
87	-997993,94967	0	1
88	-997993,94967	0	1
89	-997993,94967	0	1

B.8 The eigenvectors relating the states to the dominant eigenvalues when generator 2 is wind power with frequency controls

State name	State variable	Interarea mode (35)			Local mode, area 2 (37)		
		Controllability	Observability	Participation	Controllability	Observability	Participation
DFIG Control; Frequency; x1	x1	1,000	0,000	0,241	0,016	0,000	0,002
DFIG Control; Frequency; x2	x2	0,000	0,056	0,000	0,000	0,003	0,000
DFIG Control; Frequency; x3	x3	0,000	0,050	0,000	0,000	0,003	0,000
DFIG Control; Irot-Ctirl; xd	xd	0,008	0,002	0,009	0,001	0,000	0,000
DFIG Control; Irot-Ctirl; xq	xq	0,004	0,004	0,008	0,000	0,001	0,000
DFIG Control; MPT; xp	xp	0,000	0,002	0,000	0,000	0,000	0,000
DFIG Control; PLL WT; x1	x1	0,000	0,015	0,001	0,000	0,001	0,000
DFIG Control; PLL WT; x2	x2	0,008	0,072	0,312	0,000	0,004	0,005
DFIG Control; PQ control; xflt	xflt	0,000	0,000	0,000	0,000	0,000	0,000
DFIG Control; PQ control; xlim	xlim	0,000	0,000	0,000	0,000	0,000	0,000
DFIG Control; PQ control; xpctrl	xpctrl	0,000	0,159	0,008	0,000	0,017	0,000
DFIG Control; PQ control; xqctrl	xqctrl	0,005	0,007	0,018	0,000	0,001	0,000
DFIG Control; PQ control; xr	xr	0,000	0,000	0,000	0,000	0,000	0,000
DFIG Control; PQ control; xu	xu	0,000	0,000	0,000	0,000	0,000	0,000
DFIG Control; Pitch Control; xder	xder	0,000	0,000	0,000	0,000	0,000	0,000
DFIG Control; Pitch Control; xip	xip	0,000	0,000	0,000	0,000	0,000	0,000
DFIG Control; Pitch Control; xp	xp	0,000	0,000	0,000	0,000	0,000	0,000
DFIG Control; Shaft; dphi12	dphi12	0,027	0,000	0,004	0,000	0,000	0,000
DFIG Control; Shaft; xH	xH	0,016	0,001	0,007	0,000	0,000	0,000
DFIG Control; Speed-Controller; xi	xi	0,013	0,000	0,000	0,000	0,000	0,000
DFIG Control; Speed-Controller; xpc	xpc	0,015	0,000	0,003	0,000	0,000	0,000
Plant_G1; EXST2; xa	xa	0,000	0,989	0,000	0,000	0,617	0,000
Plant_G1; EXST2; xe	xe	0,000	0,989	0,000	0,000	0,617	0,000
Plant_G1; EXST2; xf	xf	0,000	1,000	0,100	0,000	0,467	0,024
Plant_G1; EXST2; xr	xr	0,004	0,007	0,014	0,000	0,005	0,007
Plant_G1; IEEEG1; x0	x0	0,000	0,000	0,000	0,000	0,000	0,000
Plant_G1; IEEEG1; x1	x1	0,002	0,005	0,004	0,000	0,001	0,000
Plant_G1; IEEEG1; x2	x2	0,006	0,003	0,009	0,000	0,000	0,000
Plant_G1; IEEEG1; x3	x3	0,009	0,000	0,001	0,000	0,000	0,000
Plant_G1; IEEEG1; x4	x4	0,009	0,000	0,000	0,000	0,000	0,000
Plant_G1; IEEEG1; x5	x5	0,000	0,000	0,000	0,000	0,000	0,000
Plant_G1; STAB1; x1	x1	0,086	0,002	0,103	0,004	0,000	0,005
Plant_G1; STAB1; x2	x2	0,003	0,007	0,011	0,000	0,004	0,004
Plant_G1; STAB1; x3	x3	0,029	0,000	0,006	0,001	0,000	0,000
Plant_G3; EXST2; xa	xa	0,000	0,679	0,000	0,000	1,000	0,003
Plant_G3; EXST2; xe	xe	0,000	0,679	0,000	0,000	1,000	0,000
Plant_G3; EXST2; xf	xf	0,000	0,686	0,046	0,000	0,757	0,355
Plant_G3; EXST2; xr	xr	0,003	0,021	0,027	0,004	0,007	0,081
Plant_G3; IEEEG1; x0	x0	0,000	0,000	0,000	0,000	0,000	0,000
Plant_G3; IEEEG1; x1	x1	0,002	0,021	0,022	0,000	0,002	0,003
Plant_G3; IEEEG1; x2	x2	0,007	0,013	0,045	0,002	0,001	0,004
Plant_G3; IEEEG1; x3	x3	0,010	0,001	0,007	0,003	0,000	0,000
Plant_G3; IEEEG1; x4	x4	0,010	0,000	0,000	0,003	0,000	0,000
Plant_G3; IEEEG1; x5	x5	0,000	0,000	0,000	0,000	0,000	0,000
Plant_G3; STAB1; x1	x1	0,058	0,011	0,323	0,037	0,001	0,103
Plant_G3; STAB1; x2	x2	0,002	0,032	0,035	0,003	0,008	0,083
Plant_G3; STAB1; x3	x3	0,019	0,002	0,020	0,008	0,000	0,005
Plant_G4; EXST2; xa	xa	0,000	0,802	0,000	0,000	0,873	0,003
Plant_G4; EXST2; xe	xe	0,000	0,802	0,000	0,000	0,873	0,000
Plant_G4; EXST2; xf	xf	0,000	0,811	0,062	0,000	0,661	0,330
Plant_G4; EXST2; xr	xr	0,003	0,019	0,028	0,004	0,007	0,093
Plant_G4; IEEEG1; x0	x0	0,000	0,000	0,000	0,000	0,000	0,000
Plant_G4; IEEEG1; x1	x1	0,002	0,019	0,018	0,000	0,004	0,005
Plant_G4; IEEEG1; x2	x2	0,006	0,012	0,037	0,002	0,001	0,006
Plant_G4; IEEEG1; x3	x3	0,009	0,001	0,006	0,003	0,000	0,000
Plant_G4; IEEEG1; x4	x4	0,009	0,000	0,000	0,003	0,000	0,000
Plant_G4; IEEEG1; x5	x5	0,000	0,000	0,000	0,000	0,000	0,000
Plant_G4; STAB1; x1	x1	0,066	0,010	0,329	0,039	0,001	0,158
Plant_G4; STAB1; x2	x2	0,002	0,028	0,036	0,003	0,012	0,128
Plant_G4; STAB1; x3	x3	0,022	0,002	0,021	0,009	0,000	0,007
Two Area; DFIG_1.5MW; cosphiu	cosphiu	0,000	0,034	0,000	0,000	0,000	0,000
Two Area; DFIG_1.5MW; phim	phim	0,000	0,069	0,000	0,000	0,011	0,000
Two Area; DFIG_1.5MW; psiA1_i	psiA1_i	0,000	0,026	0,000	0,000	0,004	0,000
Two Area; DFIG_1.5MW; psiA1_r	psiA1_r	0,000	0,081	0,003	0,000	0,003	0,000
Two Area; DFIG_1.5MW; psiA2_i	psiA2_i	0,000	0,000	0,000	0,000	0,000	0,000
Two Area; DFIG_1.5MW; psiA2_r	psiA2_r	0,000	0,000	0,000	0,000	0,000	0,000
Two Area; DFIG_1.5MW; psiB_i	psiB_i	0,000	0,000	0,000	0,000	0,000	0,000
Two Area; DFIG_1.5MW; psiB_r	psiB_r	0,000	0,000	0,000	0,000	0,000	0,000
Two Area; DFIG_1.5MW; sinphiu	sinphiu	0,000	0,044	0,000	0,000	0,000	0,000
Two Area; DFIG_1.5MW; speed	speed	0,003	0,000	0,001	0,000	0,000	0,000
Two Area; G1; phi	phi	0,013	0,000	0,000	0,001	0,000	0,000
Two Area; G1; psi1d	psi1d	0,000	0,039	0,009	0,000	0,007	0,007
Two Area; G1; psi1q	psi1q	0,006	0,026	0,082	0,000	0,002	0,003
Two Area; G1; psi2q	psi2q	0,004	0,026	0,049	0,000	0,002	0,001
Two Area; G1; psifd	psifd	0,008	0,044	0,190	0,002	0,009	0,047
Two Area; G1; speed	speed	0,940	0,000	0,113	0,093	0,000	0,030
Two Area; G3; phi	phi	0,012	0,166	1,000	0,013	0,005	0,225
Two Area; G3; psi1d	psi1d	0,000	0,035	0,006	0,003	0,010	0,087
Two Area; G3; psi1q	psi1q	0,005	0,012	0,033	0,003	0,002	0,022
Two Area; G3; psi2q	psi2q	0,003	0,012	0,020	0,001	0,002	0,009
Two Area; G3; psifd	psifd	0,006	0,031	0,092	0,015	0,014	0,698
Two Area; G3; speed	speed	0,951	0,001	0,533	0,919	0,000	0,636
Two Area; G4; phi	phi	0,011	0,150	0,816	0,014	0,013	0,600
Two Area; G4; psi1d	psi1d	0,000	0,039	0,007	0,003	0,010	0,092
Two Area; G4; psi1q	psi1q	0,005	0,015	0,038	0,003	0,006	0,061
Two Area; G4; psi2q	psi2q	0,003	0,015	0,022	0,002	0,005	0,024
Two Area; G4; psifd	psifd	0,006	0,038	0,126	0,016	0,013	0,686
Two Area; G4; speed	speed	0,873	0,001	0,436	1,000	0,000	1,000

C Extended results from the stability analysis of synchronous generation

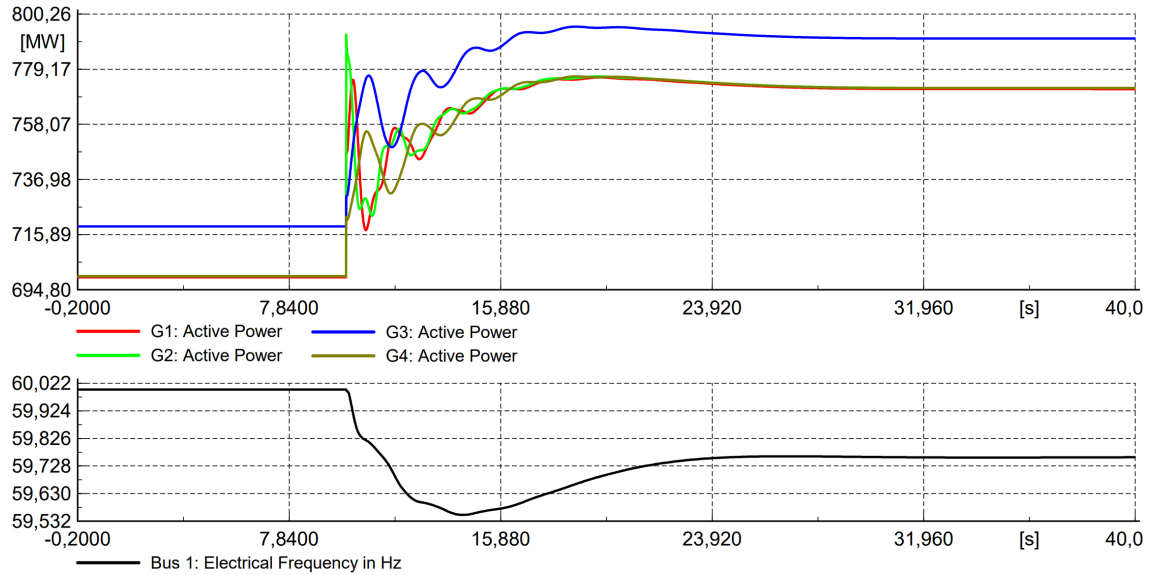


Figure C.1: The active power- and frequency response for a load step of 300MW at $t=10$ s on bus 7. The turbine governor gain is at its nominal value of 20.

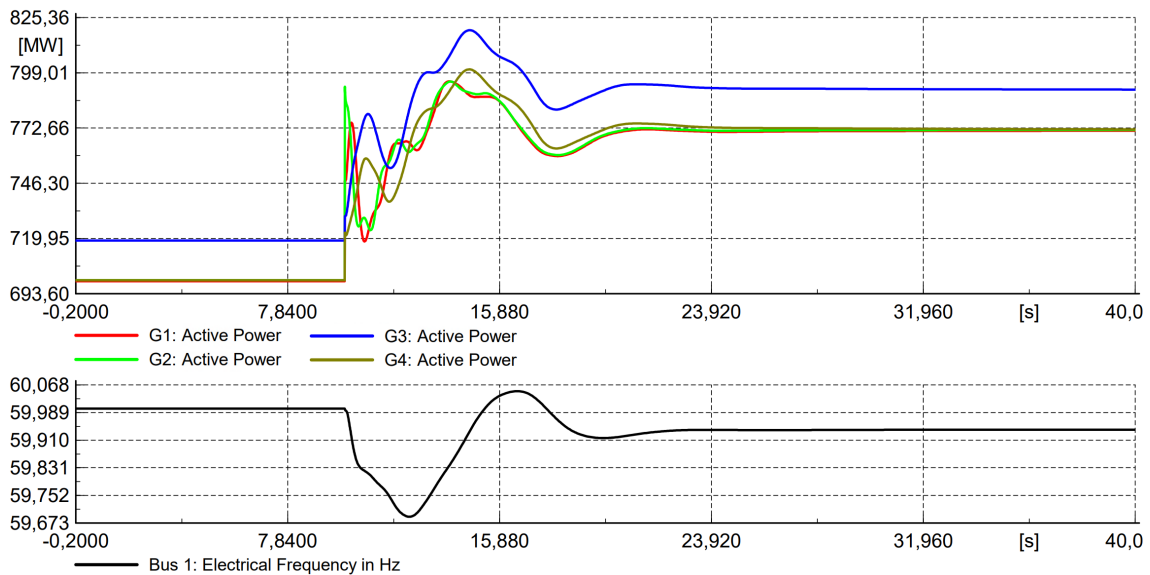


Figure C.2: The active power- and frequency response for a load step of 300MW at $t=10$ s on bus 7. The turbine governor gain is increased to 80.

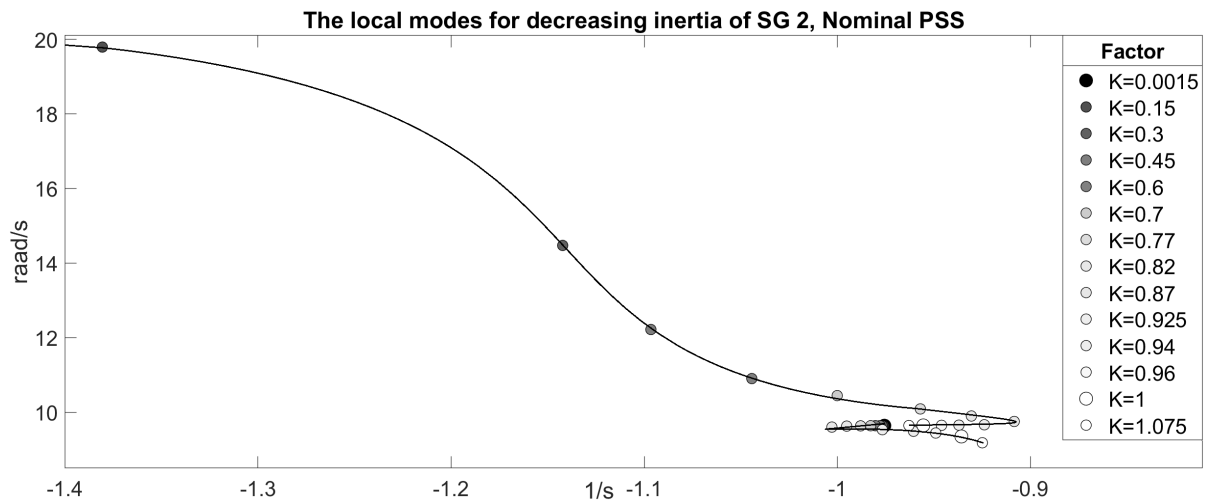


Figure C.3: The local modes for decreasing inertia of synchronous generator 2. The PSS is unchanged at its nominal values.

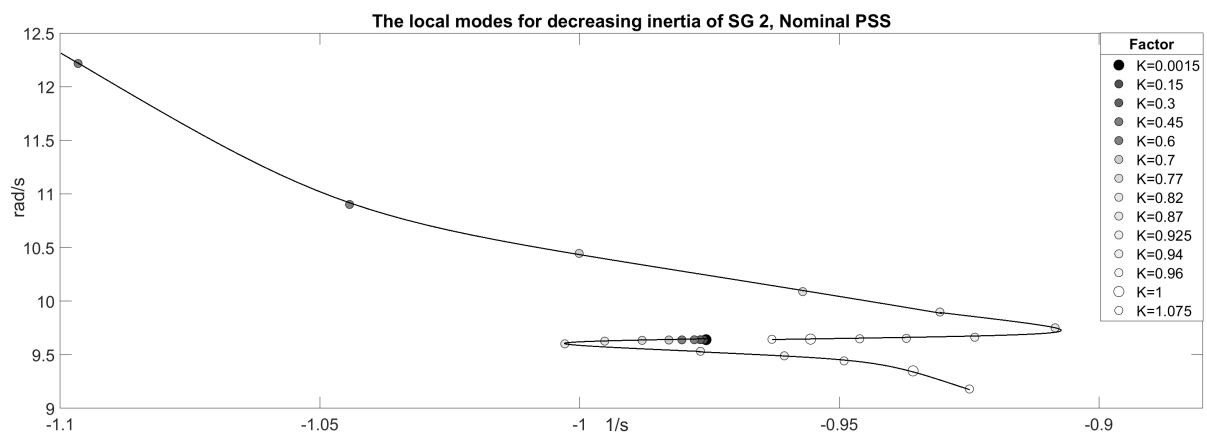


Figure C.4: The local modes for decreasing inertia of synchronous generator 2. The PSS is unchanged at its nominal values.

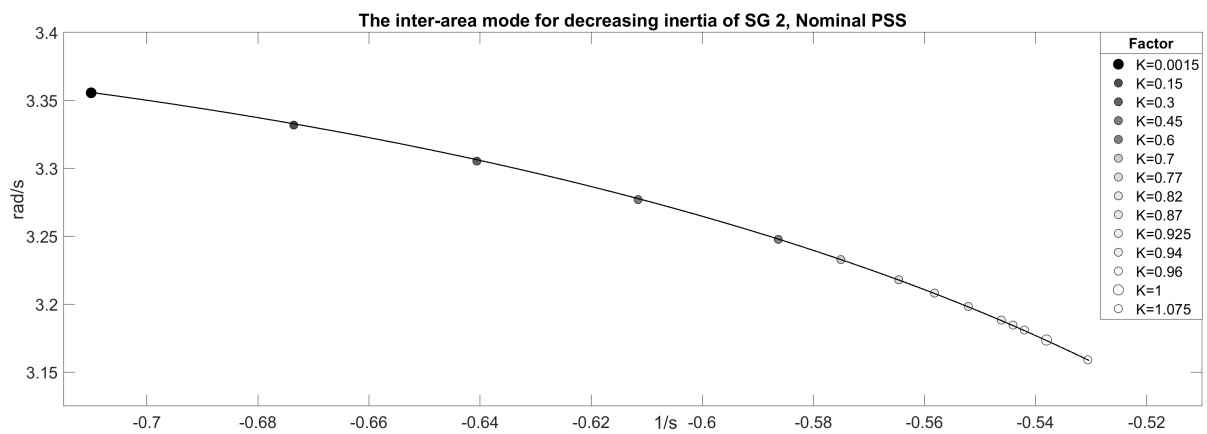


Figure C.5: The inter-area mode for decreasing inertia of synchronous generator 2. The PSS is unchanged at its nominal values.

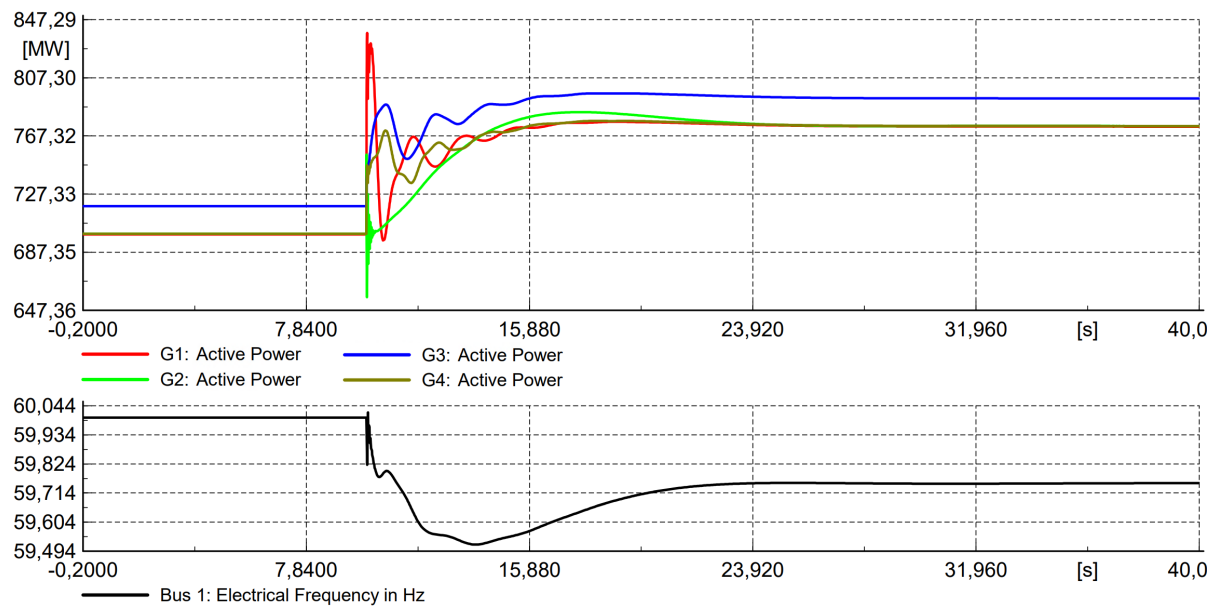


Figure C.6: The active power- and frequency response for a load step of 300MW at $t=10$ s on bus 7. Generator 2 is synchronous, and have an inertia of approximately zero.

C.1 Simple analytical eigenvalue calculation

A simplified analytical calculation of eigenvalues is deduced, for an uncontrolled system, based on the swing equation. The deduction is inspired from [15]. Firstly, the dynamics in one area are considered. Linearizing the swing equation, the damping power is proportional to the change of generator speed, and the electrical power is proportional to the change of rotor angle.

$$2H \frac{d\Delta\omega}{dt} = P_{m0} - (P_{e0} + K_e \Delta\delta_{12}) - D\Delta\omega$$

At steady-state, the sum of mechanical- and electrical power is zero.

$$2H \frac{d\Delta\omega}{dt} \Big|_{P_{m0}=P_{e0}} = -K_e(\Delta\delta_1 - \Delta\delta_2) - D\Delta\omega$$

For a tidy formulation of the state space, the quantity θ is defined.

$$\Delta\theta = \Delta\delta_1 - \Delta\delta_2 \rightarrow \Delta\dot{\theta} = \frac{d}{dt}(\Delta\delta_1 - \Delta\delta_2) = \Delta\omega_1\omega_0 - \Delta\omega_2\omega_0$$

Further, the linearised swing equations can be expressed with the quantity $\Delta\theta$.

$$2H\Delta\dot{\omega} = -K_e\Delta\theta - D\Delta\omega$$

The electrical power linearization coefficients are equal for both generators in an area.

$$K_{e1} = \frac{dP_{e1}}{d\delta_1} = \frac{E_1 E_2}{x_{e1}} \cos(\delta_1 - \delta_2) = K_{e2} \quad \text{since } \cos(\theta) = \cos(-\theta)$$

Further, the state space can be expressed, where the system's eigenvalues are calculated from the eigen-properties of the matrix.

$$\begin{bmatrix} \Delta\dot{\theta} \\ \Delta\dot{\omega}_1 \\ \Delta\dot{\omega}_2 \end{bmatrix} = \begin{bmatrix} 0 & \omega_0 & -\omega_0 \\ -\frac{K_e}{2H_1} & \frac{-D_1}{2H_1} & 0 \\ \frac{K_e}{2H_2} & 0 & \frac{-D_2}{2H_2} \end{bmatrix} \begin{bmatrix} \Delta\theta \\ \Delta\omega_1 \\ \Delta\omega_2 \end{bmatrix}$$

$$\det(A - \lambda I) = 0$$

Solving the eigenvalue vector λ , the local modes in one area are obtained. The expression can be further developed, without increasing the order of the matrix, by merging the generators in each area into one equivalent machine. The swing equations are similar to the individual generators but with the sum of inertia and damping.

$$2H_A\Delta\dot{\omega}_A = -K_i\Delta\theta_i - D_A\Delta\omega_A$$

$$2H_B\Delta\dot{\omega}_B = K_i\Delta\theta_i - D_B\Delta\omega_B$$

$$D_A = D_1 + D_2, \quad D_B = D_3 + D_4, \quad H_A = H_1 + H_2, \quad H_B = H_3 + H_4$$

The state-space now describes the dynamics of the merged generators.

$$\begin{bmatrix} \Delta\dot{\theta}_i \\ \Delta\dot{\omega}_A \\ \Delta\dot{\omega}_B \end{bmatrix} = \begin{bmatrix} 0 & \omega_0 & -\omega_0 \\ -\frac{K_i}{2H_A} & \frac{-D_A}{2H_A} & 0 \\ \frac{K_i}{2H_B} & 0 & \frac{-D_B}{2H_B} \end{bmatrix} \begin{bmatrix} \Delta\theta \\ \Delta\omega_A \\ \Delta\omega_B \end{bmatrix}$$

From the matrix, the inter-area mode can be calculated. The expression is further reduced into a one-machine system to get a simple mathematical expression for the inter-area mode and its dependency on the area inertias.

$$\begin{aligned}\Delta\dot{\omega}_A - \Delta\dot{\omega}_B &= \Delta\dot{\omega}_{AB} = \frac{-K_i\Delta\theta_i - D_A\Delta\omega_A}{2H_A} - \frac{K_i\Delta\theta_i - D_B\Delta\omega_B}{2H_B} = \\ \Delta\dot{\omega}_{AB} &= -\frac{K_i}{2(H_A||H_B)}\Delta\theta_i + \frac{D_B\Delta\omega_B * H_A - D_A\Delta\omega_A * H_B}{2H_1H_2} \\ \Delta\dot{\omega}_{AB} &= -\frac{K_i}{2(H_A||H_B)}\Delta\theta_i - \frac{D_AH_B + D_BH_A\frac{H_A}{H_B}}{2(1 + \frac{H_A}{H_B})H_AH_B}\Delta\omega_{AB}\end{aligned}$$

The second-order state space for the OMIB system can further be described.

$$\begin{bmatrix} \Delta\dot{\theta}_i \\ \Delta\dot{\omega}_{AB} \end{bmatrix} = \begin{bmatrix} 0 & \omega_0 \\ -\frac{K_i}{2H_{eq}} & -\frac{D_{eq}}{2} \end{bmatrix} \begin{bmatrix} \Delta\theta_i \\ \Delta\omega_{AB} \end{bmatrix}$$

By solving equation the characteristic equation of the A matrix, the eigenvalues of the OMIB system can be calculated. These will describe the inter-area mode.

$$\lambda = \frac{-D_{eq}}{4} \pm \sqrt{\frac{D_{eq}^2}{4} - \frac{K_i\omega_0}{2H_{eq}}}$$

This is a very simplified expression but can be used to justify the inter-area mode damping increase as the inertia in either area decreases.

D Extended results from the stability analysis of wind power without frequency service controls

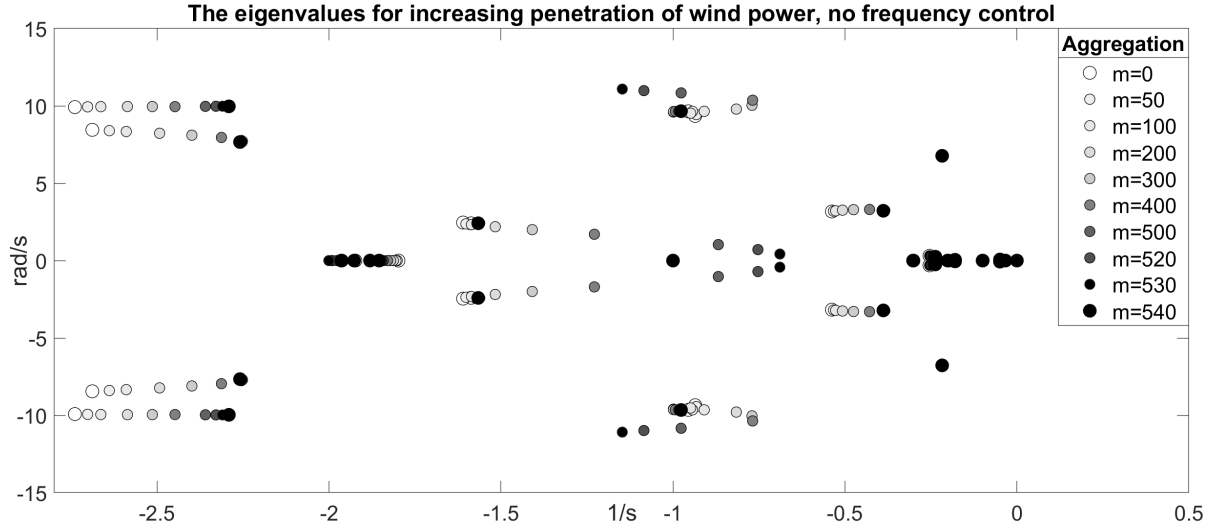


Figure D.1: The eigenvalues for an increasing wind power penetration without frequency controls. An aggregation of 540 equals complete wind power replacement of SG 2.

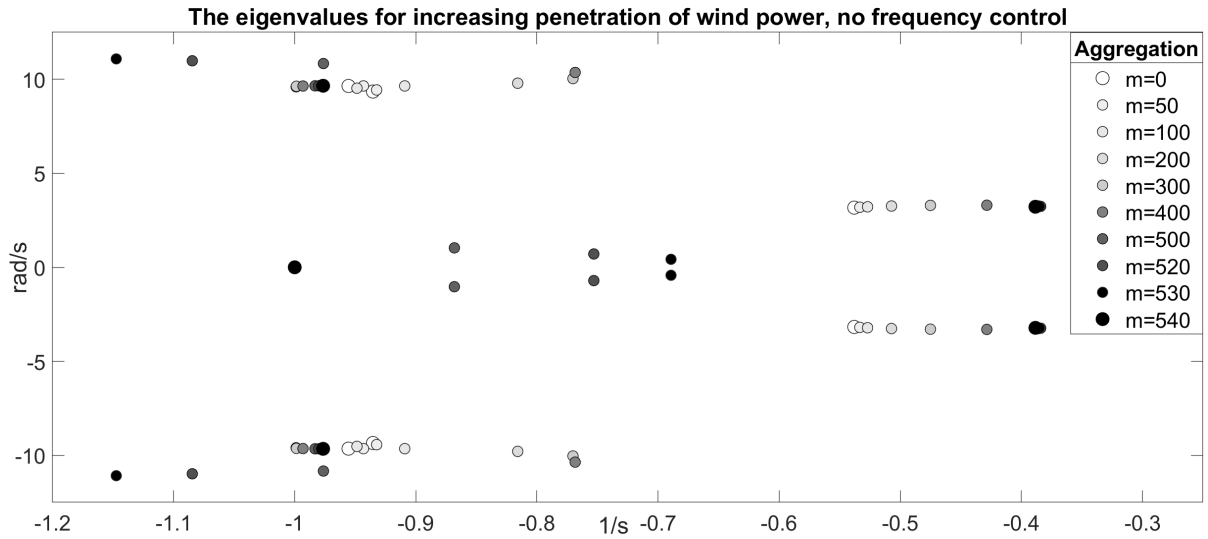


Figure D.2: The dominant eigenvalues for an increasing wind power penetration without frequency controls. An aggregation of 540 equals complete wind power replacement of SG 2.

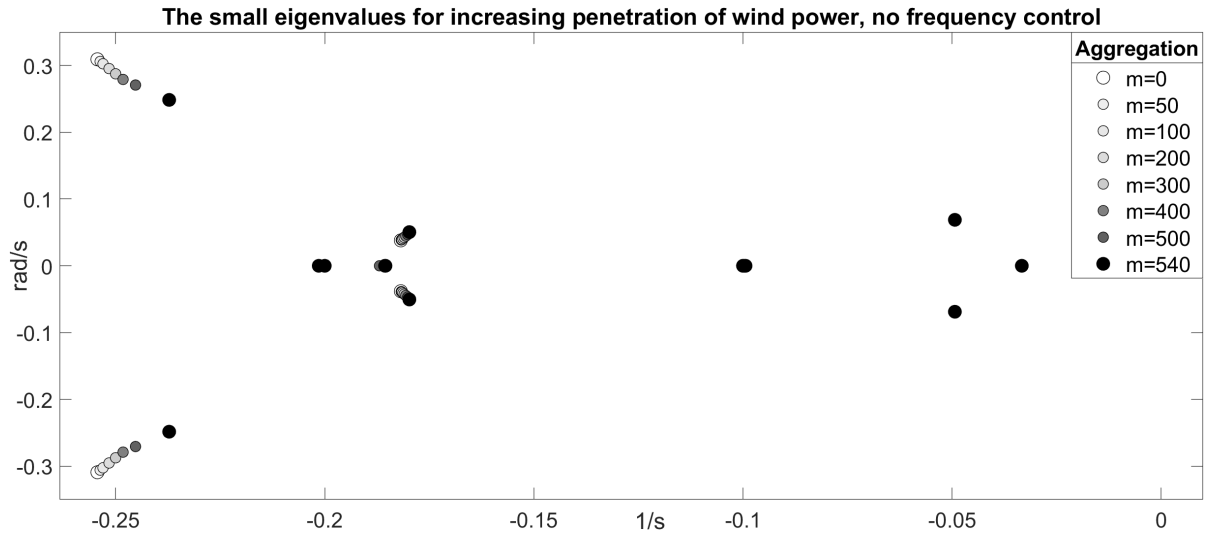


Figure D.3: The small modes for an increasing wind power penetration without frequency controls. An aggregation of 540 equals complete wind power replacement of SG 2.

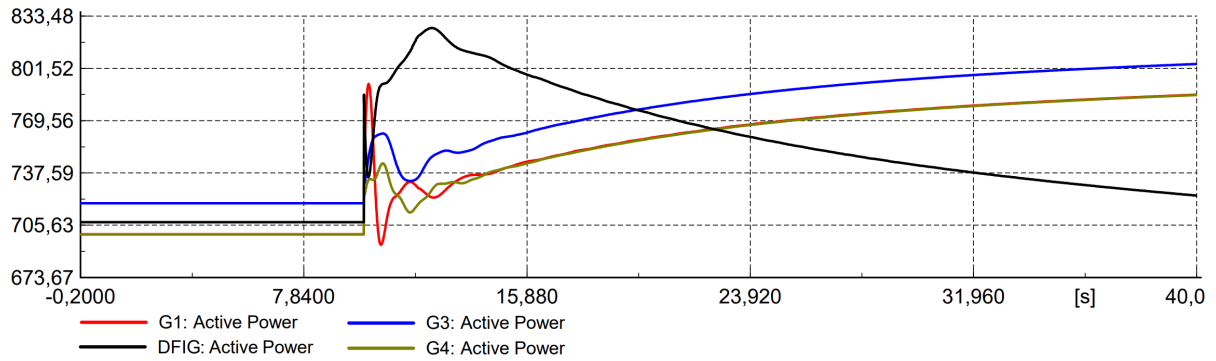


Figure D.4: Deactivated rotor current controls, meaning an unregulated rotor voltage. The compensation element is active. The active power response for a load step of 300MW at $t=10$ s on bus 7. No frequency controls are active.

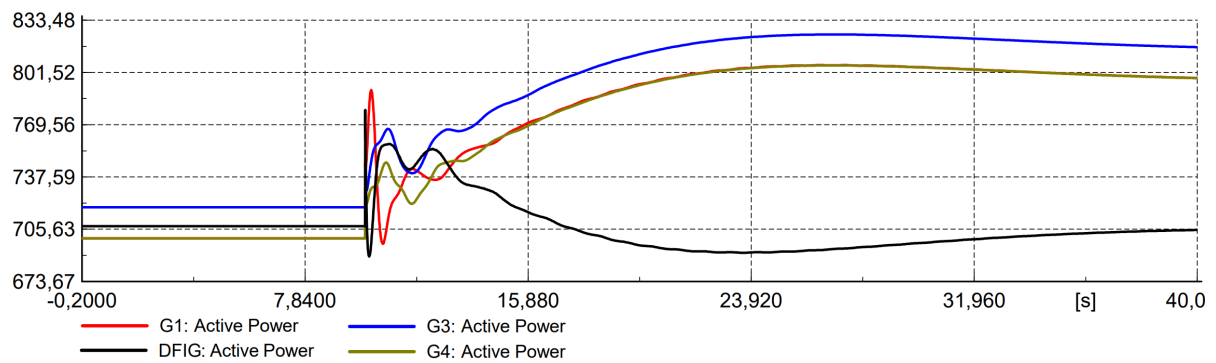


Figure D.5: Deactivated power controls, meaning a constant rotor current reference. Nominal rotor current controls. The active power response for a load step of 300MW at $t=10$ s on bus 7. No frequency controls are active.

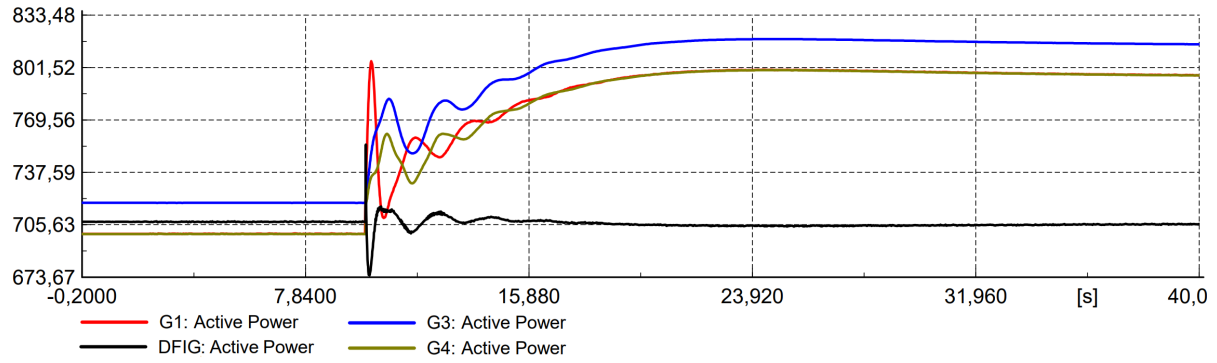


Figure D.6: Deactivated power controls, meaning a constant rotor current reference. The gain of the rotor current controls is increased. The active power response for a load step of 300MW at $t=10$ s on bus 7. No frequency controls are active.

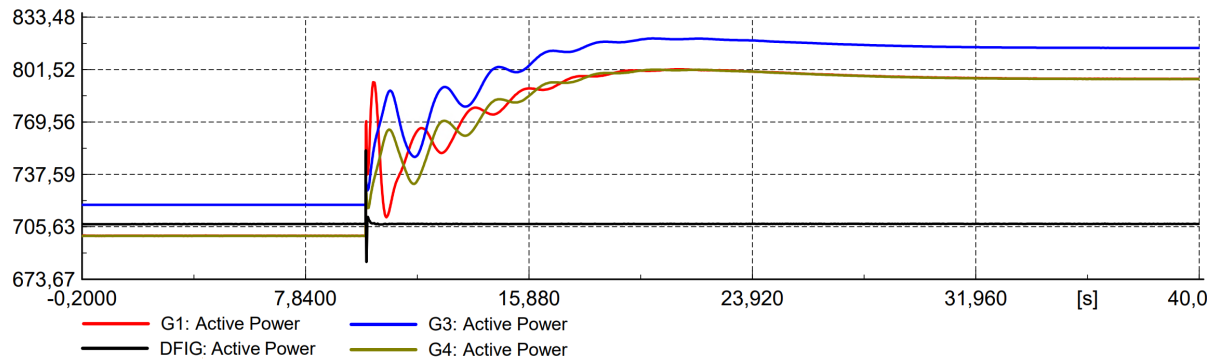


Figure D.7: Fast power- and nominal rotor current controls. The active power response for a load step of 300MW at $t=10$ s on bus 7. No frequency controls are active.

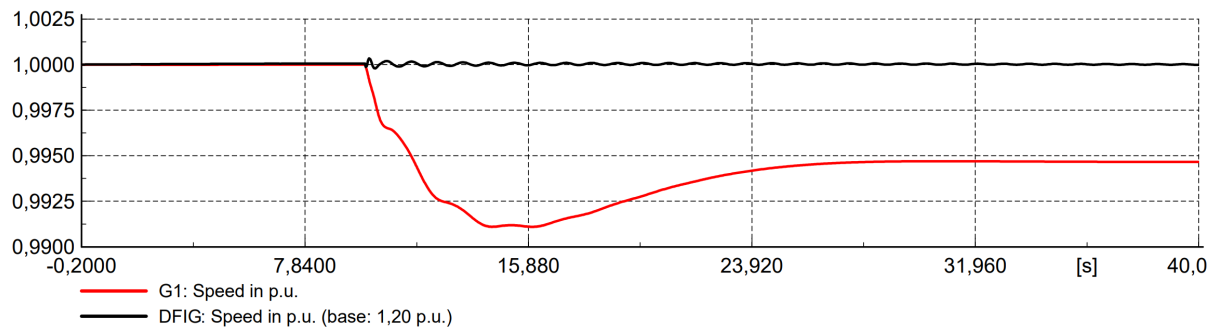


Figure D.8: Nominal power- and rotor current controls. The speed of the DFIG and generator one. As the wind turbine is nominally operated at the speed of 1.2p.u., this is the wind turbine speed base. A load step of 300MW occurs at $t=10$ s on bus 7. No frequency controls are active.

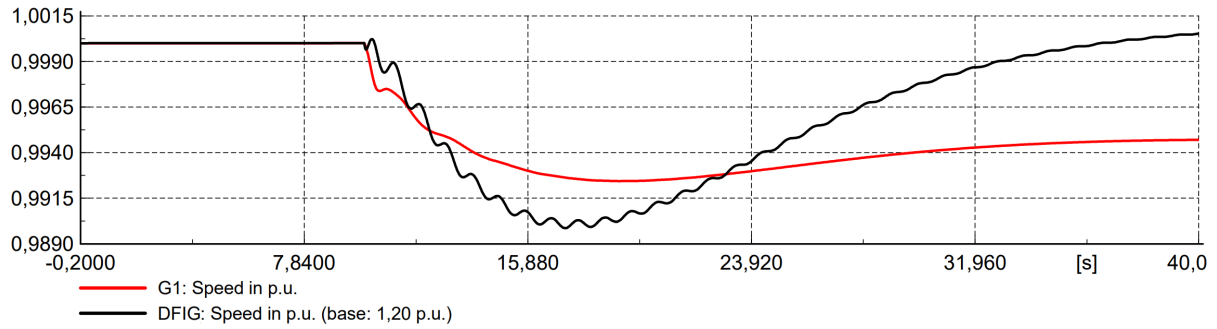


Figure D.9: Deactivated power controls, meaning a constant rotor current reference. Nominal rotor current controls. The speed of the DFIG and generator one. As the wind turbine is nominally operated at the speed of 1.2p.u, this is the wind turbine speed base. A load step of 300MW occurs at $t=10$ s on bus 7. No frequency controls are active.

	Name	Mode Index	Mode: Real part 1/s	Mode: Imaginary part rad/s	Controllability: Mag.	Observability: Mag.	Participation: Mag.
+	DFIG Control; Shaft; dphi12	29	-0,217441	6,771341	1,	0,006602	1,
+	Two Area; DFIG_1.5MW; speed	29	-0,217441	6,771341	0,261402	0,017868	0,707483
+	DFIG Control; Shaft; xH	29	-0,217441	6,771341	0,257706	0,007765	0,303131
+	DFIG Control; Speed-Controll...	29	-0,217441	6,771341	0,007909	0,009464	0,011337
+	DFIG Control; PQ control; xpctrl	29	-0,217441	6,771341	0,000111	0,115616	0,001939
+	DFIG Control; Irot-Ctrl; xd	29	-0,217441	6,771341	0,014865	0,000638	0,001436
+	Two Area; G1; psifd	29	-0,217441	6,771341	0,000929	0,007142	0,001005
+	Two Area; G1; speed	29	-0,217441	6,771341	0,031903	0,000131	0,000634
+	Plant_G1; EXST2; xf	29	-0,217441	6,771341	0,000011	0,291097	0,000504
+	Two Area; DFIG_1.5MW; psiA1_r	29	-0,217441	6,771341	0,000226	0,01253	0,000428
+	Two Area; G3; phi	29	-0,217441	6,771341	0,000334	0,007625	0,000385
+	Plant_G1; STAB1; x1	29	-0,217441	6,771341	0,003513	0,000704	0,000375
+	DFIG Control; PLL WT; x2	29	-0,217441	6,771341	0,000303	0,007113	0,000326
+	Two Area; G1; psi1q	29	-0,217441	6,771341	0,000911	0,001853	0,000256
+	Plant_G1; STAB1; x2	29	-0,217441	6,771341	0,000225	0,004747	0,000162
+	Two Area; G4; phi	29	-0,217441	6,771341	0,00015	0,007039	0,00016
+	Two Area; DFIG_1.5MW; psiA1_i	29	-0,217441	6,771341	0,000147	0,007097	0,000158
+	Two Area; DFIG_1.5MW; sinphiu	29	-0,217441	6,771341	0,000131	0,00717	0,000142
+	Two Area; G3; speed	29	-0,217441	6,771341	0,027209	0,000033	0,000134
+	Two Area; G1; psi2q	29	-0,217441	6,771341	0,00047	0,001654	0,000118
+	Plant_G1; EXST2; xr	29	-0,217441	6,771341	0,00027	0,002739	0,000112
+	DFIG Control; Speed-Controll...	29	-0,217441	6,771341	0,002802	0,000264	0,000112
+	Two Area; G1; psi1d	29	-0,217441	6,771341	0,000111	0,006135	0,000103
+	Two Area; G3; psifd	29	-0,217441	6,771341	0,000541	0,00093	0,000076
+	Two Area; G4; psifd	29	-0,217441	6,771341	0,000388	0,001097	0,000064
+	DFIG Control; PQ control; xqctrl	29	-0,217441	6,771341	0,001026	0,000395	0,000061
+	Plant_G3; STAB1; x1	29	-0,217441	6,771341	0,002047	0,000175	0,000054
+	Two Area; G4; speed	29	-0,217441	6,771341	0,010776	0,000024	0,000039

Figure D.10: The eigenvectors relating the states to the mechanical mode 19.

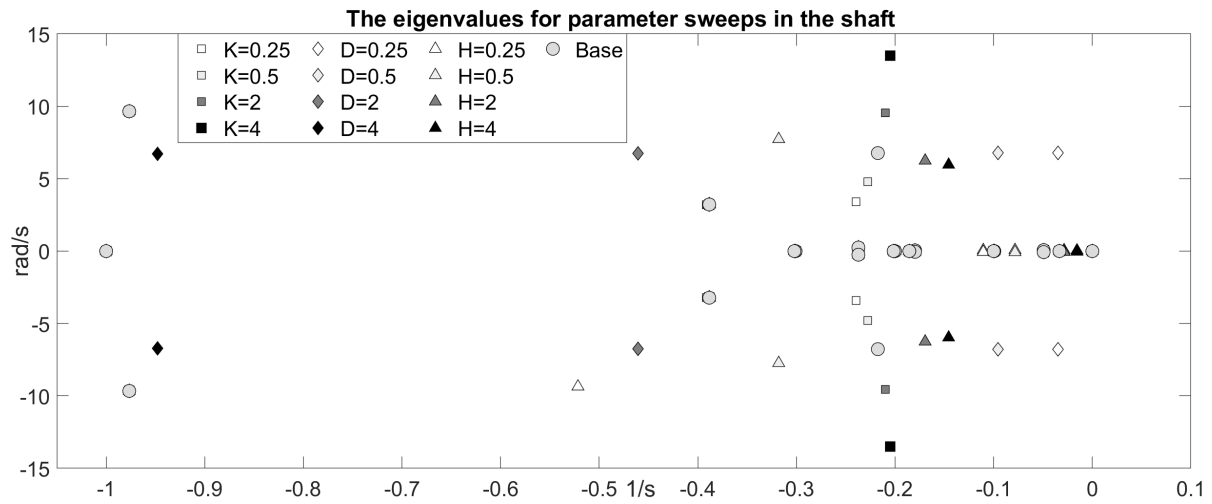


Figure D.11: The mechanical mode as a function of the shaft stiffness K , damping D , and inertia H .

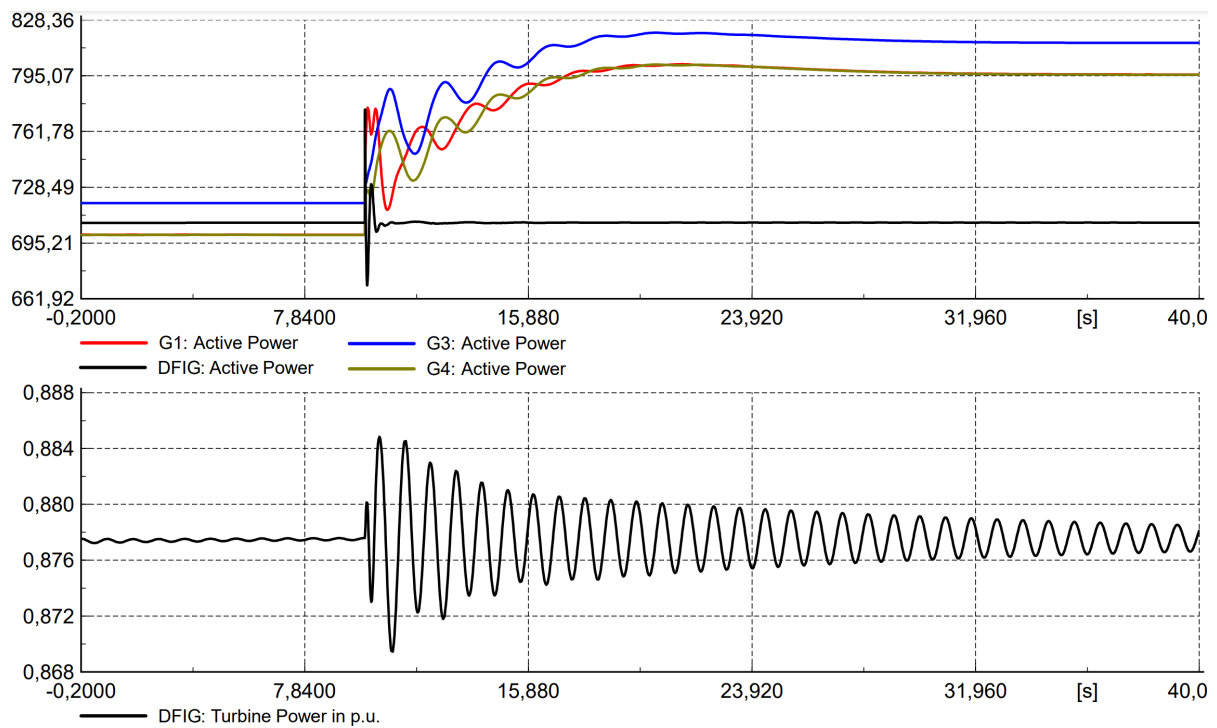


Figure D.12: The turbine power oscillations for a load step of 300MW at $t=10$ s on bus 7.

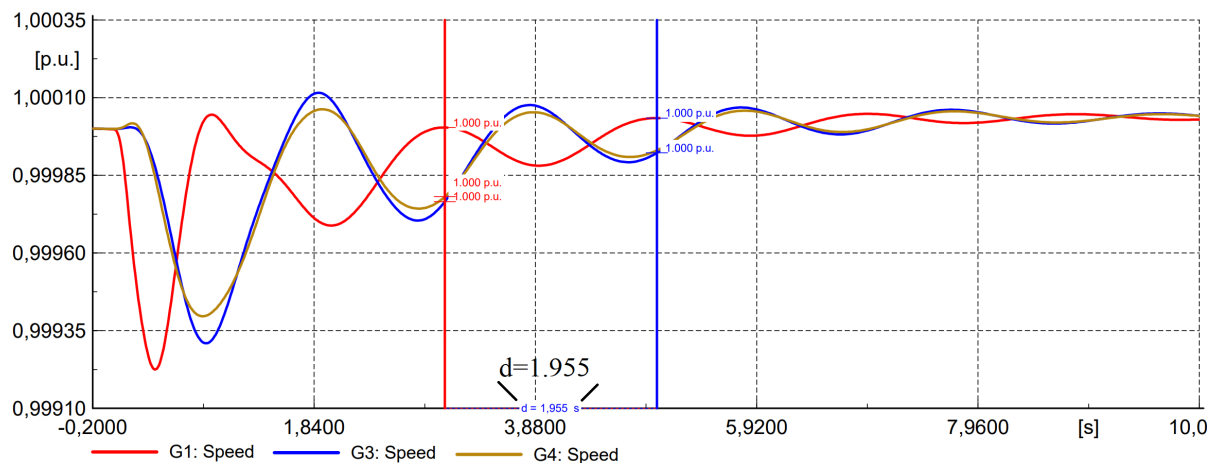


Figure D.13: The speed of the SGs for a step increase of voltage reference in generator 1, of 5% between $t=0-0.1$ s.

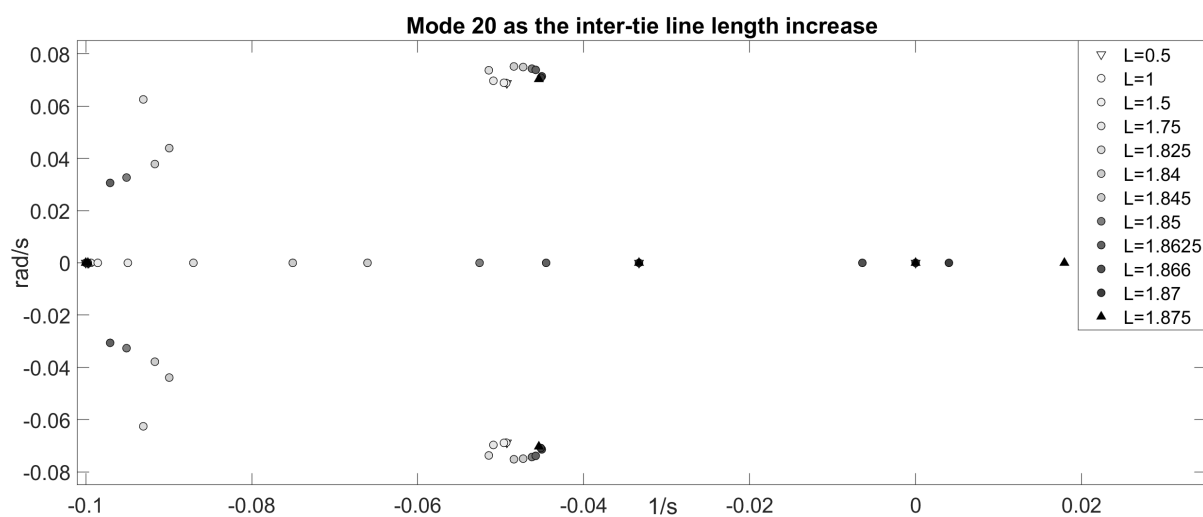


Figure D.14: The development of mode 20 for an increasing inter-tie line length. To the left is the final development of modes 23 and 24, and the mode performing the circular movement is modes 18 and 19.





	Name	Mode: Real part 1/s	Mode: Imaginary part rad/s	Controllability: Mag.
+	Plant_G1; IEEE1; x4	-0,099388	0,	1,
+	Plant_G4; IEEE1; x4	-0,099388	0,	0,505934
+	Plant_G1; IEEE1; x3	-0,099388	0,	0,494061
+	Plant_G3; IEEE1; x4	-0,099388	0,	0,493273
+	Plant_G4; IEEE1; x3	-0,099388	0,	0,249962
+	Plant_G3; IEEE1; x3	-0,099388	0,	0,243707
<div style="display: flex; justify-content: space-around; align-items: center;"> <div style="text-align: center;">  </div> <div style="text-align: center;">  </div> </div>				
+	DFIG Control; Speed-Controller; xi	-0,099388	0,	0,018848
<div style="display: flex; justify-content: space-around; align-items: center;"> <div style="text-align: center;">  </div> <div style="text-align: center;">  </div> </div>				
+	DFIG Control; Shaft; xH	-0,099388	0,	0,006535

Figure D.15: The states with the highest control over mode 20 for nominal inter-tie line length.

	Name	Mode: Real part 1/s	Mode: Imaginary part rad/s	Controllability: Mag.
+	DFIG Control; Speed-Controller; xi	-0,052546	0,	1,
+	Two Area; G1; speed	-0,052546	0,	0,801
+	Plant_G1; IEEE1; x4	-0,052546	0,	0,467437
+	Plant_G1; STAB1; x3	-0,052546	0,	0,458267
+	Two Area; G3; speed	-0,052546	0,	0,374664
+	Two Area; G4; speed	-0,052546	0,	0,367006
+	Plant_G1; IEEE1; x3	-0,052546	0,	0,275169
+	Plant_G3; IEEE1; x4	-0,052546	0,	0,230149
+	Plant_G4; IEEE1; x4	-0,052546	0,	0,225445
+	DFIG Control; Shaft; xH	-0,052546	0,	0,215586

Figure D.16: The states with the highest control over mode 20 for the inter-tie line length factor 1.85.

	Name	Mode: Real part 1/s	Mode: Imaginary part rad/s	Controllability: Mag.
+	Two Area; G1; speed	0,017929	0,	1,
+	DFIG Control; Shaft; xH	0,017929	0,	0,909629
+	Two Area; G3; speed	0,017929	0,	0,48664
+	Two Area; G4; speed	0,017929	0,	0,475423
+	Two Area; DFIG_1.5MW; speed	0,017929	0,	0,400945
+	Plant_G1; STAB1; x3	0,017929	0,	0,373371
+	Plant_G1; IEEE1; x4	0,017929	0,	0,234822
+	Plant_G1; STAB1; x1	0,017929	0,	0,16315
+	Plant_G1; IEEE1; x3	0,017929	0,	0,159442
+	Plant_G4; STAB1; x3	0,017929	0,	0,141411
+	Plant_G3; IEEE1; x4	0,017929	0,	0,120288
+	Plant_G4; IEEE1; x4	0,017929	0,	0,117516
+	DFIG Control; Speed-Controller; xi	0,017929	0,	0,102687

Figure D.17: The states with the highest control over mode 20 for the inter-tie line length factor 1.875.

E Extended results from the stability analysis of wind power with frequency service controls

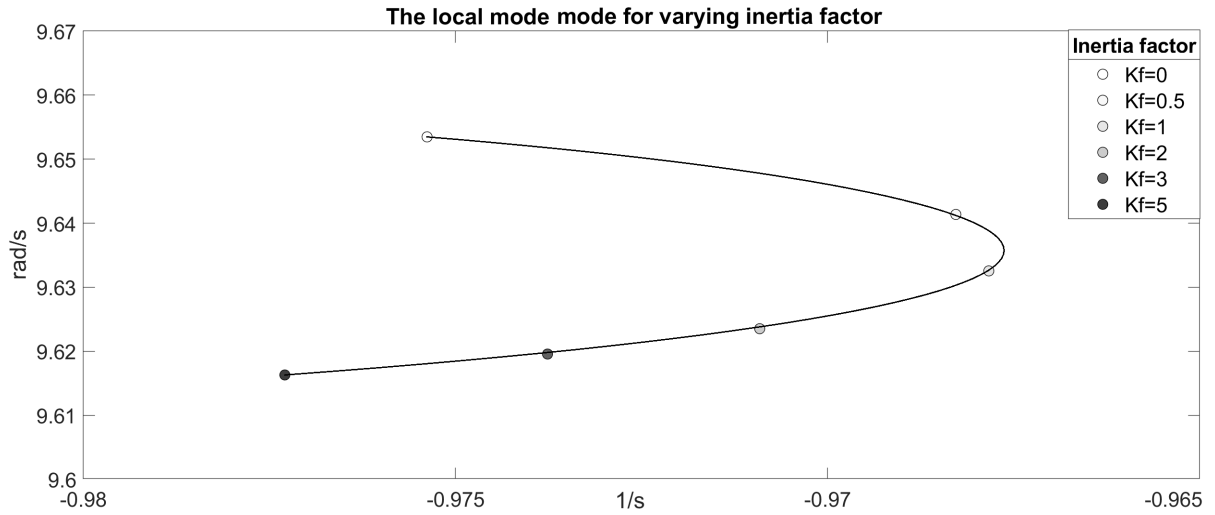


Figure E.1: The development of the local mode in area two for a varying inertia factor.

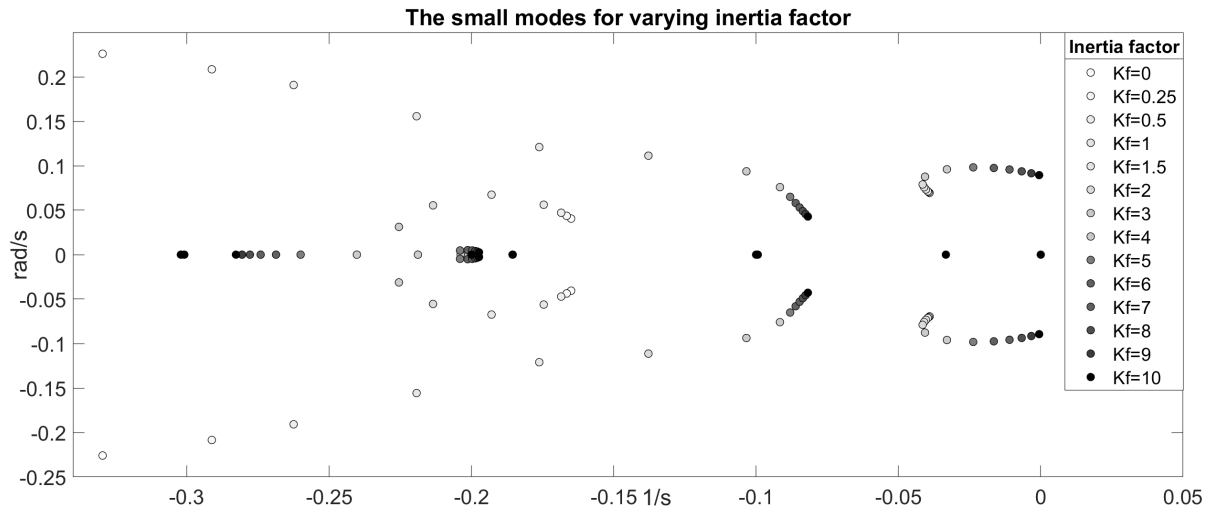


Figure E.2: The development of the small modes for a varying inertia factor.

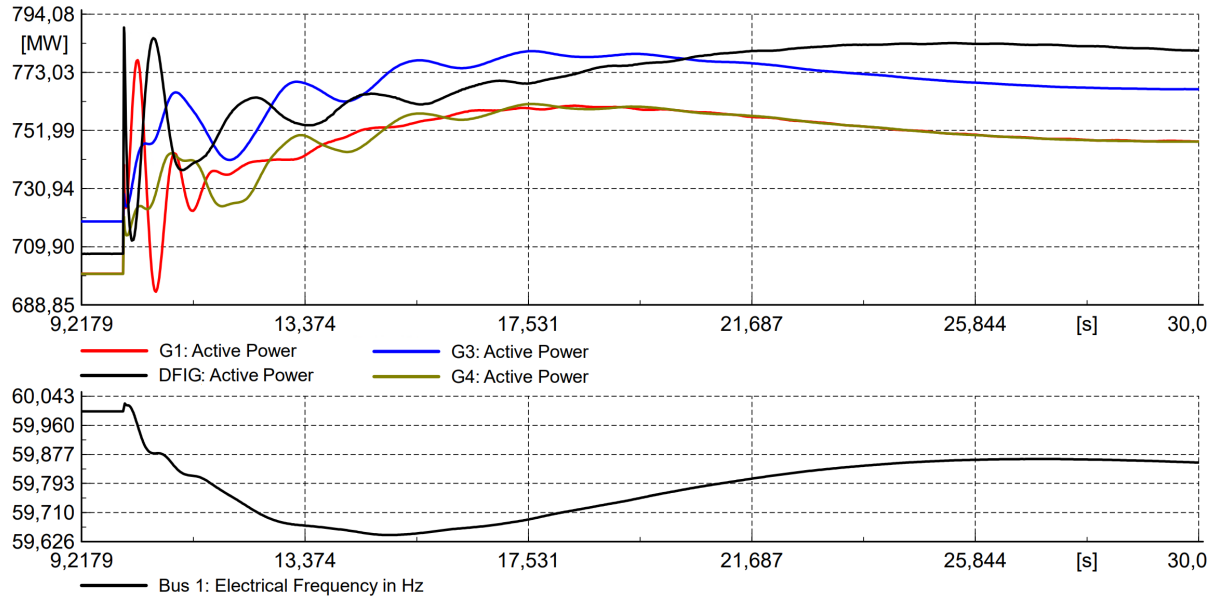


Figure E.3: The active power- and frequency response for a load step of 300MW at $t=10$ s on bus 7. The synthetic inertia derivator is extra sensitive, with a time constant multiplied by 0.3. The gain is adjusted to keep the inertial contribution in accordance with the wind turbine's stored kinetic energy. The parameters are $T_{der} = 0.09$, $K_{der} = 1.37$.

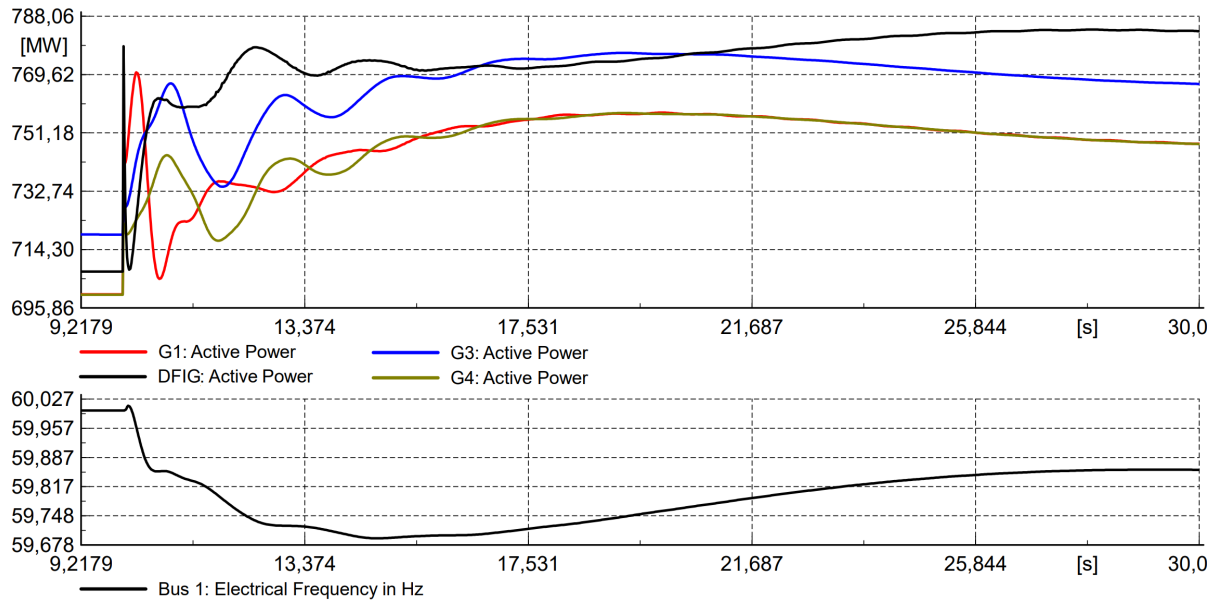


Figure E.4: The active power- and frequency response for a load step of 300MW at $t=10$ s on bus 7. The synthetic inertia derivator is slow, with a time constant multiplied by 4. The gain is adjusted to keep the inertial contribution in accordance with the wind turbine's stored kinetic energy. The parameters are $T_{der} = 1.2$, $K_{inert} = 2.75$.

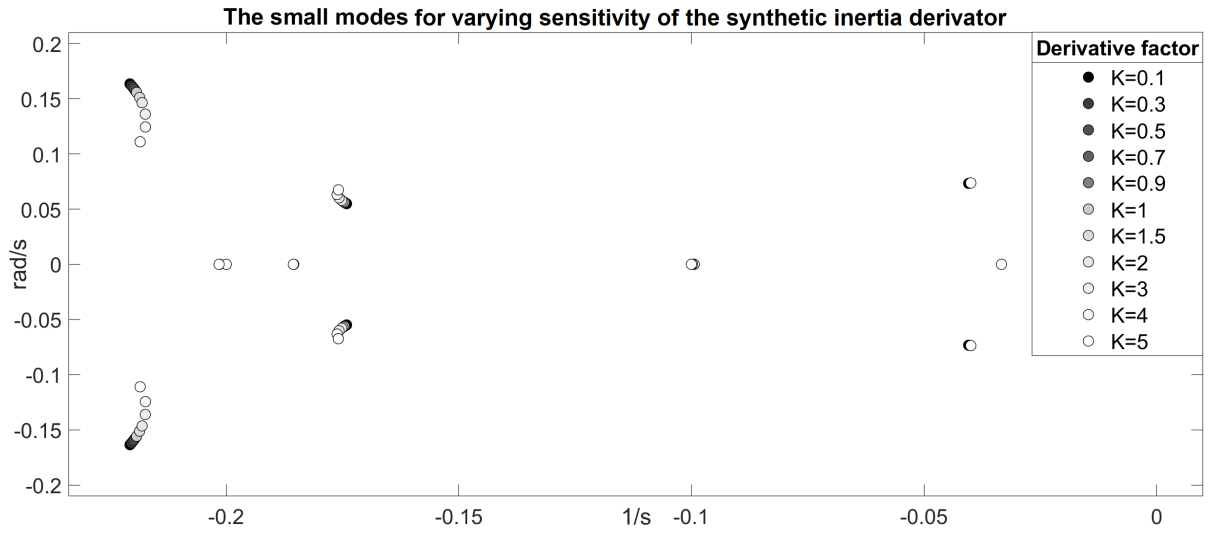


Figure E.5: The small modes for a varying synthetic inertia derivator sensitivity. The derivative factor is multiplied with the derivator time constant, and the gain is constant.

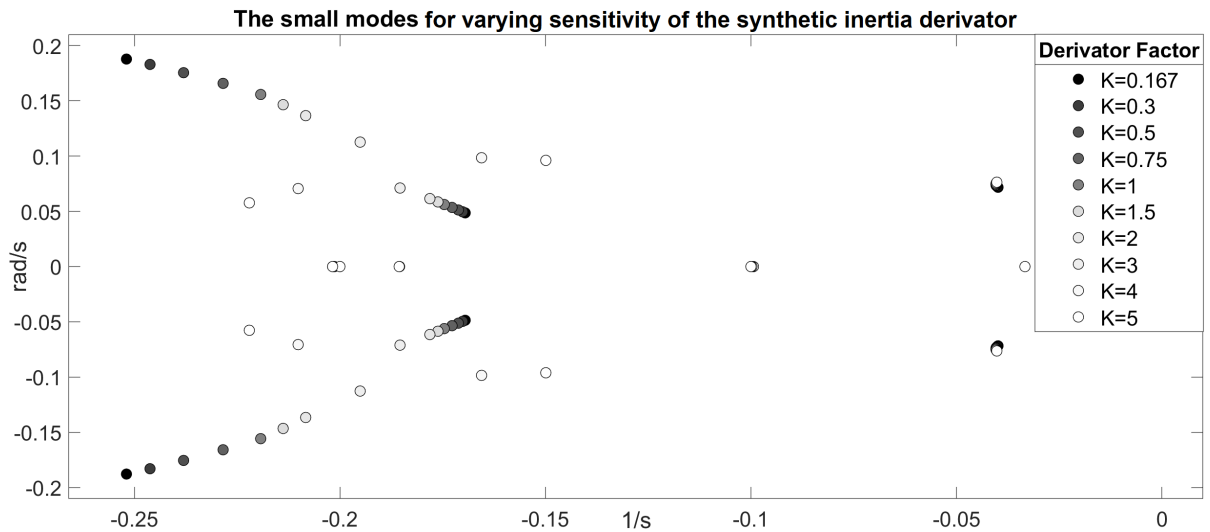


Figure E.6: The small modes for a varying synthetic inertia derivator sensitivity. The derivator factor is multiplied with the derivator time constant, and the gain is adjusted to keep the inertial contribution in accordance with the wind turbine's stored kinetic energy.

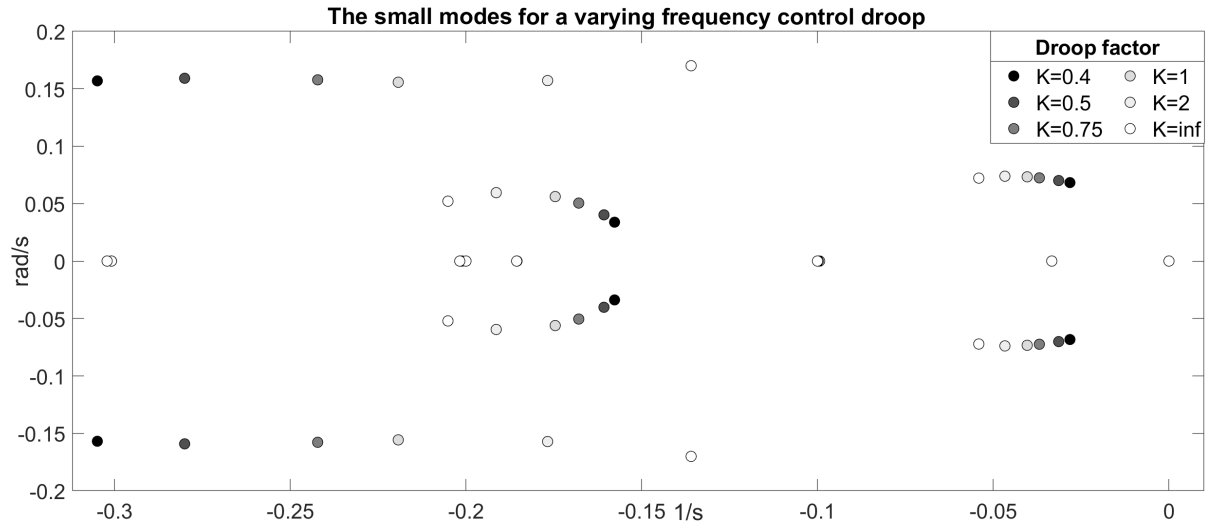


Figure E.7: The small modes for a varying primary control droop.

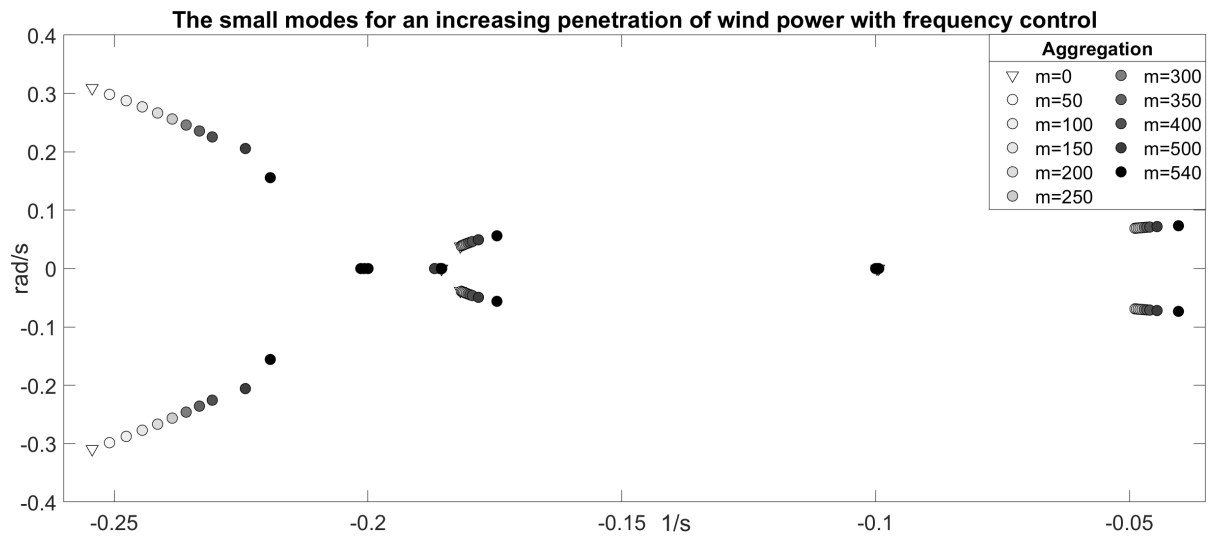


Figure E.8: The small modes for a varying wind power penetration with frequency controls.

Synchronous generation, mode 18

	Name	Mode Index	Mode: Real part 1/s	Mode: Imaginary part rad/s	Controllability: Mag.	Observability: Mag.	Participation: Mag.
+	Two Area; G1; speed	18	-0,254361	0,309238	1,	0,042678	0,548635
+	Two Area; G2; speed	18	-0,254361	0,309238	0,981643	0,042679	0,538571
+	Two Area; G3; speed	18	-0,254361	0,309238	0,602424	0,042679	0,330515
+	Two Area; G4; speed	18	-0,254361	0,309238	0,570547	0,042676	0,313001
+	Plant_G4; STAB1; x3	18	-0,254361	0,309238	0,193076	0,128106	0,31796
+	Plant_G2; STAB1; x3	18	-0,254361	0,309238	0,190542	0,128116	0,313812
+	Plant_G4; STAB1; x1	18	-0,254361	0,309238	0,082346	0,551638	0,583948
+	Plant_G2; STAB1; x1	18	-0,254361	0,309238	0,081266	0,551682	0,57633
+	Plant_G1; IEEEG1; x3	18	-0,254361	0,309238	0,080362	0,967995	1,
+	Plant_G1; IEEEG1; x4	18	-0,254361	0,309238	0,080123	0,280072	0,288471

SG 2 replaced with wind power with frequency control, mode 31

	Name	Mode Index	Mode: Real part 1/s	Mode: Imaginary part rad/s	Controllability: Mag.	Observability: Mag.	Participation: Mag.
+	DFIG Control; Frequency; x1	31	-0,219268	0,155685	1,	0,000763	0,620088
+	Two Area; G1; speed	31	-0,219268	0,155685	0,351473	0,000704	0,201292
+	DFIG Control; Speed-Controller; xi	31	-0,219268	0,155685	0,193046	0,000347	0,054416
+	DFIG Control; Shaft; xH	31	-0,219268	0,155685	0,16485	0,000931	0,124827
+	Plant_G1; STAB1; x3	31	-0,219268	0,155685	0,152583	0,002805	0,347997
+	Plant_G4; STAB1; x3	31	-0,219268	0,155685	0,07447	0,002797	0,16938
+	Two Area; DFIG_1.5MW; speed	31	-0,219268	0,155685	0,07272	0,000932	0,055123
+	Two Area; G3; speed	31	-0,219268	0,155685	0,067405	0,000702	0,038502
+	Two Area; G4; speed	31	-0,219268	0,155685	0,058921	0,000702	0,033653

Synchronous generation, mode 13

	Name	Mode Index	Mode: Real part 1/s	Mode: Imaginary part rad/s	Controllability: Mag.	Observability: Mag.	Participation: Mag.
+	Plant_G4; STAB1; x3	13	-0,18181	0,038054	1,	0,190136	0,977918
+	Plant_G2; STAB1; x3	13	-0,18181	0,038054	0,993652	0,190118	0,971621
+	Two Area; G1; speed	13	-0,18181	0,038054	0,633576	0,016728	0,054512
+	Two Area; G2; speed	13	-0,18181	0,038054	0,62008	0,016729	0,053352
+	Plant_G3; STAB1; x3	13	-0,18181	0,038054	0,418997	0,190138	0,409749
+	Plant_G1; STAB1; x3	13	-0,18181	0,038054	0,413347	0,190113	0,404171
+	Two Area; G3; speed	13	-0,18181	0,038054	0,37922	0,016731	0,032632
+	Two Area; G4; speed	13	-0,18181	0,038054	0,357279	0,01673	0,030743
+	Plant_G4; STAB1; x1	13	-0,18181	0,038054	0,205406	0,212332	0,224319
+	Plant_G2; STAB1; x1	13	-0,18181	0,038054	0,204102	0,212312	0,222875
+	Plant_G1; IEEEG1; x4	13	-0,18181	0,038054	0,194454	0,99987	1,

SG 2 replaced with wind power with frequency control, mode 23

	Name	Mode Index	Mode: Real part 1/s	Mode: Imaginary part rad/s	Controllability: Mag.	Observability: Mag.	Participation: Mag.
+	DFIG Control; Frequency; x1	23	-0,174614	0,056148	1,	0,000406	0,218955
+	Plant_G1; STAB1; x3	23	-0,174614	0,056148	0,378743	0,002872	0,586417
+	Two Area; G1; speed	23	-0,174614	0,056148	0,313144	0,000384	0,064753
+	DFIG Control; Speed-Controller; xi	23	-0,174614	0,056148	0,280696	0,000171	0,025833
+	DFIG Control; Shaft; xH	23	-0,174614	0,056148	0,194479	0,000313	0,032782
+	Plant_G4; STAB1; x3	23	-0,174614	0,056148	0,183628	0,00287	0,284035
+	Plant_G1; IEEEG1; x4	23	-0,174614	0,056148	0,092865	0,019977	1,
+	Two Area; DFIG_1.5MW; speed	23	-0,174614	0,056148	0,085826	0,000313	0,014488
+	Plant_G1; STAB1; x1	23	-0,174614	0,056148	0,083657	0,004857	0,219026

Figure E.9: The eigenvectors, sorted by controllability, relating modes 18 and 13 to the dominant states for the synchronous generation. Furthermore, the eigenvectors of the successor modes 31 and 23 for wind power with frequency service controls.

	Name	Mode Index	Mode: Real part 1/s	Mode: Imaginary part rad/s	Controllability: Mag.	Observability: Mag.	Participation: Mag.
👤	DFIG Control; Speed-Controller; xi	18	-0.040333	0.073337	0.597267	0.000281	1,
👤	DFIG Control; Shaft; xH	18	-0.040333	0.073337	0.564134	0.000235	0.790841
👤	Two Area; DFIG_1.5MW; speed	18	-0.040333	0.073337	0.24853	0.000235	0.34827
👤	DFIG Control; PLL WT; x2	18	-0.040333	0.073337	0.000482	0.068279	0.196205
👤	DFIG Control; Frequency; x1	18	-0.040333	0.073337	1,	0.000015	0.091493
👤	Plant_G1; IEEE1; x4	18	-0.040333	0.073337	0.029123	0.000365	0.063447
👤	DFIG Control; Speed-Controller; xpc	18	-0.040333	0.073337	0.020829	0.00041	0.05098
👤	Plant_G1; IEEE1; x3	18	-0.040333	0.073337	0.018762	0.000345	0.038643
👤	Plant_G1; STAB1; x1	18	-0.040333	0.073337	0.015866	0.000184	0.017407
👤	Plant_G3; IEEE1; x4	18	-0.040333	0.073337	0.005991	0.000365	0.013051
👤	Plant_G4; IEEE1; x4	18	-0.040333	0.073337	0.005194	0.000365	0.011316
👤	Two Area; G1; speed	18	-0.040333	0.073337	0.099429	0.000015	0.008983
👤	Plant_G4; STAB1; x1	18	-0.040333	0.073337	0.007832	0.000184	0.008592
👤	Plant_G3; IEEE1; x3	18	-0.040333	0.073337	0.003859	0.000345	0.007949
👤	Plant_G1; IEEE1; x2	18	-0.040333	0.073337	0.003784	0.000311	0.007015
👤	Plant_G4; IEEE1; x3	18	-0.040333	0.073337	0.003346	0.000345	0.006892
👤	Plant_G1; STAB1; x3	18	-0.040333	0.073337	0.041577	0.000018	0.004349
👤	Plant_G3; STAB1; x1	18	-0.040333	0.073337	0.003357	0.000184	0.003683
👤	Plant_G4; STAB1; x3	18	-0.040333	0.073337	0.020522	0.000018	0.002147
👤	Plant_G1; IEEE1; x1	18	-0.040333	0.073337	0.001142	0.000305	0.002076
👤	Two Area; G3; speed	18	-0.040333	0.073337	0.01943	0.000015	0.001755
👤	Two Area; G4; speed	18	-0.040333	0.073337	0.016846	0.000015	0.001522
👤	Plant_G3; IEEE1; x2	18	-0.040333	0.073337	0.000778	0.000311	0.001443
👤	Plant_G4; IEEE1; x2	18	-0.040333	0.073337	0.000675	0.000311	0.001251
👤	Plant_G3; STAB1; x3	18	-0.040333	0.073337	0.008796	0.000018	0.00092
👤	Two Area; G1; psifd	18	-0.040333	0.073337	0.000547	0.000214	0.000697

Figure E.10: The eigenvectors relating the dominant states to mode 18. The participation factors sort the states.

